MICROPOROUS MATERIALS FOR THE SELECTIVE ADSORPTION OF PERFLUORINATED SURFACTANTS

Matthias VAN DEN BERGH

Supervisors:
Prof. Dr. D. De Vos, KU Leuven
Dr. S. Mullens, VITO

Members of the Examination Committee:
Prof. R. Merckx, KU Leuven, Chairman
Prof. E. Smolders, KU Leuven
Prof. C. Kirschhock, KU Leuven
Prof. I. Vankelecom, KU Leuven
Dr. A. Georgi, Helmholtz Centre for Environmental Research – UFZ

Dissertation presented in partial fulfilment of the requirements for the degree of Doctor of Bioscience Engineering (PhD)

February 2021

Doctoraatsproefschrift nr. 1683 aan de faculteit Bio-ingenieurswetenschappen van de KU Leuven.

© 2021 KU Leuven, Science, Engineering & Technology
Uitgegeven in eigen beheer, Van den Bergh Matthias, Lubbeek.

Alle rechten voorbehouden. Niets uit deze uitgave mag worden vermenigvuldigd en/of openbaar gemaakt worden door middel van druk, fotokopie, microfilm, elektronisch of op welke andere wijze ook zonder voorafgaandelijke schriftelijke toestemming van de uitgever.

All rights reserved. No part of the publication may be reproduced in any form by print, photoprint, microfilm, electronic or any other means without written permission from the publisher.

PREFACE

Well, here it is: my PhD booklet. Finally. When I started my PhD 5 years ago, those years ahead of me seemed almost infinite. So much time, so much to do, but the years flew by so fast. I feel extremely lucky with so many of the people and events that crossed my path. This is my chance to express some gratitude.

First of all, I would like to thank Prof. Dirk De Vos, my promotor. Without him, this booklet would have never existed. As big a stereotype as this may be, it is nothing but the truth. For some reason, I had a connection with Dirk as a student that I did not have with other professors. It might have been his aspiring way of teaching, and the fact that he did remember my name (and that of many others) out of those 200 fresh faces that appeared every year in front of him. This is the reason why I shifted from Environmental Technology to the Catalysis group for doing my thesis and PhD. This is significant, because the desire to do something good for our environment was and still is the main reason why I studied for becoming a bio-engineer. I am also very thankful for Dirk giving me this PhD topic on PFAS removal. 5 years ago, I had never heard of PFASs before. Searching for this topic in general media did not generate many hits. Now it seems to be everywhere from time to time, there is even a Hollywood movie about it. Thank you Dirk for being ahead in time and realizing this would be a very relevant and hot topic today. Thank you for granting me this environmental topic, while initially you had foreseen a purely chemical one. Starting a new research topic from scratch surely had it challenges, but yet I am very happy for it. Thank you for proposing the idea of investigating hydrophobic zeolites. Without your intellectual input, I would still be in the lab, searching for my first good result. And most importantly, thank you for convincing me to go on in the moments where I wanted to quit.

I am grateful to all parties that supported me financially during this PhD: Prof. Dirk De Vos, VITO and FWO. Without them, this PhD would have been nothing more than some good ideas. Obtaining a scholarship turned out to be a difficult process, and I am very happy that VITO made the bet to invest in me and my topic. I would like to thank all people at VITO that helped me during my PhD. In the first place my co-promotor Steven Mullens, who had the difficult task to introduce me in the world of structured materials. Stefan Voorspoels and Ellen Poelmans for the analysis of PFAS concentrations; this turned out to be challenging and without them, I would have had only experiments and no results. Jasper Lefevere for helping me around in the lab and for providing me with some good recipes. A big thanks to all colleagues who

made this once-in-a-while-appearing person yet feel welcome at VITO. Thank you Mieke Quaghebeur for taking me into your group and for preparing me for the jury. I am also grateful to all members of my examination committee and for the time they invested in me and in improving this manuscript.

My understanding of PFAS adsorption would be non-existent without the help and support of some external research groups. For this, I would like to sincerely thank Andraž Krajnc and Gregor Mali from the National Institute of Chemistry in Slovenia; Sergio Rodrigues Tavares and Guillaume Maurin from the Institut Charles Gerhardt in Montpellier; and Isabelle Beurroies from Aix Marseille Université. Above all, their input made me realize how little you know as a researcher and how important it is to collaborate among people and institutions.

Arguably the best thing about doing a PhD were my colleagues. I think there are very few working environments where your colleagues are just a bunch of friends, with little to no difference in function and hierarchy. Patrick, Joris, Dries, Willem, Koen, Mickaël and Kwinten, thank you for all those fun days in the office. Thank you Simon: our friendship started somewhere in the North of Europe but luckily it did not stay there. Thank you for enduring my spam of PhD-related, administrative questions. Thank you Carlos, Cherry, Niels, Maxime, Wouter, … the list is long and not inclusive but they all contributed to a fine work environment and to fun after-work baarr moments. I would also like to thank Renewi and my new colleagues there for giving me a big new opportunity in these professionally difficult times.

A big thank you for the honorable members of De Gilde. I will never win a Noble prize, but if I would, they would still keep me modest with their skeptical jokes about doing a PhD. I have a warm heart and lots of love for my family. They might not always have known what exactly I was doing in my PhD, but they were always there for me. I am absolutely aware of how blessed I am for having such a warm family that unconditionally loves and supports me. Mama and papa, thank you for everything. Kenneth and Tinne, thank you bringing Suze and Lotte into my life. Seeing these girls grow up is a significant source of happiness in my life. Nacho, thank you for all those hours we spent riding our bikes together. For all those hours driving a car in order to ride our bikes. And for all those hours thinking about driving a car to somewhere nice in order to ride our bikes. Thank you for travelling the world for a year and organizing a goodbye party where I could meet your sister. Isa, thank you for everything. You are, within a 100 % confidence interval, the best result of my PhD. There is no chapter as compelling and as fun as the one I am writing with you. Let’s do our research thoroughly and make it a long term experiment.

ABSTRACT

Perfluorinated alkylated substances (PFASs) are a class of persistent organic pollutants which, in recent years, have been gaining a lot of attention. Extensively used over the past 40 years, they are only now fully recognized as top priority pollutants, due to their widespread occurrence in (drinking) water, food products, animals and even humans. Exposure to PFASs is associated with a series of health risks, including liver and kidney cancer and it affects fetus and child growth. Increased awareness on the risks of PFASs has led to governmental regulations worldwide, ranging from restrictions on production and consumption to the implementation of threshold concentrations for PFASs in tap, surface and waste water. Most of this new regulation focuses on perfluorooctanoic acid (PFOA) and perfluorooctanesulfonic acid (PFOS), the two most used and spilled PFASs. The restrictions on PFOA and PFOS have pushed industrial players to use other fluorinated surfactants as drop-in replacements. Most of these fluorinated alternatives are not (yet) restricted, meaning that levels of persistent and bioaccumulative fluorinated chemicals continue to build up in natural waters. In addition, historical emissions of PFOA and PFOS still cause locally elevated concentrations.

Because conventional waste water treatment plants are unable to remove PFASs from water, the recent implementation of environmental quality standards in Belgium (as well as in many other countries) requires new and suitable techniques to remove PFASs at low concentrations from complex water matrices. More specifically, PFAS concentrations have to be reduced from a µg/L concentration range (or mg/L in the case of extreme contaminations) to less than 1 ng/L. Adsorption is arguably the best technique to treat large water volumes while keeping energy costs modest. This makes the selection (and synthesis) of an adsorbent with adequate capacity and high selectivity for PFASs of utmost importance.

Since hydrophobicity was suggested to be a favorable factor for PFAS adsorption, a hydrophobic all-silica zeolite was studied as PFAS adsorbent and compared to activated carbon, the current benchmark adsorbent for PFASs. Activated carbon has a relatively high adsorption capacity and it is a widely applicable adsorbent for many types of (organic) compounds, but it therefore lacks selectivity. Based on various adsorption experiments (screening for capacity, affinity, selectivity and kinetics), all-silica zeolite Beta showed to be an outstanding adsorbent for PFAS adsorption. Zeolite Beta is a zeolite type with wide pores and straight channels, providing an

open and accessible material. The PFAS uptake was higher and quicker on this zeolite than on activated carbon. It was especially for PFAS selectivity that all-silica zeolite Beta showed truly outstanding results. PFAS uptake was undisturbed by competition of other organic compounds, even when these compounds were present in a 15-fold molar excess. In contrast, PFAS uptake on activated carbon was drastically reduced.

The question why all-silica zeolite Beta has such a high affinity and selectivity for PFASs was resolved by combining the results of advanced characterization techniques and computational modelling. Calorimetry measurements showed that PFOA adsorption on all-silica zeolite Beta is associated with a negative adsorption enthalpy. Together with the increase in entropy that is common for many hydrophobic interactions, this results in a favorable adsorption reaction. Computational simulations demonstrated that the adsorbed PFOA molecules interact in very stable head-head interactions, resulting from the formation of carboxylic acid dimers and driven by H-bonding. This contributes significantly to the favorable adsorption process. These characterization experiments made it very clear that the adsorption of PFOA on all-silica zeolite Beta is very favorable in terms of enthalpy, while the perfluorinated chains are situated in the hydrophobic, straight channels of the zeolite. The helical conformation of the perfluorinated chains makes a very tight packing at maximal capacity sterically possible, explaining the exceptionally high affinity and selectivity of all-silica zeolite Beta for PFOA and similar perfluorinated compounds.

Before industrial application is possible, four main aspects need further research and development; i) extending the scope of PFASs than can be removed, ii) regeneration of the adsorbent by PFAS degradation, iii) shaping of the adsorbent and optimization of the adsorption process and iv) upscaling of the all-silica zeolite Beta synthesis process. Effective shaping of a commercial zeolite Beta into microspheres was achieved, but this procedure could not be implemented on all-silica zeolite Beta.

SAMENVATTING

Geperfluoreerde chemicaliën (PFASs) zijn een klasse van persistente, organische polluenten die recent veel aandacht hebben gekregen. Ook al zijn ze reeds een veertigtal jaar intensief gebruikt, het is pas nu dat ze erkend worden als contaminanten die de hoogste aandacht verdienen. Dit komt o.a. omdat ze wijdverspreid zijn in (drink)water, voedingsproducten, flora en fauna en zelfs in het bloed van de meeste mensen. Blootstelling aan deze PFASs wordt geassocieerd met een reeks gezondheidsproblemen, waaronder lever- en nierkanker en een aangetaste ontwikkeling van foetussen en jonge kinderen. Door het toegenomen besef over de verspreiding en risico's van deze PFASs, zijn er de laatste jaren wereldwijd maatregelen getroffen om het gebruik en de verspreiding van deze PFASs tegen te gaan. Daarnaast zijn er in verschillende landen normen opgelegd voor de maximale concentraties van deze componenten in leiding- en oppervlaktewater. Deze maatregelen richten zich voornamelijk op perfluorooctaanzuur (PFOA) en perfluorooctaansulfonzuur (PFOS), de twee meest gebruikte en verspreide PFAS moleculen. Door deze nieuwe regelgeving zijn veel spelers in de fluorindustrie reeds overgeschakeld naar zeer gelijkaardige alternatieven die nog niet of slechts beperkt gereglementeerd zijn. Dit betekent dat er nog steeds geperfluoreerde chemicaliën in het milieu terecht komen en daar accumuleren, bovenop de historische vervuiling van PFOA en PFOS die reeds aanwezig is.

Conventionele waterzuiveringsinstallaties zijn niet in staat om PFOA en PFOS uit water te halen. Hierdoor vereist de recente implementering van milieukwaliteitsnormen in België (alsook in vele andere Westerse landen) de ontwikkeling en implementatie van nieuwe, innovatieve zuiveringstechnieken. Deze moeten in staat zijn om lage concentraties van PFAS chemicaliën (ca 1 µg/L tot 1 mg/L)nog verder te verlagen tot minder dan 1 ng/L, en dit uit een complexe waterige omgeving waar ook veel andere (organische) componenten aanwezig zijn. Adsorptie is waarschijnlijk de beste techniek om grote volumes aan water te behandelen en dit met een beperkt energieverbruik. Hierdoor wordt de selectie van een adsorbens met voldoende capaciteit en een hoge selectiviteit voor PFASs van uitermate belang.

In deze thesis werden een reeks hydrofobe zeolieten onderzocht. Deze zeolieten bestonden volledig (*all-silica*) of grotendeels (*high-silica*) uit silica, in tegenstelling tot meer conventionele zeolieten die ook aluminium (Al) in hun rooster hebben. Deze adsorbentia werden vergeleken met actieve kool, de huidige referentie inzake PFAS adsorptie. Actieve kool is vlot beschikbaar en heeft een hoge

adsorptiecapaciteit voor vele organische componenten, maar het ontbreekt hierdoor aan selectiviteit voor één specifiek type van chemicaliën. Op basis van verschillende adsorptie-experimenten (die o.a. de capaciteit, affiniteit, selectiviteit en kinetiek onderzochten), werd all-silica zeoliet Beta geselecteerd als uitstekend adsorbens voor PFAS. Zeoliet Beta is een type zeoliet met relatief grote poriën en rechte, open kanalen, waardoor het een open en toegankelijk rooster heeft. In vergelijking met actieve kool was de opname van PFAS niet alleen hoger maar ook sneller op dit type zeoliet. Maar vooral inzake selectiviteit toonde all-silica zeoliet Beta uitzonderlijke resultaten. PFAS adsorptie op deze zeoliet werd amper tot niet gehinderd door competitie van andere, natuurlijke organische stoffen, zelfs wanneer deze componenten 15-maal hogere concentraties hadden dan PFOA of PFOS. PFAS adsorptie op actieve kool daarentegen werd sterk gereduceerd door deze competitie.

De vraag waarom all-silica zeoliet Beta zo goed is voor de adsorptie van PFAS werd beantwoord door een reeks geavanceerde analyse- en simulatietechnieken te combineren. Calorimetrie metingen toonden aan dat de adsorptie van PFOA op all-silica zeoliet Beta een negatieve enthalpie kent. In combinatie met een toename van de entropie, eigen aan hydrofobische interacties, resulteert dit in een gunstige adsorptiereactie. Geavanceerde simulaties toonden bovendien aan dat de geadsorbeerde PFOA moleculen zeer gunstige kop-kop interacties aangaan in de zeoliet. Deze kop-kop interacties zijn het gevolg van waterstofbruggen die tussen twee zuurgroepen worden gevormd. Dit levert een significante bijdrage tot het gunstige karakter van deze adsorptie. Het geheel van deze experimenten toonde aan dat de PFAS moleculen net de volledige porieruimte van de zeoliet kunnen bezetten. Deze krappe maar volledig bezetting draagt mee bij tot de uitzonderlijk hoge affiniteit en selectiviteit van all-silica zeoliet Beta voor PFOA en andere, gelijkaardige geperfluoreerde chemicaliën.

Alvorens een (grootschalige) industriële toepassing van dit adsorbens mogelijk is, zijn er nog vier domeinen waar verdere ontwikkeling en onderzoek nodig is: i) een uitbreiding van het aantal verschillende types PFAS die verwijderd kunnen worden met deze zeoliet, ii) het hergebruik en de regeneratie van het adsorbens door de afbraak van geadsorbeerde PFAS moleculen, iii) de praktische vormgeving van het materiaal en de optimalisatie van het adsorptieproces als geheel, en tenslotte iv) het opschalen van de zeoliet synthese naar industriële schaal. Wat betreft vormgeving, werd de productie van microsferen uit het poeder van een zeoliet Beta onderzocht. Dit was succesvol voor een klassieke, commerciële zeoliet Beta (die Al bevat), maar (nog) niet voor de all-silica zeoliet Beta.

3DFD	Three Dimensional Fiber Deposition
AC	Activated Carbon
AEC	Anion Exchange Capacity
BDE	Bond Dissociation Energy
BET	Brunauer–Emmett–Teller
C_0	Feed Concentration
CA	Citric Acid
cc	Cubic Centimeter
CD	Cyclodextrin
C_e	Equilibrium Concentration
CLRC	Closed Loop Recycling Chromatography
CMC	Critical Micelle Concentration
COF	Covalent Organic Frameworks
CP	Cross Polarization
CTABr	Cetyltrimethylammonium Bromide
CUR	Carbon Usage Rate
d.m.	Dry Mass
DFT	Density Functional Theory
DI	Deionized (Water)
DQ	Double-Quantum
DSP	Downstream Processing
DTGS	Deuterated Triglycine Sulfate
DVB	Divinylbenzene
EBCT	Empty Bed Contact Time
ECF	Electrochemical Fluorination
EDX	Energy-Dispersive X-Ray Spectroscopy
EQS	Environmental Quality Standard
ESI	Electrospray Ionization
FEGSEM	Field Emission Gun Scanning Electron Microscope
FTIR	Fourier-Transform Infrared Spectroscopy
GAC	Granular Activated Carbon
GGA	Generalized Gradient Approximation
GIPAW	Gauge Including Projector Augmented Waves
HETP	Height Equivalent Of A Theoretical Plate
HFPO-DA	Hexafluoropropylene Oxide Dimer Acid
HMS	Hexagonal Mesoporous Silica
HPLC	High Performance Liquid Chromatography
IEP	Isoelectric Point
IgG	Immunoglobin G
IPA	Isopropyl Alcohol
K	Equilibrium Constant
K_f	Freundlich Constant

K_h	Henry Constant
K_l	Langmuir Constant
L	Liquid Flow
LAS	Linear Alkylbenzene Sulfonate
LTA	Linde Type A
MAS	Magic Angle Spinning
MC	Methylcellulose
MCM	Mobil Composition Of Matter
MIP	Molecular Imprinted Polymer
MOF	Metal Organic Framework
MR	Membered Ring
MRM	Multiple Reaction Monitoring
MS	Mass Spectrometry
MTZ	Mass Transfer Zone
n_f^{-1}	Heterogeneity Factor (Freundlich Model)
NMR	Nuclear Magnetic Resonance
NOM	Natural Organic Matter
OSDA	Organic Structure Directing Agent
PAC	Powder Activated Carbon
PBE	Perdew-Burke-Ernzerhof
PET	Polyethylene Terephthalate
PFAS	Perfluorinated Alkylated Substances
PFBA	Perfluorobutanoic Acid
PFBS	Perfluorobutanesulfonic Acid
PFC	Perfluorinated Compounds
PFCA	Perfluorinated Carboxylic Acid
PFDS	Perfluorodecanesulfonic Acid
PFHA	Perfluorohexanoic Acid
PFHS	Perfluorohexanesulfonic Acid
PFOA	Perfluorooctanoic Acid
PFOS	Perfluorooctanesulfonic Acid
PFPA	Perfluoropentanoic Acid
PFSA	Perfluorinated Sulfonic Acid
pK_a	Acid Dissociation Constant
POP	Persistent Organic Pollutant
PP	Polypropylene
PTFE	Polytetrafluoroethylene
PVP	Poly(4-Vinylpyridine)
PVPP	Polyvinylpolypyrrolidone
q_e	Equilibrium Adsorption Capacity
q_m	Maximum Adsorption Capacity
RT	Room Temperature
RV	Rotary Valve
S	Simulated Solid Flow
SAPO	Silicoaluminophosphate

SCS	Side Crushing Strength
SDA	Structure Directing Agent
SDS	Sodium Dodecylsulfate
SEM	Scanning Electron Microscope
Si-OH	Silanol Group
SMB	Simulated Moving Bed
SQ	Single-Quantum
SSRC	Steady-State Recycling Chromatography
TEA	Tetraethylammonium
TEOS	Tetraethylorthosilicate
TGA	Thermogravimetric Analysis
TPABr	Tetrapropylammonium Bromide
u	Simulated Interstitial Fluid Velocity
UOP	Universal Oil Products
u_s	Simulated Solid Velocity
UV	Ultraviolet
WWTP	Wastewater Treatment Plant
XRD	X-Ray Diffraction
ZIF	Zeolitic Imidazolate Framework

TABLE OF CONTENTS

Preface i
Abstract iii
Samenvatting v
List of Symbols and Abbreviations vii
Table of Contents xi
List of Tables xiii
List of Figures xiv

1. An introduction to perfluorinated substances 3
   1.1. General Introduction 3
   1.2. Fluorine chemistry 3
   1.3. Perfluorinated surfactants 4
   1.4. Emissions and pollution 5
   1.5. Toxicity 6
   1.6. Legislation and regulation 7
   1.7. Prospectives and PFAS alternatives 8
   1.8. Outline of PhD thesis 9
   1.9. References 10

2. Adsorption, Liquid Separation 15
   2.1. Introduction 15
   2.2. Fundamentals 15
   2.3. Process modes 18
   2.4. Adsorbents 38
   2.5. Industrial Applications 42
   2.6. Cited references 59
   2.7. General references 63

3. Adsorption and Selective Recovery of Citric Acid with Poly(4-vinylpyridine) 67
   3.1. Introduction 67
   3.2. Results and discussion 69
   3.3. Conclusion 81
   3.4. References 82
   3.5. Experimental section 83

4. Exploring the potential of siliceous microporous materials for adsorption of PFASs 87
   4.1. Introduction 87
   4.2. State of the art: PFAS adsorbents 87
   4.3. Results and discussion 91
   4.4. Conclusion 98
   4.5. References 100

4.6. Supporting Information 103

5. Highly selective removal of perfluorinated contaminants by adsorption on all-silica zeolite Beta 111
5.1. Introduction 111
5.2. Results and discussion 112
5.3. Conclusion 121
5.4. References 122
5.5. Supporting Information 124

6. Structured zeolitic adsorbents for the adsorptive separation of PFASs by droplet coagulation 145
6.1. Introduction 145
6.2. Results and discussion 153
6.3. Conclusion 173
6.4. References 175
6.5. Supporting Information 178

7. General conclusions and future perspectives 191
7.1. Conclusions 191
7.2. Future perspectives 195
7.3. References 202

List of Publications 203

Table 1.1: Environmental quality standards (EQS) imposed by Flemish legislation in VLAREM II. 8

Table 2.1: Overview of relevant industrial applications of the SMB process for adsorptive separation. 33
Table 2.2: Overview of different adsorbent types and their target compounds for waste water treatment. 51

Table 3.1: pK_a, $\Sigma\alpha^H_2$ and log P values of the different solvents tested for the regeneration of PVP. 76
Table 3.2: Anion exchange capacity (AEC) of the different resins, as stated by the manufacturer and according to our own potentiometric titrations. 77
Table 3.3: Model parameters obtained by fitting the adsorption data of IRA-900, IRA-67 and PVP to the Langmuir and Freundlich adsorption models. 78

Table S5.1: Model parameters obtained by fitting the adsorption data of different zeolite Beta types and activated carbon to the Langmuir and Freundlich adsorption models.. 140
Table S5.2: Stock concentrations of PFOA and PFOS solutions used for the determination of the single compound adsorption isotherms. 140

Table 6.1: Overview of the selected binders for the structuration of all-silica zeolite Beta and Beta-22. 154
Table 6.2: Overview of the different recipes used for the shaping of Beta-22 microspheres via gravitational droplet extrusion. 158
Table 6.3: Effect of ball milling on the average diameter of agglomerates in recipe V4 for different percentiles. 159
Table 6.4: Overview of self-shaped microspheres obtained by gravitational droplet extrusion. 160
Table 6.5: Surface and pore properties of all-silica zeolite Beta and Beta-22 (powder) vs. extruded microspheres based on Beta-22. 161
Table 6.6: Overview of the most common characterization techniques for as-shaped microspheres and the information retrieved thereof. 166

Figure 1.1: Chemical structure of perfluorooctanoic acid (PFOA) and perfluorooctanesulfonic acid (PFOS). 5
Figure 1.2: Chemical structure of GenX™ (left) and ADONA™ (right), two widely used perfluoro(poly)ether alternatives. 8

Figure 2.1: Graphical representation of the different isotherm models. 18
Figure 2.2: Sketch showing the migration of the mass transfer zone (MTZ) through a packed bed adsorption column and the corresponding concentration profile. 21
Figure 2.3: Principle of chromatography. 24
Figure 2.4: Schematic view of co-current vs. countercurrent flows. 27
Figure 2.5: Schematic illustration of a continuous countercurrent adsorption process. 28
Figure 2.6: McCabe-Thiele diagram for an ideal continuous countercurrent process with different adsorption and desorption units. 29
Figure 2.7: Schematic illustration of a moving bed process for the adsorptive separation of compounds A and B. 30
Figure 2.8: McCabe-Thiele diagram for an ideal continuous countercurrent process for the separation of a binary stream (A+B), with adsorption and desorption occurring in the same vessel. 31
Figure 2.9: Schematic diagram of the Sorbex process. 34
Figure 2.10: Schematic overview of a countercurrent SMB process by a cascade of fixed beds. 36
Figure 2.11: McCabe-Thiele diagrams for SMB adsorption processes with convex and concave adsorption isotherms. 37
Figure 2.12: Schematic representation of the IUPAC classification of pores. 38
Figure 2.13: Two of the most employed zeolites: a) type A and b) faujasite (type X and Y) 40
Figure 2.14: Typical process to produce p-xylene and m-xylene with a Parex and MX Sorbex unit 44
Figure 2.15: Comparision of the extraction and adsorption selectivity between C11-C14 paraffins and olefins. 46
Figure 2.16: Structure of a typical immunoglobulin antibody. 49

Figure 3.1: Overview of the conventional recovery of citric acid. 68

Figure 3.2: CA adsorption capacities *q* for CA (in water and at RT) for five different resins at different pH levels.....70
Figure 3.3: Schematic overview of the different interactions possible between CA and a strong and weak anion exchanger.....71
Figure 3.4: Simulated CA speciation in function of pH.....72
Figure 3.5: The effect of sulfate competition on the adsorption capacities *q* for CA of four synthetic adsorbents.....73
Figure 3.6: Desorption of CA from PVP and IRA-67 by elution with water and ethanol at RT and at 60 °C.....74
Figure 3.7: Screening of different organic solvents for the regeneration of PVP at RT.....75
Figure 3.8: Langmuir isotherms for IRA-900, IRA-67 and PVP.....80
Figure 3.9: Sorption isotherms for CA on PVP (in water and at RT) with and without the presence of sulfate competition.....80

Figure 4.1: XRD plot of as-synthesized all-silica zeolite Beta compared to a simulated powder plot of polymorph B and polymorph A.....92
Figure 4.2: XRD plot of as-synthesized silicalite-1 compared to a simulated powder plot of ZSM-5.....93
Figure 4.3: Isotherms for PFOA adsorption on all-silica zeolite Beta, silicalite-1 and chabazite.....96
Figure 4.4: PFOA adsorption isotherms for all-silica zeolite Beta, SBA-15 and MCM-41.....96
Figure 4.5: Langmuir isotherms for adsorption of PFOA on as-synthesized all-silica zeolite Beta, Beta-22 (CP814E-22) and Beta-300 (CP811C-300).....96
Figure 4.6: The effect of competing organics on the adsorption of PFOA on all-silica zeolite Beta and on the commercial zeolite Beta-22 (CP814E-22).....97
Figure 4.7: Isotherms for PFOA and PFOS adsorption on all-silica zeolite Beta and on PTFE (powder form).....99
Figure 4.8: PFOA adsorption on ZIF-8.....99
Figure S4.1: Isotherms for PFOS adsorption on all-silica zeolite Beta, silicalite-1 and chabazite.....107
Figure S4.2: PFOS adsorption isotherms for all-silica zeolite Beta, SBA-15 and MCM-41.....107
Figure S4.3: PFOS adsorption isotherms for all-silica zeolite Beta, Beta-22 (CP814E-22) and Beta-300 (CP811C-300).....107

Figure 5.1*:* A) Adsorption isotherms (293 K) for PFOA and PFOS on all-silica Beta and activated carbon. (B) Adsorption kinetics for PFOA and (C) PFOS on all-silica Beta and activated carbon.....113

Figure 5.2: PFOA and PFOS adsorption on all-silica Beta (β) and activated carbon (AC) under competitive conditions. 115
Figure 5.3: PFOA and PFOS adsorption on all-silica Beta (β) and activated carbon (AC) under competitive conditions. 115
Figure 5.4: Optimized binding geometry of all-silica zeolite Beta and PFOA. 119
Figure 5.5: NMR-based inspection of the arrangement of PFOA molecules within the all-silica zeolite Beta. 120
Figure 5.6: Graphical representation of all-silica zeolite Beta with adsorbed PFOA molecules. 121
Figure S5.1: FTIR spectrum of the hydroxyl stretching region for as-synthesized all-silica Beta (All-Si Beta) and for the commercial zeolite Beta types Beta-22 and Beta-300. 131
Figure S5.2: Characterization of all-silica zeolite Beta via N_2 and water vapor physisorption isotherms. 132
Figure S5.3: The effect of pH upon the adsorption of PFOA on all-silica zeolite Beta and activated carbon. 133
Figure S5.4: Adsorption isotherms for linear perfluorinated carboxylic acids of varying chain length on all-silica zeolite Beta. 133
Figure S5.5: Adsorption isotherms for linear perfluorinated sulfonic acids of varying chain length on all-silica zeolite Beta. 134
Figure S5.6: PFOA adsorption on all-silica Beta and activated carbon under competition of inorganic anions. 134
Figure S5.7: Adsorption isotherms for PFOA on all-silica Beta (β) and the aluminum-containing zeolites Beta-22 and Beta-300. 135
Figure S5.8: Studying the impact of thermal treatment on a PFOA-saturated all-silica zeolite Beta. 135
Figure S5.9: Integral adsorption enthalpies for all-silica zeolite Beta and the aluminum-containing zeolites Beta-22 and Beta-300 as a function of the surface concentration of PFOA, measured via calorimetry. 136
Figure S5.10: Snapshots of DFT-optimized caprylic acid conformations adsorbed in all-silica zeolite Beta, as well as their associated total energy differences with respect to the head-head dimer taken as reference. 136
Figure S5.11: Snapshots of the geometry optimized PFOA and caprylic acid dimers. 137
Figure S5.12: ^{13}C and ^{19}F MAS NMR spectra of pure, crystalline PFOA and of PFOA loaded into the all-silica zeolite Beta in two different concentrations. 137
Figure S5.13: Two-dimensional ^{1}H-^{13}C heteronuclear correlation and ^{19}F-^{19}F homonuclear correlation NMR spectra of PFOA loaded into the all-silica zeolite Beta. 138

Figure S5.14: Two-dimensional ^{1}H-^{1}H DQ-SQ homonuclear correlation NMR spectrum of pure, crystalline PFOA and schematic presentation of the arrangement of PFOA molecules and of the hydrogen-bonding among these molecules in the crystals. 138
Figure S5.15: Langmuir adsorption isotherms for PFOA and its sodium salt on all-silica zeolite Beta. 139

Figure 6.1: Different microsphere morphologies. 148
Figure 6.2: Graphical representation of droplet formation by gravitional droplet extrusion and vibrational droplet extrusion. 150
Figure 6.3*:* Overview of the monomeric units and different block co-polymers of alginate polysaccharides. 152
Figure 6.4: SEM pictures of the calcined powder mixtures M29, M30 and M31. 154
Figure 6.5: PFOA adsorption on mixtures of all-silica zeolite Beta and different inorganic binders at three different starting concentrations of PFOA. 156
Figure 6.6: PFOA adsorption on different mixtures of all-silica zeolite Beta and three different inorganic binders. 156
Figure 6.7: Schematic overview of the gravitational coagulation set-up and picture of the experimental set-up. 157
Figure 6.8: SEM pictures of a single type of microspheres (Beta-22/Ludox AS-40 80/20). 160
Figure 6.9: PFOA adsorption kinetics for M48 and M49, compared to the all-silica zeolite Beta powder. 162
Figure 6.10: PFOA adsorption kinetics for M63 and M64, compared to the all-silica zeolite Beta powder). 163
Figure 6.11: Side crushing strength results for different types of microspheres, varying in binder content and nozzle diameter. 165
Figure 6.12: Shrinkage overview upon drying and calcination of Ludox-based microspheres. 167
Figure 6.13: SEM images of M50 microspheres: Beta-22/Ludox AS-40 80/20 extruded from a 1.19 mm nozzle. 168
Figure 6.14: SEM-EDX analysis of microspheres with different weight ratio of Ludox AS-40 binder. 170
Figure 6.15: SEM-EDX analysis of microspheres with different binder types: Ludox AS-40 (colloidal silica) vs. Dispersal P2 (boehmite). 171
Figure 6.16: Isoelectric point titration of all-silica zeolite Beta and the aluminum containing Beta-22. 173
Figure S6.1: PFOA adsorption on mixtures of Beta-22 and different inorganic binders at three different initial PFOA concentrations. 181
Figure S6.2: N_2 physisorption isotherms for M48 and M49. 181

Figure S6.3: N_2 physisorption isotherm for pure, as-synthesized all-silica zeolite Beta. 182
Figure S6.4: Results of the side crushing strength (SCS) experiments for different types of microspheres. 182
Figure S6.5: Image analysis for M48 microspheres. 183
Figure S6.6: Image analysis for M49 microspheres. 183
Figure S6.7: SEM images of M54 microspheres: Beta-22/Ludox AS-40 70/30 extruded from a 1.19 mm nozzle. 184
Figure S6.8: SEM images of M56 microspheres: Beta-22/Ludox AS-40 90/10 extruded from a 1.19 mm nozzle. 185
Figure S6.9: SEM images of M52 microspheres: Beta-22/Dispersal P2 80/20 extruded from a 1.19 mm nozzle. 186
Figure S6.10: Pore volume and pore size distribution plots of Ludox based microspheres, derived from mercury intrusion porosimetry measurements. 187
Figure S6.11: Pore volume and pore size distribution plots of microspheres made with different types of binders. 188
Figure S6.12: Pore volume and pore size distribution plots of microspheres made with different weight ratio of Dispersal HP14/7 and/or extruded from different tip sizes. 188
Figure S6.13: Particle size distributions of 2 wt% suspensions of all-silica zeolite Beta (left) and Beta-22 (right) in pure water. 188

Figure 7.1: Schematic visualization of an adsorption-regeneration cycle. 200

CHAPTER 1

AN INTRODUCTION TO PERFLUORINATED SUBSTANCES

Matthias Van den Bergh[a], Dirk De Vos[a]

[a] M. Van den Bergh, Prof. D. De Vos
Centre for Membrane Separations, Adsorption, Catalysis and Spectroscopy for Sustainable Solutions (cMACS)
KU Leuven
Celestijnenlaan 200F, 3001 Leuven, Belgium

Abstract

This chapter is a general introduction to the topic of perfluorinated substances. Their unique characteristics, chemistry, toxicity and environmental behavior will be discussed, as well as the environmental regulations regarding these compounds.

Contributions

M.V.d.B. wrote the manuscript. D.D.V. supervised the work.

1. An introduction to perfluorinated substances

1.1. General Introduction

Perfluorinated alkylated substances (PFASs), also named perfluorinated compounds (PFCs), are a particular class of persistent organic pollutants. They contain a wide variety of molecules, varying in length, structure and functionalities, but they are all defined by having a completely fluorinated (stretch of) carbon chain.[1] Compared to other (synthetic) organic compounds, PFASs have many unique and remarkable properties. Most of these are due to the particular character of the carbon-fluorine bond, explained in detail further below. Perfluorinated carbon chains are extremely hydrophobic; they strongly repel every droplet of water. Very remarkably though, they are also oleophobic. Whereas most molecules are either hydrophobic or oleophobic (repelling either fat-like or aqueous components), PFAS chains repel both hydrophobic and hydrophilic compounds. A very well-known example of this is the anti-sticking pan, coated with the linear perfluorinated polymer polytetrafluorothylene, better known as PTFE or Teflon®. Animal fats, vegetable oils and watery solutions all do not stick to these pans, as can be witnessed by the high contact angles of liquid droplets in these types of cooking material. Additionally, PFASs are highly inert against high temperatures, electrical currents and other chemicals. They cannot be broken down by UV-light or microbiota, making them nearly indestructible. They have very low surface tensions, making them extremely suitable for a variety of applications, ranging from lubricants to firefighting foams.[2] All these features are very desirable for both household and industrial applications, but it is the combination of all these features in just one class of organic chemicals that is really unique. This makes the fluorochemical industry a thriving and lucrative business that will not go away in the near or distant future.[3]

1.2. Fluorine chemistry

The remarkable properties of these PFAS compounds can be explained by the peculiarities of the fluorine atom. Foremost, fluorine is the most electronegative element in the periodic table, meaning that it exerts a strong and attractive force on the electrons of any kind of fluorine bond.[4] In the case of the C-F bond, this means that the bond is strongly polarized and has not only a covalent but also a partially ionic character, making it one of the strongest bonds in organic chemistry. The bond dissociation energy (BDE) of H_3C-F is 481 kJ/mol (at 298 K), compared to 439 kJ/mol for H_3C-H, which is even one of the strongest aliphatic C-H bonds. The C-F bond becomes stronger with every additional C-F bond on the same geminal carbon atom.

This is because with every additional fluorine bond, the partial charge on the carbon atom becomes more positive, hence increasing the electrostatic interactions between the fluorine and carbon atoms (BDE of F_3C-F = 544 kJ/mol).[5,6] Also the C-C bond strength increases through vicinal C-F bonds, due to quantum chemistry effects that will not be dealt with here. All this explains why perfluorinated compounds and polymers are extremely strong and difficult to degrade. But it does not explain why these compounds are so inert and both hydrophobic and oleophobic. The hydrophobicity of perfluorinated chemicals can be explained by the extremely apolar character of these chemicals. This might seem remarkable at first, since a single C-F bond is very polar. Due to the symmetry of a perfluorinated chain, however, the dipole moments of all C-F bonds nullify each other: their summation results in a very apolar carbon chain.

The inertness and oleophobicity are explained by the low polarizability of the fluorine atom. The polarizability of an atom expresses the tendency of its electron cloud to be affected and displaced by an external electrical field. A low polarizability means that the electrons of the fluorine atom are strongly attached to the fluorine core and are not displaced by the attractive or repulsive force of an external electrical field. The electrons of an atom with a higher polarizability are easily affected by such an external field, causing fluctuations of the electron cloud and hence instantaneous dipole moments. These instantaneous dipole moments are the driving force for London dispersion forces, also known as Van der Waals forces (even though they are not exactly the same). These interactions often make apolar and hydrophobic compounds attract each other, explaining for a part why hydrophobic compounds tend to cluster together.[1] The absence of these interactions for fluorine atoms is the reason why PFASs are not only hydrophobic but also oleophobic. The low polarizability of the fluorine atoms also lowers the capacity and tendency of the fluorine atom to donate a lone electron pair and to take part in hydrogen bonding, further increasing its apolar and hydrophobic character. Simply put, perfluorinated compounds hardly interact with other types of chemicals, making them extremely inert and resistant to any kind of reactant.[7]

1.3. Perfluorinated surfactants

An important subgroup of PFASs are the surfactants in which the perfluorinated chain (or tail) is linked to a hydrophilic head, often a carboxylic or sulfonic acid group. These perfluorinated carboxylic acids (PFCAs) and perfluorinated sulfonic acids

[1] Besides by Van der Waals forces, hydrophobic interactions can also be driven by entropic effects.

(PFSAs) still have all the features mentioned above but they are water-soluble due to their polar functionality. Their carbon chains contain in general 8 to 12 C-atoms, but both longer and shorter variants exist. Two of the historically most used and hence studied PFASs are perfluorooctanoic acid (PFOA) and perfluorooctanesulfonic acid (PFOS), both having a perfluorinated C_8-chain linked to a carboxylic acid group or sulfonic acid group, respectively (**Figure 1.1**).[8] Compared to e.g. PTFE, their shorter chain length and water solubility make them easier to apply as a coating or to dissolve in solutions or suspensions. Because of their surfactant character (i.e. their tendency to spread on interfaces and surfaces) and hydrophobicity, they are very well suited for specific cleaning applications (e.g. during the etching procedure of semiconductors) or for use in lubricants, stain- and water-repellent coatings for textiles, fat-repellent food wraps, etc. One of their industrially most relevant applications is as emulsifier in the emulsion polymerization of Teflon (PTFE).[9–11]

The synthesis of PFOA and PFOS has long been covered by patents, leading to a PFAS niche market dominated by two chemical companies. In general, there are two ways to produce PFASs: electrochemical fluorination (ECF) and fluorotelomerization. During ECF, aliphatic hydrogen atoms are replaced by fluorine atoms in an electrolytic cell, with HF acting as fluorine donor. ECF is not a very selective reaction: it is difficult to steer the process in the desired direction and the products are often fragmented and branched. In contrast, fluorotelomerization is a more selective synthesis procedure. In this method, perfluoroethyliodide reacts with perfluoroethylene and the resulting product is oxidized with SO_3 towards the respective PFAS. PFASs produced by telomerization are more linear.[12,13] Analysis of PFAS isomers (branched vs. linear) allows to reveal the source and producer of PFASs. Historical emissions are mostly of the branched types, while actual emissions contain more linear PFASs.

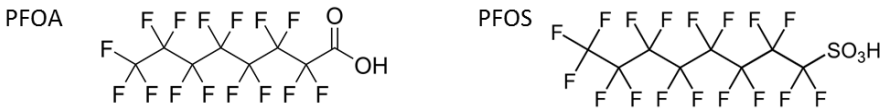


Figure 1.1: Chemical structure of perfluorooctanoic acid (PFOA) and perfluorooctanesulfonic acid (PFOS).

1.4. Emissions and pollution

Emissions of PFASs are mostly due to industrial production and usage: up to 60% of consumed PFASs in industry is believed to be emitted into the environment.[14] Contaminations can be direct from the (industrial) source (e.g. firefighting foams that

soak into the soil) or indirect (e.g. leaking percolate from a landfill or atmospheric degradation of volatile precursors). The most remarkable point sources of PFAS contamination are wastewater treatment plants (WWTPs). This is because the conventional treatment techniques and processes of most WWTPs for municipal and industrial wastewater are able to degrade PFAS precursors, but not PFAS products like PFOA and PFOS. Therefore, net PFAS concentrations can be higher in the effluent than in the influent of a WWTP. A common class of precursors are fluorotelomer alcohols: these compounds contain both a perfluorinated and an aliphatic stretch of the carbon chain with an alcohol functionality at the end. It is the aliphatic part that can be naturally or chemically degraded in the atmosphere or in WWTPs by UV-light, radicals or microbiota, while the hydroxyl group will be oxidized to an acid functionality, resulting in a fully perfluorinated acid as end product.[15,16]

PFAS pollution is a global phenomenon, since industrial sites that use or consume PFASs are spread all over the world.[17] On top of that, PFASs can be transported over long distances by either atmospheric transport of volatile precursors, or by distribution of water-soluble PFASs via water streams and oceans. Traces of PFAS pollution have been found in both the Arctic and Antarctic, where no industrial emission sources are present.[15,18,19] Nevertheless, PFAS concentrations are often the highest close to industrial production and/or consumption sites. PFOA and PFOS were only produced on a large scale at three production sites in the world: two in the US and one in Belgium (Port of Antwerp). It is no coincidence that some of the highest concentrations of PFASs ever reported (in both water streams and fauna) are found in Zwijndrecht and its surroundings.[20,21]

1.5. Toxicity

Global spreading of anthropogenic chemicals would not necessarily be troublesome if these compounds were not harmful for humans, fauna, flora and/or ecosystems. Persistent organic pollutants (POPs) are contaminants that i) are persistent, ii) accumulate in individual organisms and/or in ecosystems and iii) are toxic. Even though very high concentrations are found in animals close to pollution sources, PFASs do not tend to accumulate in organisms, neither do PFAS levels rise significantly with increasing trophic level.[22,23] For humans, however, long-chain PFASs like PFOA and PFOS have very long half-life values of 3 to 5 years. There are serious indications that chronic exposure to even low levels of PFAS poses a harmful threat for human health, with diseases like thyroid and kidney cancer, hormone disruptions and impaired fetal growth during pregnancies directly linked to PFOA and PFOS exposure.[24,25] This exposure is of course drastically different for a factory worker in a PFAS production plant compared to the average person. Nevertheless,

up to 95% of the population in the Western world has traces of PFASs in their blood, with food products being the most important source of exposure.[26,27] Since most PFASs are water-soluble, every type of food that has a significant uptake of (ground)water can carry traces PFAS compounds; e.g. grains, fruits, vegetables, potatoes etc.[28,29]

1.6. Legislation and regulation

Because PFASs match the three criteria for being classified as a POP (for human exposure), they are recognized by the EU (and other countries) as compounds of very high concern.[8,30,31] PFOA, PFOS and their direct derivatives are listed on Annex XVII of REACH – the European authority for regulation of chemicals, meaning that the use of these compounds is restricted. More specifically, the marketing and use of these compounds are no longer allowed, with the exception of applications for which no viable alternatives are present.[32] Since PFASs are a rather unique class of chemicals, the number of applications without an equally working alternative is still significant. Some of these applications (in lithography, semiconductor industry, aerospace, etc.) are among the industrially most relevant PFOA and PFOS applications. Their usage and emissions are therefore still ongoing (albeit on a lower scale), even though they are legally restricted.

The increased knowledge on and awareness of PFAS spreading and the potential health risks thereof have evoked new legislation and regulations, both in the EU and the US. In 2013, the EU issued a directive on priority substances in the field of water policy, including restrictions on PFOA and PFOS in water streams.[33] This European directive has been translated into Flemish legislation (VLAREM II), with newly imposed environmental quality standards (EQSs) for PFOS and its derivatives (see **Table 1.1**).[34] No EQSs are in place yet for PFOA and its derivatives, but regulation and monitoring on PFASs are in full development, in Flanders but also in many other regions and countries, so more restrictions on a variety of PFASs are expected in the near future. The imposed EQSs for PFOS and its derivatives are in place since 2018, yet they will only be strictly monitored from 2027 onwards. On top of the restrictions for PFOS concentrations in water bodies, both PFOA and PFOS emissions for some specific industrial sectors are strictly regulated by VLAREM II. PFOA and PFOS emissions higher than 100 ng/L have to reported to the regional authorities and the upper limit for PFOA, PFOS and other PFAS concentrations in effluents from the textile industry is 50 µg/L, 10 µg/L and 200 µg/L, respectively.

Table 1.1: Environmental quality standards (EQS) imposed by Flemish legislation in VLAREM II. YA = yearly average. MAC = maximum allowed concentration. EQS for biota are expressed on wet weight.[34]

Compound	YA-EQS land surface waters	YA-EQS other waters	MAC-EQS land surface waters	MAC-EQS other waters	EQS Biota (µg/kg)
PFOS and derivatives	0.65 ng/L	0.13 ng/L	36 µg/L	7.2 µg/L	9.1 µg/kg

1.7. Prospectives and PFAS alternatives

The restrictions on PFOA and PFOS have pushed industrial players to use other fluorinated surfactants as drop-in replacements. Besides, a part of the PFOA and PFOS production that has been largely phased out in the Western world has moved to Asia. The alternatives include shorter aliphatic PFASs, fluorotelomers, perfluoro(poly)ethers and non-functionalized aliphatic PFASs.[35–37] Shorter aliphatic PFASs (C_4 and C_6) are regarded as less harmful because they have shorter half-life times in the human body, even though their long term health effects are not yet fully revealed.[38–40] As noted before, fluorotelomers contain a stretch of non-fluorinated carbon chain. Natural degradation of these compounds can result in a net increase of PFAS emissions. A popular choice of fluorotelomers are compounds with a non-fluorinated backbone and short perfluorinated side chains. These type of compounds are already commercially applied in consumer products like Scotchgard™. Finally, also perfluoro(poly)ethers are a popular alternative for the industry. This group of PFASs is not strictly limited to ethers but also contains ketones and epoxides. The most known example is GenX™, the ammonium salt of hexafluoropropylene oxide dimer acid (HFPO-DA, **Figure 1.2**). The name GenX is sometimes used ambiguously for a group of similar perfluoroethers. GenX has already provoked controversy in the US due to pollutions of local water supplies and its potential health risks. ADONA™ (**Figure 1.2**) is another commercially branded perfluoroether alternative. The industrial shift from C_8 PFASs to shorter chain PFASs and other variants has already been witnessed in European monitoring studies.[41]

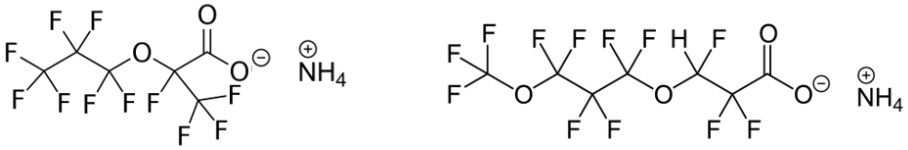


Figure 1.2: Chemical structure of GenX™ (left) and ADONA™ (right), two widely used perfluoro(poly)ether alternatives.

Most of these fluorinated alternatives are not (yet) restricted, meaning that levels of persistent and bioaccumulative fluorinated chemicals continue to build up in natural waters. In addition, historical emissions of PFOA and PFOS still cause locally elevated concentrations.[15] In this light, the recent introduction of environmental quality standards imposes the urgent need for a clean-up strategy and removal technologies. Adsorption is arguably the best technique to treat large volumes of water with low concentrations, while keeping energy costs modest. This makes the selection of an adsorbent with adequate capacity and high selectivity for PFASs of utmost importance.

1.8. Outline of PhD thesis

This dissertations deals with the selective adsorption of organic acids in general and of PFASs more specifically. It consists of seven chapters: two introductory chapters, four experimental chapters and a general conclusion. After a general introduction on PFASs in this chapter, **Chapter 2** delves into in the diverse topic of liquid separations via adsorption. In **Chapter 3**, a first example is given of how selectivity for the adsorption of an organic acid can be obtained, and which factors play an important role in this process. This chapter deals with citric acid; many of the experimental approaches and insights gained during this research have contributed to the work in the other chapters. **Chapter 4** explores the potential of siliceous microporous adsorbents for PFAS molecules, especially high- and all-silica zeolites. **Chapter 5** investigates the adsorption capacities of all-silica zeolite Beta, the best performing adsorbent for PFOA and PFOS, including an extensive study of the adsorption mechanism at the molecular level. In **Chapter 6**, the possibilities of shaping and structuring the zeolitic adsorbent into microspheres are explored. This dissertation concludes with **Chapter 7**, in which a general conclusion and future perspectives are given.

1.9. References

[1] Z. Du, S. Deng, Y. Bei, Q. Huang, B. Wang, J. Huang, G. Yu, *Journal of Hazardous Materials* **2014**, *274*, 443–454.

[2] S. Posner, in *Polyfluorinated Chemicals and Transformation Products* (Eds.: T.P. Knepper, F.T. Lange), Springer, Berlin, Heidelberg, **2012**, pp. 25–39.

[3] A. B. Lindstrom, M. J. Strynar, E. L. Libelo, *Environmental Science & Technology* **2011**, *45*, 7954–7961.

[4] D. M. Lemal, *J. Org. Chem.* **2004**, *69*, 1–11.

[5] G. Leroy, M. Sana, C. Wilante, R. M. Nemba, *Journal of Molecular Structure* **1989**, *198*, 159–173.

[6] S. J. Blanksby, G. B. Ellison*, Bond Dissociation Energies of Organic Molecules, **2002**.

[7] D. O'Hagan, *Chem. Soc. Rev.* **2008**, *37*, 308–319.

[8] G. B. Post, P. D. Cohn, K. R. Cooper, *Environmental Research* **2012**, *116*, 93–117.

[9] E. Dhanumalayan, G. M. Joshi, *Advanced Composites and Hybrid Materials* **2018**, *1*, 247–268.

[10] C. M. Teaf, M. M. Garber, D. J. Covert, B. J. Tuovila, *Soil and Sediment Contamination: An International Journal* **2019**, *28*, 258–273.

[11] G. Lewandowski, E. Meissner, E. Milchert, *Journal of Hazardous Materials* **2006**, *136*, 385–391.

[12] L. Conte, G. Gambaretto, *Journal of Fluorine Chemistry* **2004**, *125*, 139–144.

[13] S. Rayne, K. Forest, Journal of Environmental Science and Health, Part A **2009**, 44, 1145–1199.

[14] K. Prevedouros, I. T. Cousins, R. C. Buck, S. H. Korzeniowski, *Environ. Sci. Technol.* **2006**, *40*, 32–44.

[15] L. Ahrens, *J. Environ. Monit.* **2011**, *13*, 20–31.

[16] D. A. Ellis, J. W. Martin, A. O. De Silva, S. A. Mabury, M. D. Hurley, M. P. Sulbaek Andersen, T. J. Wallington, *Environ. Sci. Technol.* **2004**, *38*, 3316–3321.

[17] M. F. Rahman, S. Peldszus, W. B. Anderson, *Water Research* **2014**, *50*, 318–340.

[18] S. Castiglioni, S. Valsecchi, S. Polesello, M. Rusconi, M. Melis, M. Palmiotto, A. Manenti, E. Davoli, E. Zuccato, *Journal of Hazardous Materials* **2015**, *282*, 51–60.

[19] S. Fujii, S. Tanaka, N. P. Hong Lien, Y. Qiu, C. Polprasert, *Journal of Water Supply: Research and Technology—AQUA* **2007**, *56*, 313.

[20] W. D'Hollander, L. D. Bruyn, A. Hagenaars, P. de Voogt, L. Bervoets, *Environ Sci Pollut Res* **2014**, *21*, 11856–11866.

[21] K. I. V. De Vijver, P. T. Hoff, W. Van Dongen, E. L. Esmans, R. Blust, W. M. De Coen, *Environ. Toxicol. Chem.* **2003**, *22*, 2037–2041.

[22] S. Taniyasu, K. Kannan, Y. Horii, N. Hanari, N. Yamashita, *Environ. Sci. Technol.* **2003**, *37*, 2634–2639.

[23] E. Sinclair, D. T. Mayack, K. Roblee, N. Yamashita, K. Kannan, *Arch Environ Contam Toxicol* **2006**, *50*, 398–410.

[24] P. Grandjean, R. Clapp, *New Solut* **2015**, *25*, 147–163.

[25] L. B. Rokoff, S. L. Rifas-Shiman, B. A. Coull, A. Cardenas, A. M. Calafat, X. Ye, A. Gryparis, J. Schwartz, S. K. Sagiv, D. R. Gold, E. Oken, A. F. Fleisch, *Environmental Health* **2018**, *17*, 19.

[26] C. Cornelis, W. D'Hollander, L. Roosens, A. Covaci, R. Smolders, R. Van Den Heuvel, E. Govarts, K. Van Campenhout, H. Reynders, L. Bervoets, *Chemosphere* **2012**, *86*, 308–314.

[27] K. Kannan, S. Corsolini, J. Falandysz, G. Fillmann, K. S. Kumar, B. G. Loganathan, M. A. Mohd, J. Olivero, N. V. Wouwe, J. H. Yang, K. M. Aldous, *Environ. Sci. Technol.* **2004**, *38*, 4489–4495.

[28] W. D'Hollander, D. Herzke, S. Huber, J. Hajslova, J. Pulkrabova, G. Brambilla, S. P. De Filippis, L. Bervoets, P. de Voogt, *Chemosphere* **2015**, *129*, 179–185.

[29] V. Hlouskova, P. Hradkova, J. Poustka, G. Brambilla, S. P. De Filipps, W. D'Hollander, L. Bervoets, D. Herzke, S. Huber, P. de Voogt, J. Pulkrabova, *Food Addit. Contam. Part A-Chem.* **2013**, *30*, 1918–1932.

[30] B. O. Clarke, S. R. Smith, *Environment International* **2011**, *37*, 226–247.

[31] M. Sun, E. Arevalo, M. Strynar, A. Lindstrom, M. Richardson, B. Kearns, A. Pickett, C. Smith, D. R. U. Knappe, *Environmental Science & Technology Letters* **2016**, *3*, 415–419.

[32] Restrictions on the Marketing and Use of Certain Dangerous Substances and Preparations (Perfluorooctane Sulfonates), **2006**.

[33] Directive 2013/39/EU as Regards Priority Substances in the Field of Water Policy, **2013.**

[34] N. Bal, G. Van Gestel, F. Collet, T. Pancras, H. Slenders, M. Van Houten, J. Rabaey, R. Van Muylder, **2018**.

[35] Z. Wang, I. T. Cousins, M. Scheringer, K. Hungerbühler, *Environment International* **2013**, *60*, 242–248.

[36] P. B. Poulsen, A. A. Jensen, E. Wallström, E. Aps, *Environmental Project* **2005**, *1013*, 2005.

[37] R. Holt, **2011**.

[38] M. I. Gomis, R. Vestergren, D. Borg, I. T. Cousins, *Environment International* **2018**, *113*, 1–9.

[39] N. Sheng, R. Cui, J. Wang, Y. Guo, J. Wang, J. Dai, *Arch Toxicol* **2018**, *92*, 359–369.

[40] M. Ateia, A. Maroli, N. Tharayil, T. Karanfil, *Chemosphere* **2019**, *220*, 866–882.

[41] R. Loos, B. M. Gawlik, G. Locoro, E. Rimaviciute, S. Contini, G. Bidoglio, *Environmental Pollution* **2009**, *157*, 561–568.

CHAPTER 2

ADSORPTION, LIQUID SEPARATION

Matthias Van den Bergh[a], Simon Smolders[a], Dirk De Vos[a]

Kirk-Othmer Encyclopedia of Chemical Technology, 2020, in press

[a] M. Van den Bergh, S. Smolders, Prof. D. De Vos
Centre for Membrane Separations, Adsorption, Catalysis and Spectroscopy for Sustainable Solutions (cMACS)
KU Leuven
Celestijnenlaan 200F, 3001 Leuven, Belgium

Abstract

Adsorption has been used since history for the purification and separation of both gaseous and liquid streams. Nearly every modern day industrial chemical manufacturing process requires some form of separation in general, and adsorption in specific. In this chapter, the basic fundamentals of adsorption, the different adsorbent types and process modes and a selection of the most relevant industrial adsorptive separations will be discussed.

Contributions

M.V.d.B. and S.S. wrote the manuscript. D.D.V. supervised the work.

2. Adsorption, Liquid Separation

2.1. Introduction

In industry, recovery and purification of the desired end product is a crucial step in the production of many chemicals, arguably as important as the synthesis itself. The cost of separation and purification often contributes a large part of the total production cost. Selection of the appropriate separation technique and optimization of the purification process are hence of critical importance. Adsorption has been used since history for the purification and separation of both gaseous and liquid streams. Sand filtration is known since ancient times and is one of the first examples of human water treatment. Even though the exact nature and mechanism of adsorption processes have long not been well understood, adsorption has been used for a huge variety of applications through all of human history. The separation of dyes, contaminant removal from water, decolorization of sugars and recovery of fermented products are only a few examples. Nearly every modern day industrial chemical manufacturing process requires some form of separation in general, and adsorption in specific. For instance, every catalytic reaction on a solid catalyst is characterized by an adsorption step, potentially rate-determining. In this chapter, the basic fundamentals of adsorption, the different adsorbent types and process modes and a selection of the most relevant industrial adsorptive separations will be discussed.

2.2. Fundamentals

Adsorption (in the context of liquids separation) is defined as “an increase in the concentration of a dissolved substance at the interface of a solid and a liquid phase due to the operation of surface forces” [1]. The solid surface is called the adsorbent and the adsorbed species from the liquid phase are called the adsorbates. Adsorption is thus based on the attractive forces between molecules, which are generally higher near a solid surface and which cause a region of low potential energy at that surface. As a result, there is a local accumulation of molecules. These molecules are less mobile and adsorption is thus often accompanied by loss of entropy, but this is largely compensated by the reduced enthalpy. The accumulation is therefore defined by the entropy-enthalpy balance.

Depending on the nature and strength of the surface forces, adsorption can be classified as physisorption or chemisorption. Physical adsorption is relatively weak and mainly involves electrostatic, hydrogen bonding and van der Waals interactions

in which exchange of electrons between species is negligible. Chemisorption however involves electron transfer which causes binding energies in the range of these in chemical reactions. Chemisorption thus results in more strongly adsorbed species and more specific interactions than in physisorption, but adsorption is limited to monolayer coverage. In addition, chemisorption is often activated, slow and irreversible. As a result, separation processes mainly rely on physisorption since reversible adsorption is required. Only in the case of highly selective removal of trace impurities, chemisorption is sometimes used.

The ability of an adsorbent to retain one species (or class) from a mixture is called selectivity, and it is the key property of a separation process since it directly influences its effectiveness. Selectivity in a binary mixture is defined as the ratio of the compound A and B on the adsorbent divided by the ratio in the liquid (eq. 1).

$$Selectivity = \frac{(wt\%\ A/wt\%B)_{adsorbent}}{(wt\%\ A/wt\%B)_{liquid}} \qquad \text{eq. 1}$$

Selectivity depends on differences in chemical equilibrium or kinetics. Although adsorption is generally a fast process, many separations are performed by materials with pores of molecular dimensions (i.e. micropores, *vide infra*). In that case, diffusion is sterically restricted and can differ several orders of magnitude over small size differences, which causes kinetic selectivity. In the extreme limit, some species are even completely excluded from the pores, causing a molecular sieve separation. Selectivity can thus be controlled by tailoring the pore size. Many separation/purification processes however rely on thermodynamic differences in adsorption, which cause relative equilibrium concentrations at the surface that are significantly different from the bulk. In physisorption, this equilibrium can be controlled by adjusting the balance between the two major attractive forces at the surface: electrostatic and van der Waals forces. Polar surfaces, such as cation-rich zeolites, silica or alumina, feature mainly electrostatic interactions and preferentially adsorb polar compounds such as water and are therefore called hydrophilic surfaces. Adsorption on apolar materials (also referred to as hydrophobic materials) such as activated carbon is dominated by van der Waals forces. Since these involve induced dipole interactions, the attracting force on apolar compounds depends on the polarizability of these adsorbates, which increases roughly proportional with their molecular weight.

Before an adsorption system is applied, it is essential to obtain extensive knowledge on its separation properties. One of the key elements to achieve this is by measuring adsorption isotherms. These isotherms will provide insight in the maximum

adsorption capacity, the interaction mechanism and the thermodynamic adsorption parameters such as changes in the standard Gibbs free energy, standard enthalpy and standard entropy. This information can be extracted by correctly classifying the isotherms and fitting a meaningful model (see **Figure 2.1** for a graphical overview of the different models). The simplest model, called Henry's law, can be applied to adsorbents with a uniform surface and isolated adsorption sites, if the adsorbate concentration is sufficiently low. In this case, the adsorbed quantity is linearly dependent on the fluid phase concentration (eq. 2), with q_e (mol/kg) the adsorbed quantity, C_e (mol/m³) the equilibrium concentration of the adsorbate in the liquid phase and K_H (m³/kg) the Henry constant.

$$q_e = K_H C_e \qquad \text{eq. 2}$$

At higher concentrations, this linear trend is no longer valid because a significant fraction of the adsorption sites is already covered. As a result, Henry's law has to be adapted to cope with the changing adsorption site availability. Based on the equilibrium between adsorbing and desorbing molecules, the Langmuir equation (eq. 3) can be deduced. K_L (m³/mol) is herein the Langmuir constant and q_m (mol/kg) is the maximal adsorption capacity.

$$q_e = q_m \frac{K_L C_e}{1+K_L C_e} \qquad \text{eq. 3}$$

At low concentrations ($K_L C_e << 1$), the Langmuir equation can be simplified to Henry's law, with $K_H = q_m K_L$. The above mentioned equation describes a single adsorbate system but can easily be extended to multicomponent systems (eq. 4). The subscripts i and j represent the indices of the adsorbate in the mixture.

$$q_{e_i} = q_m \frac{K_{L_i} C_{e_i}}{1+\sum_j K_{L_j} C_{e_j}} \qquad \text{eq. 4}$$

Langmuir isotherms are extensively used but their simplicity is based on several assumptions: i) adsorption only takes place in the monolayer regime, ii) each adsorption site can only hold one adsorbate molecule, iii) neighboring adsorption sites are sufficiently spaced to avoid any mutual influence, iv) all sites are equivalent and v) the surface is uniform. In reality, adsorbents however display a heterogeneous surface with significant differences in adsorption energy. This can be described by a simple empirical equation (eq. 5), called the Freundlich equation, with K_F ((m³/kg)$^{1/n}$) the Freundlich constant and $1/n_F$ the heterogeneity factor. n_F should herein be larger than one. The Freundlich model does not reduce to Henry's law at low concentration

and is not thermodynamically consistent in that range, but it provides a good approximation over a wide range of conditions

$$q_e = K_F C_e^{1/n_F} \qquad \text{eq. 5}$$

After identifying the key properties of the adsorbate-adsorbent interactions, it is essential to determine the required purity and recovery of the separation process, since these are essential to design a separation unit. The purity of a stream leaving the unit is defined as the wt% of the desired compound in that stream. The recovery is the amount of the desired compound in that stream divided by the amount of that compound in the feed.

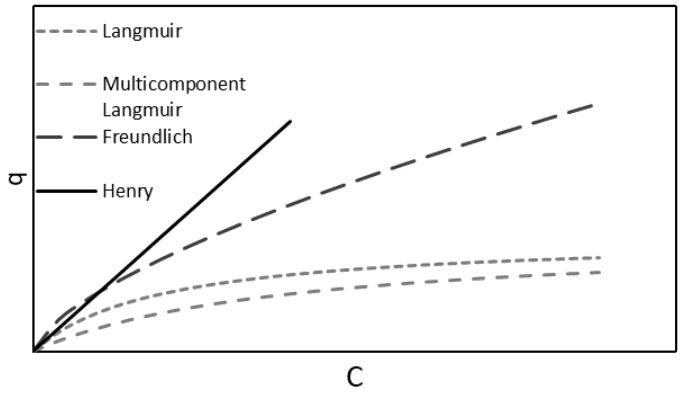


Figure 2.1: Graphical representation of the different isotherm models.

2.3. Process modes

Industrial scale adsorption processes can be performed in different process modes. All operation modes have their respective advantages and disadvantages. Which mode is most recommended for a certain industrial separation depends on the exact conditions (compounds to be separated, volumes, flows, etc.) and requirements (product purity, downstream processing, etc.) of the separations and, last but not least, their economics. In this section, the most common and important operation modes for liquid phase adsorptive separations are discussed.

2.3.1. BATCH MODE

Batch operation mode is the most simple process form, from a concept point of view. In a batch adsorption process, the adsorbent is mixed with a liquid phase in a closed vessel, without inflow or outflow of either liquids or solids. The adsorption process

is stopped when equilibrium is reached, the solid adsorbent is saturated or when the bulk concentrations of the compounds that have to be separated have reached their target values. After settling or filtration of the solid adsorbent, the container is emptied and the adsorbent is regenerated in order to be used again. The sequence of adsorption and regeneration defines one cycle of the batch adsorption process. In most industrial batch separations, these cycles will be continuously repeated. Cycle time is an import process parameter with a significant influence on the cost and efficiency of the separation. It depends on several factors, with the rates of adsorption, the saturation capacity of the adsorbent, the desired uptake and ease of regeneration among the most important ones.

In a batch adsorption, the uptake of the adsorbate is determined by its adsorptive equilibrium. Changing the operating temperature, feed composition or adsorbent type will shift the equilibrium, but it is not possible, like for continuous processes, to remove more of the adsorbate than is dictated by the adsorption isotherm. Hence, full removal of the adsorbate in a single batch is normally not achieved. In addition, adsorption rates will decrease when the system is approaching its equilibrium. Therefore, process efficiency of the batch mode will be lower than for a continuous operating mode, meaning that for a certain level of desired uptake, more adsorbent material and more process time are required. Additionally, also more desorbent will have to be used for regenerating all of the adsorbent material. Multiple batches can be used in series, with each batch being an additional equilibrium stage in the adsorption process. This way, the desired separation can be obtained using less adsorbent material and having a lower total liquid volume than when a similar separation is performed in a single batch.

2.3.2. FIXED BED

In a fixed bed adsorption process, there is constant flow of liquid stream over a physically stationary adsorbent bed. With a fixed bed, it is possible to remove almost all of the adsorbate at the end of the bed, so that the stream leaving the bed (i.e. the effluent) is practically adsorbate free. Its concept is simple and the equipment is relatively inexpensive. Another advantage is the minimal attrition of the adsorbent and hence its prolonged lifetime, compared to batch and moving bed processes where there is more liquid-solid friction. A big disadvantage, however, is the creation of a mass transfer zone (MTZ). Adsorbent particles before the MTZ are completely saturated, while the adsorbent particles behind this zone are not yet brought into contact with the adsorbate. This means that at any given time, only the adsorbent particles in the MTZ are actually active in the adsorption process. This also means that the liquid composition at a given level in the bed undergoes a change with time.

So despite the apparent simplicity of the design and concept of a fixed bed process, the factor time has to be included in the design equations, resulting in more complex, partial differential equations. Adsorption in a fixed bed will always be an unsteady state, rate controlled process, reducing the overall efficiency of the adsorption process. Similar to batch adsorption, process efficiency of a fixed bed adsorption can be increased by arranging multiple fixed bed in series or parallel. The number and arrangement of beds will determine important process variables like total flow rate, total pressure drop, energy demands etc. and the choice largely depends on economics.

Only in the MTZ, the concentration of the adsorbate in the effluent and the loading of the adsorbent are gradually changing in time; meanwhile the MTZ is migrating with the flow direction through the fixed bed (**Figure 2.2**). When the MTZ reaches the end of the packed bed, the adsorbate concentration in the effluent will surge. This is called breakthrough and should be avoided at all times. However, migration of the MTZ throughout the adsorbent bed is difficult to monitor online. It is practically more convenient to measure solute concentrations at the end of the bed, but this is unworkable in industry where one has to stop the adsorption cycle before breakthrough occurs. In industry, breakthrough is not necessarily defined as the moment where the adsorbate concentration in the effluent starts to increase, but rather as the moment where this concentration reaches a certain threshold. This can e.g. be the limit of detection for a certain adsorbate, an environmental standard for pollutants or the maximum concentration for a downstream catalytic reactor to work at optimum.

Another disadvantage of a fixed bed is the need for taking it offline for regeneration. Therefore, a second bed is required for treating a continuous liquid stream. Most commercial fixed bed processes use several beds in parallel. The mode of desorption (e.g. temperature swing or rinsing with a desorbent) has a large influence on the total cycle time and its choice is largely determined by economics (see paragraph 2.3.6). The regeneration time for the second bed must not be longer than the time to reach breakthrough in the first bed, unless additional beds are operated, either in adsorption or desorption mode. In practice more than two beds are often used, which introduces the need for complex pipe and valve arrangements together with a control system.

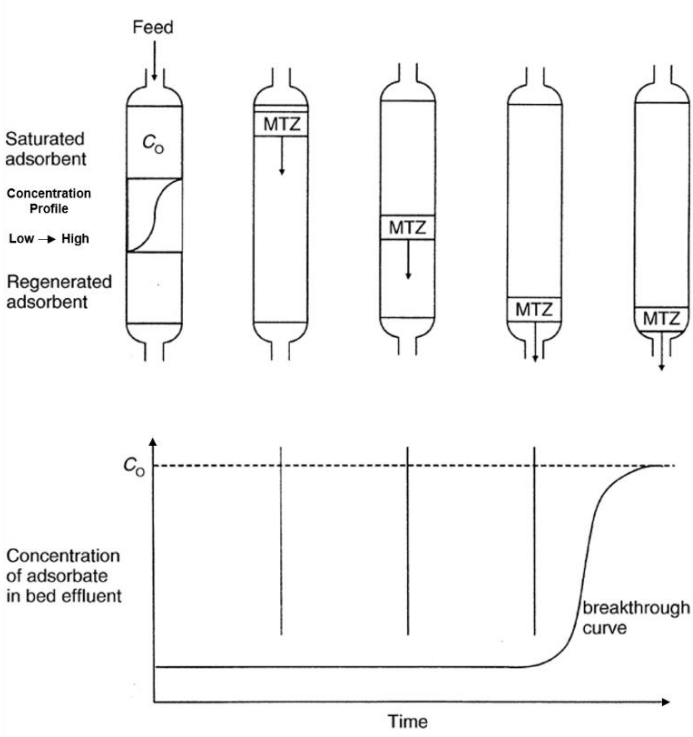


Figure 2.2: Sketch showing the migration of the mass transfer zone (MTZ) through a packed bed adsorption column (top) and the corresponding concentration profile (breakthrough curve, bottom). C_0 is the adsorbate concentration in the feed. Source: Crittenden and Thomas [2].

Compared to adsorption processes with good mixing between the liquid phase and the solid sorbent (e.g. batch mode or fluidized beds), heat transfer in a packed, fixed bed can be poor. Therefore, it can be difficult and time-consuming to increase the temperature for a temperature swing desorption. Since adsorption is an exothermic process, heat will be released. Poor heat transfer might lead to locally elevated temperatures and a less beneficial adsorption equilibrium. Despite these disadvantages, fixed bed separations are of significant industrial relevance. Compared to e.g. moving beds (*vide infra*), the equipment is less complex and less expensive. Considering both technical and economic aspects, fixed bed separations can therefore still be the optimal choice for industrial separations. Some design and operation aspects of fixed beds are discussed in more detail below.

Fixed bed set-ups are in general vertically oriented. A horizontal position of the packed beds is possible but this increases the risk of flow maldistribution. Good flow distribution through the bed is of critical importance to exploit the full capacity of

the bed and to reduce the pressure drop over the column, so preferential flow pathways have to be avoided as much as possible. Vertical flow can be down- or upward. Upward flow of the liquid has the potential to create lifting or fluidization of the bed. A light degree of bed lifting is not harmful and can even be desirable to reduce pressure drop, but one has to take care that there is not too much lifting. This would lead to extensive bed expansion and mixing of the bed. The fixed bed operation would then resemble a mixed batch process, with lower efficiency. Downward flow, on the other hand, causes the potential threat of crushing the adsorbent particles under the weight of the overlying bed. When the liquid stream contains solid particles in suspension (e.g. sludge in a wastewater treatment plant), downward flow is the preferred choice and the bed will act as a particle trap. In that case, the pressure drop will increase after time and occasional back flushing is needed. In case of downward flow, the driving force can be gravity or mechanical pressure. Gravity driven flow is the most simple process mode and resembles a sand filter. Of course, modern day gravity driven processes have additional units to remove and regenerate the adsorbent.

Fixed beds have to be regenerated before breakthrough of the adsorbate occurs. This requires drainage or replacement of the liquid feed from the bed, and after regeneration the packed bed has to be refilled with the feed stream. If desorption is done with a hot gas (i.e. purging), the bed has to be drained completely. Liquid flow during the drainage process is always downward. Drainage is mostly driven by gravitation or sometimes by a light pressure of 1-2 bar. Due to capillary forces, it can be very difficult to drain all of the liquid. This can lead to high energy consumption when purging the bed with a hot gas, e.g. steam. After purging with a gas, refilling of the bed is best done in an upward direction to rinse out any remaining gas bubbles. Trapped gas bubbles will lead to maldistribution of the liquid flow and can cause excessive bed lifting in case of upward flow during the adsorption phase.

When regeneration is done by rinsing the bed with another solvent, there is no drainage but fluid displacement. Depending on the exact characteristics of the fluids and the packed bed (particle size distribution, fluid densities and viscosities, relative surface tensions, etc.) there is a potential threat of fingering. This means that the desorbing solvent forms flow columns through the bed instead of replacing all of the liquid feed from the bed completely. This is mostly the case when the desorbing liquid is more dense or less viscous. In that case, any bulge of desorbent liquid that is created in the feed liquid will tend to grow, since liquid flow will follow the path of least resistance.

2.3.3. PREPARATIVE CHROMATOGRAPHY

Chromatography is an adsorptive separation technique that is widely used for analytical chemistry. It is also used to separate different components, dissolved in the same liquid phase, from each other for later use. In this way, it is a form of product purification and called preparative chromatography. Preparative chromatography has many applications in several sectors but it is especially common in the pharmaceuticals industry for the separation of complex and high-value chemicals that are difficult to separate with more convenient separation techniques. The adsorbent bed in preparative chromatography is very similar to a fixed bed: the solid adsorbent is packed in a column with a continuous liquid feed (called the mobile phase) flowing through the column. In a fixed bed adsorption, the adsorbate is withheld on the adsorption column and breakthrough of the adsorbate has to be avoided so that the effluent stream is adsorbate-free. This is different in adsorptive chromatography, where several compounds are fed into the adsorption column simultaneously and migrate with different speeds through the bed. In this way, all compounds elute from the column at a different time and can be collected separately for further use (**Figure 2.3**).

In preparative chromatography, adsorption and desorption processes occur simultaneously. The rates of adsorption and desorption determine the retention time of a compound in the adsorption bed. Since the compounds to be separated are meant to elute from the column, the adsorption bed will -under normal operation - never be fully saturated and will not have to be taken offline for regeneration, in contrast to the fixed bed mode (*vide supra*). This implies of course that the mobile phase is able to desorb all of the compounds that are fed into the adsorption column. Careful selection of an appropriate mobile phase is hence critical for a successful separation in preparative chromatography. If a mobile phase has no desorbing capabilities, compounds will not elute from the adsorption bed. If a mobile phase has very strong desorbing capabilities, the compounds might not be retained long enough on the adsorption bed to achieve complete separation of the different compounds. One way to handle this challenge is to change the composition of the mobile phase in time, with the desorbing effect of the mobile phase ever increasing. This is called gradient elution, while isocratic elution refers to an invariant mobile phase composition [3].

Several categories of preparative chromatography exists. The classification can be based on the interaction mechanism between the adsorbate molecules and the adsorbent column, e.g. normal phase for polar interactions, reversed phase for hydrophobic interactions, size exclusion when the adsorbent is a gel or a molecular

sieve, etc. Even complex chiral separations are possible, when the adsorbent has a chiral selector [4]. Considering the operation mode, batch chromatography, cyclic chromatography and continuous chromatography can be defined.

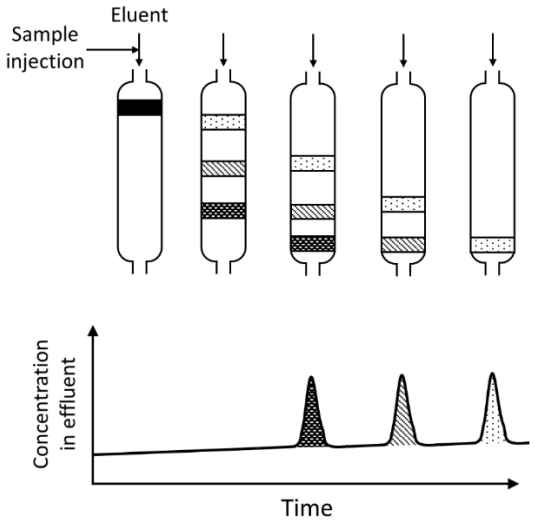


Figure 2.3: Principle of chromatography: a mixture of compounds from a sample is injected in the liquid mobile phase (eluent). Different retention times due to stronger or weaker interactions with the stationary phase will result in separation of the compounds after elution from the column.

In batch chromatography, a mixture containing the compounds to be separated is injected in the mobile phase flow at the inlet of the column. Separation of the compounds occurs due to differences in affinity between the adsorbent column and the compounds. The compound with the highest affinity will be the most strongly retained on the column and elute from the column the latest. This mode of chromatography is also practiced in HPLC (high performance liquid chromatography) for analytical purposes [5].

A disadvantage of batch chromatography is the large consumption of mobile phase and the corresponding cost. There is often a trade-off between shorter run times (i.e. time required for all compounds of an injected sample to migrate through the column) and the separation efficiency (i.e. resolution) and product purity. These disadvantages can partly be overcome by implying a strategy in which the mobile phase effluent is recycled over the adsorption column. In closed loop recycling chromatography (CLRC), the injected sample is passed several times through the column before it is collected in different fractions with a four-way valve at the end of the column. Steady-state recycling chromatography (SSRC) is another recycling

strategy rather similar to CLRC, but now fresh feed is injected in the recycling stream to avoid large concentration reductions. Even though continuous chromatography (*vide infra*) often delivers higher separation efficiencies, this does not always compensate the additional complexity and cost of these processes. Cyclic chromatography offers improved process efficiency with only a small increase in cost and complexity, compared to batch chromatography [6].

In batch chromatography, only the mobile phase flow is continuous and samples of the adsorbates mixture are only fed to the column intermittently. This means that it is practically not possible to separate a continuous product feed with batch chromatography. In continuous chromatography, the feed mixture is fed continuously to the column and the different adsorbates are withdrawn from the column in different product streams. This is similar to continuous moving bed and simulated moving bed operations, discussed in paragraph 2.3.4 and 2.3.5 [7,8].

2.3.4. CONTINUOUS MOVING BED

In a continuous, moving bed operation, there is not only a liquid flow, there is also a continuous net flow of solid adsorbent particles in and out of the bed. The main advantage of a moving bed process is that the adsorbent can be regenerated as soon as its role in the adsorption step has been completed. Because of the net movement of the solid particles, compared to a fixed bed, heat transfer in a moving bed is significantly better. An essential prerequisite however is that the adsorbent particles need to be rugged, in order to withstand the attrition that is inevitably higher than in a fixed bed. The equipment involving moving bed operations is also more complex and hence more expensive.

The efficiency of an adsorption process is significantly higher in a continuous mode of operation than in a cyclic batch or fixed bed mode. In a fixed bed, the adsorption is an unsteady state process and a large portion of the bed (i.e. all but the MTZ) does not perform any useful function at a given time. In continuous mode, the adsorption can be a steady state process (i.e. the liquid composition at a given level is invariant with time) where every part of the bed performs a useful function at all times. Therefore, the height equivalent of a theoretical plate (HETP, this is the length of the bed divided by the number of theoretical equilibrium plates) in a batch or fixed bed operation is roughly three times that in continuous mode, reflecting a much lower efficiency. For difficult separations, batch operations require up to 25 times more adsorbent inventory and twice the desorbent circulation rate. Obtaining uniform flow of both the solid and liquid stream in beds of large diameter can however be

very challenging and the performance will be drastically impaired by nonuniform flow of either phase.

Moving bed operations can be divided based on the relative flow direction of the liquid and solid stream. In a co-current process, both streams have the same flow direction, while in a countercurrent process, the liquid feed and adsorbent particles move in opposite directions. The latter is much more common in industry because it has some significant advantages. The biggest asset of a countercurrent operation is the maximization of the average driving force for mass transfer between the fluid and the adsorbent. Because liquid feed is flowing in the opposite direction of the adsorbent particles, fresh feed will first be contacted with near-saturated adsorbent. Because the adsorbate concentration in the feed is maximal at the inlet of the adsorption vessel, there will still be a net driving force for mass transfer of the adsorbate from liquid to the adsorbent, even though loading of the adsorbent is near maximal. As the liquid feed flows in opposite direction of the solid flow through the adsorption vessel, the adsorbate concentration decreases, but so does the adsorbent loading. Therefore, it is possible to maintain a net driving force for mass transfer through the whole of the adsorption column (see **Figure 2.4**). In a co-current process, mass transfer will be maximal at the beginning of the column, where the liquid feed has maximal adsorbate concentration and the adsorbent is completely unloaded. However, once equilibrium is reached, no further net mass transfer between the liquid and adsorbent is possible. Since it is possible to maintain a net mass transfer over much longer column lengths in a countercurrent process, the adsorption process is much more efficient than for a co-current operation. Once the spent adsorbent leaves the adsorption column, it is transferred to a desorbent vessel (see **Figure 2.5** for a schematic view of a continuous countercurrent adsorption process). The same principle applies for the desorption: with a countercurrent flow, the mass transfer of the adsorbate from the solid particles towards the liquid desorbent will be maximized. Consequently, almost all industrially relevant adsorptive separations with moving beds are run in countercurrent mode.

Different types of continuous moving bed operations exist. Conceptually, the most simple mode of countercurrent adsorption is when the solids adsorbent particles are falling downwards in an upward liquid stream and when both solid and liquid streams behave as plug flows. In plug flow, the flow velocity of a stream is constant across any cross-section of the column. This type of countercurrent operation can reach steady state but is more complex than it initially appears, especially considering equipment. The adsorbent particles must be returned to the inlet of the vessel and an additional unit is necessary for regeneration, either at the end of the

vessel or during the transportation (**Figure 2.5**). Furthermore, the adsorbent particles must withstand high attrition and mechanical erosion.

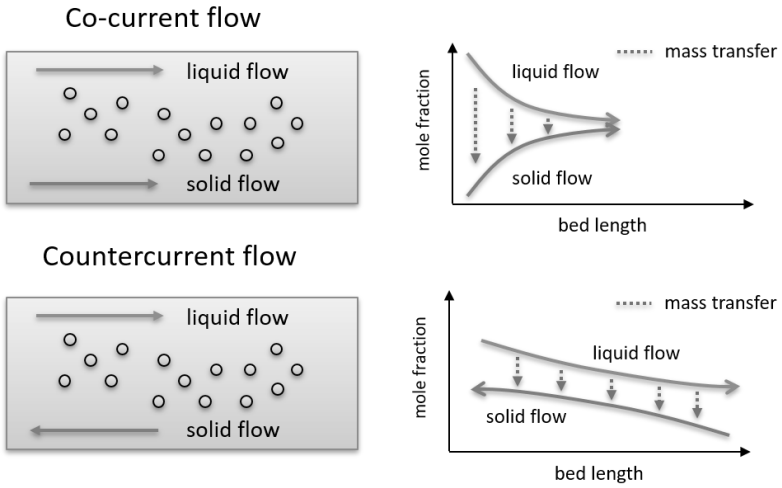


Figure 2.4: Schematic view of co-current vs. countercurrent flows with the corresponding concentration profiles of the adsorbate in the liquid and solid flow. In a countercurrent process, the net mass transfer will be maintained over a longer column length.

Not so different from the plug flow set-up is the fluidized bed, where the solid particles are more loosely packed and suspended by the liquid flow. The advantage of a fluidized bed is that the pressure drop over the bed is independent of the liquid flow rate. In addition, heat and mass transfer rates in a fluidized bed are higher. Nevertheless, a fluidized bed has several disadvantages. To start, all of the disadvantages of the plug flow set-up also apply for fluidized beds, where attrition of the adsorbent is even larger. There is also a potential risk of extensive mixing of the solid particles. This would diminish the advantages of a continuous countercurrent process and resemble a mixed batch process. Finally, obtaining uniform flow of both liquid and solids is difficult, which may drastically impair adsorption efficiency. In view of these difficulties, only a few fluidized beds are employed commercially for adsorptive separation.

Finally, pulsed flow operation is a singular example of a co-current moving bed operation. In this mode, the liquid flow enters at the bottom of the vessel and flows upward, taking with it a part of the adsorbent. The (regenerated) adsorbent is refilled at the bottom of the vessel. In this way, the MTZ is kept in the adsorbent bed and does not migrate with the liquid flow. In practice, removal and addition of the adsorbent are very often not done continuously but intermittently. The pulsed flow operation then resembles a series of fixed beds.

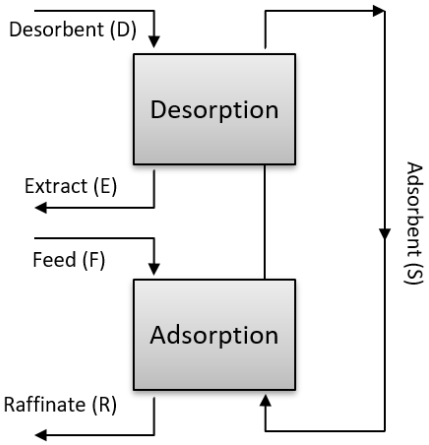


Figure 2.5: Schematic illustration of a continuous countercurrent adsorption process.

Operation of a moving bed process

The operation of a simple countercurrent flow adsorption system like the one on **Figure 2.5** can be represented by a McCabe-Thiele diagram. The McCabe–Thiele method is considered to be the most simple and perhaps most instructive method for the analysis of binary distillation, but it can also be applied for binary separations via adsorption. It uses the fact that the composition at each theoretical tray (or equilibrium stage) is completely determined by the mole fraction of one of the two components of the binary stream. **Figure 2.6** shows a linear McCabe-Thiele diagram that corresponds with the separation of a compound A from a binary feed in a countercurrent adsorption set-up such as the one presented in **Figure 2.5**. The McCabe-Thiele diagram shows a single straight equilibrium line for the strongly adsorbing compound A. The equilibrium line is ideal, assuming adsorption and desorption occur at the same temperature. The thin lines are the operating lines for the adsorption and desorption units and are defined by the mass balance of A over these units. With these operation lines, mole fractions of A on the adsorbent and in the different liquid streams (feed, desorbent, raffinate and extract) can be deduced.

In countercurrent moving bed operations, regeneration of the spent adsorbent can also occur in the same vessel as where the adsorption takes place. A theoretical example of such a set-up, representative for many industrial moving bed operations, is shown in **Figure 2.7**. Both set-up types are common for industrial separations and conceptually they are very similar. **Figure 2.7** shows a hypothetical moving bed for the separation of a binary feed (A+B), where A is the strongly adsorbing compound. The adsorbent circulates continuously and countercurrent-wise to the downward

liquid flow. The feed (F) is introduced in the middle of the bed, while the desorbing liquid D is fed to the column at the top. The raffinate stream (R) consists of the less strongly adsorbed component B mixed with the desorbent D and is withdrawn below the feed. Only a portion of the liquid flowing in the bed is withdrawn at this point; the remainder continues to the next section of the bed. The extract stream (E), consisting of the more strongly adsorbed component A mixed with the desorbent D, is withdrawn above the feed. Again, only a portion of the flowing liquid in the bed is withdrawn as extract; the remainder continues to flow into the next bed section. The positions of introduction and withdrawal of streams divide the bed into four zones, each of which performs a different function as described below.

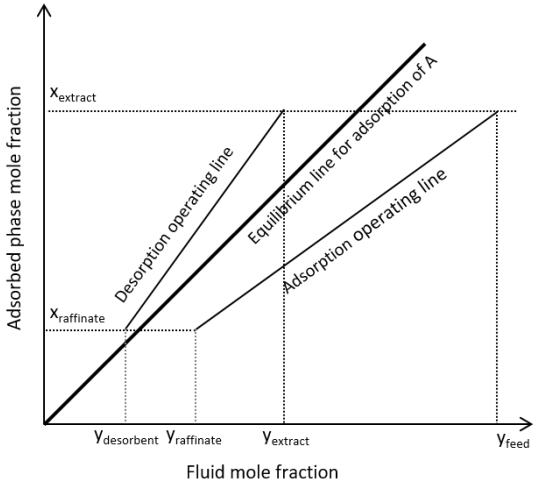


Figure 2.6: McCabe-Thiele diagram for an ideal continuous countercurrent process with different adsorption and desorption units (Figure 2.5). $x_{raffinate}$ and $x_{extract}$ refer to the adsorbed phase concentration in the solid stream at the positions in the bed where the extract and raffinate are withdrawn. No solid particles are withdrawn in these streams.

Zone 1: The main purpose of this zone is the adsorption of A from the liquid.

Zone 2: The main purpose of this zone is the desorption of B from the solid adsorbent particles.

Zone 3: The main purpose of this zone is the desorption of A from the solid adsorbent particles.

Zone 4: This zone acts as a buffer to prevent component B being transferred from zone 1 to zone 3, where it would contaminate the extract stream.

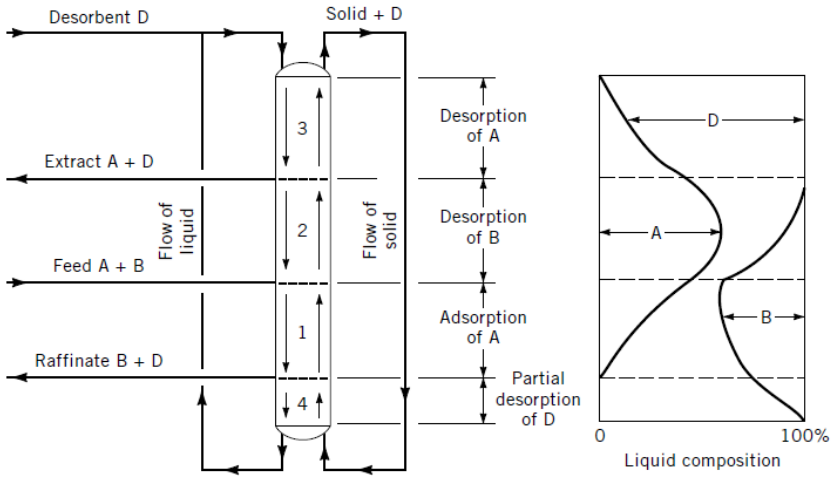


Figure 2.7: Schematic illustration of a moving bed process for the adsorptive separation of compounds A and B, with an overview of the four different zones in a moving bed and the corresponding concentration profiles of A and B in the liquid phase. Figure taken from Gembicki *et al.*(2002) [9].

The concentration profiles of components A and B in these four zones of the bed are also shown on **Figure 2.7**. The corresponding McCabe-Thiele diagram is now somewhat more complex and has several operating lines, associated with the different zones of the bed (see **Figure 2.8**). The adsorption equilibrium line for A lies above the one for B, which is essential for the selective separation of A from B in the product stream (i.e. the extract). In general, most of the separation of the component for the extract product occurs in zones 1 and 3, while the separation of the component for the raffinate stream occurs in zones 2 and 4. This can be seen from the operating lines on the McCabe-Thiele diagram; operating lines 1 and 3 for component A have the same relative position as operating lines 2 and 4 for component B. Note that for component A, no operating line for zone 4 can be seen. Similarly, the operating cycle for component B does not show zone 3. This is because the liquid flow concentration of the respective compound in these zones is zero (see again the concentration profiles on **Figure 2.7**). The horizontal operating lines without zone association on **Figure 2.8** correspond with the transition at the inlet and extract ports. At these ports, there will be sudden changes in the fluid phase composition without a concomitant change in adsorbed phase concentration.

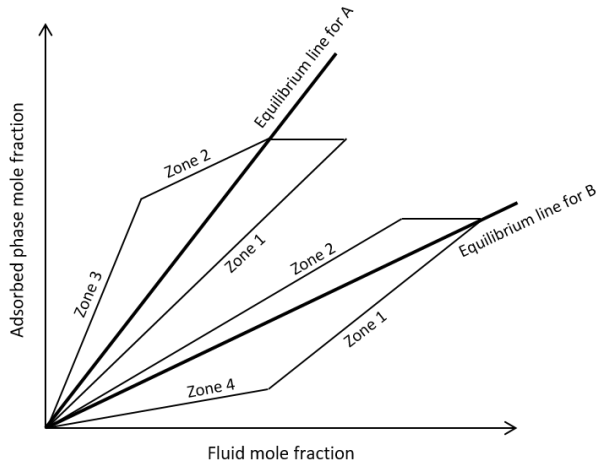


Figure 2.8: McCabe-Thiele diagram for an ideal continuous countercurrent process for the separation of a binary stream (A+B), with adsorption and desorption occurring in the same vessel (see set-up on Figure 2.7).

2.3.5. SIMULATED MOVING BED (SMB)

In a moving bed system as shown on **Figure 2.7**, solid adsorbent particles are continuously moving in a circuit past fixed points of feed introduction and raffinate and extract withdrawal. Many of the advantages of moving beds can be retained – while overcoming disadvantages like high attrition - by holding the adsorbent bed stationary and instead moving the points of liquid introduction and withdrawal. Such a shift of the feed and withdrawal points simulates a countercurrent movement of the adsorbent bed in the liquid stream and this operation mode is therefore called simulated moving bed (SMB). Of course, moving the liquid feed and withdrawal positions continuously is impractical, but approximately the same effect can be achieved by providing multiple liquid-access lines to the bed and by periodically switching each stream to the adjacent line. In this way, the four different zones of a countercurrent adsorption bed (*vide supra*) can move through the bed, always maintaining the same distance between the various streams. This mode of operation is nowadays common practice in the chemical industry and known as the Sorbex process [10]. Many industrial adsorptive separations are applications of a SMB process, an overview of some is given in **Table 2.1**.

In a Sorbex process (schematic diagram on **Figure 2.9**), a pump is provided to circulate the liquid stream downwards through the column and back from the bottom outlet to the top inlet. The flow rate and position of the liquid introduction and extraction point are controlled by a rotary valve (i.e. a fluid-directing device).

The rotary valve (RV) directs each of several streams to different lines connected to the adsorption bed. At the right hand side of the rotary valve, the four streams to and from the process are continuously fed and withdrawn. At the left hand side, a number of lines (e.g. 12 lines on **Figure 2.9**) are connected that terminate in distributors within the adsorbent bed. At any moment, only four of all available lines from the RV to the column are active. When the rotating element of the rotary vale is moved to its next position, each net flow is transferred to the adjacent line. The rotary valve is the most widely used method in industrial scale applications for accomplishing the stepwise movement of external streams, but the same function can be accomplished by using manifolds of on-off valves [11].

In a true moving bed (e.g. **Figure 2.7**), the liquid flow rate is different in each of the four zones, because of the addition or withdrawal of the various streams. In a SMB the liquid flow is controlled by the circulating pomp and not by the RV. On **Figure 2.9**, the circulating pump is positioned between the raffinate and desorbent ports and the pumping rate should hence be optimized for zone 4 (vide supra for description of the different zones). The relative position of the circulating pump to the different zones of the bed changes after each switch of the rotary valve. Therefore, the pump must be programmed to operate at four different flow rates, each one optimized for one specific zone. The control point of the pump is then altered each time an external stream is transferred from the bottom to the top of the column (e.g. from line 12 to line 1 on **Figure 2.9**).

When the feed rate is fixed (e.g. controlled by an upstream process), the primary control variable is the process cycle time, i.e. the time required for the rotary valve to complete one full rotation. The rotation speed of the rotary valve is analogous to the adsorbent circulation rate in a true moving bed. Another primary control variable is the liquid flow rate through the bed, controlled by the circulating pump. To make the simulation of a moving bed complete, the liquid flow rate relative to the solid adsorbent particles must be the same in both a SMB and a true moving bed operation. This means that the liquid flow rate in a SMB operation must be higher because the adsorption bed is physically stationary. When these two variabeles are set, all other net flow rates to and from the bed are fixed. Temperature and pressure are generally not considered as primary operating variables in a SMB. In practice, temperature is set sufficiently high to ensure rapid mass transfer, while pressure is set high enough to avoid vaporization of the liquid streams. In liquid phase adsorption, the required bed temperature is not related to the boiling range of the feed (as is the case for distillative separations), which is an advantage when handling heat sensitive stocks. Various aspects of process control for SMB operations are described in the scientific and patent literature, but these are beyond the scope of

this chapter. SMB adsorption processes are generally not restrictive on the adsorbent type that can be used and most common adsorbents are applied in several SMB operations

Table 2.1: Overview of relevant industrial applications of the SMB process for adsorptive separation.

Process	Separation	Adsorbent	Desorbent	Ref.
Parex/Eluxyl	p-xylene from C8 aromatics	K-BaX	p-diethylbenzene	[10]
MX Sorbex	m-xylene from C8 aromatics	NaY	Indane	[12]
Gasoline Molex	n-pentane/n-hexane from light naphtha	5A	Iso-/n-butane	[13]
Maxene	C5-C10 n-paraffins from naphtha	5A	n-dodecane	[14,15]
Detergent Molex	C10-C13 n-paraffins from kerosene	5A	n-pentane/ iso-octane	[16]
C4 Olex	Isobutene from C4 isomers	CaX/SrX	n-hexane/ n-hexane	[17,18]
Detergent Olex	C10-C16 linear olefins from isomers	CaX/SrX	n-hexane/ n-hexane	[17]
Toray's Aromax	p-xylene from C8 aromatics	K-BaX	diethylbenzene	[19]
Sarex	Fructose from fructose-glucose	CaY	water	[20]
Arosorb	Separation of aromatics from naphta	silica gel	pentane	[21]
Biltricide (Bayer)/ Praziquantel	Chiral separation of racemic drug mixture	Chiralcel OZ	ethanol	[22,23]
Lexapro (Lundbeck)/Cipralex	Chiral separation of racemic drug mixture	Chiralpak M AD	acetonitrile	[24]
Keppra (UCB)/Levetiracetam	Chiral separation of racemic drug mixture	silica gel/ amylose	ethanol/ heptane	[25]
Nuvigil (Cephalon)/ Armodafinil	Chiral separation of racemic drug mixture	Chiralpak AD	methanol	[26]
Zoloft (Pfizer)/ Sertraline	Chiral separation of racemic drug mixture	Chiralpak AD	acetonitrile/ methanol	[27,28]
Taxol (Genentech)/ Paclitaxel	Chiral separation of racemic drug mixture	polystyrene–divinylbenzene	ethanol	[29,30]
Xyzal (UCB)/ Levocetirizine	Chiral separation of racemic drug mixture	Chiralpak AD	heptane/ n-propanol	[31]
Zyrtec UCB)/ Cetirizine	Chiral separation of racemic drug mixture	Chiralpak AD	hexanesulfonic acid/methanol	[32]

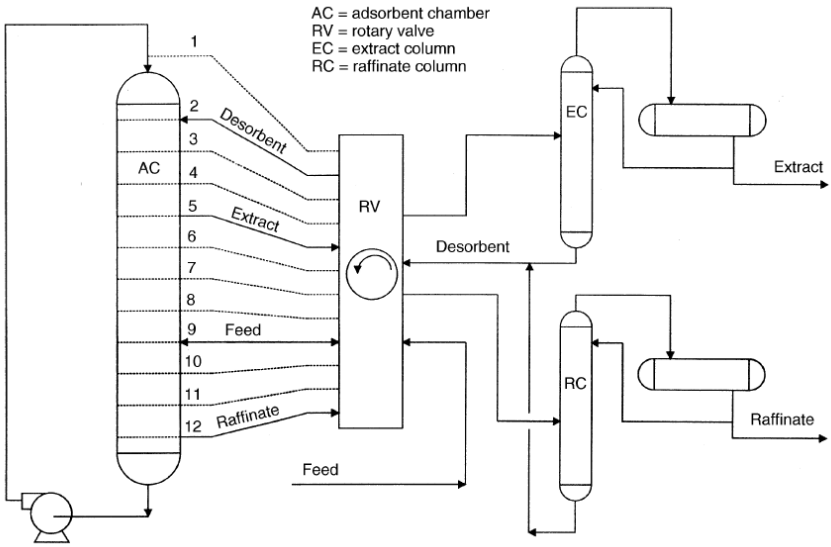


Figure 2.9: Schematic diagram of the Sorbex process. Figure taken from Broughton *et al.* (1970) [10].

Besides the Sorbex process, there is another approach to simulate a moving bed. In this approach, a cascade of multiple fixed beds is put in series. At intermittent time periods, a completely regenerated bed is added to the end of the cascade, just before breakthrough is about to occur. Simultaneously, a fully saturated bed is removed at the start of the cascade and placed at the end of a parallel regeneration train. In this way, the adsorbent effectively moves countercurrent relative to the solvent stream, in both the adsorption and the regeneration train (see **Figure 2.10**). If, hypothetically, the number of fixed beds in series would be infinitely increased, the system would evolve into a true countercurrent moving bed system. Note that this approach is also a bit similar to the pulsed flow reactor.

Operation of a simulated moving bed process

To describe the operation of a SMB process, the separation of a binary feed over a hypothetical SMB is discussed. This hypothetical SMB is schematically the same as the true moving bed on **Figure 2.7**, so this will be used again here as example. The only difference now is that the solid bed is stationary while the stream access points will move throughout the bed. The binary feed again consists of components A and B, with A being the strongly adsorbing compound and D the desorbent. A, B and D are separated in an isothermal continuous countercurrent operation; the system is linear and ideal (i.e. non-interacting). To achieve complete separation of A and B, certain conditions of flow must be met. With γ_i (dimensionless) as the product of the

equilibrium constant K_i (dimensionless[2]) for component *i* and the ratio of simulated solid motion *S* (m/s) to the liquid flow *L* (m/s), the following equation (eq. 6) holds true:

$$\gamma_i = K_i \left(\frac{S}{L}\right) = K_i \left(\frac{1-e}{e}\right)\left(\frac{u_s}{u}\right) \qquad \text{eq. 6}$$

In this equation, u_s (m/s) and *u* (m/s) are the simulated solid and interstitial fluid velocities, respectively, while *e* is the bed voidage. The flow conditions that must be observed for each section of the bed are then the following, with *F, D, R* and *E* being the flow rates (m³/s) of the feed, desorbent, raffinate and extract stream, respectively:

Section	Condition
I	$\gamma_A > 1$, $\gamma_B < 1$
II	$\gamma_A > 1$, $\gamma_B < 1$
III	$\gamma_A < 1$, $\gamma_B < 1$
IV	$\gamma_A > 1$, $\gamma_B > 1$

The system has four flow rate variables and four inequality constraints, one for each of the four bed sections. If each of the above conditions is met by the same separation factor α (α being K_A/K_B and > 1) the inequalities can be written as mass balances:

Section	Mass balance
I	$\alpha\ (D - E - + F)/S = K_A$
II	$(D - E)/S = K_B\ \alpha$
III	$S/D = K_A\ \alpha$
IV	$\alpha\ (D - E - + F - R)/S = K_B$

Solving these mass balances will result in a set of flow rates that can be used in a McCabe-Thiele diagram [34,35]. The McCabe-Thiele diagram for this SMB process and the interpretation of the operating lines will be the same as the McCabe-Thiele diagram (see **Figure 2.8**) discussed for a true moving bed process (*vide supra*). Reducing the ratio *L*/*S* will force the operating lines on the McCabe-Thiele diagram closer to the equilibrium line, reducing the mass transfer driving force and hence the process efficiency. By analogy with distillation, a reduced mass transfer efficiency

[2] Concentrations in the liquid phase and adsorbent phase should be expressed in similar units, e.g. mol/kg.

means that a larger number of theoretical stages is required to achieve a similar separation. For SMB operations, this means that each of the four beds needs to be increased in size. As the conditions for separation of A and B imply that $\gamma_A > 1$ and $\gamma_B < 1$, then the following inequality (eq. 7) must hold true:

$$K_A > \frac{D+F}{S} > \frac{D}{S} > K_B \qquad \text{eq. 7}$$

Therefore, there is an optimum choice to be made between the size of each bed and the desorbent flow rate. The McCabe-Thiele diagram on **Figure 2.8** is only valid for a linear, ideal system without interactions between different compounds. In reality, non-linear systems are more common, leading to concave or convex adsorption isotherms [36]. Convex isotherms (**Figure 2.11**, left) are generally seen for hydrocarbon separations on zeolite adsorbents, while concave adsorption isotherms (**Figure 2.11**, right) are rather seen for ion-exchange resins in sugar separation, among others. Both examples of industrial adsorptive separations are still used in large scale SMB processes.

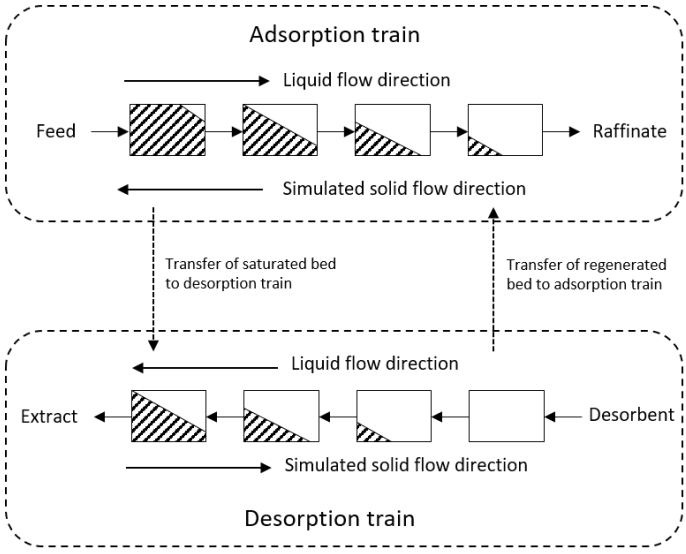


Figure 2.10: Schematic overview of a countercurrent SMB process by a cascade of fixed beds. Shading indicates the concentration profiles of the adsorbate on the solid adsorbent phase. Switching of adsorption columns between the adsorption and desorption train effectively simulates a flow of the solid phase. Redrawn from Ruthven and Ching [33].

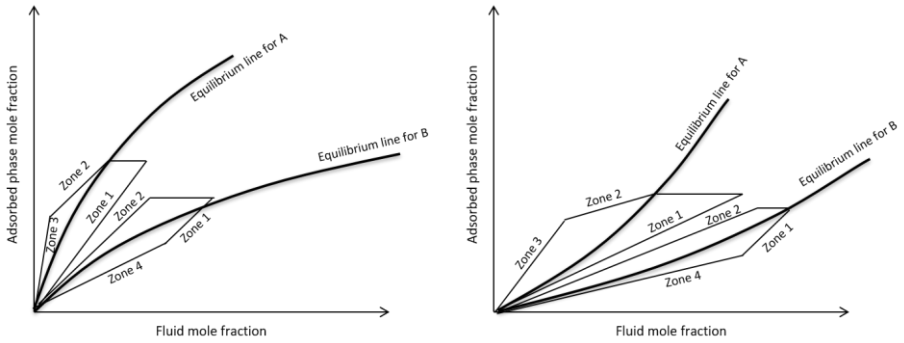


Figure 2.11: McCabe-Thiele diagrams for SMB adsorption processes with convex (left) and concave (right) adsorption isotherms.

2.3.6. ECONOMICS OF ADSORPTIVE SEPARATIONS

In industry, the choice for a specific separation mode and type is generally based on the cost of operation. Pharmaceutical separations might be an exception, where for instance ultra-high purity or even enantiopurity are the most important targets. When comparing the economics of different process modes, the costs of capital, operation, chemicals and lost crude all have to be accounted for. Often, the costs for SMB operations are equivalent or superior to those of batch processes, especially for large scale processing. For small scale processes, batch operation can still be the best option. The optimum number of stages (i.e. the bed length) is often determined by an economical evaluation where the capital and operational costs of extra bed material are balanced against the increased separation efficiency. The regeneration of the adsorbent bed can contribute significantly to the cost of operation and the choice of desorption mode is therefore generally based on economics. Thermal regeneration of lengthy adsorption beds requires large amounts of thermal energy, while heat losses from the bed can weigh against high efficiency and a large thermal capacity of an adsorbent bed will lead to long times of heating and cooling and thus lengthy cycle times. Regeneration via liquid desorption on the other hand can consume large amounts of chemicals and produce stochiometric amounts of waste or byproducts that have be disposed of. In some cases, it might be more economical to simply discard the adsorbent than to attempt its regeneration. These processes are called non-regenerative and they can occur when the regeneration process is complex, technically challenging or energy- and resource-intensive, or when both the adsorbate and adsorbent are of low value (e.g. pollutant removal on a cheap activated carbon).

2.4. Adsorbents

Since adsorption is a process that occurs at the interface of a liquid/gaseous phase with a solid adsorbent, promising adsorbents feature a large specific surface area. This requires either very large outer surfaces or the presence of pores with their associated internal surface area. Only nanomaterials feature sufficiently large outer surfaces, but their potential health hazards hinder broad applicability. Therefore, all well-known adsorbents are porous and the majority of their surface area originates from their pore structure. IUPAC classifies pores depending on their size (**Figure 2.12**). The smallest pores (< 2 nm) are called micropores and are subdivided in ultramicropores (< 0.7 nm) and supermicropores (0.7 – 2.0 nm). Mesopores are between 2 nm and 50 nm wide and macropores are larger than 50 nm. Nanopores are smaller than 100 nm and therefore include all previous classes, although macropores are not necessarily nanopores [37]. Adsorption takes mainly place in the micropores with some contribution from the mesopores, although this depends on the application; macromolecules such as proteins cannot enter micropores and will thus adsorb mainly in the mesopores. Macropores feature virtually no contribution to the adsorption, but can be essential to allow fast transport to the smaller micro- and mesopores.

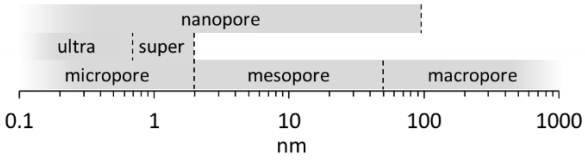


Figure 2.12: Schematic representation of the IUPAC classification of pores.

The uniformity of the adsorbent severely affects the selectivity of the separation. For this reason, adsorbents are classified as amorphous or crystalline materials. The latter display order on the molecular level, i.e. there is a translational repetition of a certain unit cell (i.e. the brick from which the material is built) resulting in pores of exact diameter and chemical nature. The distinction between the two types of adsorbents is however not absolute. Crystalline materials often contain non-structural mesopores (e.g. cracks) and/or disordered atoms on a molecular level (e.g. position of Al^{3+} ions can vary in zeolites). On the other hand, amorphous materials such as the mesoporous silica MCM-41 feature narrow pore size distributions in the mesopore range.

The choice of the appropriate adsorbent is largely guided by the nature of the separation/purification. If a highly selective chemisorption process is targeted, a

material will be selected that specifically displays adsorption sites that can chemically bond with the adsorbate. The majority of the adsorption processes however rely on physisorption and in these cases, the key properties of the adsorbent depend on whether a thermodynamic or kinetic selectivity is required. In general, chemically different compounds will be separated thermodynamically whereas similar compounds with different size/geometry will be separated based on kinetic differences. In thermodynamic separations, the nature of the adsorbents' surface mainly determines the success of the adsorption; hence adsorbents will be selected based on their surface functionalities. In contrast, adsorbents for kinetic separations will be designed to feature the necessary pore size/shape. Several classes of adsorbents for liquid separations can be distinguished:

1) Organic adsorbents:

a. **Activated carbons** have already been used for centuries as adsorbent to remove colors and odors from water. These purely carbonaceous compounds are produced by first carbonizing organic matter under inert conditions and subsequently physically and/or chemically activating them to increase their surface area. Physical activation typically occurs at elevated temperatures (~800°C) with CO_2, air or steam, whereas chemical activation is performed with agents like KOH, H_3PO_4 or $ZnCl_2$. Activated carbons display a high specific surface area (up to 3000 m^2/g) and are originally apolar, although it is possible to synthesize polar variants via chemical modification. They are generally cheap and amorphous, resulting in a broad pore size distribution. They are therefore often used as purification agent to remove poorly defined impurities such as toxins, colorants etc. Carbonaceous adsorbents with a narrow pore size distribution can also be synthesized and are called carbon molecular sieves.

b. **Polymeric resins** can be both synthetic or originating from natural sources. They feature a large variety in chemical composition and can be highly tuned by adapting the functional groups present on the polymer chains. They can be both aromatic and aliphatic and often contain basic or acidic functionalities such as amino groups or sulfonic and carboxylic acids to perform ion exchange. Due to their wide functionality range but swelling and thermal stability issues, resins are often used for thermodynamic separations, although separation of fragments with large mass differences is possible. Their main applications include ion-exchange separations and affinity chromatography.

2) Inorganic adsorbents:

a. **Clays** are naturally available layered silicalites (i.e. compounds containing SiO_2) that can adsorb guest molecules between their inorganic sheets. As the molecules stack between the layers, the interlayer distance can increase and cause general swelling of the hydrophilic crystals. As a result, the pore size depends on the presence of guest molecules. Adsorption on clays is often driven by ion exchange. Besides naturally available materials, clays can also by synthesized to tailor their ion exchange properties to the desired applications, such as colorant removal.

b. **Zeolites** were already known by the ancient Greeks as rocks that could ad/desorb water. Although several zeolites are naturally available, most materials are synthetic. Zeolites are aluminosilicates consisting of SiO_4 and AlO_4 tetrahedra that form an open crystal structure with micropores and with a very narrow pore size distribution. Although zeolites are generally known for their water adsorbing properties, there are apolar variants known with a high Si/Al ratio. This ratio is, together with the framework topology, one of the main characteristics of a zeolite because it directly influences the charge in the structure. As a result, this ratio has to be carefully tuned for optimal performance. The pore size of a given zeolite can sometimes also be tailored by exchanging cations of different size on the Al^{3+} sites, which for instance causes the remarkably different properties of the Linde 3A (K^+), 4A (Na^+) and 5A (Ca^{2+}) materials which all feature the same LTA topology (**Figure 2.13**). Due to their narrow pore size distribution, zeolites have been the adsorbent of choice in many size-exclusion separations, such as the separation of different xylenes.

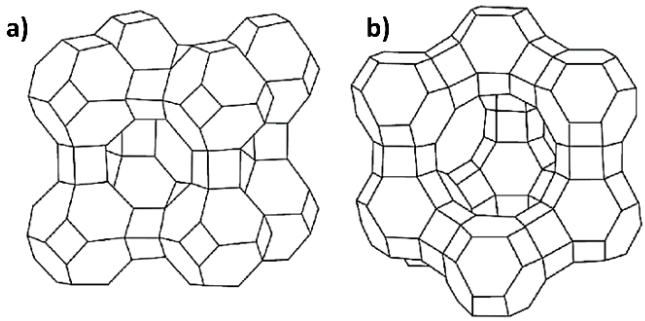


Figure 2.13: Two of the most employed zeolites: a) type A and b) faujasite (type X and Y).

c. **Mesoporous structured silicas** are synthetic materials that were reported in the 1970s. These amorphous all-silica materials feature ordered mesopores with well-defined sizes because they are synthesized using liquid crystal templates. They were mainly studied because they were the first class of materials with a narrow pore size distribution in the mesopore range, although more recent materials, such as MOFs (*vide infra*), also display well-defined mesopores. Owing to their large pores, mesoporous structured silicas can be functionalized with organic molecules that allow selective removal of metal ions from solutions [38].

d. **Silica/alumina** are mostly known as desiccants and adsorbents in the gas phase. However this class of relatively simple inorganic compounds encompasses many different amorphous or crystalline varieties with their own characteristics. A well-known liquid phase application of silica gel is its use in chromatographic separations, in which its polarity causes non-polar compounds to elute before more polar ones. In addition, silica can be covalently modified to generate an apolar surface, which is for instance used in reversed-phase chromatography.

3) Hybrid organic-inorganic adsorbents:

a. **Metal-organic frameworks** (MOFs) are a new class of synthetic porous materials that have been intensely studied since the early 2000s. These hybrid materials are chemically very diverse but always contain metal cations that are linked together by organic ligands. The ease with which the metal or linker can be varied led to the concept of isoreticular chemistry, in which crystal structures with identical topologies but with different pore size, functionality etc. can be synthesized. Similar to zeolites, MOFs feature well-defined pores but these pores can be extend to the mesopore range, which is not possible for zeolites. Due to the large variation in chemical composition, MOFs can be both hydrophilic or hydrophobic and can contain the adsorption site types of all above mentioned materials. In addition, some MOFs feature variable pore sizes upon introduction of guest molecules, similar to the swelling effect of clays. However, irrespective of their broad application window, their current high price hinders commercial application [39].

Besides selecting an adsorbent based on its chemistry and pore size, some practical issues have to be considered. Firstly, the adsorption capacity (volumetric or gravimetric) of the adsorbent directly relates to its required amount, which strongly affects the total cost of the adsorbent and the size of the separation unit. In addition,

the stability and recyclability are important inherent properties of the adsorbent, but also the size and shape of the adsorbent particles influence the efficacy. Large particles suffer from too long diffusion paths and diffusion is thus limited to the outer shell of the adsorbents, which should be avoided. However, small particles hinder fast transport through the interparticle voids, leading to a high pressure build-up. As a result, large pellets (up to mm scale) that consist of small particles are often prepared to guarantee sufficiently fast mass transport on all length scales. In some cases, an inert binder material is added to the adsorbent to prepare pellets with high mechanical stability.

2.5. Industrial Applications

In the last part of this chapter, a series of industrial examples for various sectors and applications will be looked at in more detail. Examples range from large scale bulk separations to smaller scale purifications for high-purity end products.

2.5.1. PETROCHEMICAL SEPARATIONS

Introduction

The petrochemical industry is characterized by extremely large quantities of products, which have to be produced very efficiently with minimal energy consumption and waste production. As a result, specialized refineries are built that operate continuously, often for many years without a shutdown. Separation installations should therefore also run continuously with minimal maintenance and at a relatively low cost, which is typically performed in robust distillation columns. However, separations of compounds with a similar boiling point are very challenging and other techniques have to be explored to allow low-cost, effective separation. Liquid phase adsorption in SMB units is herein an attractive technique for molecules with similar volume but different shape such as xylene isomers, linear vs. branched paraffins or olefins vs. paraffins. Due to the small differences in shape, adsorbents with a very narrow pore size distribution are used. In addition, the adsorbents are in operation for several years and thus have to be highly stable. As a result, zeolites are employed for petrochemical bulk separations.

Aromatic separation

The best known adsorption-based liquid phase separation of bulk petrochemicals is the separation of xylenes. These C8 aromatics are industrially highly important because para-xylene is the precursor of terephthalic acid, a key compound for the

synthesis of polyethylene terephthalate. The large demand of PET has resulted in a steady increase in *p*-xylene consumption since the first adsorptive separation in the 1970s, to a predicted global annual demand of approximately 55 Mtons in 2019 [40]. On the other hand, the production of *m*-xylene is only 2% of that of the para-isomer and is closely linked to the para market demand because *m*-xylene is used as an additive (in the form of isophthalic acid) in the PET synthesis. The demand for *o*-xylene is intermittent (approximately 10% of total xylene production) and it is mainly used as precursor for phthalic anhydride [41].

The xylene isomers are found in a stream produced by catalytic reforming or naphtha cracking which contains all three isomers (ortho, meta, para) combined with ethylbenzene [42]. Due to their similar boiling points, the isomers are very hard to separate using conventional distillation, although *o*-xylene is partially removed by distillation together with heavier fractions. The remaining isomer mixture is separated with a zeolitic adsorbent with very narrow pore size distribution. The separation of the xylene isomers is performed in counter-current simulated moving bed adsorbers (*vide supra*), a technology trademarked by UOP LLC as the Sorbex process. The particular *p*-xylene separation is called the UOP Parex process and yields *p*-xylene in high purity (99.7-99.9%) and at high recovery (>97%) [43]. Since the demand for *p*-xylene is much higher than for the other isomers, the ortho and meta xylenes are then catalytically converted to an equilibrium mixture of all three isomers and fed back upstream of the Parex unit (**Figure 2.14**). Similarly, a competitor also produces *p*-xylene via the adsorptive Eluxyl process [44]. If a pure meta-xylene stream is desired, a second Sorbex unit, referred to as the MX Sorbex unit, can be placed downstream of the Parex adsorber to yield a 99.5-99.8% pure *m*-xylene stream [12,45].

The Parex unit consists of adsorbent beds, a rotary valve that simulates a moving bed (*vide supra*) and several distillation columns to separate the products from the desorbent (*p*-diethylbenzene). It is important to notice that the boiling point of the desorbent needs to significantly differ from that of the products to allow facile distillative separation. In addition, the desorbent and product have to display a similar affinity to the adsorbent to balance the required amount of adsorbent while not hindering the adsorption of the product itself. The employed adsorbent is a proprietary zeolite X or Y (faujasite) because their large pore sizes allow fast mass transfer through the zeolite cages. By modifying the Si/Al ratio and varying the exchanged cations (e.g. K, Ba), the selectivity for one xylene isomer can be tuned. Although the Parex process is already 50 years old, continuous investigations to improve the selectivity are still performed because the intrinsically low selectivity causes any improvement to be directly translated into smaller required bed sizes.

The MX Sorbex unit is very similar to the Parex one but generally smaller due to the lower demand for *m*-xylene. In addition, the selectivity of the adsorbent is tuned differently to get a pure *m*-xylene stream. In addition to the Parex and MX Sorbex units, UOP also developed several other separation processes in the Sorbex family, such as Ebex to remove ethylbenzene from the xylene mixture, Cymex to remove *p*- or *m*-cymene from its isomers and Cresex to remove the para- or meta- isomers from a cresol mixture. These processes are however not employed on a large scale [47,48].

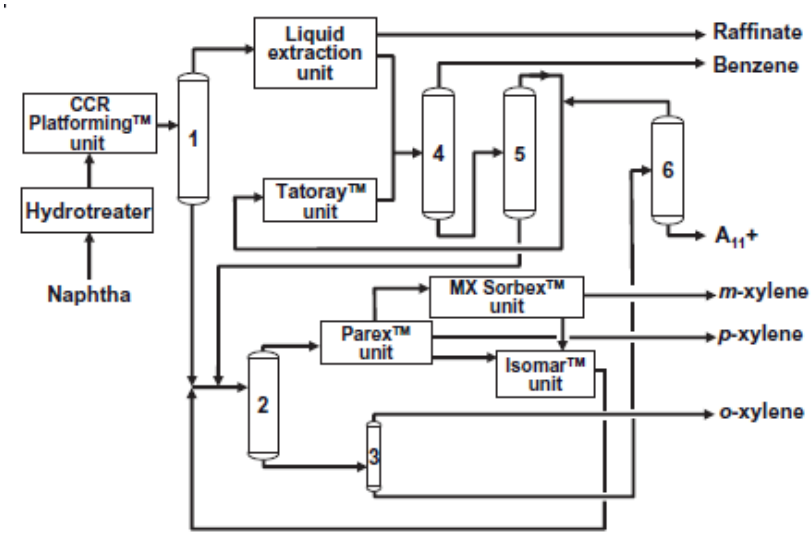


Figure 2.14: Typical process to produce p-xylene and m-xylene with a Parex and MX Sorbex unit. Taken from Kulprathipanja (2010) [46].

Linear paraffin separation

Besides the separation of xylenes, also some non-aromatic petrochemicals are separated by the liquid adsorptive Sorbex processes. The most commonly employed one is the Molex process, which separates n-paraffins from their branched, cyclic and aromatic counterparts in C5-C18 blends. The adsorbents in the Molex process are proprietary 5A zeolites with a high selectivity towards linear paraffins. As a result, the practically achieved purity of the outgoing streams is dictated by the non-ideal conditions in the adsorber such as bad flow distribution and back mixing. Since the adsorbent is very selective for polar compounds such as heteroatom-containing species, these contaminants have to be removed prior to the Molex process to avoid poisoning of the adsorber bed. Therefore, hydrotreatment of the streams is often necessary. Depending on the molecular weight of the product stream, the Molex separations can be subdivided in gasoline Molex (C5-C6), MaxEne (C5-C10) and detergent Molex (C10-C13) [16].

In the gasoline Molex, n-pentane and n-hexane are removed from light naphtha because their presence in gasoline has a detrimental effect on the octane number. After separation, the n-paraffins are isomerized to non-linear hydrocarbons in an isomerization reactor and mixed back with the light naphtha at the inlet of the separator. As a result, the naphtha stream coming out of the separator is low in n-paraffins and the final gasoline product features a highly improved octane number. Since the purity requirement of the n-paraffin stream is relatively low (desired purity >85%), the gasoline Molex adsorbers contain a lower number of total beds than other Sorbex units. The gasoline Molex system uses a light desorbent (i.e. iso-/n-butane mixture), which means that the desorbent is more volatile than the products and is recovered as the overhead product in the downstream distillation columns.

The relatively recent MaxEne process separates the C5-C10 n-paraffins from naphtha to optimize the operations of the downstream naphtha steam cracker (using a n-paraffin rich stream) and catalytic reformer (using a n-paraffin lean stream). The high n-paraffin content in the steam cracker's feed results in a 30% increased yield towards ethylene and propylene, while reducing coke formation by 50%. On the other hand, the non-normal rich stream also reduces coke formation in the catalytic reformer, reduces its operating temperature and improves its selectivity towards aromatics. Similar to the gasoline Molex system, the desired purity of the product streams is relatively low, although still slightly higher than for the gasoline system. As a result MaxEne adsorbers contain approximately half the number of beds of conventional Sorbex units. The MaxEne process employs a heavy desorbent such as n-dodecane, which means the desorbent is recovered at the bottom of the downstream fractionation columns. Due to the heavier fractions in the MaxEne process compared to the gasoline Molex, diffusion is slower and the cycle time has to be slightly increased.

The detergent Molex process isolates the linear (C10-C13) alkanes from kerosene to convert them to linear alkylbenzenes, precursors of the linear alkylbenzene sulfonate (LAS) detergent [49]. Due to the high required purity of the C10-C13 n-paraffin stream (>99%), the detergent Molex unit contains much more beds than the other Molex separators. The detergent Molex system employs a light desorbent consisting of n-pentane with some added iso-octane to balance the desorbing strength and the operating pressure of the liquid-phase adsorptive separator.

Olefin separation

A third major petrochemical adsorptive separation process is the olefin isolation from paraffins. This is particularly interesting for streams with compounds of different chain lengths, which differ often more in boiling point and solubility depending on chain length than depending on saturation of the bonds (**Figure 2.15**). The adsorptive process, better known as Olex, can however separate the olefin fraction for the entire stream using a proprietary zeolite X as adsorbent. The Olex process can be subdivided in the C4 Olex process to obtain isobutene and the detergent Olex process to get C10-C16 olefins [50].

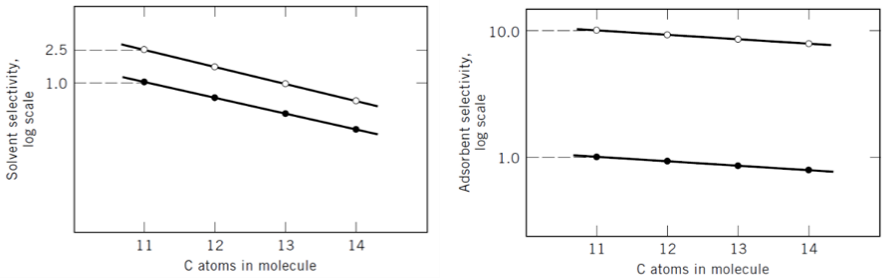


Figure 2.15: Comparision of the extraction (left) and adsorption (right) selectivity between C11-C14 paraffins (●) *and olefins* (○)*.* Taken from Gembicki *et al.* [9].

In the C4 Olex process, a mixture of primarily isobutane and isobutene is separated. The desired isobutylene has a broad use in the production of methyl *tert*-butyl ether (MTBE) and iso-octane, both additives that increase the octane number of gasoline. The separation requires a large adsorption installation to achieve sufficient product purity (>93%) and uses a heavy desorbent consisting of n-hexene isomers mixed with n-hexane. Since the feed also contains C5-C6 compounds, an additional rerun column is required to remove these compounds from the desorbent stream as they would contaminate it [18].

The detergent Olex process produces a range of linear olefins in the C10-C16 range. The length of the olefins depends on the application, such as LAB detergents (C10-C13), detergent alcohols (C12-C15) or lubricants (C15-C16). Similar to the C4 Olex and the detergent Molex processes, the detergent Olex unit requires the full allotment of the Sorbex bed to achieve sufficiently pure product streams. The unit also uses an n-hexene/n-hexane desorbent mixture, although its exact content largely depends on the molecular weight of the desired products [51].

2.5.2. PHARMACEUTICAL SEPARATIONS

Introduction

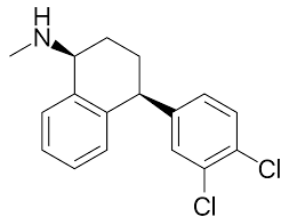
Adsorptive separation in the pharmaceutical industry significantly differs from that in the petrochemical industry. This is firstly due to the different quantities that are typically processed: petrochemical processes involve the separations in the kton-Mton/year scale, whereas pharmaceuticals are produced on a kg-ton/year scale. Secondly, the value of pharmaceutical products is much higher and the time to market is highly important, which allows more expensive adsorption systems. Thirdly, pharmaceutical compounds are generally more sensitive to high temperatures, which excludes separations at elevated temperature. As a result, pharmaceutical separators are relatively small and run mostly discontinuously (although the use of SMB units increases), in contrast to the large, continuously running units in the petrochemistry. Adsorptive pharmaceutical separations are therefore often performed via chromatographic methods.

Adsorbents for separations in the pharmaceutical industry are generally based on metal oxides (e.g. SiO_2) or polymer matrices (e.g. carbohydrate polymers), which are often functionalized to get the desired separating properties. Separations are based on chemical functionality or size, although the strict cut-off possible with microporous materials is not feasible since the larger pharmaceutical compounds cannot enter micropores. Size exclusion, for instance through gels, is thus merely based on moderate differences in diffusivity between molecules of significantly different size. The adsorbents that separate products based on their chemical nature can be classified as normal phase (polar adsorbents such as silica), reversed phase (apolar adsorbents, e.g. C18-coated silica) and ion exchangers.

A thorough overview of the major adsorptive separations in the pharmaceutical industry lies beyond the scope of this chapter due to the large variety and number of pharmaceutical products and separations. Therefore, two examples of difficult separations that significantly differ from other adsorptive application fields are discussed.

Small molecules

The separation of chiral molecules is one of the most challenging processes in the synthesis/purification of (intermediates of) active pharmaceutical ingredients. Although crystallization is sometimes possible, chromatography is often necessary to obtain an enantiopure product. This can be very important, since many cases are known where the two enantiomers have significantly different effects. Preferential adsorption of one enantiomer over the other can be achieved by using a chiral polymer or functionalizing a matrix with a chiral selector, which can be based on ligand-exchange, π-complexation, sequestration in crown ethers etc. These selectors contain at least one stereocentre and selectively bind one of the isomers. Commonly used chiral polymers include carbohydrates such as amylose and cellulose. The interactions between the mobile and stationary phases are similar to those in other chromatographic separations, but the exact location of the interactions has a much higher influence since one of the isomers should have a significantly higher affinity for the stationary phase. Because of the strong constrains and large flexibility in chemical nature, many different chiral stationary phases are known and commercially available [31].



One of the most prescribed chiral drugs is the antidepressant Sertraline (in the top 15 of most prescribed drugs in the US in 2017, [52]), which is produced in large quantities and therefore initially separated using an SMB unit instead of a regular fixed-bed column. The employed stationary phase was amylose tris(3,5-dimethylphenylcarbamate) coated on silica-gel and the solvent was an acetonitrile-methanol mixture. After separation, the undesired isomer was racemized and fed back into the separator [53]. The sertraline production process was however improved by a chiral separation of the tetralone intermediate over a clay-supported optically pure Ru complex (e.g. $Ru(phen)_3^{2+}$) with an ethyl acetate-supercritical CO_2 mobile phase. The clay-support allows a higher operating temperature than previous stationary phases, thereby improving the products' solubility and thus productivity. Furthermore, the separation is performed in a non-steady state continuous process with variable zone length (i.e. the Varicol process) [54].

Biological agents

Besides synthetic small molecules, many pharmaceutical compounds are harvested from cells (i.e. biological agents). The last few decades much attention has herein been devoted to the development of monoclonal antibodies, which are produced

from genetically modified cells and include for instance the best-selling (in USD) drug of 2018 (adalimumab) [55]. Isolation of adalimumab involves several steps, of which affinity chromatography is particularly interesting since it is a widely used, highly effective method to isolate/purify antibodies. Affinity chromatography involves specific and reversible interactions between the stationary phase and the target protein, which allows isolation from a complex crude mixture. It is furthermore the only technique that enables purification of a molecule based on its biological function. Although hundreds of different monoclonal antibodies have been produced, the majority can be isolated using only a few adsorbents. This is due to general affinity of the immobilized protein A, G or L for a few relatively invariant domains in the Fc region of immunoglobin G (igG), the most common type of human antibodies (**Figure 2.16**). The chromatographic separation includes a first adsorption step in which the antibodies bind to the immobilized proteins with high affinity. In a second step, the antibodies are released from the stationary phase, which involves elution with a buffer solution of different pH and/or ionic strength than the initial mobile phase [56].

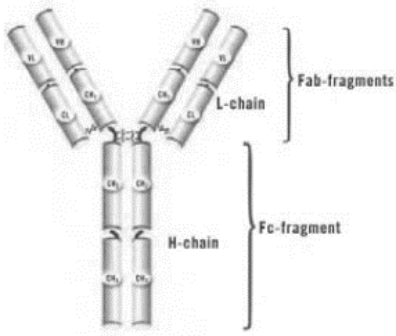


Figure 2.16: Structure of a typical immunoglobulin antibody. Source: GE Healthcare [57].

2.5.3. WASTE WATER TREATMENT

Introduction

Clean water is an essential commodity for human beings, not only for drinking water but also for agriculture, industry and almost every human activity on earth. Contamination of natural water resources and emissions of industrial effluents pose the need for water treatment to protect both humans and ecosystems. Water purification techniques date back to ancient times, with sand filtration being one of the oldest known examples of filtration via adsorption. Modern day water treatment techniques vary from fairly simple, large scale bulk treatment to highly complex purification techniques for the removal of specific contaminants from industrial

effluent streams. The scale and degree of complexity depend on the volumes to be treated, the contaminants to be removed, the degree of contamination and the environmental standards that have to be met, among others. This will have an effect on the cost of purification, which typically varies between 10 and 450 USD per million liters [58]. Common methods of water purification are, among others, (membrane) filtration, sedimentation, flotation, ion-exchange, adsorption or more advanced techniques like electrodialysis, electrolysis and advanced oxidation processes. Adsorption is generally considered as one of the best water treatment methods due to its wide range of applications, ease to process large volumes and ambient conditions. In addition, it is relatively inexpensive. Depending on the adsorbent type and adsorption mode, a wide variety of organics and inorganics, both soluble and insoluble can be removed resulting in very high purity. Both batch and continuous processes can be employed for water treatment, each having different capabilities. Obviously, continuous packed bed systems are the better choice for the treatment of high volumes of water in short operating times. The short operating times for continuous water treatment can make mass transfer rates a limiting factor, while column operation can be associated with large pressure drops. If process time is not limiting, batch operation might be useful and can result in higher removal effectiveness, expressed per unit mass adsorbent. Activated carbon is the universal and most common adsorbent for waste water treatment, but a wide variety of adsorbent types can be applied for a similar variety of target compounds (see **Table 2.2**). Two relevant examples of adsorptive water treatment will be highlighted here, differing largely in scale and complexity.

Bulk removal of organic compounds by activated carbon

Both natural organic matter (NOM) and synthetic organic contaminants have to be removed during waste water treatment, until concentrations are below the environmental threshold levels. Removal of organics is also a common step in the treatment of industrial effluents before they are discharged in natural surface waters. Many natural organics are *in se* innocent and do not pose a direct threat to the health of humans. Removal of NOM from water mainly serves esthetic considerations: i.e. color and odor removal. Nevertheless, NOM can also be a precursor in the formation of hazardous disinfection byproducts, including trihalomethanes like chloroform. Since NOM is ubiquitously present in natural waters, it is mostly removed by filtration prior to adsorption. It would otherwise quickly saturate activated carbon beds and prevent more toxic organic micropollutants from being removed effectively via adsorption. Adsorption by activated carbon in waste water treatment mostly intends to remove the latter category of contaminants, together with dissolved organic matter that cannot be

removed by filtration. One of the advantages of activated carbon is that it can remove a wide variety of organic micropollutants, ranging from antibiotics, pharmaceuticals, hormones, personal care products to pesticides and hydrocarbons. This also implies that activated carbon will never show high selectivity for one specific organic compound, but this is hardly a disadvantage in bulk treatment of waste water [59].

Table 2.2: Overview of different adsorbent types and their target compounds for waste water treatment. Redrawn from Bonilla-Petriciolet *et al.* [58].

Adsorbent	**Heavy metals**	**Metalloids**	**Halogens**	**Dyes**	**Pharmaceuticals**	**Toxins**	**Radioisotopes**	**Organic pollutants**
Alumina	✓	✓	✓	✓	✓	✓		
Activated carbon	✓	✓	✓	✓	✓	✓	✓	✓
Biological materials	✓	✓	✓	✓				✓
Bone char	✓	✓	✓	✓	✓	✓	✓	✓
Clays	✓	✓	✓	✓	✓	✓		✓
Composites	✓	✓	✓	✓	✓		✓	✓
Graphene-based adsorbents	✓	✓	✓	✓	✓	✓	✓	✓
Low cost adsorbents*	✓	✓	✓	✓	✓		✓	✓
Nano adsorbents	✓	✓	✓	✓	✓	✓	✓	✓
Polymeric materials	✓	✓	✓	✓	✓	✓	✓	✓

*Biomass, agricultural and wastes and byproducts

Activated carbon exists in different sizes and shapes and can be made from many carbonaceous sources, but it is commonly divided in powder activated carbon (PAC) and granular activated carbon (GAC), referring to the grain size of the adsorbent. Both types of activated carbon are used in waste water treatment processes, but GAC is more common for packed bed operations. The typical grain size for GAC ranges between 1 – 2 mm but both smaller and larger granules exist. The adsorptive capacities of an activated carbon are denominated by the iodine and molasses number. The iodine number characterizes the ability to adsorb small molecules in the micropores of the activated carbon and is defined as the amount of iodine (in milligrams) that is adsorbed by one gram of carbon at an equilibrium concentration of 0.02N of iodine. GAC adsorbents for water treatment typically have iodine numbers ranging between 600 and 1100. The molasses number characterizes the ability to adsorb larger molecules in the mesopores of the materials. The definition

of the molasses number is less straightforward and differs between European and American standards [60].

As stated before, GAC adsorbent beds are mostly applied after a prior filtration step to remove solids and larger particles, even though in some situations the GAC bed might function as a solids trap itself. When applied after filtration, the main and only objective of the adsorption bed is to remove dissolved organic material and micropollutants. Because of the prior filtration step, fouling of the bed is normally not a problem and backwashing is not necessary. Filtration-adsorption beds require frequent backwashing and thus have shorter run times. Frequent backwashing will inevitably result in increased carbon losses and higher operation costs. The main advantage of using filtration-adsorption beds is the significant reduction in capital cost since no additional filtration units are required.

The bed length and desired capacity of an adsorption unit in wastewater treatment mainly depend on the target levels of the pollutant concentrations and the flow volumes that have to be treated. In waste water treatment, breakthrough is generally defined as the moment when effluent concentrations increase above the imposed environmental standards. Depending on the micropollutant type, these concentration standards can vary orders of magnitude and hence breakthrough time can differ significantly depending on the composition of the water stream. Another important factor is the empty bed contact time (EBCT), this is the ratio of the empty bed (i.e. the void volume of the bed) and the liquid flow. Once the desired flow rate is determined, the EBCT and corresponding bed length can be calculated. Longer EBCT values will delay breakthrough and reduce the regeneration frequency of the adsorbent bed. The latter is often expressed as the carbon usage rate (CUR), defining the rate at which the bed will be saturated and how often it will need to be replaced or regenerated. Longer EBCT values can be achieved by increasing the bed length or reducing the flow rate. Increasing the bed length results in a higher capital cost, while reducing the flow rate reduces the treatment capacity (in terms of volume) of the unit. Hence, determining the optimal EBCT is often a careful consideration of both technical and economic aspects. Typical EBCT values for water treatment range between 5 – 25 min [61].

GAC adsorption units can be operated as downflow or upflow fixed beds, or even as fluidized beds, with a single bed or multiple beds in series or in parallel. To enlarge treatment capacity and maximize carbon usage, multiple beds are often operated in parallel, with each bed in a different state of saturation. The effluent feeds are blended afterwards, so that effluent concentrations are relatively stable and breakthrough of a single bed will not result in violation of the target concentrations.

Fluidized GAC beds can be run as pulsed bed adsorbers (see paragraph 2.3.4), making it possible to run the adsorption process in continuous mode, hence avoiding breakthrough of the contaminants and column downtime for regeneration. Since activated carbon is relatively inexpensive, disposal of the spent adsorbent might be more economical than regeneration. However, disposal of saturated GAC beds can potentially result in leaching of the adsorbed pollutants. Therefore, regeneration is often still the preferred choice. Saturated GAC beds are generally regenerated by steam purging, thermal treatment or chemical treatment, of which thermal treatment is the most common.

Tailor-made adsorbents for the removal of perfluoro-compounds from industrial effluents

Whereas waste water treatment plants are designed to treat a variety of organic and inorganic pollutants, the demands for treating industrial effluents are often significantly different. Depending on the industrial activity, the effluent can be highly polluted by a single contaminant or class of pollutants that have to be removed prior to discharge in the surface water. In this case, the purpose of effluent treatment is to specifically remove one or multiple target compounds, rather than to adsorb a full range of organics like in general water treatment units (*vide supra*). An example of this is effluent treatment in the fluorine chemistry. Perfluorinated chemicals are a specific class of fully fluorinated surfactants. Compounds like perfluorooctanoic acid (PFOA) and perfluorooctanesulfonic acid (PFOS) dissolve well in water due to their acids groups, but cannot be selectively separated from other organic compounds on convenient adsorbents like activated carbon or anion-exchangers. The industry has come forward with tailored adsorbent types to efficiently remove these perfluoro-compounds from effluent streams. An example is the surface modification of native silica particles with hydrophobic groups to increase the hydrophobic interactions with the ultra-hydrophobic perfluorinated surfactant chains. Rendering the silica surface more hydrophobic can be done by reaction of the surface with e.g. fluorinated organosilanes. Several industrial patents cover the surface modification with hydrophobic organosilanes of various siliceous adsorbents (silica gel, molecular sieves, zeolites) specifically for the removal of perfluorinated pollutants from effluent streams [62–64]. Another class of tailored adsorbents for the removal of perfluorinated compounds are layered double hydroxides, where e.g. Al- and Zn-linked hydroxides can form complexes with the acid groups of the surfactants [65]. Even cellulose-based adsorbents have been modified with cationic ammonium groups [66]. Despite the tailor-made and novel character of these adsorbent types, they can be applied in convenient adsorption modes, like batch or fixed bed operations.

2.5.4. SEPARATIONS IN THE NUTRITIONAL INDUSTRY

Introduction

Separation technologies have always played a crucial role in optimizing the quality, taste and shelf life of many foods and beverages. Besides the improvement of product quality, adsorption is used for the removal of unwanted products in feed or product streams and for the recovery of desired (co)products from waste streams. In this way, adsorption technology can drastically improve the efficiency and economics of food processes. The sugar industry was one of the first to implement the simulated moving bed (SMB) technology on a large scale after its first use in the petrochemical industry (*vide supra*). Other commercial large scale applications can nowadays be found across several food and beverages manufacturing sectors, including dairy, sugar and fruit juice processing, as well as in the brewing industry.

SMB applications in the sugar processing industry

The separation of fructose and glucose in the production of high fructose corn syrup is one of the first and still one of the most important commercial applications of SMB technology. This process was developed by Universal Oil Products (UOP) and named Sarex. Similar to the Parex process (also developed by UOP, *vide supra*), Sarex makes use of a proprietary zeolite X and Y as adsorbent to selectively remove fructose from glucose after the hydrolysis of sucrose. By selecting the appropriate counterion of the zeolite (Na, K, Ba, Sr, NH_4, or Ca), the selectivity for fructose over glucose can be significantly increased from 1.4 to 6.2 [20]. The Sarex process is a SMB operation with countercurrent flow, able to recover 90% of the fructose with up to 94% (w/w) purity, at optimum process conditions [67]. The Sarex process has later been extended to operate with synthetic ion exchangers, mostly polystyrene-based resins.

Another common application of adsorption in sugar processing is the desugarization of molasses and the separation of fine sugars from biomass hydrolysates. Molasses is a typical by-product of sucrose production from beet or sugarcane and is still rich in sucrose, but it also contains other compounds like betaine, minerals and amino acids. By fractionation of the molasses into two or more streams, valuable product streams can be extracted from a vegetable-derived byproduct of the food and fermenting industry. Several companies have developed SMB technologies for these sugar/molasses separation processes. Commercial examples of patented SMB processes are FAST (separation of beet molasses, by Finnsugar), Improved Simulated Moving Bed (separation of glucose from fructose in high fructose corn syrup, by Mitsubishi Chemical Industries), Pseudo Simulated Moving Bed (fractionation of beet

molasses into raffinose, sucrose, glucose and betaine, by Japan Organo Company) and Sequential Simulated Moving Bed (several sugar applications, like the fractionation of sucrose solutions, by Novasep) [68–71].

SMB operations are also widely applied to recover other saccharides or sugar alcohols (natural sweeteners) produced by the hydrolysis of various biomass sources. Examples include the recovery of various sugars (arabinose, mannose, xylose, galactose, glucose and cellobiose) from corn-stover hydrolysates, the purification of sorbitol from glucose solutions [72] and polydextrose from a crude sugar stream [73]. SMB technology remains ubiquitous in various sectors of the sugar industry: more than 100 SMB plants for carbohydrate separations exist.

Adsorptive recovery of fermented organic acids

Several organic acids are used as acidity regulator, preservative and flavoring agent in many foods and beverages. Common examples are citric acid, lactic acid, gluconic acid and itaconic acid. Chemical synthesis of these organic acids is possible, but fermentative production is commonplace. Fermentation requires only mild conditions, consumes less energy and is based on renewable carbon sources. These carbon sources are often cheap byproducts from the sugar or plant harvesting industry. This makes fermentation relatively inexpensive, but it implies that the organic acid has to be recovered from a complex fermentation broth, consisting of a substrate stream, a cell culture and several (undesired) byproducts. Convenient methods for the recovery of fermented organic acids contain several process steps, like filtration, precipitation and adsorption, making downstream processing a significant cost in the production of organic acids (typically 30-40 %). The use of adsorbents in the recovery of organic acids has many benefits: it can increase the degree of recovery and reduce the amounts of chemicals and waste (common with e.g. extraction and precipitation). Even though SMB operations are not so common as in the sugar processing industry, SMB units have been used for the separation of lactic acid from acetic acid and for the separation of citric acid from unconverted glucose streams. Both examples use the synthetic resin polyvinylpyridine as adsorbent [74–77].

Optimization of colloidal stability in beer

Colloidal instability in beers causes visible haze, reducing the appeal and shelf life of the product. This is mostly caused by interactions between hydrophilic polypeptides and polyphenols. Polyphenols in beer originate from barley and hop and are present in a wide variety. The haze active polyphenols are known as tannoids and the

hydroxyl groups on their aromatic rings are involved in the peptide binding. When these peptides and tannoids form covalent bonds, insoluble complexes are formed and a permanent haze is created. Removal of the haze forming peptides can be achieved using adsorbents like bentonite and polyvinylpyrrolidone. However, other types of peptides (called foam-active) play a role in the stabilization of the beer foam, so selective removal of haze-active proteins over foam-active proteins is crucial. Bentonite, for instance, can remove all of the haze-active peptides but will simultaneously remove the foam-active proteins. Silica gel adsorbents remove haze-active proteins while sparing almost all foam-actives proteins, hence showing a desired high selectivity for haze-active peptides in beer. This specificity is due to silica gel binding to the same sites on the proteins as where the polyphenols attach to create haze [78].

The use of silica gel as an adsorptive beer stabilizer was first introduced in the 1960s and is now a common practice in the brewing process. The silica gel is swollen in water before use and generally added to the unfiltered beer before the filtration step. Since the silica gel does not dissolve in the beer, it can be easily removed afterwards, along with the adsorbed proteins. Another advantage is its fast mode of action: adsorption of the proteins only requires a few minutes. The two types of silica gel commonly used in brewing are hydrogels and xerogels, both commercially available. The main difference between the two gel types is the degree of hydration, with the hydrogel having a higher moisture content (typically 60-70%) than the xerogel. The hydrogel is less expensive but needs greater mixing time to be sufficiently dispersed, while the xerogel is readily dispersed in aqueous solutions. Several patents cover the synthesis and application of silica gel in the brewing process, as well as the synthesis of - or combination with - other adsorbents, like silica deposited on synthetic polyvinylpyrrolidone particles [79].

2.5.5. HIGHLY SPECIFIC ADSORBENTS IN R&D AND ANALYTICAL CHEMISTRY

Introduction

Most of the adsorption processes discussed in the previous chapters are performed on a large scale for commercial processes. Adsorption, and more specifically chromatography, is an ubiquitous technique in labs all around the world. In contrast to industrial bulk separations, chromatography in research is often used for qualitative or quantitative analysis of complex mixtures of high-value chemicals with concentrations going as low as ppm and ppb levels. Understandably, complex separations of e.g. two stereoisomers require more specific, expensive adsorbents. Therefore, many novel adsorbents are invented, synthesized and investigated for

research and analytical purposes. Many of these adsorbents are not yet implemented in pilot-scale or large-scale commercial separations, but hold great premise for complex separations at lab scale where selectivity and specificity often are more important than process times and economics.

Cyclodextrin-based chiral stationary phases

Cyclodextrins are a class of cyclic oligosaccharides, forming macrocyclic rings of glucose subunits. There are three types of cyclodextrins, called α, β and γ, having 5, 6 or 7 glucose units per macrocycle, respectively. Cyclodextrins (CDs) have been used to prepare stationary phases for HPLC separation since a few decades. The cavities formed by the macrocyclic glucose rings give these CDs a unique structure and the possibility to form inclusion complexes with a large variety of organic and inorganic guest molecules. The guest-host interactions and corresponding affinity can be heavily influenced by chemical modification of the hydroxyl groups on the glucose units. Crosslinking the macrocycles by aromatic linkers can for instance render the cavities more hydrophobic, implement steric constraints and/or introduce acid/base moieties. The formation of these inclusion complexes is therefore often highly selective, making them very attractive for chromatographic separations [80]. Modified CDs even have the potential to separate chiral enantiomers, hence the wide-spread application of CDs in the chiral resolution of racemic compounds, e.g. in pharmaceutical, agrochemical and food industries. The CDs can be applied as either mobile phase additives or chiral stationary phases, with the latter being the most common approach. CD based chiral stationary phases can be used in both GC and HPLC applications, the latter being more common. Chiral HPLC involving chiral CD stationary phases is now one of the most important techniques for enantioseparations, and various novel adsorbents have been synthesized and immobilized onto silica surfaces (via physical coating or covalent bonding) for the packing of adsorbent columns. Due to the formation of robust inclusion complexes and the facile modification of CDs with selective functional groups, the number of CD derivates and corresponding analytes (both chiral and achiral) that can be separated is very extensive and beyond the scope of this chapter. Ongoing research in CD for HPLC focuses on fast enantioseparations by developing sub-micron or nanoscale porous supports and on the stable integration and combination of multiple (novel) chiral selectors for ultra-high performance LC [81]. In addition to CDs, other macrocyclic hosts with a cavity that can be selective for the inclusion of particular guests have been developed and studied. Examples of novel, synthetic macrocycles are crown ethers, calixarenes and pillararenes. Together with cyclodextrines, these macrocyclic hosts have been used for various analytical and

adsorptive applications, including the detection and selective removal of organic micropollutants [82].

2.6. Cited references

1. Nic, M. (2006) *IUPAC Compendium of Chemical Terminology: The Gold Book*, International Union of Pure and Applied Chemistry.
2. Crittenden, B., and Thomas, J.W. (1998) *Adsorption Technology and Design*, Butterworth-Heinemann.
3. Seidel-Morgenstern, A. (2005) Preparative Gradient Chromatography. *Chemical Engineering & Technology*, **28** (11), 1265–1273.
4. Rajendran, A., Paredes, G., and Mazzotti, M. (2009) Simulated moving bed chromatography for the separation of enantiomers. *Journal of Chromatography A*, **1216** (4), 709–738.
5. Barker, P.E., and Ganetsos, G. (1988) Chemical and Biochemical Separations Using Preparative and Large Scale Batch and Continuous Chromatography. *Separation and Purification Methods*, **17** (1), 1–65.
6. Schlinge, D., Scherpian, P., and Schembecker, G. (2010) Comparison of process concepts for preparative chromatography. *Chemical Engineering Science*, **65** (19), 5373–5381.
7. Guiochon, G. (2002) Preparative liquid chromatography. *Journal of Chromatography A*, **965** (1), 129–161.
8. Aniceto, J.P.S., and Silva, C.M. (2015) Preparative Chromatography: Batch and Continuous, in *Analytical Separation Science*, American Cancer Society, pp. 1207–1313.
9. Gembicki, S.A., Rekoske, J., Oroskar, A., and Johnson, J. (2002) Adsorption, Liquid Separation. *Kirk-Othmer Encyclopedia of Chemical Technology*.
10. Broughton, D., Neuzil, R., Pharis, J., and Brearley, C. (1970) Parex Process for Recovering Paraxylene. *Chem. Eng. Prog.*, **66** (9), 70-+.
11. Chin, C.Y., and Wang, N.-H.L. (2004) Simulated Moving Bed Equipment Designs. *Separation & Purification Reviews*, **33** (2), 77–155.
12. Neuzil, R.W. (1982) Process for the separation of meta-xylene. United States US4326092A, filed Jul. 17, 1980 and issued Apr. 20, 1982.
13. Broughton, D. (1968) Molex - Case History of a Process. *Chem. Eng. Prog.*, **64** (8), 60
14. Rice, L., Sohn, S., and Kulprathipanja, S. (2006) Ethylene production by steam cracking of normal paraffins. United States US20060205988A1, filed Mar. 11, 2005 and issued Sep. 14, 2006.
15. Foley, T.D., and Sohn, S.W. (2004) Ethylene production by steam cracking of normal paraffins. World Intellectual Property Organization WO2002036716A8, filed Oct. 26, 2001 and issued Mar. 4, 2004.
16. Bieser, H.J. (1977) Process for separating normal paraffins. United States US4006197A, filed Nov. 19, 1975 and issued Feb. 1, 1977.
17. Tajbl, D.G., Kanofsky, J.S., and Braband, J.M. (1987) UOP's OLEX Process: New Applications. *Energy Process/Canada*, **72** (5), 61–63.
18. Neuzil, R.W., and Kulprathipanja, S. (1984) Separation of C4 olefins. United States US4455445A, filed Dec. 20, 1982 and issued Jun. 19, 1984.
19. Mori, T., Tsuchiya, T., Noguchi, Y., Yamamoto, T., Takeuchi, I., Matsumura, K., Akita, S., Sando, K., Kanaoka, M., Otani, S., and Iwamura, T. (1973) Separation process of components of feed mixture utilizing solid sorbent. United States US3761533A, filed Jul. 20, 1971 and issued Sep. 25, 1973.
20. Neuzil, R.W., and Priegnitz, J.W. (1980) Process for separating a ketose from an aldose by selective adsorption. United States US4226977A, filed May 27, 1976 and issued Oct. 7, 1980.

21. Pollock, A.W. (1958) Separation of aromatic from saturate hydrocarbons. United States US2856444A, filed Apr. 13, 1956 and issued Oct. 14, 1958.
22. Ching, C.B., Lim, B.G., Lee, E.J.D., and Ng, S.C. (1993) Preparative resolution of praziquantel enantiomers by simulated counter-current chromatography. *Journal of Chromatography A*, **634** (2), 215–219.
23. Cunha, F.C., Secchi, A.R., Souza, M.B. de, and Barreto, A.G. (2019) Separation of praziquantel enantiomers using simulated moving bed chromatographic unit with performance designed for semipreparative applications. *Chirality*, **31** (8), 583–591.
24. Ahmadian, H., Assenza, S.P., Brosen, P., Cox, G., Dapremont, O., Geiser, F., Hariharan, S., Lee, J., Nair, U., Nielsen, O., Pedersen, H., Petersen, H., Sommer, M.B., and Suteu, C. (2009) Method for the preparation of Escitalopram. AU2009200448A1, filed Feb. 6, 2009 and issued Mar. 5, 2009.
25. Futagawa, T., Canvat, J.-P., Cavoy, E., Deleers, M., Hamende, M., and Zimmermann, V. (2000) Process for the preparation of levetiracetam. United States US6107492A, filed May 7, 1999 and issued Aug. 22, 2000.
26. Hauck, W., Adam, P., Bobier, C., and Landmesser, N. (2008) Use of large-scale chromatography in the preparation of armodafinil. *Chirality*, **20** (8), 896–899.
27. McCoy, M., Gish, E., Behr, H., Lomas, S., and Jacob, M. Chiral Separation of the Drug Product Sertraline Hydrochloride on Lux® Amylose-1 According to Ph. Eur. Monograph 1705. 4.
28. Zinnen, H.A., and Gattuso, M.J. (2002) Process for preparation of pharmaceutically desired sertraline and sertraline analogs. United States US6455736B1, filed Nov. 3, 2000 and issued Sep. 24, 2002.
29. Mun, S., and Wang, N.-H.L. (2008) Optimization of productivity in solvent gradient simulated moving bed for paclitaxel purification. *Process Biochemistry*, **43** (12), 1407–1418.
30. Lin, K., Nannini, M., Punnoose, E., Sampath, D., Wallin, J., and Patel, P. (2017) Combinations of akt inhibitor compounds and chemotherapeutic agents, and methods of use. United States US20170157124A1, filed Feb. 21, 2017 and issued Jun. 8, 2017.
31. Subramanian, G. (2008) Chiral Separation Techniques: A Practical Approach, John Wiley & Sons.
32. Pflum, D.A., Wilkinson, H.S., Tanoury, G.J., Kessler, D.W., Kraus, H.B., Senanayake, C.H., and Wald, S.A. (2001) A Large-Scale Synthesis of Enantiomerically Pure Cetirizine Dihydrochloride Using Preparative Chiral HPLC. *Org. Process Res. Dev.*, **5** (2), 110–115.
33. Ruthven, D.M., and Ching, C.B. (1989) Counter-current and simulated counter-current adsorption separation processes. *Chemical Engineering Science*, **44** (5), 1011–1038.
34. Carta, G., and Pigford, R. (1986) Periodic Countercurrent Operation of Sorption Processes Applied to Water Desalination with Thermally Regenerable Ion-Exchange Resins. *Industrial & Engineering Chemistry Fundamentals*, **25** (4), 677–685.
35. Ching, C., Hidajat, K., Ho, C., and Ruthven, D. (1987) Modeling of a Simulated Countercurrent Adsorption Process. *React. Polym.*, **6** (1), 15–20.
36. Migliorini, C., Gentilini, A., Mazzotti, M., and Morbidelli, M. (1999) Design of Simulated Moving Bed Units under Nonideal Conditions. *Ind. Eng. Chem. Res.*, **38** (6), 2400–2410.
37. Thommes, M., Kaneko, K., Neimark, A.V., Olivier, J.P., Rodriguez-Reinoso, F., Rouquerol, J., and Sing, K.S.W. (2015) Physisorption of gases, with special reference to the evaluation of surface area and pore size distribution (IUPAC Technical Report). *Pure Appl. Chem.*, **87** (9–10), 1051–1069.

38. Benhamou, A., Baudu, M., Derriche, Z., and Basly, J.P. (2009) Aqueous heavy metals removal on amine-functionalized Si-MCM-41 and Si-MCM-48. *Journal of Hazardous Materials*, **171** (1), 1001–1008.
39. Voorde, B.V. de, Bueken, B., Denayer, J., and Vos, D.D. (2014) Adsorptive separation on metal–organic frameworks in the liquid phase. *Chemical Society Reviews*, **43** (16), 5766–5788.
40. Bhattacharya, N. (2017) Advances in Aromatics Technology: Lowers Paraxylene Cost of Production.
41. Zhu, F. (Xin X.), Johnson, J.A., Ablin, D.W., and Ernst, G.A. (2019) *Efficient Petrochemical Processes: Technology, Design and Operation*, John Wiley & Sons.
42. Meyers, R.A. (2003) *Handbook of Petroleum Refining Processes*, McGraw Hill Professional.
43. Spiller, J.C.A. (1958) Paraxylene purification system. United States US2866833A, filed Sep. 14, 1953 and issued Dec. 30, 1958.
44. Ash, G., Barth, K., Hotier, G., Mank, L., and Renard, P. (1994) Eluxyl: a new paraxylene separation process. *Revue de l'Institut français du pétrole*, **49** (5), 541–549.
45. Kulprathipanja, S. (1999) Process for adsorptive separation of metaxylene from xylene mixtures. United States US5900523A, filed Aug. 8, 1997 and issued May 4, 1999.
46. Kulprathipanja, S. (2010) *Zeolites in Industrial Separation and Catalysis*, John Wiley & Sons.
47. Derosset, A.J. (1975) Process for the separation of ethylbenzene. United States US3917734A, filed Apr. 8, 1974 and issued Nov. 4, 1975.
48. Neuzil, R.W., and Rosback, D.H. (1976) Process for the separation of cresol isomers. United States US3969422A, filed Feb. 19, 1975 and issued Jul. 13, 1976.
49. Kulprathipanja, S., and Neuzil, R.W. (1983) Process for separating normal paraffins using silicalite adsorbent. United States US4367364A, filed Jul. 30, 1981 and issued Jan. 4, 1983.
50. Neuzil, R.W., and Rosset, A.J.D. (1970) Olefin separation process. United States US3510423A, filed Apr. 5, 1968 and issued May 5, 1970.
51. Rosback, D.H., and Neuzil, R.W. (1977) Olefin separation process. United States US4036744A, filed Jul. 28, 1975 and issued Jul. 19, 1977.
52. ClinCalc DrugStats Database.
53. Dapremont, O., Geiser, F., Zhang, T., Guhan, S.S., Guinn, R.M., and Quallich, G.J. (2002) Process for the production of enantiomerically pure or optically enriched sertraline-tetralone using continuous chromatography. United States US6444854B1, filed Apr. 27, 1999 and issued Sep. 3, 2002.
54. Berger, L., Duval, R., Taillasson, P., Weber, I., and Wick, A. (2004) Process for the preparation of optically pure or enriched racemic tetralone. United States US6683220B2, filed Sep. 18, 2002 and issued Jan. 27, 2004.
55. The top 20 drugs by 2018 U.S. sales. *FiercePharma*.
56. Mendiratta, S.K., Bandyopadhyay, S., and SINGH, A.K. (2014) Purification process for monoclonal antibodies. World Intellectual Property Organization WO2014207763A1, filed Jun. 25, 2014 and issued Dec. 31, 2014.
57. (2007) Antibody Purification Handbook.
58. Bonilla-Petriciolet, A., Mendoza-Castillo, D.I., and Reynel-Ávila, H.E. (2017) *Adsorption Processes for Water Treatment and Purification*, Springer.
59. Shannon, M.A., Bohn, P.W., Elimelech, M., Georgiadis, J.G., Marinas, B.J., and Mayes, A.M. (2008) Science and technology for water purification in the coming decades. *Nature*, **452** (7185), 301–310.

60. Dias, J.M., Alvim-Ferraz, M.C.M., Almeida, M.F., Rivera-Utrilla, J., and Sánchez-Polo, M. (2007) Waste materials for activated carbon preparation and its use in aqueous-phase treatment: A review. *Journal of Environmental Management*, **85** (4), 833–846.
61. EPA Drinking Water Treatability Database.
62. Badri, B.B., David, M.M., Oritani, T., Rong, H., and Veeraraghavan, B. (2011) Absorbent articles comprising treated porous particles and methods of desiccating using treated porous particles. World Intellectual Property Organization WO2011063372A2, filed Nov. 23, 2010 and issued May 26, 2011.
63. Badri, B.B., David, M.M., Rong, H., and Veeraraghavan, B. (2015) Methods of surface treating porous particles. United States US9078946B2, filed Nov. 23, 2010 and issued Jul. 14, 2015.
64. Funaki, H.A., Hirano, S.S., Kamiya, H., Nagatomo, K., Nishimura, Y., Ohno, S., Uehara, M., and Yanase, K. (2005) Process for the recovery of fluorine-containing emulsifiers. European Union EP1514848A1, filed Jun. 19, 2003 and issued Mar. 16, 2005.
65. Fuda, K., Matsunaga, T., Kamiya, T., and Omori, K. (2002) Method of treating fluorine compound and treated substance. World Intellectual Property Organization WO2002010105A1, filed Jul. 26, 2001 and issued Feb. 7, 2002.
66. Bruzzano, S., Somborn-Schulz, A., Möhle, E., Fastabend, A., and Volkert, B. (2013) Adsorbens zur Abtrennung fluorierter organischer Verbindungen aus kontaminierten Fluiden, Verfahren zu dessen Herstellung und Verwendung desselben. Germany DE102011114952A1, filed Oct. 6, 2011 and issued Apr. 11, 2013.
67. Bieser, H.J., and Rosset, A.J.D. (1977) Continuous Countercurrent Separation of Saccharides with Inorganic Adsorbents. *Starch - Stärke*, **29** (11), 392–397.
68. Paananen, H., Heikkila, H., Puuppo, O., Koivikko, H., Monten, K.-E., Manttari, M., and Nystrom, M. (2004) Process for recovering betaine. United States US20040006222A1, filed Feb. 25, 2003 and issued Jan. 8, 2004.
69. Paananen, H., Hyöky, G., Cornelius, G., and Cotillon, M. (2000) Multiple value-added products using the FAST Separation Technology. *International Sugar Journal (Worldwide Edition)*, **102** (1213), 26–30.
70. Masuda, T., Sonobe, T., Matsuda, F., and Horie, M. (1993) Process for fractional separation of multi-component fluid mixture. United States US5198120A, filed Dec. 18, 1990 and issued Mar. 30, 1993.
71. Inamuddin, D., and Luqman, M. (2012) *Ion Exchange Technology II: Applications*, Springer Science & Business Media.
72. Konetzke, G.D.R.N.D.-C., Schmidt, K.D.R.N.D.-C., Theoleyre, M.-A., and Weidemann, R.D.-I. (2005) Verfahren zur Herstellung von Sorbitolen aus Standard-Glucose. European Union EP1176131B1, filed Jul. 19, 2001 and issued Mar. 9, 2005.
73. An, S.C., Jee, H.S., and Doh, M.H. (1998) Process for obtaining, by separation, highly pure water-soluble polydextrose. United States US5831082A, filed Oct. 17, 1996 and issued Nov. 3, 1998.
74. Straathof, A.J.J. (2011) The Proportion of Downstream Costs in Fermentative Production Processes, in *Comprehensive Biotechnology*, Elsevier, pp. 811–814.
75. López-Garzón, C.S., and Straathof, A.J.J. (2014) Recovery of carboxylic acids produced by fermentation. *Biotechnology Advances*, **32** (5), 873–904.
76. Lee, H.-J., Xie, Y., Koo, Y.-M., and Wang, N.-H.L. (2004) Separation of Lactic Acid from Acetic Acid Using a Four-Zone SMB. *Biotechnol Progress*, **20** (1), 179–192.
77. Van den Bergh, M., Van de Voorde, B., and De Vos, D. (2017) Adsorption and Selective Recovery of Citric Acid with Poly(4-vinylpyridine). *ChemSusChem*, **10** (24), 4864–4871.

78. Leiper, K.A., Stewart, G.G., McKeown, I.P., Nock, T., and Thompson, M.J. (2005) Optimising Beer Stabilisation by the Selective Removal of Tannoids and Sensitive Proteins. *Journal of the Institute of Brewing*, **111** (2), 118–127.
79. Oliver, G. (2012) *The Oxford Companion to Beer*, Oxford University Press, USA.
80. Hinze, W.L. (1981) Applications of Cyclodextrins in Chromatographic Separations and Purification Methods. *Separation and Purification Methods*, **10** (2), 159–237.
81. Xiao, Y., Ng, S.-C., Tan, T.T.Y., and Wang, Y. (2012) Recent development of cyclodextrin chiral stationary phases and their applications in chromatography. *Journal of Chromatography A*, **1269**, 52–68.
82. Zheng, Z., Yu, H., Geng, W.-C., Hu, X.-Y., Wang, Y.-Y., Li, Z., Wang, Y., and Guo, D.-S. (2019) Guanidinocalix[5]arene for sensitive fluorescence detection and magnetic removal of perfluorinated pollutants. *Nat Commun*, **10** (1), 1–9.

2.7. General references

Bonilla-Petriciolet, Adrián, Didilia Ileana Mendoza-Castillo, and Hilda Elizabeth Reynel-Ávila. 2017. *Adsorption Processes for Water Treatment and Purification*. Springer.

Crittenden, Barry, and John W. Thomas. 1998. *Adsorption Technology and Design*. Butterworth-Heinemann.

Faust, Samuel D., and Osman M. Aly. 2013. *Adsorption Processes for Water Treatment*. Elsevier.

Knoerzer, Kai, Pablo Juliano, and Geoffrey W. Smithers. 2016. Innovative Food Processing Technologies: Extraction, Separation, Component Modification and Process Intensification. Woodhead Publishing.

Kulprathipanja, Santi. 2010. *Zeolites in Industrial Separation and Catalysis*. John Wiley & Sons.

Meyer, Veronika R. 2004. Practical High-Performance Liquid Chromatography. John Wiley & Sons.

Meyers, Robert A. 2003. *Handbook of Petroleum Refining Processes*. McGraw Hill Professional.

Rousseau, Ronald W. 1987. *Handbook of Separation Process Technology*. John Wiley & Sons.

Ruthven, Douglas M. 1984. Principles of Adsorption and Adsorption Processes. John Wiley & Sons.

Schmidt-Traub, H. 2006. Preparative Chromatography: Of Fine Chemicals and Pharmaceutical Agents. John Wiley & Sons.

Subramanian, Ganapathy. 2008. *Chiral Separation Techniques: A Practical Approach*. John Wiley & Sons.

Worch, Eckhard. 2012. Adsorption Technology in Water Treatment: Fundamentals, Processes, and Modeling. Walter de Gruyter.

Zhu, Frank (Xin X.), James A. Johnson, David W. Ablin, and Gregory A. Ernst. 2019. *Efficient Petrochemical Processes: Technology, Design and Operation*. John Wiley & Sons

CHAPTER 3

ADSORPTION AND SELECTIVE RECOVERY OF CITRIC ACID WITH POLY(4-VINYLPYRIDINE)

Matthias Van den Bergh[a], Ben Van de Voorde[a], Dirk De Vos[a]

With permission from Wiley, adapted from:

ChemSusChem, 2017, vol 10 (24), p 4864-4871

[a] M. Van den Bergh, B. Van de Voorde, Prof. D. De Vos
Centre for Membrane Separations, Adsorption, Catalysis and Spectroscopy for Sustainable Solutions (cMACS)
KU Leuven
Celestijnenlaan 200F, 3001 Leuven, Belgium

Abstract

Citric acid (CA) is an important organic acid that is produced on a large scale by fermentation. Current methods to recover CA from the fermentation broth require large amounts of chemicals and produce considerable amounts of waste, while not all CA can be recovered. The use of adsorbents can increase the degree of product recovery and reduce chemical consumption and waste generation. In this work poly(4-vinylpyridine) (PVP) is evaluated as adsorbent for CA recovery. It has a high adsorption capacity (>30 wt.%) at low pH and a high selectivity for CA at moderate pH in the presence of sulfate anions, two conditions that are frequently encountered during CA recovery. PVP could be efficiently regenerated after adsorption using simple alcohols like methanol and ethanol. Considering selectivity and regeneration, PVP distinctly outperforms more common adsorbents for organic acids, like commercial strongly and weakly basic anion exchangers. The desirable adsorptive features of PVP for CA can be attributed to the low basicity of the pyridine group.

Contributions

M.V.d.B., B.V.d.V. and D.D.V. conceived the study. All experiments were performed by M.V.d.B., who also wrote the paper. D.D.V. supervised the work.

3. Adsorption and Selective Recovery of Citric Acid with Poly(4-vinylpyridine)

3.1. Introduction

Citric acid (CA) is a tricarboxylic acid with widespread applications in a variety of fields. Most of its production goes to the food industries, where it is used as an acidulant, antioxidant, preservative and buffering and flavouring agent in beverages and food products. Another significant fraction goes to the pharmaceutical industries, where it is often applied as an effervescent and flavouring agent for medicines.[1] Global CA production rose above 1.7 million tons in 2007, making it the most produced organic acid worldwide on a mass basis.[2] The global market for CA is still expanding steadily, as witnessed by an annual increase in production of 5%.[3] CA production will further benefit from an increasing market share of bio-based chemicals in the chemical industry. With current attention to limiting greenhouse gas emissions and petroleum dependency, the share of renewable organic acids is expected to rise. Organic acids, including CA, are a key group among the bio-based chemicals. Because of their functional groups, they have high potential as chemical building blocks.[4]

CA production is almost completely based on fermentation.[5] An important part of any fermentation process is downstream processing (DSP). The goals of DSP are obtaining a high purity of the end product while maintaining a high degree of recovery. Modern DSP techniques also aim at low consumption of energy and chemicals and try to reduce waste production as much as possible.[6] Since DSP costs typically contribute to 30-40% of the total production cost, a competitive recovery process is critical to make CA production economically viable.[7] Because several unwanted by-products can be formed during fermentation, selective recovery of the CA product is of utmost importance but very challenging.[8] The conventional method for industrial CA recovery is a multi-step process, based on the precipitation of CA from the fermentation broth (**Figure 3.1**).[9]

Because fermentation of CA is performed at low pH (pH 2), the acid molecules are present in their protonated form (denoted as H_3CA).[10] After clarification of the fermentation broth, $Ca(OH)_2$ is added to convert CA into an insoluble carboxylate salt. The precipitate is filtered off and reconverted to the carboxylic form by acid treatment with sulfuric acid, yielding 1.5 moles of gypsum ($CaSO_4 \cdot H_2O$) as low value by-product for every mole of CA. The final step is the crystallization of CA from aqueous solution. Not all CA is recovered during precipitation, due to the low

aqueous solubility of calcium citrate (0.96 g/l at room temperature (RT)).[11] Also during acid treatment and crystallization, a fraction of CA is not recovered. These loss streams, together with the high consumption of acids and bases and the generation of gypsum as waste product considerably increase production costs and reduce the sustainable character of fermentative CA production, thereby driving the search for new, enhanced recovery techniques.

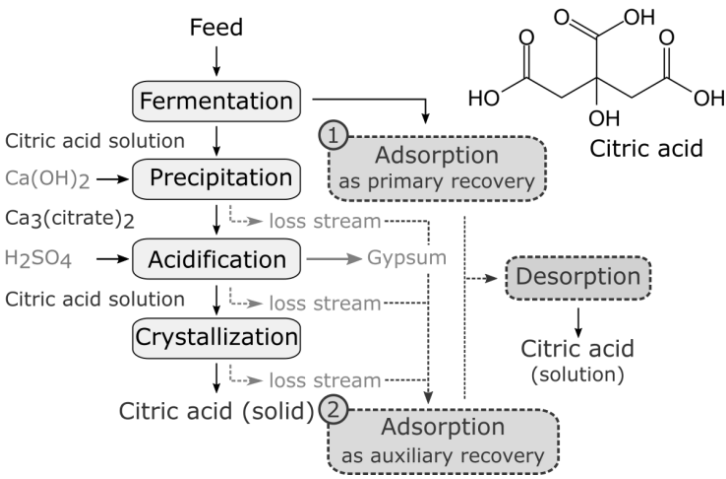


Figure 3.1: Overview of the conventional recovery of citric acid (CA). Adsorbents can be applied either directly after the fermentation as the primary mean of recovery (box 1) or as auxiliary mean to reduce loss streams, further down the recovery process (box 2). A regeneration step (i.e. desorption) is needed to recover the adsorbed acid.

The use of adsorbents can increase the degree of CA recovery and reduce the consumption of chemicals as well as waste production. Adsorbents can be applied either directly after fermentation (at low pH) or after primary recovery (at moderate pH). Adsorption can be considered as the primary strategy for carboxylic acid recovery (**Figure 3.1**, box 1) or as an auxiliary mean to reduce loss streams (**Figure 3.1**, box 2). Common adsorbents for organic acids are strong and weak anion exchangers such as Amberlite® IRA-900 and Amberlite® IRA-67, respectively.[12] These commercial anion exchangers have high adsorption capacities for carboxylic acids and are stable in normal process conditions.[13] Gluszcz *et al.* (2004) investigated 18 different ion exchange resins for the adsorption of citric acid, with the weak anion exchange resin IRA-67 showing the highest adsorption capacity.[12] However, these commercial ion exchangers often show only low or moderate selectivity for the desired organic acid compared to other organic and inorganic anions.[14] This is of specific importance for CA recovery, since the acid treatment of the citrate precipitate results in high sulfate concentrations. In addition,

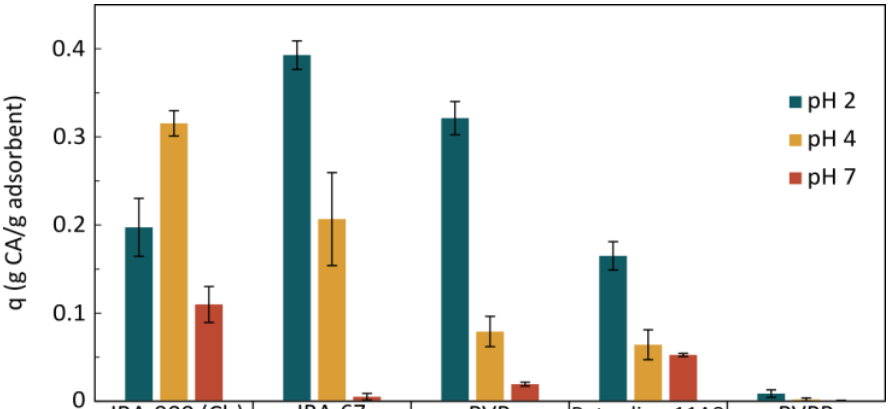
regeneration of these anion exchangers requires the use of acids and bases, increasing the cost of recovery and suppressing the benefits of adsorbents.

In this work, different adsorbents are screened for their proficiency in enhancing the degree and efficiency of CA recovery. An adsorbent ideally has high adsorption capacity and selectivity for the desired compound, is stable in adsorption conditions and can be regenerated with a 'benign' solvent such as water or ethanol, avoiding waste generation and consumption of chemicals. Poly(4-vinylpyridine) (PVP) is proposed and investigated as an excellent adsorbent for CA recovery, meeting all four criteria mentioned above. Kawabata *et al.* (1981) were the first to report on the adsorption and regeneration characteristics of PVP for a series of different organic acids.[15] Lee *et al.* (2004) and Wu *et al.* (2009) used PVP for the recovery of lactic and citric acid, respectively, in a simulated moving bed (SMB), but their reports mainly focused on SMB modelling.[16,17] Despite these promising results on the use of PVP for recovery of organic acids, specific research on PVP as adsorbent for CA recovery is very limited. This work reports on the different adsorptive features of PVP for CA recovery, with a particular focus on the mechanisms that explain the desirable adsorption behavior of PVP. Besides PVP, two other less common adsorbents were screened for their usefulness in the recovery of CA, being the zwitterionic resin Dowex® Retardion 11A8 and the very weak base polyvinylpolypyrrolidone (PVPP).

3.2. Results and discussion

3.2.1. Screening of synthetic adsorbents for CA capacity

In a first stage, all resins were screened for their adsorption capacity for CA under different pH conditions and in the presence of competing ions. In this way, a first indication was acquired of the affinity and selectivity of some less common adsorbents for CA, compared to those of IRA-900 and IRA-67 as benchmark materials. The adsorption capacities q (g CA/g adsorbent) for all resins at different pH levels (pH 2, 4 and 7; 5 g CA/l) are shown in **Figure 3.2**. The different pH levels are representative for different possible conditions during the industrial CA recovery process. The highest CA uptake is witnessed for IRA-67 (39 wt% at pH 2), followed by IRA-900 and PVP (32 wt% at pH 4 and 2, respectively). The zwitterionic resin Retardion 11A8 shows a notably lower CA uptake at all three pH levels, while there is almost no CA uptake with PVPP.



	IRA-900 (Cl-)	IRA-67	PVP	Retardion 11A8	PVPP
pH 2	0.20	0.39	0.32	0.17	0.01
pH 4	0.32	0.21	0.08	0.06	0.00
pH 7	0.11	0.01	0.02	0.05	0.00

Figure 3.2: CA adsorption capacities *q* for CA (in water and at RT) for five different resins at different pH levels. Reference adsorbents: IRA-900 (Cl^- form, strong anion exchanger) and IRA-67 (free base, weak anion exchanger). Other resins: poly(4-vinylpyridine) (PVP, weak anion exchanger), Retardion 11A8 (zwitterionic ion exchanger) and polyvinylpolypyrrolidone (PVPP). Error bars show the standard deviation of triplicate experiments.

While CA uptake for IRA-900 reaches a maximum around pH 4, CA adsorption is reduced with increasing pH for all other resins. This observation is in agreement with the different exchange mechanisms of strong and weak anion exchangers, as generally reported in literature.[6,12] A strong anion exchanger is permanently charged, so CA needs to be deprotonated at least once (pK_{a1} = 3.13) before anion exchange can take place (**Figure 3.3A**). This explains the strong increase in CA uptake for IRA-900 when shifting from pH 2 to 4. The reduction in CA uptake when going to pH 7 might be explained by a multiple-site occupancy of exchange sites by HCA^{2-} and CA^{3-} molecules (pK_{a2} = 4.76, pK_{a3} = 6.40, see **Figure 3.4** for CA speciation in function of pH), as previously suggested for dicarboxylic acids.[18] In contrast, weak anion exchangers (often containing tertiary amines, e.g. IRA-67) have no permanent charge: the protonation of the amine groups is pH dependent. At low pH, a higher fraction of the carboxylic acid is protonated and as such able to perform an acid-base reaction with the basic groups of the resin. The carboxylate anion is subsequently attracted to the resin via ion-pair coupling (**Figure 3.3C**). With increasing pH, acid-base reaction between the resin and the carboxylic acid becomes less favorable, resulting in a lower adsorption on the resin. This effect is enhanced by the increasing electrostatic repulsion between the adsorbed carboxylate anions.

Finally, the decrease in q when shifting from pH 2 to 4 is remarkably larger for PVP than for IRA-67, even though they are both weak anion exchangers. This can be explained by the weaker basicity of pyridine (pK_a 5.25) compared to that of tertiary amines (e.g. pK_a 10.75 for trimethylamine). The strength of the acid-base interaction between CA and PVP is consequently lower and PVP will be protonated to a lesser degree than IRA-67 at pH 4 and 7.

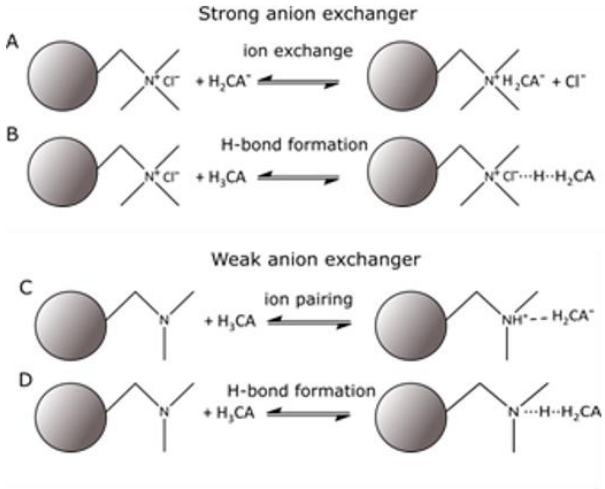


Figure 3.3: Schematic overview of the different interactions possible between CA and a strong and weak anion exchanger.

3.2.2. Screening of synthetic adsorbents for CA selectivity

If adsorbents are used during the purification of CA, selectivity towards sulfate anions is a key aspect. Sulfuric acid is used to reconvert the precipitated calcium citrate to CA, so in the end, any residual CA molecule should be recovered from a sulfate-rich background (typically 5-10 g/l). The selective adsorption of CA from a sulfate-rich rest stream is nontrivial. Not only do sulfate concentrations generally exceed CA concentrations, sulfuric acid is also a much stronger acid (pK_{a1} = -3, pK_{a2} = 2) and bears a divalent negative charge in the relevant pH range of 4-7. Even though CA can have a negative charge of -2 or -3 in this pH range (see **Figure 3.4)**, sulfate is a more compact ion and will therefore have a higher charge density. This favors the selectivity of sorbents towards sulfate ions in situations where ion exchange and ion-pairing are the dominant sorption mechanisms.

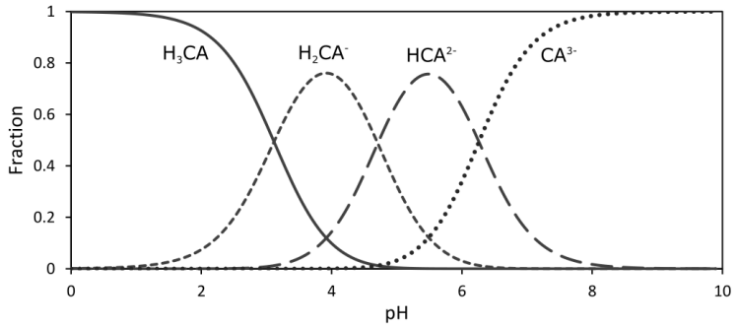
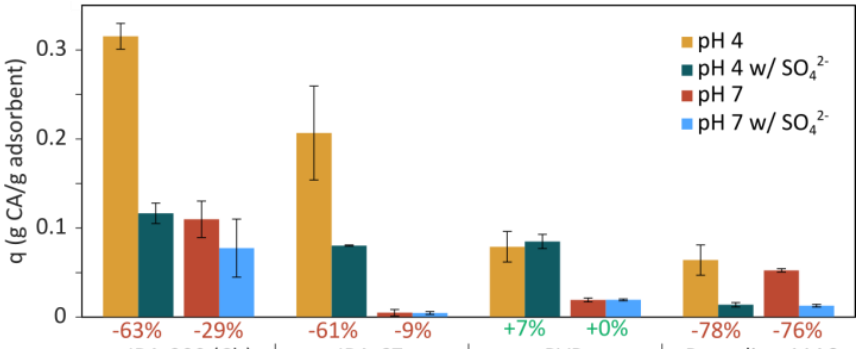


Figure 3.4: Simulated CA speciation in function of pH. (CA: pK_{a1} = 3.13; pK_{a2} = 4.76; pK_{a3} = 6.40).

The different synthetic adsorbents were screened for CA adsorption (at 5 g CA/l) with sulfate competition (8 g/l) at two different pH levels (4 and 7). All results are shown and compared to the adsorption results without sulfate competition in **Figure 3.5**. PVPP was no longer considered, since CA uptake was insignificant. **Figure 3.5** immediately shows distinct differences between PVP and the other resins. CA uptake on commercial resins like IRA-900 and IRA-67 is reduced dramatically under the influence of sulfate competition (especially at pH 4), confirming that ion exchange and ion-pairing are the dominant sorption processes on IRA-900 and IRA-67, respectively. In contrast, CA adsorption on PVP is completely unaffected by the presence of SO_4^{2-} ions. Selectivity experiments indicate an identical uptake, within the experimental error. The robustness of PVP for CA uptake in conditions of sulfate competition is a clear advantage of the resin over the commercial Amberlite® resins, even though absolute adsorption capacities at pH 4 are of the same order. This robustness indicates that PVP is a reliable adsorbent that is rather insensitive to the presence of other inorganic ions like sulfate, a key advantage for the recovery of a fermentation product from a broth. Even though robustness towards sulfate is crucial for adsorbents to be applied in industrial CA recovery processes, this feature was never investigated or reported before for PVP, nor for many other adsorbents. Nevertheless, the fact that CA uptake of PVP is unaffected by sulfate does not necessarily indicate that PVP has a specific selectivity for CA.

Figure 3.5 also shows selectivity results for the zwitterionic resin Retardion 11A8. This resin contains both carboxyl and quaternary ammonium functions. We hypothesized that especially at pH 4, when most of the CA molecules have a -1 charge, the divalent SO_4^{2-} anions would be repelled more by the anionic groups of the zwitterionic resin than the predominant H_2CA^- species, and that the net effect of attraction by positive ammonium groups and repulsion by negative carboxylate groups would favor CA adsorption in the presence of SO_4^{2-}. However **Figure 3.5** shows mediocre results for this material, both at pH 4 and at pH 7. Therefore, it is

probably incorrect to assume that the cationic and anionic functionalities of a zwitterionic resin interact separately with CA or sulfate. These functional groups are in very close proximity of each other, probably in an electrostatic interaction. In that case, the interaction within the amphoteric entity has to be broken in order for anions to adsorb on the zwitterionic resin, meaning that the attractive force of the cationic group might be more important than the repulsive effect of the anionic group. Also steric effects are very likely to play an important role, explaining why zwitterionic resins are most often employed for separation of small ions and not for large, organic molecules.[19,20]



	IRA-900 (Cl-)	IRA-67	PVP	Retardion 11A8
pH 4	0.32	0.21	0.08	0.06
pH 4 w/ SO_4^{2-}	0.12	0.08	0.08	0.01
pH 7	0.11	0.01	0.02	0.05
pH 7 w/ SO_4^{2-}	0.08	0.00	0.02	0.01

Figure 3.5: The effect of sulfate competition [8 g/l] (in water and at RT) on the adsorption capacities *q* for CA of four synthetic adsorbents. Only poly(4-vinylpyridine) (PVP) is unaffected by the presence of sulfate. Error bars show the standard deviation of triplicate experiments.

3.2.3. Regeneration of adsorbents

In order to be applied in industrial processes, an adsorbent must be easy to regenerate. Strong and weak ion exchangers are usually regenerated by a strong acid or base, but this generates chemical waste products and increases the cost of recovery. An adsorbent that can be regenerated by elution with water or e.g. an alcohol without excessive dilution of the recovered acid is much more eco-friendly while simultaneously reducing costs. However, none of the few previous reports on PVP as an adsorbent for CA investigated the use of 'benign' solvents for the regeneration of the resin. Therefore, PVP was tested for its desorption characteristics and compared to IRA-67 as the commercial benchmark (**Figure 3.6**). Both resins are weak anion exchangers. Desorption of CA is measured at RT and at

60 °C, the latter being the generally reported maximum operation temperature of commercial resins.

As expected, based on the relatively strong basicity of a tertiary amine, IRA-67 can hardly be regenerated with either water or ethanol. Also temperature has little or no influence, even though adsorption is an exothermic process so increasing the temperature can enhance desorption. PVP, on the contrary, shows far better desorption characteristics, especially in ethanol and at higher temperature. The easy desorption of CA from PVP, compared to IRA-67, can be explained by the weak basicity of the pyridine group: it is more easy to shift the acid-base equilibrium towards desorption. The large effect of the temperature swing for PVP, as seen on **Figure 3.6**, is in line with the Van 't Hoff equation which predicts a larger temperature effect for a lower reaction enthalpy. Accordingly, the stronger basicity of IRA-67 results in a lower temperature effect for the desorption from this resin.

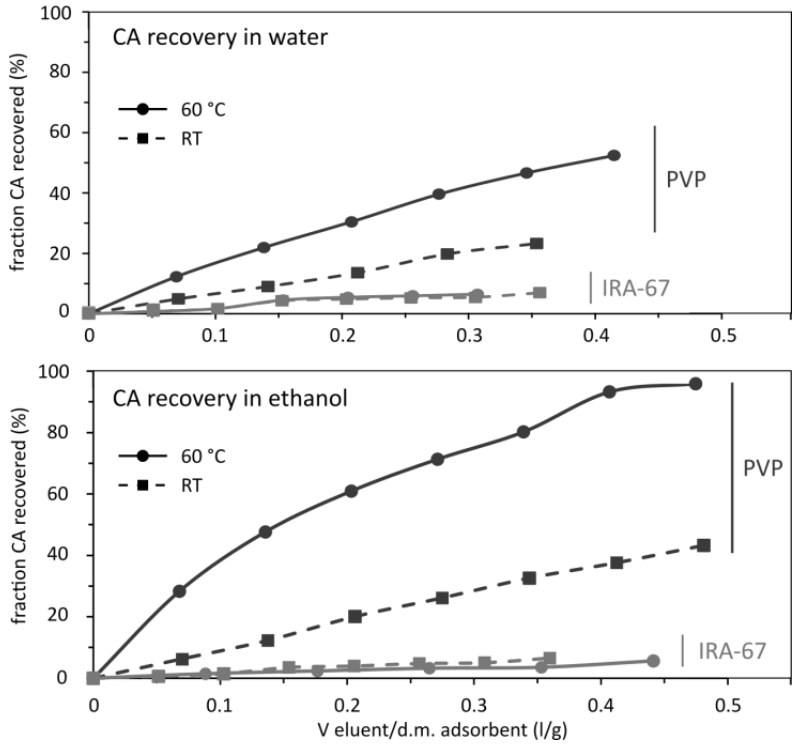


Figure 3.6: Desorption of CA from PVP and IRA-67 by elution with water and ethanol at RT and at 60 °C.

Ethanol was selected as a reference alcohol to compare the difference in desorption behavior between PVP and IRA-67. Other organic solvents were screened at RT for the desorption of PVP in order to select the best eluent (**Figure 3.7**). Methanol is distinctively the best solvent to regenerate a CA loaded PVP resin, followed by ethanol. 1-Propanol, 2-propanol, acetone and acetonitrile seemed much less effective for CA desorption. Remarkably, the desorption efficiency of the organic solvents increases with increasing acidity (i.e. decreasing pK_a, see **Table 3.1**), but it is unlikely that desorption of CA is caused by an acid-base reaction between the solvent and the resin, since CA is still much more acidic than any of the screened solvents. Besides, desorption of other fermented acids does not follow this trend.[15] The partition of CA between the resin and the solvent is influenced by hydrophobic interactions (with the carbon backbone of CA) and polar interactions such as hydrogen bonds (with the carboxyl and hydroxyl groups of CA). Especially hydrogen bonding seems to play an important role here: the desorption efficiencies of the solvents correlate with their hydrogen bond donor capacities (see $\Sigma\alpha^{H}_{2}$ values in **Table 3.1**: hydrogen bonding acidity parameters according to Abraham's scale).[21] Hydrophobicity of the solvent seems less important for the desorption of CA (see log *P* values in **Table 3.1**).

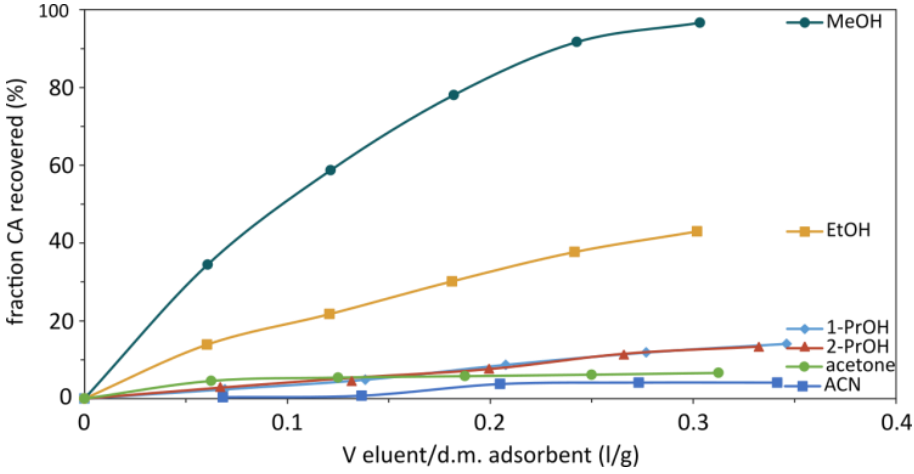


Figure 3.7: Screening of different organic solvents for the regeneration of PVP at RT. MeOH = methanol; EtOH = ethanol; 1-PrOH = 1-propanol; 2-PrOH = 2-propanol; ACN = acetonitrile.

Clearly, CA seems to have the best partitioning behavior in methanol, which is backed by some reports in literature stating that methanol is a good extractant for CA in liquid-liquid separations.[22,23] Methanol, however, is toxic and unfit for consumption, so it might not be the first choice for the recovery of a product with pharmaceutical and food applications. Taking this into account, desorbing a loaded PVP resin with ethanol at elevated temperature is a very good and efficient

alternative, especially since the effect of a temperature swing in methanol appeared to be very limited. Regardless the choice of ethanol or methanol, PVP completely outperforms a more common weak anion exchanger like IRA-67. The regeneration of a strong anion exchanger like IRA-900 will be even harder, being a major drawback of these common anion exchangers. Even though CA desorption from a PVP resin is efficient, further processing is still needed to recover CA in its pure form. Solvent evaporation and crystallization are commonly used to obtain pure CA monohydrate crystals.[6]

Table 3.1: pK_a, $\Sigma\alpha^{H}_2$ and log P values of the different solvents tested for the regeneration of PVP. MeOH = methanol; EtOH = ethanol, 1-PrOH = 1-propanol; 2-PrOH = 2-propanol; ACN = acetonitrile.

Solvent	MeOH	EtOH	1-PrOH	2-PrOH	acetone	ACN
pK_a	15.5	15.9	16	16.5	19.2	25
$\Sigma\alpha^{H}_2$	0.43	0.37	0.37	0.33	0.04	0.07
log *P*	-0.69	-0.18	0.33	0.05	-0.04	-0.33

3.2.4. Adsorption isotherms and mechanisms

PVP has shown a high adsorption capacity for CA at low pH, a good robustness against sulfate competition at moderate pH and a favorable desorption behavior. To explain these adsorption characteristics and their differences with typical strong and weak anion exchangers, the adsorption mechanism and behavior of CA on the different resins were investigated. Firstly, the anion exchange capacity (AEC) of IRA-900, IRA-67 and PVP was measured by potentiometric titrations using HCl or KOH as a titrant (**Table 3.2**). The AEC gives an indication of the total capacity to recover ions from solution, regardless of the exchange or adsorption mechanism. Remarkably, the measured AEC of PVP is much higher than that of IRA-900 and IRA-67, even though this does not result in a much higher adsorption capacity for CA, as presented earlier. The high AEC of PVP can be attributed to the fact that the pyridine groups are an inherent part of the resin matrix, thus minimizing the monomer weight, whereas for IRA-900 and IRA-67, the specific functional groups are introduced onto the aromatic polymer structure after the proper polymerization. Also remarkable is the deviation between the advertised and measured AEC, indicating that not all functional groups of the resins are available for ion exchange under the conditions of the potentiometric titration.

To compare the different ion exchange resins and their sorption behavior, isotherms were constructed for different resins and at different pH levels (**Figure 3.8**). All data were fitted to the Langmuir or Freundlich adsorption models, resulting in a set of model parameters (see **Table 3.3**). Q_{max} and K_L are Langmuir parameters and indicate

the maximum adsorption capacity and affinity, respectively, of the adsorbent. K_F and n, on the other hand, are Freundlich parameters. K_F is an indicator for the adsorption capacity, while n represents the heterogeneity of the adsorption. All isotherms could be very adequately plotted by the Langmuir model, except for IRA-67 at pH 6 and for PVP at pH 4. These isotherms had a much better fit to the Freundlich model. Several isotherms had good fits to both models. This is possible, because Langmuir and Freundlich are no contradicting models. Langmuir is a simplistic, theory-based model that assumes homogeneous adsorption sites and no multilayer adsorption, while Freundlich is an empirical model that allows for heterogeneous adsorption sites and multilayer adsorption. [18,24]

Table 3.2: Anion exchange capacity (AEC) of the different resins, as stated by the manufacturer and according to our own potentiometric titrations. No product info for the AEC of PVP was available.

AEC [meq/g]	IRA-900	IRA-67	PVP
Product Info	3.8	6.0	n.a.
Measurement	2.6	5.3	8.2

The isotherms for IRA-900 (**Figure 3.8**, top) confirm that CA adsorption on a strong anion exchanger is largely influenced by pH. There is a maximum adsorption capacity around pH 4, when all exchange sites are occupied (100% of AEC). When shifting from pH 4 to 6, there is a large decrease in Q_{max}, while K_L rises significantly. This apparently stronger interaction confirms the multiple-site occupancy, as mentioned earlier. When two carboxylate groups of a single CA anion occupy two cationic groups of the resin, the adsorption interaction will be much stronger (hence the high K_L value), but adsorption capacity will be halved. This is also seen on the isotherms: site occupation reduces from 100% at pH 4 to <50% at pH 6.

In contrast with IRA-900, the isotherms for IRA-67 show a monotonous decrease in both capacity (Q_{max}) and affinity (K_L) with increasing pH (**Figure 3.8**, mid). The pH 6 isotherm clearly deviates from a Langmuir isotherm and is plotted according to the Freundlich model. Remarkable for this isotherm is the exponential increase of adsorption capacity with increasing equilibrium concentration, whereas Langmuir isotherms trend towards a plateau phase. This is indicative of cooperative adsorption, where CA molecules adsorb in an 'all-or-no-one' manner. This is also reflected in the small n value at pH 6: low n values (<1) indicate cooperative adsorption. The isotherms for PVP (**Figure 3.8**, bottom) are similar to those for IRA-67, since both resins are weak anion exchangers (even though they differ in basicity). No pH 6 isotherm for PVP was plotted, because almost no adsorption was measured.

If the Langmuir parameters in **Table 3.3** for PVP are compared with those for IRA-67, it can be seen that Q_{max} is higher for PVP at pH 2 and 4, in line with the higher AEC. On the other hand, K_L values are lower for PVP, reflecting the weaker acid-base interaction with the pyridine group of PVP.

Table 3.3: Model parameters obtained by fitting the adsorption data of IRA-900, IRA-67 and PVP to the Langmuir and Freundlich adsorption models. Bold parameters indicate the model with the best fit. Q_{max} [g/g] and K_L [l/g] are Langmuir parameters. Q_{max} is the maximum adsorption capacity, while K_L is an indicator of the affinity of the adsorbent. K_F [$(l/g)^{1/n}$] is the Freundlich parameter and n is the Freundlich exponent. K_F is an indicator for the adsorption capacity, while n represents the heterogeneity of the adsorption.

		Langmuir model			**Freundlich model**		
Resin	**pH**	Q_{max}	K_L	R^2	K_F	**n**	R^2
IRA-900	2	0.25	0.12	1	0.05	2.57	1
	4	0.71	0.09	0.95	0.08	1.66	0.94
	6	0.18	1.11	0.99	0.11	5.57	0.75
IRA-67	2	0.91	0.74	1	0.39	3.37	0.95
	4	0.76	0.19	0.99	0.15	2.11	0.96
	6	-0.03	-0.04	0.46	0.00	0.52	0.91
PVP	2	1.14	0.45	1	0.37	2.48	0.96
	4	1.07	0.03	0.88	0.04	1.26	0.98

The isotherms for IRA-67 and PVP are in line with the assumed acid-base reaction and subsequent ion-pairing, as generally reported for the adsorption of an organic acid onto weak anion exchangers and as discussed earlier (**Figure 3.3C**).[6,12] The decrease in adsorption capacity for an increasing pH is, according to the general assumption, explained by the lower degree of CA protonation. In that case, CA is less likely to interact with the base group of the resin, since for the tricarboxylic acid $pK_{a1} < pK_{a2} < pK_{a3}$; hence the acid-base interaction becomes weaker with every deprotonation step. This is also reflected in the decreasing K_L values when pH increases. Obviously, this model is only correct when the pH of the solution is solely governed by CA, and not by any other (stronger) acid, like e.g. sulfuric acid. In that case, the resin can be protonated by free protons available in the solution, without the involvement of CA. In addition to these acid-base and ion-pairing interactions, also hydrogen bond formation is believed to play a significant role, for any type of resin.[25] Hydrogen bonds can be formed between the OH-moiety of CA and the (halide) counter ion of a strong anion exchanger (**Figure 3.3B**), or with the nitrogen atom of an unprotonated weak anion exchanger (**Figure 3.3D**).

Insight in the different types of adsorption interactions is helpful in explaining the apparent selectivity of PVP towards CA, a remarkable and very desirable feature for the resin. No reports about selectivity of PVP for CA towards other (inorganic) anions are found in literature. There is one publication, however, that reports on the adsorption of organic acids on PVP in the presence of a strong acid. Kawabata *et al.* (1981) state that there is no decrease in adsorption of adipic acid on PVP in the presence of HCl. Based on a significant increase in pH of a test solution after contact with the resin, the authors concluded that the organic and inorganic acid were coadsorbed.[15] To investigate the selectivity of PVP for CA towards sulfate, together with the underlying mechanism, the isotherm experiments for CA adsorption on PVP were repeated in the presence of sulfate (**Figure 3.9**). These isotherms reveal an interesting feature: there is a significant decrease in CA adsorption at pH 2 due to sulfate competition, whereas there is no significant reduction in CA adsorption at pH 4. If an acid can only adsorb on PVP by a direct protonation reaction, as commonly suggested, then sulfate is unable to adsorb by itself, since it is fully deprotonated at any of the test conditions. This would also mean that adsorption of sulfate can only occur by anion exchange with a CA molecule that has previously protonated the basic group of the resin. In that case, every adsorbed sulfate molecule is at the cost of an adsorbed CA molecule, which is in contrast with the observation of high CA adsorption on PVP at pH 4. On the other hand, the reduced CA adsorption due to sulfate for PVP at pH 2 indicates that there actually is exchange of CA molecules for sulfate anions under some conditions.

If it is considered, as stated above, that PVP can be protonated by free protons from the solution, then PVP will be positively charged at pH < pK_a of the basic group (pK_a of pyridine = 5.25) and attract both CA and sulfate anions. This explains the negative impact of sulfate on CA adsorption at pH 2. At pH 4, pyridine groups will still be protonated but to a lesser extent. Because of its low basicity, the pK_a of pyridine is close to pK_{a2} (4.76) and even below pK_{a3} (6.40) of CA. This means that in the specific situation of the CA solution at pH 4, there will be both unprotonated pyridine groups and undissociated carboxyl groups of CA. This is a situation that is not encountered for IRA-67 at pH 4 or for PVP at pH 2. In this specific situation, H-bond formation and/or acid-base interactions between PVP and CA can occur, while these interactions are not possible between sulfate and PVP. This explains the selectivity of PVP for CA at pH 4, a very desirable feature since the recovery of CA at this pH level from a sulfate-rich fermentation broth is very relevant. It also shows the positive impact of lowering the basicity of a weak anion exchanger with respect to the acid that needs to be recovered. Not only does a weaker basicity facilitate an easier desorption; it also circumvents selectivity problems when adsorption is mainly (or only) governed by electrostatic interactions. IRA-67, for instance, will have a

higher degree of protonation at pH 4 because of its stronger basicity. Consequently, the adsorption of CA on IRA-67 will be largely based on electrostatic interactions, resulting in the observed negative impact of SO_4^{2-} competition.

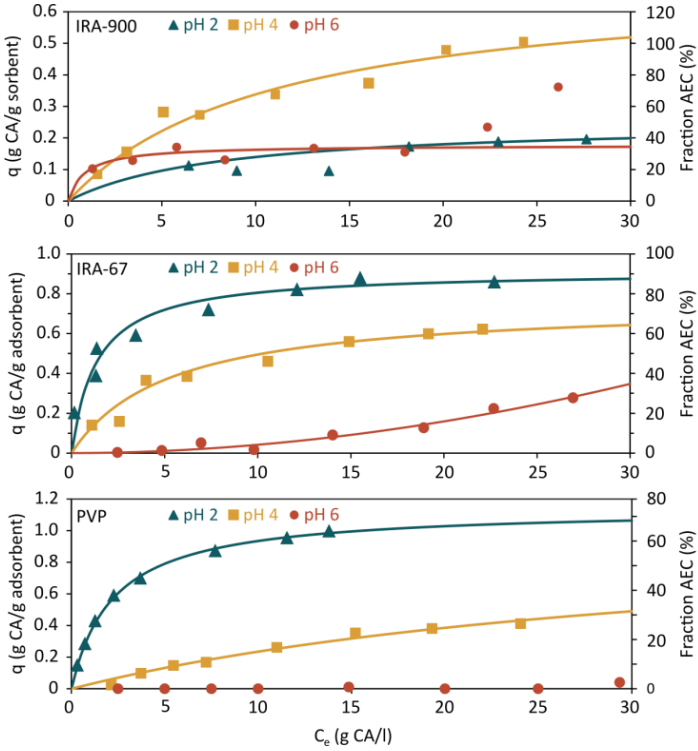


Figure 3.8: Langmuir isotherms (in water and at RT) fitted to the experimental data of the adsorption experiments for IRA-900 (top), IRA-67 (mid) and PVP (bottom). Only the pH 6 isotherm of IRA-67 and the pH 4 isotherm of PVP are fitted according to the Freundlich model. Note that the isotherms are plotted as a fraction of the anion exchange capacity (AEC) of the respective resins, so the scale of the y-axis differs.

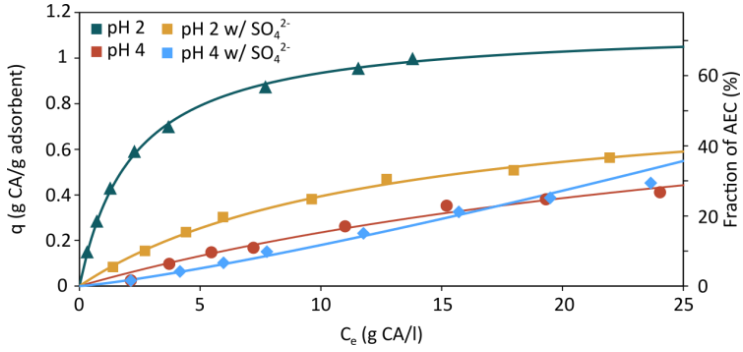


Figure 3.9: Sorption isotherms for CA on PVP (in water and at RT) with and without the presence of sulfate competition.

3.3. Conclusion

This work reports on the promising adsorption behavior of poly(4-vinylpyridine) in the recovery of citric acid, and its advantages compared to more common, commercial adsorbents for organic acids like IRA-900 and IRA-67. PVP shows a high adsorption capacity for CA at low pH (>30 wt%) and a high selectivity for CA at a moderate pH in a sulfate-rich environment. This makes PVP very suitable for the recovery of CA, either directly after fermentation (at low pH) as primary mean of recovery, or as auxiliary mean of recovery after the conventional precipitation process (at moderate pH and with high sulfate concentrations). The robustness of PVP towards sulfate competition is in contrast with other resins, which show dramatic reductions in CA adsorption in the presence of sulfate. PVP is efficiently regenerated with methanol as eluent or with ethanol at elevated temperature, while regeneration of IRA-900 and IRA-67 requires the use of acids or bases, creating salts as low value waste products. The good adsorptive features of PVP for CA recovery can be attributed to the weak basicity of the pyridine group: it facilitates an easier desorption and circumvents selectivity problems when adsorption is dominated by electrostatic interactions, as is the case for most commercial strong and weak anion exchangers. It shows the potential of fine-tuning the basicity of a weakly basic anion exchanger, with respect to the organic acid to be recovered, in optimizing the recovery procedure.

Acknowledgements

M. Van den Bergh is grateful to Fonds Wetenschappelijk Onderzoek (FWO – Vlaanderen) and Vlaamse Instelling voor Technologisch Onderzoek (VITO) for his doctoral fellowship. D. De Vos acknowledges FWO for research project funding, the Flemish government for long-term structural funding through Methusalem and Belspo (IAP-PAI 7/05) for financial support.

3.4. References

[1] C. R. Soccol, L. P. Vandenberghe, C. Rodrigues, A. Pandey, *Food Technol. Biotechnol.* **2006**, *44*, 141.

[2] G. S. Dhillon, S. K. Brar, M. Verma, R. D. Tyagi, *Food Bioprocess Technol.* **2010**, *4*, 505–529.

[3] T. V. Finogenova, I. G. Morgunov, S. V. Kamzolova, O. G. Chernyavskaya, *Appl. Biochem. Microbiol.* **2005**, *41*, 418–425.

[4] M. Sauer, D. Porro, D. Mattanovich, P. Branduardi, *Trends Biotechnol.* **2008**, *26*, 100–108.

[5] B. Max, J. M. Salgado, N. Rodríguez, S. Cortés, A. Converti, J. M. Domínguez, *Braz. J. Microbiol.* **2010**, *41*, 862–875.

[6] C. S. López-Garzón, A. J. J. Straathof, *Biotechnol. Adv.* **2014**, *32*, 873–904.

[7] A. J. J. Straathof, *Compr. Biotechnol.* **2011**, *2*, 811–814.

[8] H. Song, S. Y. Lee, *Enzyme Microb. Technol.* **2006**, *39*, 352–361.

[9] E. Heinzle, A. P. Biwer, C. L. Cooney, in *Dev. Sustain. Bioprocesses*, John Wiley & Sons, Ltd, **2006**, pp. 125–136.

[10] M. Papagianni, M. Mattey, B. Kristiansen, *Enzyme Microb. Technol.* **1999**, *25*, 710–717.

[11] R. C. Weast, M. J. Astle, W. H. Beyer, others, *CRC Handbook of Chemistry and Physics*, CRC Press Boca Raton, FL, **1988**.

[12] P. Gluszcz, T. Jamroz, B. Sencio, S. Ledakowicz, *Bioprocess Biosyst. Eng.* **2004**, *26*, 185–190.

[13] Q. Gao, F. Liu, T. Zhang, J. Zhang, S. Jia, C. Yu, K. Jiang, N. Gao, *PLOS ONE* **2010**, *5*, e13948.

[14] Y. Dai, C. J. King, *Ind. Eng. Chem. Res.* **1996**, *35*, 1215–1224.

[15] N. Kawabata, J. Yoshida, Y. Tanigawa, *Ind Eng Chem Prod Res Dev* **1981**, *20*, 386–390.

[16] H.-J. Lee, Y. Xie, Y.-M. Koo, N.-H. L. Wang, *Biotechnol. Prog.* **2004**, *20*, 179–192.

[17] J. Wu, Q. Peng, W. Arlt, M. Minceva, *J. Chromatogr. A* **2009**, *1216*, 8793–8805.

[18] K. Zhang, S.-T. Yang, *Sep. Sci. Technol.* **2015**, *50*, 56–63.

[19] P. N. Nesterenko, P. R. Haddad, *Anal. Sci.* **2000**, *16*, 565–574.

[20] E. P. Nesterenko, P. N. Nesterenko, B. Paull, *Anal. Chim. Acta* **2009**, *652*, 3–21.

[21] M. H. Abraham, P. L. Grellier, D. V. Prior, P. P. Duce, J. J. Morris, P. J. Taylor, *J. Chem. Soc. Perkin Trans. 2* **1989**, *0*, 699–711.

[22] R. P. Metivier, F. J. Francis, F. M. Clydesdale, *J. Food Sci.* **1980**, *45*, 1099–1100.

[23] N. Kawabata, S. Yasuda, T. Yamazaki, *Process for Recovering a Carboxylic Acid*, **1982**, US4323702 A.

[24] K. Y. Foo, B. H. Hameed, *Chem. Eng. J.* **2010**, *156*, 2–10.

[25] S. M. Husson, C. J. King, *Ind. Eng. Chem. Res.* **1999**, *38*, 502–511.

3.5. Experimental section

3.5.1. Materials

The resins evaluated in this study include Amberlite® IRA-900 and Amberlite® IRA-67 (both commercial products bought from Sigma-Aldrich). They are used as reference materials throughout this study. Other materials are Dowex® Retardion 11A8 (Sigma Aldrich), poly(4-vinylpyridine) (PVP, Fluka) and polyvinylpolypyrrolidone (PVPP, Sigma-Aldrich).

3.5.2. Adsorption and desorption experiments

All adsorbents were first screened with single-point triplicate measurements at a fixed CA concentration of 5 g/l (26 mM) and at three different pH levels (2, 4 and 7). pH of the CA solutions was adjusted using H_2SO_4 and KOH. K_2SO_4 was added to some samples to simulate the effect of sulfate competition at industrial relevant concentrations (8 g/l or 83 mM).

All batch adsorption experiments were performed at 298 K in 1.8 ml glass vials filled with 250 mg of sorbent material, 1.8 ml of an aqueous CA solution and a magnetic stirring bar. Prior to the adsorption experiments, all adsorbents were dried overnight at 333 K. All samples were stirred for 2h, where after equilibrium was reached. The vials were centrifuged at 4500 rpm for 15 min to separate the adsorbent from the liquid phase. Uptakes were calculated by measuring CA concentrations with High Performance Liquid Chromatography (HPLC) on an Agilent 1200 HPLC instrument, equipped with a BIO-RAD Aminex HPX-87H column (300 x 7.8 mm) at 303 K with 5 mM H_3PO_4 in Milli-Q water as mobile phase and at a flow rate of 0.6 ml/min. The column was coupled to a UV-detector (λ = 212 nm).

Adsorption isotherms were constructed with similar adsorption experiments, also ran in triplicate. CA adsorption was measured at 8 different concentrations (2.5, 5, 7.5, 10, 15, 20, 25 and 30 g CA/l) and at three different pH levels (pH 2, 4 and 6). After the experiments, all results were fitted to the Langmuir and Freundlich adsorption model and isotherms were plotted according to the model with the best fit.

For regeneration (i.e. desorption) experiments, all adsorbents were first preloaded with CA. Therefore, 12 ml vials were filled with 0.125 g of sorbent material and 10 ml of the CA solution which gave the highest uptake capacity during the screening. The vials were stirred for 2h and then centrifuged at 3000 rpm for 10 min. The supernatants were removed and the sorbents dried overnight in air at 298 K. Afterwards, the vials were filled with 10 ml of the eluent and stirred for 2h at either

298 K or 333 K. The vials were again centrifuged and the supernatants were analyzed for CA concentrations with HPLC. This desorption step was repeated at least four times for every sample.

3.5.3. Potentiometric titrations

The anion exchange capacity (AEC) of the resins was determined via potentiometric titrations. All resins were titrated forward and backward to exclude the effect of hysteresis. Ca. 1g of adsorbent was wetted with 30 ml of an electrolyte solution (1M KCl). As titrant solution, 2M HCl and 2M KOH were used for forward and backward titration, respectively. This order was reversed for the titration of IRA-900, since this strong anion exchanger has originally chloride as counter anion. Both titrant solutions had an electrolyte concentration of 1M KCl, in order to minimize electrostatic interactions. Titrant solutions were added in steps of 100 µl and pH was measured 10 min after every step. AEC values were calculated based on the inflection point of the titration curves.

CHAPTER 4

EXPLORING THE POTENTIAL OF SILICEOUS MICROPOROUS MATERIALS FOR ADSORPTION OF PFASS

Matthias Van den Bergh[a] and Dirk De Vos[a]

Unpublished results

[a] M. Van den Bergh, Prof. D. De Vos
Centre for Membrane Separations, Adsorption, Catalysis and Spectroscopy for Sustainable Solutions (cMACS)
KU Leuven
Celestijnenlaan 200F, 3001 Leuven, Belgium

Abstract

In this chapter, microporous, siliceous materials were explored for their potential as PFAS adsorbents. A selection of materials was synthesized, characterized and screened in adsorption experiments. Comparison with other microporous and mesoporous (silica-based) materials learned that i) hydrophobicity of the material and ii) adequate (micro)porosity and specific surface area appear to be key parameters for PFAS adsorption. The experiments in this chapter showed that both criteria have to be fulfilled simultaneously in order to achieve both high affinity and capacity. All-silica zeolites have no framework charge due to the absence of aluminum, but this is not sufficient: all-silica zeolite Beta showed a much higher uptake for PFOA and PFOS than a commercial, high-silica Beta 300.

Contributions

M.V.d.B. wrote the manuscript. D.D.V. supervised the work.

4. Exploring the potential of siliceous microporous materials for adsorption of PFASs

4.1. Introduction

Very recently, the European Union imposed environmental quality standards (EQSs) for PFOS and its derivates in water streams and bodies. These limitations are valid from 2018 and will be strictly monitored from 2027 onwards (see paragraph 1.6). Very likely, additional EQSs for PFOA and similar compounds will follow in the near future. These EQSs come on top of limitations on the discharge of PFASs via industrial effluent streams. These limitations are already in place for several years and vary from industry to industry. Even though the removal of PFASs from water is never easy, treating highly concentrated spills in industrial effluents is more manageable than treating large volumes of surface water with very low concentrations. Because conventional waste water treatment plants (WWTPs) are unable to remove PFASs from water, the implementation of EQSs in Belgium (as well as in many other countries) requires new and suitable techniques to remove PFASs in low concentrations from complex water matrices. More specifically, PFAS concentrations have to be reduced from a µg/L range (or mg/L range in the case of extreme contaminations) to less than 1 ng/L.[1] Several techniques, like sonolysis and electrochemical or photochemical catalysis are being explored for the degradation of PFASs in water, but they suffer from high energy demands and require several pre-treatment steps.[2–4] This makes them unsuitable for the treatment of large water volumes. In this regard, adsorption is arguably the best technique to treat large volumes while keeping energy costs modest. Even if a chemical degradation process would be considered as removal and treatment technique, adsorption would often be the go-to method as an essential preconcentration step. This makes the selection (and synthesis) of an adsorbent with adequate capacity and high selectivity for PFASs of utmost importance. In the next paragraph, the state-of-the-art background of adsorbents for PFAS removal will be outlined. The as-synthesized adsorbents in the rest of this chapter will be set against this background.

4.2. State of the art: PFAS adsorbents

Up until now, a considerable amount of research has been carried out on the isolation of PFASs from water via adsorption. Very different material types have been investigated for this application, ranging from inorganic, natural clays to synthetic, organic resins.[5,6] The current benchmark adsorbent is without a doubt activated carbon (AC), an organic and commercial adsorbent. It exists in many forms, e.g.

powder activated carbon (PAC) vs. granular activated carbon (GAC), referring to the size of the adsorbent particles.[7,8] On a weight basis, PAC has a higher adsorption capacity for PFASs (and other adsorbates) than GAC due to the higher specific surface area. Important adsorption features like porosity and surface chemistry highly depend on the method of activation (physical vs. chemical activation) and on the carbonaceous substrate material, hence the wide variety in different AC materials. AC mainly interacts with PFASs via hydrophobic interactions, but also more polar interactions between the PFAS head groups and the functionalities of the AC surface can occur. AC is a highly versatile and relatively cheap adsorbent that shows high capacity for many different target molecules; it is therefore the current benchmark adsorbent and it can be efficiently used in cases of high-concentration single-point emissions (e.g. industrial spills). It lacks in selectivity for PFASs over other organic compounds though, and it is therefore very uneconomical and impractical as adsorbent for the treatment of high volumes with low concentration of PFASs (e.g. most surface water bodies in Flanders).

Another type of organic adsorbent that is commonly used and studied for PFAS removal are the synthetic ion-exchange resins.[6,7,9–16] Since almost all perfluorinated acids are deprotonated at relevant pH levels for surface waters, they behave as anions and can be removed with anion-exchange resins. These resins contain either quaternary ammonium or tertiary amine groups which interact with the acidic groups of the PFASs. The interactions between anion-exchange resins and (non-fluorinated) organic acids, and the effects of factors like pH and ionic competition have been explained in detail in Chapter 3. The porosity (gel-type, macroporous or mesoporous) and chemical backbone (polyacrylic, polystyrene, polystyrene-divinylbenzene, among others) of the resin matrix can have a large influence on the intraparticle diffusion and uptake capacity. Various anion-exchange resins have among the highest adsorption capacities ever reported for PFASs. The highest uptake capacity for PFOS is reported by Deng *et al.* (2010) for the polyacrylic resin IRA-67 at 2500 mg/g resin.[11] Yu *et al.* (2009) note the highest exchange capacity for PFOA with 1400 mg/g resin at the polystyrene-DVB resin IRA400.[13] Also non-ionic resins can adsorb PFASs, however in much lower quantities than their anionic counterparts. The highest reported uptake for PFOA and PFOS on non-ionic resins is ca. 40 mg/g resin.[6,7]

Anion-exchange resins are widely applied in industry for the recovery of PFASs, especially in product streams and waste streams with very high PFAS concentrations. Some of these resins are patented by the industrial manufacturers of PFASs.[17–19] Similar to activated carbon, it is very difficult for anion-exchangers to obtain a high selectivity for anionic PFASs over other compounds. These resins often suffer from a

strong decline in exchange capacity in the presence of competing inorganic anions and organic matter. They are especially susceptible to the competition of divalent inorganic anions like sulfate and organic anionic compounds like sodium dodecylsulfate (SDS) and humic acid.[5,14] For instance, Zaggia *et al.* (2016) studied three different resins for the uptake of PFOA and PFOS and reported a reduction of >99.9% in PFAS adsorption for the best performing resin (Purolite® A532E) when switching from single-solute batch experiments to continuous-flow experiments with real case groundwater.[16] Additionally, the regeneration of the spent anion-exchangers is often cumbersome and requires elution with a mixed methanol and salt solution, involving the use of volatile and toxic solvents and the generation of stoichiometric amounts of waste products. The resulting waste eluate cannot always be recycled and needs to be incinerated.[5]

Also cyclodextrin-based polymers are found to adsorb PFASs in significant amounts. Xiao *et al.* (2017) report β-cyclodextrin, a macrocycle composed of seven glucose units with an uptake capacity for PFOA of 34 mg/g and an apparent 10-fold higher affinity for PFOA than activated carbon.[20] Such type of polymer is specifically constructed to target a certain adsorbate compound and is therefore called a molecular imprinted polymer (MIP). Another example of a MIP for PFAS adsorption is a chitosan-based polymer, studied by Yu *et al.* (2008). They report a maximum uptake capacity for PFOS of 280 mg/g.[21] Also cellulose-based polymers are investigated for PFAS adsorption, however, adsorption capacity of these cellulose-type polymers is rather low compared to other adsorbents. Ateai *et al.* (2018) report a maximum uptake capacity of 2.3 mg PFOA/g for poly(ethylenimine)-functionalized cellulose microcrystals. As for anion-exchangers, a strong decline of PFAS adsorption in the presence of divalent anions like sulfate is mentioned.[22]

Besides organic adsorbents, a variety of inorganic materials has been considered for the adsorptive removal of PFASs. Many of these materials can be synthetically shaped into highly dispersed structures, like metal-oxide nanoparticles or meso- and microporous silicas and zeolites for instance. This opens the door towards adsorbents with very high specific surfaces and/or porosity, hence increasing capacity and diffusion kinetics. Microporous structures may also allow shape selectivity for linear PFASs over large and branched organic molecules (e.g. humic and fulvic acids). The variety of inorganic adsorbents and the possibilities of synthetic finetuning (e.g. the combination of different metal oxides or the isomorphic substitution of a metal cation into a zeolite framework) are enormous.

Different metal oxides have shown to be capable of adsorbing PFOA and/or PFOS, even though often only with modest capacity, e.g. less than 1 wt.% of PFOS for

boehmite, a high surface aluminum oxide hydroxide (γ-AlO(OH)).[23] Nassi *et al.* (2014) studied siliceous (meso)porous materials for the adsorption of PFOA from aqueous solutions. These materials, well known in literature as MCM-41 or HMS have ordered mesopores but they lack the short range crystalline order that is defining for zeolite materials. Relatively modest uptake capacities were observed for PFOA, with maximally 8 mg PFOA per g of HMS.[24] Ochoa-Herrera and Sierra-Alvarez (2008) studied the adsorption of perfluorinated surfactants on various zeolites, in a comparative study in which GAC showed generally better performance, e.g. higher uptake capacity and higher affinity, than the zeolites studied. The best performing zeolite was a faujasite type zeolite (FAU topology) with a Si/Al ratio of 80. This material has a maximal capacity for PFOS uptake of only 105 mg/g zeolite.[8]

Lastly, there are also hybrid materials that combine organic and inorganic characteristics. An example are metal-organic frameworks (MOFs), where metal nodes are connected via organic linkers in a crystalline order. Similar to anion-exchange resins, MOFs can be used for the ion-exchange of PFASs. This is especially the case for zirconium-based MOFs (e.g. UiO-66) or chromium-based MOFs (e.g. MIL-101 (Cr)), where the positively charged metal nodes act as exchange sites. Clark *et al.* (2019) studied a highly defective UiO-66 MOF with a maximal uptake capacity for PFOS of 620 mg/g.[25] The uptake capacity of these MOFs for PFASs can be further tuned by modification of the organic linkers, e.g. amine-grafted terephthalate linkers for MIL-101 (max. uptake capacity: 782 mg PFOA/g) or fluorinated terephthalate linkers for UiO-66 (max. uptake capacity: 470 mg PFOA/g).[26,27] Related to MOFs, Ji *et al.* (2018) studied the use of covalent organic frameworks (COFs) for the uptake of PFASs. COFs are porous, crystalline polymers. They report a maximal uptake capacity of 200 mg/g for the perfluoro-compound GenX with an imine-linked, primary amine-bearing polymer.[20]

In this chapter, the potency of hydrophobic zeolites will be explored. Ochoa-Herrera and Sierra-Alvarez (2008) were the first to point out that the adsorption capacity of a Zeolite Y for PFOS increased with increasing Si/Al ratio. Nevertheless, the potential of hydrophobic high-silica and all-silica zeolites for the adsorption of PFASs has never been studied before. The lower the Al content, the higher the hydrophobicity of a zeolite; isomorphic substitution of Si^{4+} with Al^{3+} introduces a negative charge in the zeolite structure that is compensated by a counter cation. This is not the only factor though: also silanol groups (Si-OH) contribute to the hydrophilic character of a zeolite. Silanol groups are found at the crystal edges and inside the zeolite where there is a framework defect. Hence one should not only strive towards a high-silica content but also towards a defect-free framework. Since zeolites exist in many varieties, it is possible to study the influence of pore size, channel structure,

topology, Al-content, etc. on important adsorption features like capacity and selectivity. This should result in the selection of a high-silica/all-silica zeolite adsorbent for PFASs and lead to new insights in which concepts result in a high selectivity and/or capacity for fluorinated surfactants.

4.3. Results and discussion

4.3.1. Synthesis of adsorbents

The primary focus was the synthesis of all-silica zeolite Beta (*BEA), because it seemed the most relevant and promising zeolite for PFAS adsorption that can be synthesized in an all-silica variant. Its 12-membered ring openings and 3D channel structure provide an accessible and open framework. Synthesis was based on literature and carried out in fluoride media in order to maximally reduce local defects, hence increasing the hydrophobicity of the framework. The fluoride anions (F^-) act as a mineralizing agent and compensate the positive charge of the organic template, tetraethylammonium (TEA^+) in the case of zeolite Beta. The organic template is introduced in the hydroxide form into the synthesis mixture. Since F^- has a smaller radius than OH^-, charge compensation by F^- can occur inside the growing zeolite channels without sterically disrupting them.[28,29] Synthesis proved to be cumbersome without the use of seeds, even though it was described that way in literature. After several attempts, successful synthesis of all-silica zeolite beta was only achieved after adding 5 wt.% of seeds (a dealuminated CP814E-22 zeolite Beta) to the synthesis mixture. The CP814E-22 zeolite was dealuminated according to the method described by Dijkmans *et al.* (2015), resulting in zeolite Beta seeds with a SiO_2/Al_2O_3 ratio of 175.[30] XRD measurements confirmed the correct crystallographic topology of the as-synthesized material (**Figure 4.1**). Zeolite Beta actually is an intergrowth of two different but closely related crystal phases, being polymorphs A and B. Also polymorph C and other, less common types exist, but these are not always present. In a usual (i.e. not all-silica) zeolite Beta, polymorphs A and B are present in a 44:56 ratio, but in the all-silica type, enrichment of polymorph A is often seen. The XRD pattern of the as-synthesized zeolite Beta clearly shows an overlap of both the polymorph A and B pattern. It is not possible to deduce the exact ratio of polymorphs with high accuracy from XRD measurements. The presence of both sharp and broad peaks in the XRD pattern is an indication of stacking faults. This is characteristic for zeolite Beta, which is a partially disordered, crystalline material; hence the asterisk in the topology code for zeolite Beta (*BEA).[31–34] More details on the synthesis of zeolite Beta are given in the Supporting Information.

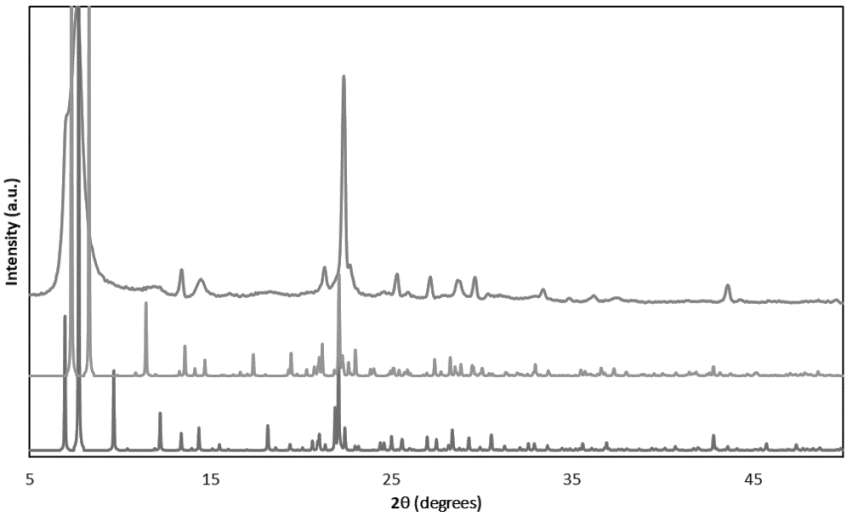


Figure 4.1: XRD plot of as-synthesized all-silica zeolite Beta (top) compared to a simulated powder plot of polymorph B (middle) and polymorph A (bottom).

Besides all-silica zeolite Beta, other high-silica and all-silica zeolites do exist. Their synthesis is sometimes (but not always) described in literature and can be very cumbersome. A selection of relevant high-silica and all-silica zeolites was synthesized in our labs. Many of these zeolites are not commercially available, since the all-silica variants of (common) zeolite types often remain rather exotic specimens. Silicalite-1 is an all-silica variant of the ZSM-5 zeolite (MFI topology). It has a 10-membered ring (10-MR) opening and 3D channels, so it is a good candidate to study the effect of pore size on the adsorption of PFASs in zeolites (cfr. zeolite Beta has a 12MR ring opening). The synthesis of this zeolite was based on literature.[35] XRD measurements confirmed the correct crystallographic structure of the as-synthesized material (**Figure 4.2**).

A high-silica chabazite (CHA) was synthesized by dr. Trees De Baerdemaeker. Chabazite has 8-membered ring openings (8-MR) and a 3D channel structure. Given the smaller cage windows, a high PFAS uptake is not really expected, but it is interesting to study the effect of pore size on PFAS adsorption. SSZ-24 is the all-silica analogue of AlPO-5 (AFI), a common aluminophosphate. It has 12-membered ring openings and a 1D channel system, so it is a good candidate to study the effect of channel structure on the adsorption of PFASs in zeolites (cfr. zeolite Beta has a 3D channel system). Synthesis procedures from literature seemed poorly reproducible, however.[36,37] An alternative recipe for the synthesis of an all-silica AFI structure was provided by Prof. Dusselier. This recipe proved to be very time-dependent: there was only a very limited time window during the crystallization stage wherein a pure

crystalline phase could be obtained. Despite many efforts, a pure phase was never obtained. The best results showed some typical AFI peaks on the XRD diffractograms, but broad amorphous shoulders were still present.

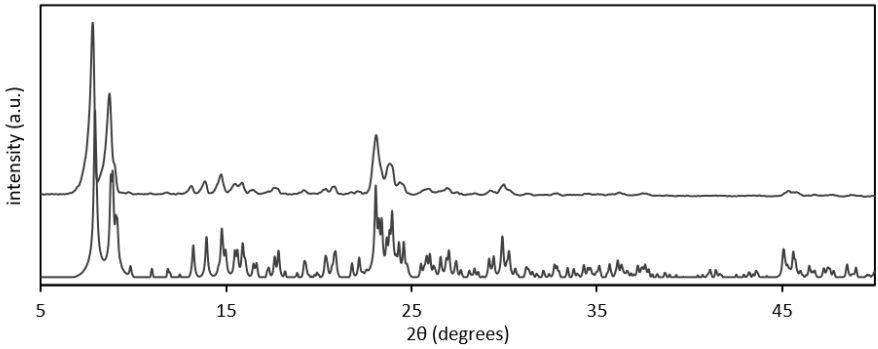


Figure 4.2: XRD plot of as-synthesized silicalite-1 (top) compared to a simulated powder plot of ZSM-5 (bottom).

Unfortunately, SSZ-24 was not the only all-silica zeolite of which the synthesis could not successfully be achieved. Also ITQ-4 (IFR, 12-MR, 1D channels) and CIT-5 (CFI, 14-MR, 1D channels) were planned for synthesis but no pure zeolite product could be obtained. This was due to difficulties during the synthesis and purification of the organic structure directing agents (SDAs), used for the all-silica variants of the abovementioned zeolites. Even though synthesis of the zeolites themselves is described in literature, preparation of the correct SDAs is largely uncovered and not straightforward.[38–41] Since successful adsorption results were obtained rather quickly for all-silica zeolite Beta (see Chapter 5), any further attempts for the successful synthesis of all-silica AFI, IFR and CFI zeolites were adjourned. Lastly, two mesoporous silica materials, being MCM-41 and SBA-15, have been synthesized with the goal of comparing high surface area mesoporous silica adsorbents with microporous all-silica zeolites. Synthesis of these materials was based on literature and turned out successfully: pore volumes and BET-surfaces of the as-synthesized materials were very well in agreement with literature data. [42–44]

4.3.2. Screening of adsorbents for PFAS adsorption

After synthesizing a selection of micro- and mesoporous, siliceous materials, they were screened and compared for their adsorption of PFOA and PFOS. These two PFAS components will act as model and reference compounds throughout a large part of this research. All adsorption experiments were performed in plastic (PP) vials, in order to reduce PFAS sorption onto glass surfaces, as often suggested in literature on PFAS analysis. The use of PTFE (coated) materials was avoided as much as

possible. Since their manufacture has often involved the use of PFASs as emulsifier, leaching of remnant PFAS can affect the adsorption results. However, during post-experiment analysis (HPLC-MS), avoidance of PTFE tubing and parts is often difficult.[45] The effect hereof is screened for by analyzing blank samples (see 4.6.1 Experimental Procedures). The ratio of adsorbent to solvent was 5 mg of adsorbent (d.m., dry mass) for 5 ml of stock solution throughout all experiments. More experimental details are given in the Supporting Information. Since Chapter 5 is fully dedicated to the exceptional adsorption behavior of all-silica zeolite Beta (and its comparison to the benchmark adsorbent activated carbon), this chapter will focus on the exploration, screening and comparison of the various siliceous adsorbents for PFAS adsorption.

All-silica zeolite Beta will show to be an excellent adsorbent for PFOA and PFOS, with not only high capacity but also a high affinity and selectivity for these compounds. On top of that, adsorption uptake is relatively fast. By comparing all-silica zeolite Beta with relatively similar materials, first evidence can be gathered about the factors that contribute to this remarkable adsorbent behavior. Strikingly, all-silica silicalite-1 (10-MR, 3D) and high-silica chabazite (8-MR, 3D) had an almost insignificant PFOA uptake, compared to all-silica zeolite Beta (**Figure 4.3**). These isotherms suggest that there is a minimal window size in order for PFOA molecules to enter the zeolite channels, and that this size limit is situated between those of a 12-MR and 10-MR window channel. This is remarkable, since the dimensions of a 10-MR window (5.1 Å x 5.5 Å for silicalite-1) are large enough to accommodate C_8-alkanes and even para-disubstituted aromatics like p-xylene.[46,47] (Chabazite, on the other hand, can only accommodate alkanes up to pentane (C_5) due to its smaller cage size.[48]) Therefore, based on the molecular dimensions of a single PFOA molecule, it was expected that PFOA could well pass 10-MR windows and would fit in the cages of e.g. silicalite-1. This expectation is wrong and might indicate that PFOA does not adsorb onto zeolite Beta as a single molecule, but for instance rather as a dimer of two PFOA molecules, axially aligned along their perfluorinated chains. This is (for now) just an hypothesis based on the adsorption isotherms of the different zeolites. Elucidation of the adsorption mechanism will be dealt with later on.

Even though PFOS adsorption on all-silica zeolite Beta is lower than PFOA uptake under identical conditions, a similar trend can be seen when comparing zeolite Beta with silicalite-1 and chabazite (see **Figure S4.1**). PFOS uptake in these 10-MR and 8-MR zeolites, respectively, is drastically lower compared to the 12-MR zeolite Beta, while there is little to no difference between silicalite-1 and chabazite. Note that for these zeolites, PFOS uptake is somewhat higher than PFOA uptake, not only on a mass basis but also on molar basis.

Besides all-silica and high-silica zeolites, also two common mesoporous silica materials were screened: SBA-15 and MCM-41. These silica materials have one-dimensional, cylindrical mesopores (2 to 6.5 nm) and can be used to study whether the pore size and/or internal surface is a limiting factor for PFAS adsorption.[43] The isotherms are given in **Figure 4.4** and clearly show that there is no uptake of PFOA at all on MCM-41 and SBA-15. Similar results for PFOA adsorption on various mesoporous silica materials were found by Nassi *et al.* (2014). Compared to all-silica zeolite Beta, these materials have much more hydroxyl groups at their surface, hence giving these materials a more hydrophilic character.[24] This shows that surface hydrophobicity may be an important factor in the adsorption of long-chain PFASs like PFOA. PFOS uptake is a bit higher on these mesoporous silica materials compared to PFOA uptake, but once again, it is much lower when compared to all-silica zeolite Beta (**Figure S4.2**).

This conclusion was confirmed when all-silica zeolite Beta was compared with two commercial zeolite Beta samples, being Beta-22 (CP814E-22) and Beta-300 (CP811C-300). The numbers 22 and 300 refer to the SiO_2/Al_2O_3 ratio of the commercial samples. These zeolites are of course similar in topology and channel structure and only differ in their Al content and in the amount of local defects. The corresponding isotherms (**Figure 4.5**) show a clear difference between the all-silica and the Al-containing types of zeolite Beta. This was surprising at first, since Beta-300 is considered as hydrophobic, given its low Al-content. Apparently, it is not enough for a zeolite Beta to have a low Al content in order to be a good adsorbent for PFASs: PFOA uptake of Beta-300 is more or less similar to that of the less hydrophobic Beta-22 and much lower than that of all-silica Beta. Also here, a similar trend was seen when comparing the different zeolite Beta types for PFOS adsorption (**Figure S4.3**). The importance of surface hydrophobicity was yet again suggested when the selectivity of all-silica zeolite Beta for PFOA (in competition with other organic molecules) was compared to that of Beta-22 (**Figure 4.6**). Even though they are both zeolites Beta, the selectivity of Beta-22 towards PFOA was tremendously lower. All these results seem to indicate that the presence of even a few hydroxyl groups (or other polar functions) in the zeolite framework has a detrimental effect on the adsorption uptake of PFASs.

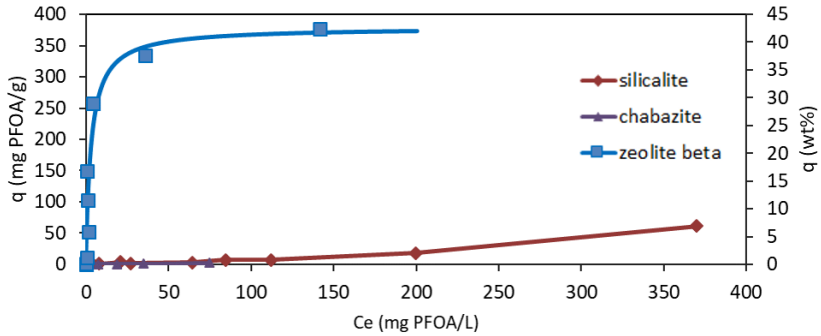


Figure 4.3: Isotherms for PFOA adsorption on all-silica zeolite Beta (Langmuir), silicalite-1 and chabazite. No Langmuir isotherms were plotted for silicalite-1 and chabazite because of their low PFOA uptake. q = mg PFAS adsorbed per g of dry matter; C_e = equilibrium concentration in water.

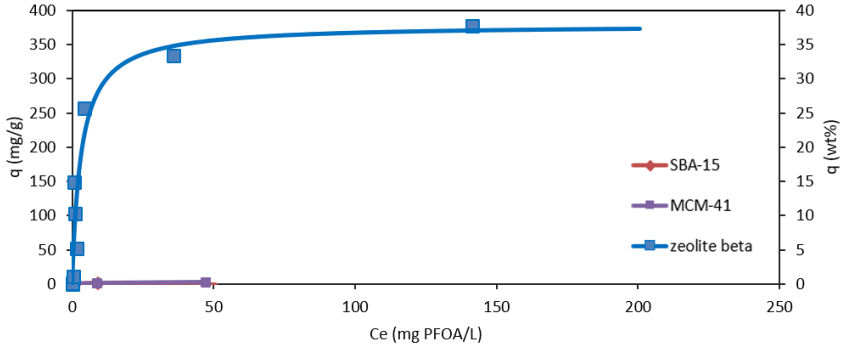


Figure 4.4: PFOA adsorption isotherms for all-silica zeolite Beta (Langmuir), SBA-15 and MCM-41. No Langmuir isotherms were plotted for SBA-15 and MCM-41 because of their low PFOA uptake. q = mg PFAS adsorbed per g of dry matter; C_e = equilibrium concentration in water.

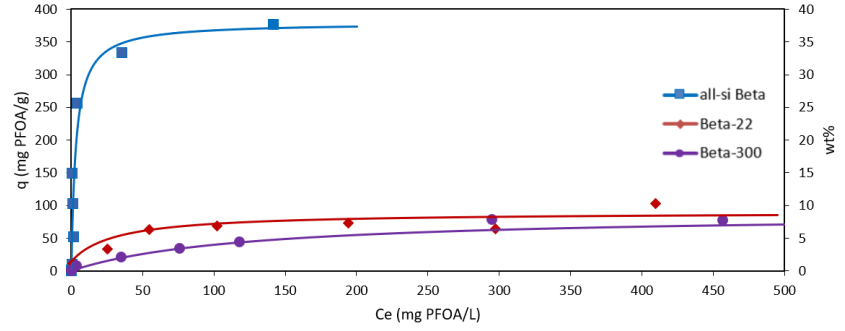


Figure 4.5: Langmuir isotherms for the adsorption of PFOA on as-synthesized all-silica zeolite Beta, Beta-22 (CP814E-22) and Beta-300 (CP811C-300). q = mg PFAS adsorbed per g of dry matter; C_e = equilibrium concentration in water.

As additional experiments, also non-microporous and/or non-siliceous materials were investigated for their capacity in the adsorption of PFASs. As mentioned in Chapter 1, PFASs do not tend to strongly interact with other types of chemicals. There are reports in literature that (long-chain) PFASs adsorb better on hydrophobic materials, and also the experimental results in this chapter suggest the impact and importance of the adsorbents' hydrophobicity. However, the interaction between PFASs and hydrophobic adsorbents is believed to be driven by entropy. For very hydrophobic molecules like long-chain PFASs, total entropy of the system can be higher when they are adsorbed on a surface than when they are dissolved in an aqueous solution. This might seem counterintuitive at first, but water molecules have to form a very rigid 'basket' around dissolved hydrophobic molecules. Therefore, entropy is often lower for a system of dissolved hydrophobic molecules as compared to a system with phase separation (e.g. adsorption).[49,50] In this light, a powder form of PTFE (6 µm diameter) was screened for the adsorption of PFOA and PFOS (**Figure 4.7**). There was very little uptake of these PFASs on the PTFE powder though, showing that it is not sufficient to have a perfluorinated surface for high PFAS adsorption. Adequate porosity, pore volume and surface area are important to capture high amounts of adsorbate; this forms the basis of the adsorptive capacities of many microporous materials.

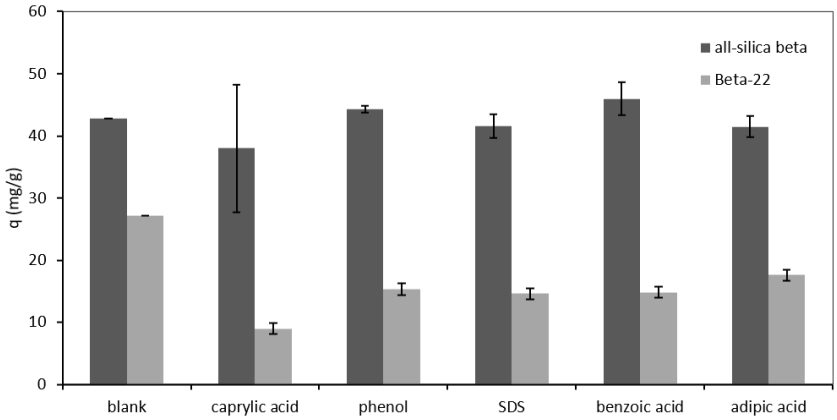


Figure 4.6: The effect of competing organics on the adsorption of PFOA on all-silica zeolite Beta and on the commercial zeolite Beta-22 (CP814E-22). Starting concentrations for both PFOA and the organic competitors are 100 µM. *q* = mg PFAS adsorbed per g of dry matter. Error bars indicate standard deviations for triplicate experiments.

Lastly, PFOA adsorption on ZIF-8 was investigated. ZIF-8 is a Zeolitic Imidazolate Framework (ZIF), a subtype of MOF materials. ZIFs are composed of tetrahedral metal nodes linked with imidazolate linkers. They have zeolite-like topologies because the metal-linker-metal angle is similar to the Si-O-Si angle in zeolites, hence the adjective 'zeolitic'.[51] The ZIF-8 framework consists of Zn^{2+} ions connected by 2-

methylimidazolate linkers. It has large cage diameters (1.16 nm) but with small aperture (0.34 nm). Its porosity (0.5 mL/g) and BET surface (1400 m^2/g) are very high and the imidazolate linkers render the material rather hydrophobic, which has been substantiated in the literature by selective uptake of hydrocarbons and rejection of water.[52] It is therefore an interesting, alternative candidate for PFAS adsorption. even though the small aperture might be a limiting factor.[53] Nevertheless, the ZIF-8 framework is known to be flexible, with a gate opening effect upon increasing adsorption. The adsorption of molecules that are theoretically too large to pass through the window openings has been described in literature.[54]

The adsorption data for PFOA on ZIF-8 are shown in **Figure 4.8**. At first sight, these data might suggest cooperative adsorption, where multilayer adsorption takes place only after a threshold concentration (in the liquid solution and on the adsorption sites) is reached.[55,56] In the case of cooperative adsorption, high uptake capacities are largely driven by intermolecular interactions between the adsorbate molecules and not by a strong adsorbate-adsorbent interaction. Because of their surface-active character, PFASs are definitely capable of multilayer adsorption. Reports of hemi-micelle formation onto solid surfaces are known in literature. Nevertheless, even with the flexibility of the ZIF-8 framework in mind, the large cages of the ZIF material do not provide enough space to accommodate multiple stacked PFOA molecules. The adsorption data might rather reflect the gate opening effect, where diffusion of the PFOA molecules through the cage openings is facilitated only upon reaching a certain threshold concentration. Even though maximum PFOA uptake at ZIF-8 is high, uptake and affinity at low concentrations are very low because of the gate opening effect. This is undesired for the remediation of PFAS pollutions with low concentrations.[57,58]

4.4. Conclusion

In this chapter, microporous, siliceous materials were explored for their potential as PFAS adsorbents. A selection of materials was synthesized, characterized and screened in adsorption experiments. All-silica zeolite Beta is a promising PFAS adsorbent and will be investigated in detail in a next chapter. Comparison with other microporous and mesoporous (silica-based) materials showed that i) hydrophobicity of the material and ii) adequate (micro)porosity and specific surface area appear to be key parameters for PFAS adsorption. The experiments in this chapter showed that both criteria have to be fulfilled simultaneously in order to achieve both high affinity and capacity. Adsorption of PFAS on zeolites is limited by the radius of the cage windows, with 12-membered ring openings appearing to be the minimal window size to allow adequate PFAS adsorption. All-silica zeolites have no framework charge due

to the absence of aluminum, but a high SiO_2/Al_2O_3 ratio alone is not sufficient. This was clearly shown by comparing the high PFOA uptake on all-silica zeolite Beta with the low uptake on the commercial zeolite Beta-300. A possible explanation for this is the suggested higher content of framework defects (i.e. silanol nests) in the commercial Beta-22 and Beta-300 samples.

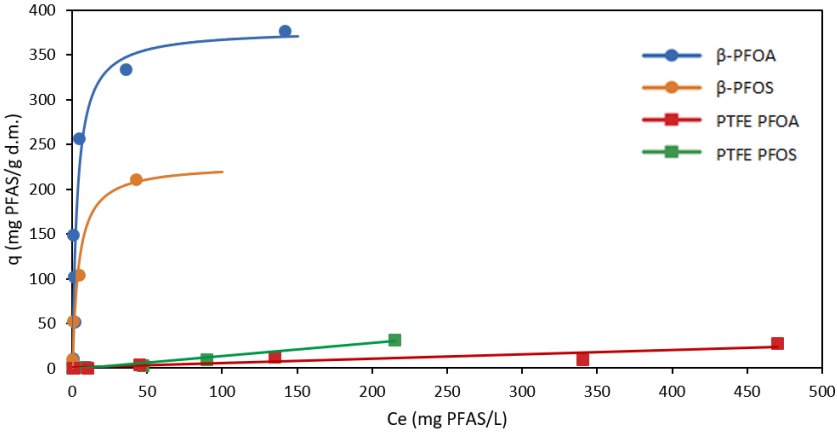


Figure 4.7: Isotherms for PFOA and PFOS adsorption on all-silica zeolite Beta (Langmuir) and on PTFE (powder form). No Langmuir isotherms were plotted for PTFE because of the very low PFAS uptake. q = mg PFAS adsorbed per g of dry matter; C_e = equilibrium concentration in water.

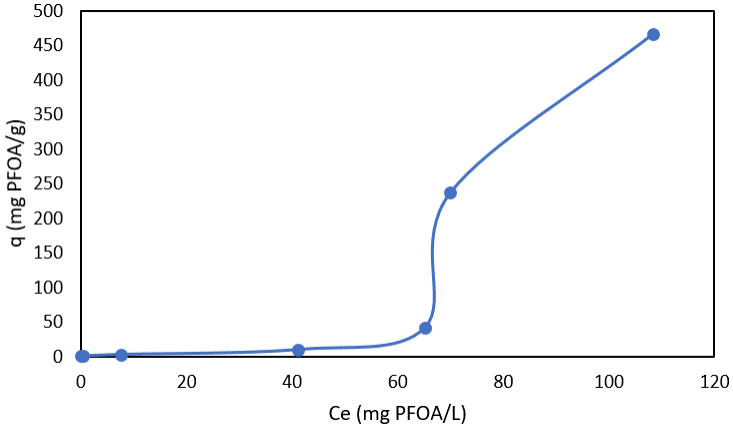


Figure 4.8: PFOA adsorption on ZIF-8. The fitted curve serves only as a guide to the eye. q = mg PFAS adsorbed per g of dry matter; C_e = equilibrium concentration in water.

4.5. References

[1] N. Bal, G. Van Gestel, F. Collet, T. Pancras, H. Slenders, M. Van Houten, J. Rabaey, R. Van Muylder, **2018**.

[2] K. H. Kucharzyk, R. Darlington, M. Benotti, R. Deeb, E. Hawley, *Journal of Environmental Management* **2017**, *204*, 757–764.

[3] B. T. Mader, Ultrasonically Induced Cavitation of Fluorochemicals, **2010**, US20100072134A1.

[4] K. Welcker, Removal and Recovery of Ammonium Perfluorooctanoate (APFO) from Contaminated Water, **2007**, US20070138110A1.

[5] Z. Du, S. Deng, Y. Bei, Q. Huang, B. Wang, J. Huang, G. Yu, *Journal of Hazardous Materials* **2014**, *274*, 443–454.

[6] S. T. M. L. D. Senevirathna, S. Tanaka, S. Fujii, C. Kunacheva, H. Harada, B. R. Shivakoti, R. Okamoto, *Chemosphere* **2010**, *80*, 647–651.

[7] P. Chularueangaksorn, S. Tanaka, S. Fujii, C. Kunacheva, *Journal of Applied Polymer Science* **2014**, *131*, DOI 10.1002/app.39782.

[8] V. Ochoa-Herrera, R. Sierra-Alvarez, *Chemosphere* **2008**, *72*, 1588–1593.

[9] Lampert David J., Frisch Michael A., Speitel Gerald E., *Practice Periodical of Hazardous, Toxic, and Radioactive Waste Management* **2007**, *11*, 60–68.

[10] F. Schuricht, E. S. Borovinskaya, W. Reschetilowski, *Journal of Environmental Sciences* **2017**, *54*, 160–170.

[11] S. Deng, Q. Yu, J. Huang, G. Yu, *Water Research* **2010**, *44*, 5188–5195.

[12] J. Li, Q. Li, L. Li, L. Xu, *Chemical Engineering Journal* **2017**, *320*, 501–509.

[13] Q. Yu, R. Zhang, S. Deng, J. Huang, G. Yu, *Water Research* **2009**, *43*, 1150–1158.

[14] A. Maimaiti, S. Deng, P. Meng, W. Wang, B. Wang, J. Huang, Y. Wang, G. Yu, *Chemical Engineering Journal* **2018**, *348*, 494–502.

[15] S. Woodard, J. Berry, B. Newman, *Remediation Journal* **2017**, *27*, 19–27.

[16] A. Zaggia, L. Conte, L. Falletti, M. Fant, A. Chiorboli, *Water Research* **2016**, *91*, 137–146.

[17] B. Felix, R. Sulzbach, S. Führer, T. Kaiser, H. Kniep, A. Budesheim, *Method for Recovering Fluorinated Alkanoic Acids from Waste Waters*, **2003**, US6613941B1.

[18] B. Felix, T. Zipplies, S. Führer, T. Kaiser, A. Budesheim, *Process for the Recovery of Fluorinated Alkandic Acids from Wastewater*, **2003**, US6518442B1.

[19] R. Epsch, K. Hintzer, G. Löhr, W. Schwertfeger, Process for Reducing the Amount of Fluorinated Surfactant in Aqueous Fluoropolymer Dispersions, **2004**, US6825250B2.

[20] W. Ji, L. Xiao, Y. Ling, C. Ching, M. Matsumoto, R. P. Bisbey, D. E. Helbling, W. R. Dichtel, *J. Am. Chem. Soc.* **2018**, DOI 10.1021/jacs.8b06958.

[21] Q. Yu, S. Deng, G. Yu, *Water Research* **2008**, *42*, 3089–3097.

[22] M. Ateia, M. F. Attia, A. Maroli, N. Tharayil, F. Alexis, D. C. Whitehead, T. Karanfil, *Environ. Sci. Technol. Lett.* **2018**, *5*, 764–769.

[23] F. Wang, K. Shih, J. O. Leckie, *Chemosphere* **2015**, *118*, 213–218.

[24] M. Nassi, E. Sarti, L. Pasti, A. Martucci, N. Marchetti, A. Cavazzini, F. D. Renzo, A. Galarneau, *J Porous Mater* **2014**, *21*, 423–432.

[25] C. A. Clark, K. N. Heck, C. D. Powell, M. S. Wong, *ACS Sustainable Chem. Eng.* **2019**, DOI 10.1021/acssuschemeng.8b05572.

[26] K. Liu, S. Zhang, X. Hu, K. Zhang, A. Roy, G. Yu, *Environ. Sci. Technol.* **2015**, *49*, 8657–8665.

[27] K. Sini, D. Bourgeois, M. Idouhar, M. Carboni, D. Meyer, *New J. Chem.* **2018**, DOI 10.1039/C8NJ03312A.

[28] D. P. Serrano, R. Van Grieken, P. Sánchez, R. Sanz, L. Rodríguez, *Microporous and Mesoporous Materials* **2001**, *46*, 35–46.

[29] M. A. Camblor, A. Corma, S. Valencia, *Chemical Communications* **1996**, *0*, 2365–2366.

[30] J. Dijkmans, M. Dusselier, D. Gabriëls, K. Houthoofd, P. C. M. M. Magusin, S. Huang, Y. Pontikes, M. Trekels, A. Vantomme, L. Giebeler, S. Oswald, B. F. Sels, *ACS Catal.* **2015**, *5*, 928–940.

[31] M. M. J. Treacy, J. M. Newsam, *Nature* **1988**, *332*, 249–251.

[32] J. M. Newsam, M. M. J. Treacy, W. T. Koetsier, C. B. D. Gruyter, J. M. Thomas, *Proceedings of the Royal Society of London. A. Mathematical and Physical Sciences* **1988**, *420*, 375–405.

[33] Á. Cantín, A. Corma, M. J. Díaz-Cabañas, J. L. Jordá, M. Moliner, F. Rey, *Angewandte Chemie* **2006**, *118*, 8181–8183.

[34] M. Tong, D. Zhang, W. Fan, J. Xu, L. Zhu, W. Guo, W. Yan, J. Yu, S. Qiu, J. Wang, F. Deng, R. Xu, *Scientific Reports* **2015**, *5*, 11521.

[35] C. Wang, J. Liu, J. Yang, J. Li, *Microporous and Mesoporous Materials* **2017**, *242*, 231–237.

[36] Z. Liu, Nobuhisa Fujita, O. Terasaki, T. Ohsuna, K. Hiraga, M. A. Camblor, M.-J. Díaz-Cabañas, A. K. Cheetham, *Chem. Eur. J.* **2002**, *8*, 4549–4556.

[37] R. Bialek, W. M. Meier, M. Davis, M. J. Annen, *Zeolites* **1991**, *11*, 438–442.

[38] P. A. Barrett, M. A. Camblor, A. Corma, R. H. Jones, L. A. Villaescusa, *J. Phys. Chem. B* **1998**, *102*, 4147–4155.

[39] O. Axelsson, D. Peters, *Journal of Heterocyclic Chemistry* **1997**, *34*, 461–463.

[40] P. A. Barrett, M. J. Díaz-Cabañas, M. A. Camblor, R. H. Jones, *Journal of the Chemical Society, Faraday Transactions* **1998**, *94*, 2475–2481.

[41] P. Wagner, M. Yoshikawa, K. Tsuji, M. E. Davis, P. Wagner, M. Lovallo, M. Taspatsis, *Chemical Communications* **1997**, 2179–2180.

[42] F. de Clippel, M. Dusselier, R. Van Rompaey, P. Vanelderen, J. Dijkmans, E. Makshina, L. Giebeler, S. Oswald, G. V. Baron, J. F. M. Denayer, P. P. Pescarmona, P. A. Jacobs, B. F. Sels, *J. Am. Chem. Soc.* **2012**, *134*, 10089–10101.

[43] M. Grün, I. Lauer, K. K. Unger, *Adv. Mater.* **1997**, *9*, 254–257.

[44] D. Zhao, Q. Huo, J. Feng, B. F. Chmelka, G. D. Stucky, *J. Am. Chem. Soc.* **1998**, *120*, 6024–6036.

[45] S. Lath, E. R. Knight, D. A. Navarro, R. S. Kookana, M. J. McLaughlin, *Chemosphere* **2019**, *222*, 671–678.

[46] J. F. Denayer, A. Bouyermaouen, G. V. Baron, *Ind. Eng. Chem. Res.* **1998**, *37*, 3691–3698.

[47] B. F. Mentzen, P. Gelin, *Materials Research Bulletin* **1995**, *30*, 373–380.

[48] I. Daems, R. Singh, G. Baron, J. Denayer, *Chemical Communications* **2007**, *0*, 1316–1318.

[49] F.-Y. Lin, W.-Y. Chen, *Anal. Chem.* **2001**, *73*, 3875–3883.

[50] N. A. Kotov, *Nanostructured Materials* **1999**, *12*, 789–796.

[51] K. S. Park, Z. Ni, A. P. Côté, J. Y. Choi, R. Huang, F. J. Uribe-Romo, H. K. Chae, M. O'Keeffe, O. M. Yaghi, *PNAS* **2006**, *103*, 10186–10191.

[52] K. Zhang, R. P. Lively, C. Zhang, R. R. Chance, W. J. Koros, D. S. Sholl, S. Nair, *J. Phys. Chem. Lett.* **2013**, *4*, 3618–3622.

[53] J. Lefevere, B. Claessens, S. Mullens, G. Baron, J. Cousin-Saint-Remi, J. F. M. Denayer, *ACS Appl. Nano Mater.* **2019**, *2*, 4991–4999.

[54] D. Fairen-Jimenez, S. A. Moggach, M. T. Wharmby, P. A. Wright, S. Parsons, T. Düren, *J. Am. Chem. Soc.* **2011**, *133*, 8900–8902.

[55] S. Liu, Journal of Colloid and Interface Science **2015**, 450, 224–238.

[56] A. Chakraborty, B. Sun, *Applied Thermal Engineering* **2014**, *72*, 190–199.
[57] X. Zhao, J. Li, Y. Shi, Y. Cai, S. Mou, G. Jiang, *Journal of Chromatography A* **2007**, *1154*, 52–59.
[58] J. Xu, Z. Liu, D. Zhao, N. Gao, X. Fu, *Science of The Total Environment* **2020**, *723*, 137757.

4.6. Supporting Information

4.6.1. Experimental Procedures

A. Synthetic Procedures

Reagents and standards

All reagents and standards were acquired from Sigma-Aldrich in the highest grade available. Aqueous solutions were prepared in Milli-Q water. Both native and mass-labelled analytical reference standards used for characterization were acquired from Wellington Laboratories (Guelph, Ontario, Canada). Commercial zeolite samples (CP814-E22, referred to as Beta-22, CP811C-300, referred to as Beta-300 and USY) were acquired via Zeolyst International. The Activated Carbon was a powder type Norit SX 1G (Cabot).

Dealumination of zeolite Beta

A zeolite adsorbent with *BEA topology and a SiO_2/Al_2O_3 ratio of 22 was dealuminated according to the literature method of Dijkmans *et al.*[1] An amount of 3 g of the zeolite was dispersed in 165 mL of a 7 M aqueous HNO_3 solution and the solution was left stirring overnight. The zeolite was separated, rinsed thoroughly with deionized water and dried overnight at 333K.

Synthesis of all-silica and high-silica zeolites

All-silica zeolite Beta was prepared in fluoride media, according to a method described earlier in literature.[2] Tetraethylorthosilicate (TEOS) was used as silica source and an aqueous solution of tetraethylammonium hydroxide (TEAOH) was used as organic structure directing agent (OSDA). The gel composition was: SiO_2 : 0.55 TEAOH : 0.55 HF : 9 H_2O, with an addition of 5 wt% of dealuminated zeolite Beta seeds. Crystallization of the zeolite was carried out in a Teflon liner under static conditions at 408 K for 168 hours. After crystallization, the solid product was separated from the liquid phase by filtration and washed repeatedly with deionized water. The zeolite product was obtained after thermal treatment at 823 K for 6 hours.

All-silica silicalite-1 was prepared in basic media according to a procedure described in literature.[3] Silica sol was used as silica source, ethylamine (C_2H_7N) and tetrapropylammonium bromide (TPABr) were used as OSDA. The final gel composition was: SiO_2 : 0.1 C_2H_7N : 0.1 TPABr : 0.15 NaOH : 50 H_2O. Crystallization of the zeolite was carried out in a Teflon liner under static conditions at 453 K for 20

hours. After crystallization, the solid product was washed and thermally activated in a similar way as all-silica zeolite Beta.

Synthesis of high-silica chabazite was performed in basic media, like described earlier in literature.[4] USY zeolite was used as silica source and TEAOH as OSDA. The final gel composition was: SiO_2 : 0.2 TEAOH : 0.2 NaOH : 5 H_2O. Crystallization of the zeolite was carried out in a Teflon liner under static conditions at 433 K for 72 hours. After crystallization, the solid product was washed and thermally activated in a similar way as all-silica zeolite Beta.

Synthesis of mesoporous silica materials

Two highly ordered hexagonal mesoporous silica materials (SBA-15 and MCM-41) were synthesized according to the respective literature methods.[5,6] For the synthesis of SBA-15, TEOS was used as silica source and Pluronic P123 (a nonionic alkyl poly(ethylene oxide) oligomeric surfactant) as OSDA. Typically, 4 g of Pluronic P123 and 8.5 g of TEOS were dissolved in 30 g of water and 120 g of a 2 M HCl solution and stirred at 308 K for 20h. The solid product was then washed with water, air-dried at 298 K and thermally activated at 773 K for 6 h.

For the synthesis of MCM-41, TEOS was again used as silica source and cetyltrimethylammonium bromide (CTABr) as OSDA. The procedure started by dissolving 2.50 g of CTABr in 50 mL of water. Afterwards, 60 g of ethanol and 13.2 g of ammonium hydroxide were added and stirred for 15 min to obtain a homogeneous solution. Then 4.67 g of TEOS was added and the resulting solution was stirred for 2 h. The precipitate was washed with water and methanol. The solid product was dried overnight at 343 K and thermally treated at 823 K for 8 h.

B. Characterizations

Physisorption measurements

N_2 physisorption experiments were performed using a Micromeritics 3Flex apparatus at 77 K. Samples (ca. 50 mg) were activated at 413 K under dynamic vacuum (10^{-3} mbar) prior to the measurements. Micropore volumes were calculates using the t-plot model. Surface areas were calculated using the multipoint BET (Brunauer-Emmett-Teller) method, all in accordance with the Rouquerol consistency criteria. Water vapor physisorption was performed on the same apparatus with degassed water at 298 K. Degassing consisted of connecting a pressure resistant stainless steel canister with water (ca. 15 mL) to the 3Flex apparatus and cooling it to freezing temperature (273 K). After 15 min of cooling the head space of the container was removed under dynamic vacuum (10^{-3} mbar), the canister's connection valve was

closed and water was left to defrost. The process was repeated 3 times to ensure complete degassing.

XRD measurements

Powder X-ray diffraction (XRD) patterns of all zeolites were recorded on a Malvern PANalytical Empyrean diffractometer in transmission mode over a 1.3–45° 2θ range, using a PIXcel3D solid-state detector and Cu anode (Cu Kα1: 1.5406 Å; Cu Kα2: 1.5444 Å). Data were analyzed with the PANalytical Data Viewer Software.

HPLC-MS analysis

Samples containing perfluorinated carboxylates or sulfonates were analyzed by LC-ESI-(-)-MS/MS using a Waters UPLC and a XEVO Triple Quad tandem mass spectrometer. Analytes were separated on a Waters Acquity BEH Shield RP_{18} column (2.1 × 100 mm; 1.7 µm) at 313 K. An elution gradient was used, with 2 mM ammonium acetate either in 95:5 (*v/v*) water:MeOH (solvent A), or in MeOH (solvent B). Two multiple reaction monitoring (MRM) transitions were used for each analyte. The method was validated and the method precision (which is the most important performance parameter for this study) ranged from < 1 % (repeatability) to 2-4 % (intermediate precision). During analysis, a quality control scheme was in place to monitor good performance of the method. Further details can be found in literature [7].

C. Experiments

Adsorption experiments

All batch adsorption experiments were performed in polypropylene vials, in order to avoid PFAS adsorption onto the surface of glass vials. For all the experiments, a commercial powder activated carbon (Norit SX 1 G) was used as benchmark material. For the determination of the single compound adsorption isotherms, an amount of 5 mg of adsorbent was contacted with 5 mL of an aqueous sample with a known PFOA or PFOS concentration (C_0). PFOA stock concentrations ranged from 0.1 mg/L to 500 mg/L, while PFOS stock concentrations ranged from 0.1 mg/L to 250 mg/L. A lower maximum concentration was used for PFOS in order to avoid micelle formation; PFOS has a lower critical micelle concentration (CMC) than PFOA. Stock concentrations for other PFAS alternatives were similar to those of PFOS. The samples were shaken for 24 hours where after PFAS concentrations of the aqueous solutions were measured via HPLC-MS (see above). PFAS uptake on the zeolite adsorbents was calculated using equation 1, where V is the sample volume (L), q (mg/g) is the amount of PFAS adsorbed per g of dry matter (m) and C_e (mg/L) is the

equilibrium PFAS concentration in the aqueous solutions, upon contact with the adsorbent.

$$q = (C_0 - C_e)\, V_{sample} / m_{adsorbent} \quad (1)$$

After the isotherm experiments, the results of the better performing adsorbents were fitted to the Langmuir and Freundlich adsorption model and isotherms were plotted according to the model with the best fit. For the selectivity experiments, 5 mg of adsorbent was again mixed with 5 mL of a 100 µM aqueous solution of PFOA or PFOS. This time, an organic competitor (either caprylic acid, phenol, sodium dodecyl sulfate (SDS), benzoic acid or adipic acid) was present in the sample in a 1:1 molar ratio. Measurements of the PFAS concentrations and calculations of PFAS uptakes were performed as described previously.

4.6.2. Supporting Figures

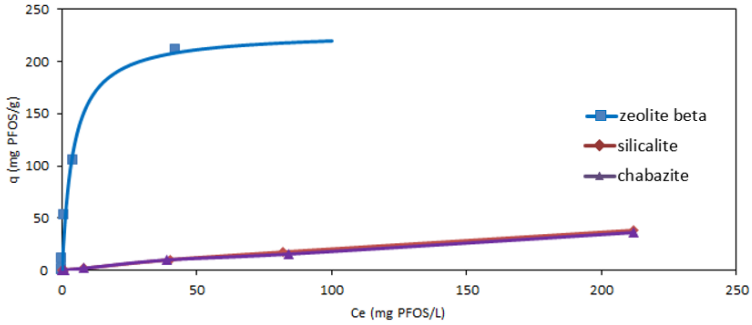


Figure S4.1: Isotherms for PFOS adsorption on all-silica zeolite Beta, silicalite-1 and chabazite. No Langmuir isotherms were plotted for silicalite-1 and chabazite because of their low PFOA uptake. q = mg PFAS adsorbed per g of dry matter; C_e = equilibrium concentration in water.

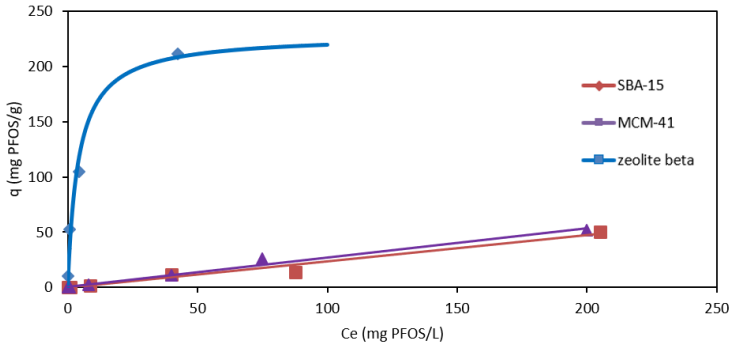


Figure S4.2: PFOS adsorption isotherms for all-silica zeolite Beta, SBA-15 and MCM-41. No Langmuir isotherms were plotted for SBA-15 and MCM-41 because of their low PFOA uptake. q = mg PFAS adsorbed per g of dry matter; C_e = equilibrium concentration in water.

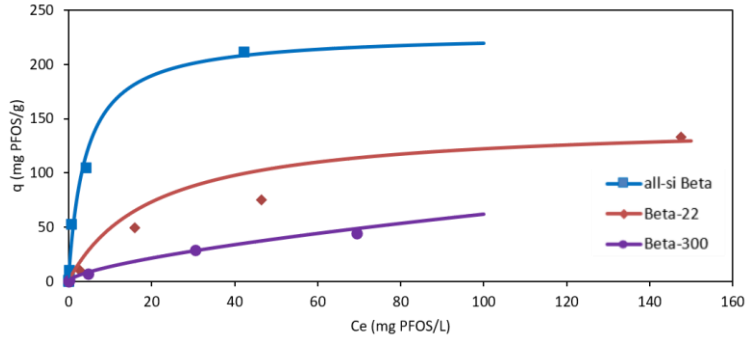


Figure S4.3: PFOS adsorption isotherms for all-silica zeolite Beta, Beta-22 (CP814E-22) and Beta-300 (CP811C-300). All-silica zeolite Beta and Beta-22 are plotted as Langmuir isotherms, while Beta-300 is plotted as Freundlich isotherm. q = mg PFAS adsorbed per g of dry matter; C_e = equilibrium concentration in water.

4.6.3. References Supporting Information

[1] J. Dijkmans, M. Dusselier, D. Gabriëls, K. Houthoofd, P. C. M. M. Magusin, S. Huang, Y. Pontikes, M. Trekels, A. Vantomme, L. Giebeler, S. Oswald, B. F. Sels, *ACS Catal.* **2015**, *5*, 928–940.

[2] D. P. Serrano, R. Van Grieken, P. Sánchez, R. Sanz, L. Rodríguez, *Microporous and Mesoporous Materials* **2001**, *46*, 35–46.

[3] C. Wang, J. Liu, J. Yang, J. Li, *Microporous and Mesoporous Materials* **2017**, *242*, 231–237.

[4] N. Martín, M. Moliner, A. Corma, *Chem. Commun.* **2015**, *51*, 9965–9968.

[5] D. Zhao, Q. Huo, J. Feng, B. F. Chmelka, G. D. Stucky, *J. Am. Chem. Soc.* **1998**, *120*, 6024–6036.

[6] M. Grün, I. Lauer, K. K. Unger, *Adv. Mater.* **1997**, *9*, 254–257.

[7] A. Alves, G. Jacobs, G. Vanermen, A. Covaci, S. Voorspoels, *Talanta* **2015**, *144*, 574–583.

CHAPTER 5

HIGHLY SELECTIVE REMOVAL OF PERFLUORINATED CONTAMINANTS BY ADSORPTION ON ALL-SILICA ZEOLITE BETA

Matthias Van den Bergh,[a] Andraž Krajnc,[b] Stefan Voorspoels,[c] Sergio Rodrigues Tavares,[d] Steven Mullens,[c] Isabelle Beurroies,[e] Guillaume Maurin,[d] Gregor Mali,[b] and Dirk De Vos*[a]

With permission from Wiley, adapted from:

Angewandte Chemie International Edition, 2020, vol 59 (33), p 14086-14090

[a] M. Van den Bergh, Prof. D. E. De Vos
Centre for Membrane Separations, Adsorption, Catalysis and Spectroscopy for Sustainable Solutions (cMACS)
KU Leuven
Celestijnenlaan 200F, 3001 Leuven, Belgium
[b] A. Krajnc, G. Mali
National Institute of Chemistry
Hajdrihova 19, SI-1001 Ljubljana, Slovenia
[c] M. Van den Bergh, S. Voorspoels, S. Mullens
Flemish Institute for Technological Research, VITO
Boeretang 200, 2400 Mol, Belgium
[d] S. R. Tavares, Prof. G. Maurin
Institut Charles Gerhardt Montpellier
UMR 5253, CNRS, ENSCM, Pl. E. Bataillon, F-34095 Montpellier, France
[e] Prof. I. Beurroies
MADIREL
Aix Marseille Université, F-13013 Marseille, France

Abstract

Perfluorinated alkylated substances (PFASs) are widely used in industrial and commercial applications, leading to a widespread occurrence of these persistent and harmful contaminants in our environment. Removal of these compounds from surface and waste waters is being mandated by European and U.S. governments. Currently, there are no treatment techniques available that lower the concentrations of these compounds for large water bodies in a cost- and energy-efficient way. We hereby propose a hydrophobic, all-silica zeolite Beta material that is a highly selective and high-capacity adsorbent for PFASs, even in the presence of organic competitors. Advanced characterization data demonstrate that the adsorption process is driven by a very negative adsorption enthalpy and favorable steric factors. Even though not measured, in increase in entropy is also believed to play an import role in these hydrophobic interactions.

Contributions

M.V.d.B. and D.D.V. conceived the study; M.V.d.B. performed zeolite syntheses and adsorption experiments; other experimental contributions and text revisions by A.K. and G.Mali (NMR), S.R.T. and G.Maurin (calculations), I.B. (calorimetry) and S.V. (LC-MS analysis). M.V.d.B. wrote the paper; D.D.V. supervised the work.

5. Highly selective removal of perfluorinated contaminants by adsorption on all-silica zeolite Beta

5.1. Introduction

Perfluorinated compounds (PFASs) have seen extensive industrial use over the past 40 years, but are now considered top priority pollutants, due to their chemical persistence, and their pervasive presence in (drinking) water, food products, animals and even humans.[1,2] Exposure to PFASs entails serious health risks like liver and kidney cancer, and may affect fetus and child growth.[3–5] Current PFAS regulations range from restricting production to imposing threshold PFAS concentrations in tap, surface and waste water.[6,7] Most regulation focuses on perfluorooctanoic acid (PFOA) and perfluorooctanesulfonic acid (PFOS), two of the most spilled PFASs.

Conventional waste water treatment plants are unable to remove PFASs in low concentration from complex waste and surface waters. Sonolysis and electro- or photocatalysis have been explored, but these suffer from high energy demand and require pretreatment steps, impeding treatment of large water volumes.[8–10] Adsorption may be a better, lower cost approach.[11–16] So far, most PFAS adsorption studies use solutions of individual compounds, without the non-fluorinated organics that are present in real situations. A single study exploring the impact of organic matter on PFAS adsorption reports a drastic decline of capacity for PFASs on conventional adsorbents like activated carbon.[17] Even though a large variety of different adsorbent types has been screened so far, not many adsorbents are known that selectively accumulate PFOA or PFOS in the presence of competing organics. A particular and promising adsorbent type are macrocyclic, polymeric adsorbents that possess a cavity that can be highly selective for specific guest molecules. Recent examples are a β-cyclodextrin polymer network and a guanidinocalix[5]arene network, both showing high adsorption capacity and selectivity for PFOA and PFOS.[18,19] However, these materials are expensive, difficult to recover from aqueous streams and hard to regenerate. In a study of Na-exchanged Y zeolites, a higher Si/Al ratio appears to enhance the PFOS adsorption, but the nature of the zeolite sorbent and the role of the Na^+ are unclear, and more importantly, no competitive sorption data are given.[15] Since zeolites, as crystalline microporous materials, present a multitude of pore architectures and compositions, we initiated a detailed search into the best zeolite adsorbent for adsorptive PFAS removal. Here, we report direct experimental and spectroscopic evidence that all-silica zeolite Beta is a highly-selective and high-capacity adsorbent for removing PFOA and PFOS from water, even in the presence of organic competitors.

5.2. Results and discussion

All-silica zeolite Beta was synthesized using fluoride as the mineralizing agent. The resulting zeolite framework is almost free of local defects, as proven by the very weak intensity of the silanol ν_{OH} vibration at 3733 cm^{-1} in the FTIR spectrum (**Figure S5.1**).[20,21] It exhibits high pore volumes of 0.21 cm^3/g and high surface areas of 624 m^2/g (calculated by the t-plot and Brunauer-Emmet-Teller equations, respectively via nitrogen physisorption isotherms, see **Figure S5.2**). The lack of defects and Al in the zeolite framework (i.e. the absence of silanol groups) renders the interior surface extremely hydrophobic, as can be seen on water vapor adsorption isotherms, when compared to a more hydrophilic zeolite Beta type (**Figure S5.2**). Besides Beta, other all-silica and high-silica adsorbents were synthesized and screened for PFOA adsorption in a concentration range of 0.1 – 500 mg/L. On most zeolites, such as all-silica silicalite-1 and high-silica chabazite, there was no significant PFOA uptake. Mesoporous materials like SBA-15 and MCM-41, with all-silica composition, but with significant numbers of defect –OH groups, showed no sign of PFOA adsorption. All-silica zeolite Beta, on the contrary, showed both high affinity (in the lower concentration range) and high saturation capacity for PFOA (37 wt%), strongly outperforming the industrial benchmark adsorbent activated carbon (AC) (**Figure 5.1** (A)). Especially the high affinity at lower concentrations, even below 1 mg/l, is highly relevant in an environmental context.[22,23] This is also reflected in higher Langmuir (K_L) and Freundlich (K_F) coefficients for all-silica zeolite Beta. All adsorption coefficients for the isotherm experiments in this chapter are given in **Table S5.1.** A log-log plot of the adsorption isotherms is shown in **Figure S5.3** (A), for better visualization of adsorption performances at lower concentrations.

In similar experiments for adsorption of PFOS (0.1-250 mg/L), the capacity of all-silica Beta (21 wt%) proved to be similar to that of AC, but the affinity at lower concentrations was again much higher (**Figure 5.1** (A)). Also for PFOS, a log-log plot of the isotherms is given (**Figure S5.3** (B)). The fact that all-silica zeolite Beta does not outperform AC on maximum PFOS adsorption capacity is due to AC being a better adsorbent for PFOS than for PFOA; indeed the sulfonic acid group of PFOS is a stronger and more polar acid compared to the carboxyl group of PFOA, which allows a stronger interaction with cationic surface functionalities of AC. The anion-exchange capacity of most AC types originates from basic-oxygen containing groups and from positively charged sites created by protons on π-electron-rich regions.[24] In addition,. Fast adsorption kinetics are essential for efficient PFAS removal in waste water treatment. Kinetic experiments revealed that adsorption equilibrium is reached much faster for PFOA on all-silica zeolite Beta than on AC, while the time profiles for PFOS adsorption are similar for both adsorbents (**Figure 5.1** (B & C)).

Hence, considering kinetics, all-silica zeolite Beta looks very well suited to be used in a flow-through adsorption column.

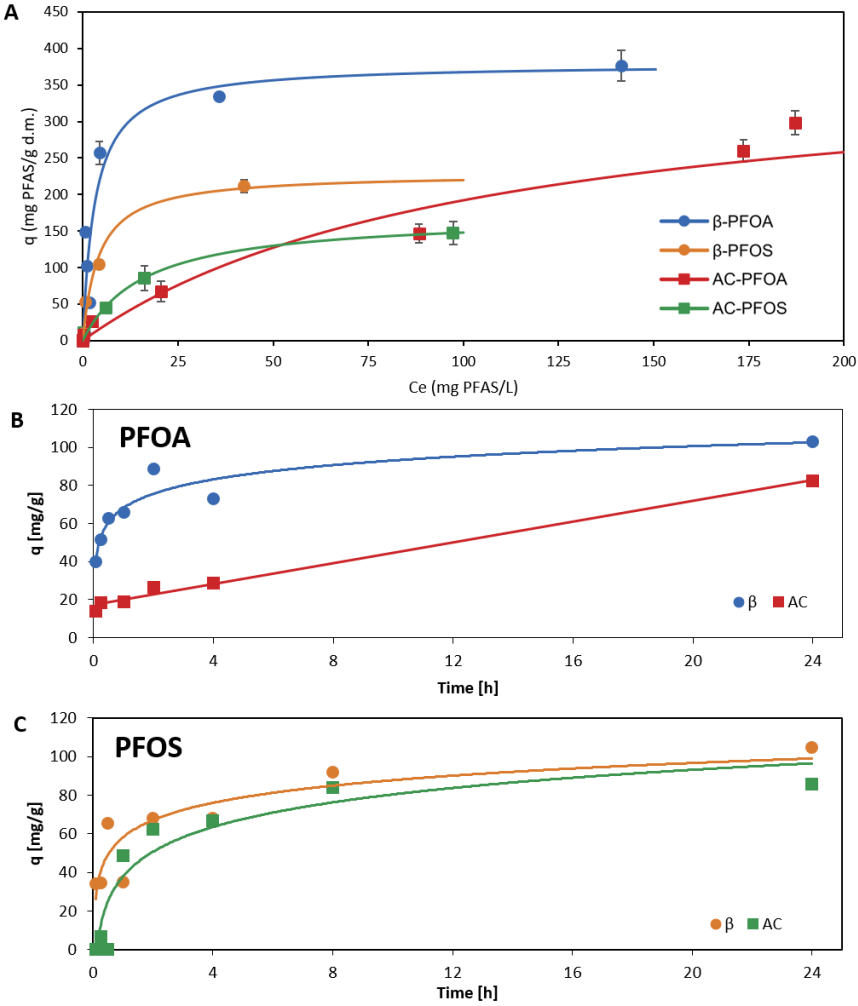


Figure 5.1*:* A) Langmuir isotherms (293 K) for PFOA and PFOS on all-silica Beta (β) and activated carbon (AC). *q* = mg PFAS adsorbed per g of dry matter; C_e = equilibrium concentration in water. (B) Adsorption kinetics for PFOA and (C) PFOS on all-silica Beta (β) and activated carbon (AC). Errors bars indicate standard deviation for triplicate experiments.

Since PFOA and PFOS are strong acids, their concentration will influence the pH of the test solutions, unless this is adjusted for by addition of a base and/or a buffer. PFOA adsorption, however, is remarkably unaffected by pH changes in a range of pH 2-7 (see **Figure S5.4**). During the isotherm experiments, the highest stock concentration (500 mg PFOA/l) resulted in a pH of 2.9, whereas the lowest stock

concentration (0.100 mg PFOA/l) lead to a pH of 6. Because these pH levels fall in the region where PFOA adsorption is unaffected by pH, no pH adjustments where performed, hereby avoiding the impracticalities of adjusting pH levels in 1.8 mL vials.

Even though adsorption might be the best available technique for the low-cost and energy efficient removal of PFASs from water, many adsorbents with good or high capacity (like AC) simply lack the selectivity that is required to be used for real waters. Adsorption selectivity is therefore arguably the most important feature for adsorbent selection, since natural waters contain various organic competitors, often in molar excess. For this study, a series of selectivity experiments were performed, in order to assess the influence of organic competitors on the uptake of PFOA and PFOS. Five non-fluorinated compounds were selected to represent the wide array of organics in real waters: the aromatics phenol and benzoic acid, which carry motives of more complex humic acids; adipic acid, as a representative dicarboxylic acid, and caprylic acid and sodium dodecyl sulfate, being non-fluorinated analogues of PFOA and PFOS, respectively.

First, PFOA and PFOS uptakes were measured in the presence of an equimolar amount (100 µM) of each organic compound. The results for all-silica Beta are outstanding: the uptakes of both PFOA and PFOS remain the same as in the reference experiment without organic competitor (see **Figure 5.2**). In contrast, PFOA uptake on AC was reduced significantly by other organics, with an average reduction in uptake capacity of 43%. PFOS adsorption on AC in the presence of competing organics proved more resilient compared to PFOA adsorption, but a reduction of PFOS uptake (-17% on average) is still seen (**Figure 5.2**). Next, PFOA and PFOS uptakes on all-silica Beta and on AC were measured in the presence of an excess of organic material, like in waste or natural waters. All five organics were added simultaneously in either 1:1 or 3:1 ratio towards 100 µM of PFOA or PFOS, resulting in organics to PFAS ratios of 5:1 and 15:1, respectively. Even in these challenging conditions, PFOA adsorption on all-silica zeolite Beta was not reduced, demonstrating the outstanding PFOA selectivity of Beta (**Figure 5.3**). In contrast, PFOA uptake on AC was cut down dramatically with 43% and 60% in the 5:1 and 15:1 test solutions. Also PFOS adsorption was reduced significantly on AC in the 5:1 (-22%) and 15:1 (-51%) solution. On all-silica zeolite Beta, PFOS adsorption remained relatively stable under excess competition, with only minor reductions in uptake (-9% for the 5:1; -14 % for the 15:1 solution). This shows that the high selectivity of all-silica Beta is not limited to PFOA, but also applies to other PFASs. The adsorbate scope of all-silica zeolite Beta can thus be extended towards other types of perfluoro-compounds like non-functional perfluoroalkanes; it has for instance been found that also perfluorooctane and perfluorodecane are adsorbed in high quantities. Also

perfluorinated carboxylic and sulfonic acids with chain lengths shorter and longer than C_8 can be adsorbed; here adsorption capacity and affinity decreases with shorter chain lengths (see **Figure S5.5** and **Figure S5.6**). Additionally to these experiments, also selectivity towards naturally occurring inorganic anions was screened for (see **Figure S5.7**). Both all-silica zeolite Beta and activated carbon showed no reduction in PFOA uptake under competition of either chloride or carbonate anions, neither in equimolar conditions nor for triple molar excess of the inorganic anion.

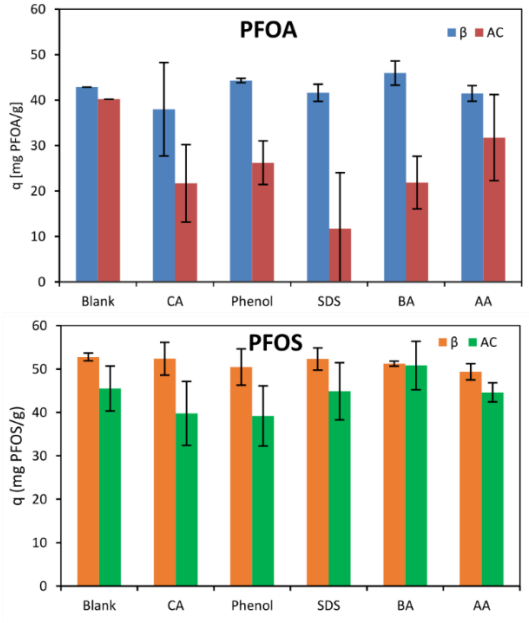


Figure 5.2: PFOA (top) and PFOS (bottom) adsorption on all-silica Beta (β) and activated carbon (AC) under competitive conditions (100 µM of PFOA or PFOS and 100 µM of a single organic competitor). CA = caprylic acid, SDS = sodium dodecyl sulfate, BA = benzoic acid, AA = adipic acid.

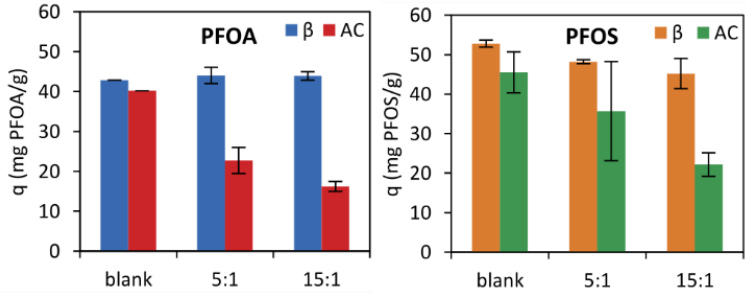


Figure 5.3: PFOA (left) and PFOS (right) adsorption on all-silica Beta (β) and activated carbon (AC) under competitive conditions. The 5:1 solution has a 5-time molar excess of organic competitors, the 15:1 solution has a 15-time molar excess.

To study the impact of framework aluminum and silanol groups on PFAS uptake, a comparison was made with two Al-containing Beta samples, with SiO_2/Al_2O_3 ratios of 22 (Beta-22) and 300 (Beta-300). These have an identical pore architecture, but were prepared via templated synthesis in OH^- medium (for Beta-22), eventually followed by dealumination (for Beta-300). At SiO_2/Al_2O_3 = 300, the zeolite would be considered hydrophobic. However, PFOA uptakes on Beta-300 and Beta-22 are similar, and much lower than on all-silica Beta: a maximum uptake of 78 mg PFOA/g was measured, 79% lower than the maximum uptake on the all-silica analogue (**Figure S5.8**). A similar trend was seen for PFOS adsorption, with all zeolites based on an Al-containing synthesis being poor adsorbents. This indicates that not only Al, but also the silanol defects formed during dealumination have a detrimental effect on PFAS adsorption, even in very small amounts. Also the stability and reusability of all-silica zeolite Beta were assessed by a performing a thermal treatment. This revealed that after complete saturation with PFOA, all adsorbed molecules can be removed at 350 °C without any damage to the zeolite's framework and its crystallinity (**Figure S5.9**). The possibility of a thermal regeneration is a significant asset for all-silica zeolite Beta, because such a simple treatment cannot be applied for organic adsorbents like the aforementioned macrocyclic polymers or ion-exchange resins.

An intriguing question is why all-silica zeolite Beta has such a high affinity and selectivity for PFASs. Calorimetric experiments were performed to resolve whether the adsorption process is mostly driven by enthalpy or entropy. One may expect an entropy-driven process, given the very hydrophobic nature of both the all-silica zeolite Beta and the perfluorinated chains of the surfactants; many hydrophobic effects are indeed entropic phenomena. Moreover, perfluorinated carbon chains hardly engage in Van der Waals interactions, due to the extremely low polarizability of the fluorine-carbon bonds. However, calorimetry shows that PFOA adsorption on the different zeolite Beta types is associated with a negative adsorption enthalpy, both at low and at higher occupation of the zeolite surface (**Figure S5.10**). Adsorption enthalpies for all-silica zeolite Beta are much more negative, at -30 to -40 kJ mol^{-1}, than for the aluminated zeolite Beta types, where the enthalpy increases from -20 to 0 kJ mol^{-1} at higher concentrations (Beta-22 and Beta-300, see **Figure S5.10**). Entropy changes during the adsorption process could not be measured; nevertheless an increase in entropy is still considered as a main driving force for the hydrophobic adsorption interaction. The negative adsorption enthalpy measured here is an additional factor favoring the adsorption of PFOA on all-silica zeolite Beta.

Given the estimated dimensions of PFOA (ca. 13Å x 6.5Å x 6.5Å) and zeolite Beta (channel diameter of 6.7 Å, intersection spacing of 12.62 Å), the packing of PFOA in

the Beta pores must be tight. The fluorous tails of PFOA may assume a helical or a zig-zag conformation; and the PFOA surfactant may be packed in a head-head, tail-tail or head-tail conformation.[25,26] Through Density Functional Theory (DFT) simulations, the total energy of different optimized conformations of PFOA and caprylic acid molecules in zeolite Beta was calculated. These DFT calculations demonstrate a strong preference of PFOA for head-head interactions, with a total energy difference of -16.5 kJ mol^{-1} and -76.8 kJ mol^{-1} over the head-tail and tail-tail conformations, respectively (**Figure 5.4** (A)). The stability of the head-head interactions results from the formation of carboxylic acid dimers, driven by H-bonding.[27,28] The same scenario is observed for caprylic acid (**Figure S5.11**), associated, however, with a guest/zeolite Beta interaction energy (-181.1 kJ mol^{-1}) that is much lower than that obtained for the head-head conformation of PFOA (-264.6 kJ mol^{-1}). This observation shows that the observed selectivity of all-silica zeolite Beta for PFOA is enthalpy-driven, confirming the calorimetry results. Note that the interaction energies are calculated using the single point total energy of the adsorbate molecules and the zeolite in the gas phase as reference, hence no solvation effects are accounted for (see 5.5.1. Experimental Procedures). DFT simulations also show that a helical conformation of PFOA is slightly more favorable than the zig-zag one; the corresponding total energy difference between the two is -4.2 kJ mol^{-1}, in contrast to caprylic acid for which a zig-zag structure is more stable (**Figure S5.12**). Since the helical conformation is slightly shorter than the zig-zag one, PFOA might also have a steric advantage over caprylic acid when the zeolite is fully packed. The PFOA molecules are aligned according to the straight channels in the *a*- and *b*-directions; DFT calculations show a total energy penalty of 19.7 kJ mol^{-1} for the PFOA in the tortuous channels along *c* (**Figure 5.4** (B)).

Experimental evidence supporting the computational prediction is offered by solid-state NMR spectroscopy. ^{19}F MAS and ^{1}H-^{13}C CP/MAS NMR (Cross Polarization/Magic Angle Spinning) spectra of pure, crystalline PFOA and of PFOA loaded into all-silica zeolite Beta show large similarity and confirm the presence of PFOA inside the zeolite (**Figure S5.13** and **Figure S5.14**). With increasing concentration of PFOA in the zeolite, the NMR linewidths become smaller, meaning that the molecular arrangement becomes more ordered. In the carbon spectrum there is a slight difference in the chemical shift of the carboxylate carbon signal between pure PFOA and PFOA in the zeolite, suggesting that the polar heads experience different environments in both cases. The 2D ^{1}H-^{1}H homonuclear correlation spectrum of the zeolite Beta loaded with the highest concentration of PFOA exhibits a strong diagonal signal at about 8 ppm, proving that hydrogen atoms of the PFOA carboxyl groups see identical hydrogen atoms in their proximity (**Figure 5.5** (A)). This strongly suggests that PFOA within the zeolite forms head-to-head hydrogen-bonded dimers. The chemical shift

of the hydrogen nuclei involved in these bonds is different from the chemical shifts of the hydrogen nuclei within the crystalline PFOA, indicating that the geometries of bonds between the PFOA molecules within the zeolite and the molecules within the pure PFOA are different. Indeed, molecules in pure PFOA are involved in a network of hydrogen bonds; they cannot be regarded as isolated head-to-head bonded dimers (**Figure S5.15**). The ^{1}H-^{1}H homonuclear correlation spectrum also shows that the PFOA carboxyl groups do not interact with the hardly detectable hydroxyl groups of the zeolite framework (resonating between 3 and 5 ppm). The latter groups are rare in the all-silica zeolite Beta; they most probably only appear at defects on the surface of the crystals. The ^{29}Si NMR spectrum of the all-silica zeolite Beta exhibits several partly overlapped signals (**Figure 5.5** (B)). The signals can be grouped into three chemical shift ranges, one between -111 and -113 ppm, one between -113 and -114 ppm, and one around -116 ppm.

According to DFT/GIPAW calculations the first and the third groups of signals belong to framework silicon atoms that form the straight channels of zeolite Beta, whereas the second group of signals belongs to silicon nuclei at the channel intersections. Close inspection of the ^{19}F-^{29}Si heteronuclear correlation spectrum suggests that the hydrophobic part of the molecule (fluorine atoms F3-F6) is located within the straight channels, since the corresponding ^{19}F-^{29}Si cross peaks emphasize the ^{29}Si resonances between -111 and -113 ppm and the resonances around -116 ppm. The tail of the molecule, with fluorine atoms F8, is closer to the channel intersections (the corresponding ^{19}F-^{29}Si cross peaks emphasize the ^{29}Si resonances between -113 and -114 ppm). All these findings are in line with the computational predictions.

Despite the experimental evidence from both the calorimetry measurements and the DFT simulations, it remains intriguing that the adsorption of such a nonpolar and non-polarizable molecule as PFOA (see Paragraph 1.2: Fluorine chemistry) on all-silica zeolite Beta is associated with a negative enthalpy. So far, the exact explanation hereof is not clear, however some hypotheses can be made. The low polarizability of the fluorine atom will impede the formation of instantaneous dipoles, which form the basis for London dispersion forces (a large contributor to Van der Waals forces and thus hydrophobic interactions). The interaction energy of London dispersion forces is correlated with r^{-6}, with r being the distance between two nuclei. Given the more or less similar diameter of a PFOA molecule and a straight channels of zeolite Beta, it can be assumed that the distance between the PFOA molecules and the zeolite wall is rather small, which would amplify the London dispersion forces significantly given the exponent of 6 for r.[29] Next, the polarizability of an atom is often determined and analyzed for (electro)dynamic systems, where molecules can move freely. It is possible that the polarizability of the fluorine atom is different in

confined situations like for PFOA molecules adsorbed in the channels of zeolite Beta. Logically, molecular rigidity of these adsorbed PFOA molecules will be much higher than for PFOA molecules dissolved in the liquid bulk phase. At last but not least; PFAS molecules are very nonpolar because all intramolecular dipole moments neutralize each other. Nevertheless, a single C-F bond has a large dipole moment, because of the high electronegativity of the fluorine atom. Again, in a very confined environment like the one discussed here, this might possibly allow the formation of very local dipole interactions.

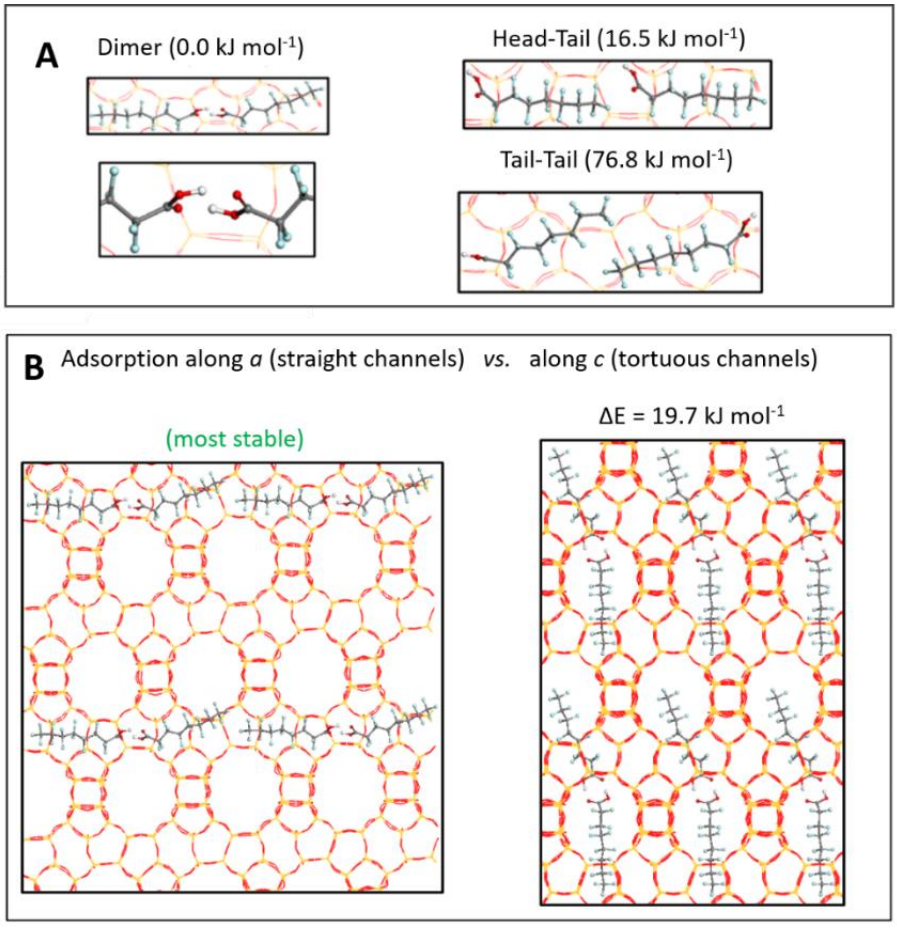


Figure 5.4: Optimized binding geometry of all-silica zeolite Beta and PFOA. (A) Snapshots of DFT-optimized conformations of PFOA molecules, adsorbed on all-silica zeolite Beta, and the associated total energy differences with respect to the head-head dimer taken as reference. (B) Snapshots of the PFOA dimers, adsorbed in the straight channels (along a) vs. tortuous channels (along c) of all-silica zeolite Beta.

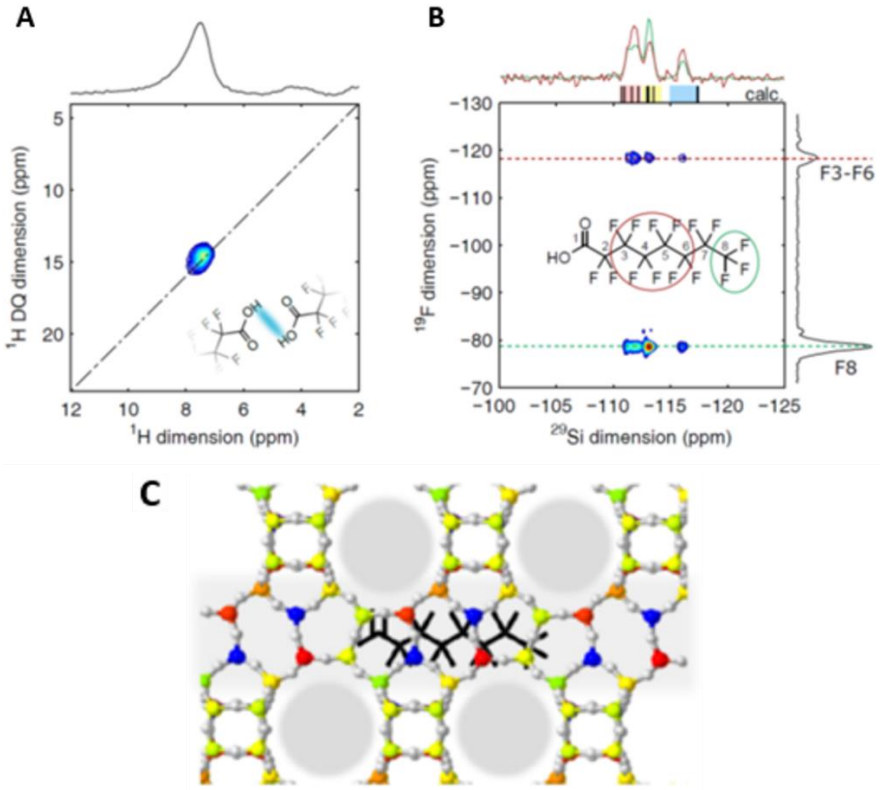


Figure 5.5: NMR-based inspection of the arrangement of PFOA molecules within the all-silica zeolite Beta. (A) 2D ^{1}H-^{1}H DQ-SQ homonuclear correlation and (B) ^{19}F-^{29}Si heteronuclear correlation NMR spectrum. In (B) traces through cross-peaks that describe correlations (proximities) between F8 and Si atoms and F3-F6 and Si atoms are shown above the 2D spectrum with green and red line, respectively. Below the traces, vertical black solid lines mark the values of ^{29}Si chemical shifts calculated by GIPAW. Location of Si atoms with specific chemical shift within the framework of zeolite Beta can be read from the scheme in (C): Si atoms with chemical shifts between -111 and -113 ppm are plotted in red and orange, atoms with shifts between -113 and -114 ppm are shown in yellow and green, and atoms with shifts around -116 ppm are presented in blue.

A final enticing question is whether the PFAS molecules, which are all strong acids, enter the zeolite pores in their protonated or dissociated form. Their acidity would suggest the latter, while the limited free volume in the zeolite pores (especially at higher adsorbent loadings) promotes the idea of PFOA molecules entering as dimers. So far, there is no experimental evidence answering this question. However, the adsorption uptake of all-silica zeolite Beta for the Na-salt of PFOA is almost similar (even a bit higher) to that of the pure PFOA acid (**Figure S5.16**). This proves that PFOA can be adsorbed by the zeolite as protonated dimers in high amounts, even when its predominant speciation in the liquid phase is the anionic carboxylate. How

counterintuitive it may be for a strong acid like PFOA, this suggests a protonation step before adsorption.

5.3. Conclusion

Summarizing, the PFOA molecules are positioned in the straight *a*- and *b*-channels of the zeolite, with the hydrophobic chains in the channels and the carboxylic heads, forming hydrogen bonded pairs, in the intersections. This results in a very favorable adsorption enthalpy. Even though not measured, also favorable entropy changes upon adsorption are believed to play an import role in these hydrophobic interactions. The helical conformation of the perfluorinated chains makes a very tight packing at maximal capacity sterically possible, as shown in **Figure 5.6**. This explains the exceptionally high affinity and selectivity of all-silica zeolite Beta for PFOA and similar perfluorinated compounds. These properties position this unusual zeolite as the lead candidate for combating PFAS pollution.

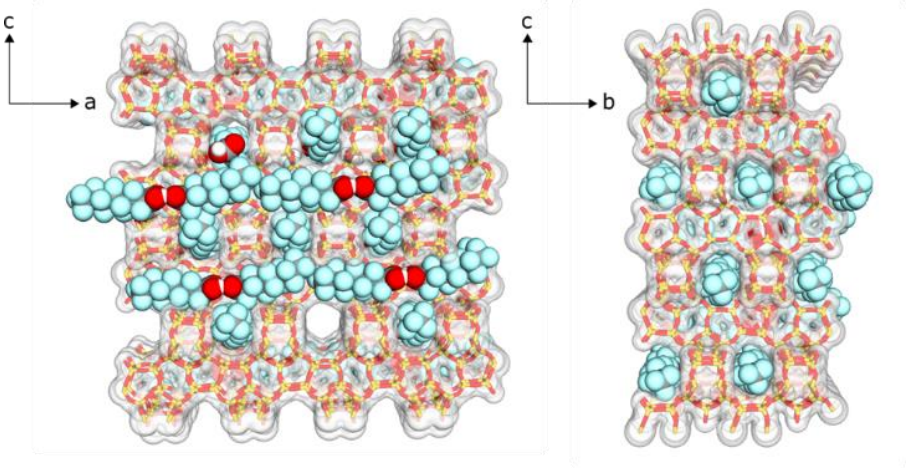


Figure 5.6: Graphical representation of all-silica zeolite Beta with adsorbed PFOA molecules. The PFOA molecules are positioned in the *a* and *b* channels and the helical conformation of the perfluorinated chains makes a very tight packing at maximal capacity sterically possible.

Acknowledgements

M.V.d.B. thanks FWO Flanders for a doctoral fellowship; G. Mali and D.D.V. thank FWO for a research grant (G0781118N, G0D0518N); D.D.V. thanks KULeuven for Metusalem funding (METU14/04). A.K. and G.Mali acknowledge the financial support from the Slovenian Research Agency (research core funding No. P1-0021 and project No. N1-0079).

5.4. References

[1] B. O. Clarke, S. R. Smith, *Environment International* **2011**, *37*, 226–247.

[2] K. E. Murray, S. M. Thomas, A. A. Bodour, *Environmental Pollution* **2010**, *158*, 3462–3471.

[3] P. Grandjean, R. Clapp, *New Solut* **2015**, *25*, 147–163.

[4] M. I. Gomis, R. Vestergren, D. Borg, I. T. Cousins, *Environment International* **2018**, *113*, 1–9.

[5] A. B. Lindstrom, M. J. Strynar, E. L. Libelo, *Environmental Science & Technology* **2011**, *45*, 7954–7961.

[6] The European Parliament and the Council of the European Union, "Restrictions on the Marketing and Use of Certain Dangerous Substances and Preparations"(Perfluorooctane Sulfonates) (Directive 2006/122/EC, 2006), **2006**.

[7] U.S. Environmental Protection Agency, (EPA), "Revisions to the Unregulated Contaminant Monitoring Regulation (UCMR 3) for Public Water Systems" (Bill Code 6560-50-P, 2015)., **2012**.

[8] K. H. Kucharzyk, R. Darlington, M. Benotti, R. Deeb, E. Hawley, *Journal of Environmental Management* **2017**, *204*, 757–764.

[9] N. Merino, Y. Qu, R. A. Deeb, E. L. Hawley, M. R. Hoffmann, S. Mahendra, *Environmental Engineering Science* **2016**, *33*, 615–649.

[10] M. Trojanowicz, A. Bojanowska-Czajka, I. Bartosiewicz, K. Kulisa, *Chemical Engineering Journal* **2018**, *336*, 170–199.

[11] Z. Du, S. Deng, Y. Bei, Q. Huang, B. Wang, J. Huang, G. Yu, *Journal of Hazardous Materials* **2014**, *274*, 443–454.

[12] M. Nassi, E. Sarti, L. Pasti, A. Martucci, N. Marchetti, A. Cavazzini, F. D. Renzo, A. Galarneau, *J Porous Mater* **2014**, *21*, 423–432.

[13] R. Rattanaoudom, C. Visvanathan, S. K. Boontanon, *Journal of Water Sustainability* **2012**, *2*, 245–258.

[14] R. M. Wallace, P. J. Chen, S. A. Henck, D. A. Webb, *Journal of Vacuum Science & Technology A* **1995**, *13*, 1345–1350.

[15] V. Ochoa-Herrera, R. Sierra-Alvarez, *Chemosphere* **2008**, *72*, 1588–1593.

[16] L. Xiao, Y. Ling, A. Alsbaiee, C. Li, D. E. Helbling, W. R. Dichtel, *J. Am. Chem. Soc.* **2017**, *139*, 7689–7692.

[17] J. Yu, L. Lv, P. Lan, S. Zhang, B. Pan, W. Zhang, *Journal of Hazardous Materials* **2012**, *225–226*, 99–106.

[18] M. J. Klemes, Y. Ling, C. Ching, C. Wu, L. Xiao, D. E. Helbling, W. R. Dichtel, *Angewandte Chemie* **2019**, *131*, 12177–12181.

[19] Z. Zheng, H. Yu, W.-C. Geng, X.-Y. Hu, Y.-Y. Wang, Z. Li, Y. Wang, D.-S. Guo, *Nat Commun* **2019**, *10*, 1–9.

[20] M. A. Camblor, A. Corma, S. Valencia, *Chem. Commun.* **1996**, 2365–2366.

[21] D. P. Serrano, R. Van Grieken, P. Sánchez, R. Sanz, L. Rodríguez, *Microporous and Mesoporous Materials* **2001**, *46*, 35–46.

[22] K. Prevedouros, I. T. Cousins, R. C. Buck, S. H. Korzeniowski, *Environ. Sci. Technol.* **2006**, *40*, 32–44.

[23] P. Zareitalabad, J. Siemens, M. Hamer, W. Amelung, *Chemosphere* **2013**, *91*, 725–732.

[24] N. Saeidi, F.-D. Kopinke, A. Georgi, *Chemical Engineering Journal* **2020**, *381*, 122689.

[25] F. Wang, K. Shih, *Water Research* **2011**, *45*, 2925–2930.

[26] C. Quarti, A. Milani, C. Castiglioni, *J. Phys. Chem. B* **2013**, *117*, 706–718.

[27] R. W. Gora, S. J. Grabowski, J. Leszczynski, *J. Phys. Chem. A* **2005**, *109*, 6397–6405.

[28] B. M. Weckhuysen, A. A. Verberckmoes, I. P. Vannijvel, J. A. Pelgrims, P. L. Buskens, P. A. Jacobs, R. A. Schoonheydt, *Angewandte Chemie International Edition in English* **1996**, *34*, 2652–2654.
[29] T. Hasegawa, *Chemical Physics Letters* **2015**, *627*, 64–66.
[30] C. Wang, J. Liu, J. Yang, J. Li, *Microporous and Mesoporous Materials* **2017**, *242*, 231–237.
[31] N. Martín, M. Moliner, A. Corma, *Chem. Commun.* **2015**, *51*, 9965–9968.
[32] D. Zhao, Q. Huo, J. Feng, B. F. Chmelka, G. D. Stucky, *J. Am. Chem. Soc.* **1998**, *120*, 6024–6036.
[33] M. Grün, I. Lauer, K. K. Unger, *Adv. Mater.* **1997**, *9*, 254–257.
[34] A. Alves, G. Jacobs, G. Vanermen, A. Covaci, S. Voorspoels, *Talanta* **2015**, *144*, 574–583.
[35] P. Giannozzi, S. Baroni, N. Bonini, M. Calandra, R. Car, C. Cavazzoni, D. Ceresoli, G. L. Chiarotti, M. Cococcioni, I. Dabo, A. D. Corso, S. de Gironcoli, S. Fabris, G. Fratesi, R. Gebauer, U. Gerstmann, C. Gougoussis, A. Kokalj, M. Lazzeri, L. Martin-Samos, N. Marzari, F. Mauri, R. Mazzarello, S. Paolini, A. Pasquarello, L. Paulatto, C. Sbraccia, S. Scandolo, G. Sclauzero, A. P. Seitsonen, A. Smogunov, P. Umari, R. M. Wentzcovitch, *J. Phys.: Condens. Matter* **2009**, *21*, 395502.
[36] J. P. Perdew, K. Burke, M. Ernzerhof, *Phys. Rev. Lett.* **1996**, *77*, 3865–3868.
[37] S. Grimme, Journal of Computational Chemistry **2006**, 27, 1787–1799.
[38] D. Vanderbilt, *Phys. Rev. B* **1990**, *41*, 7892–7895.

5.5. Supporting Information

5.5.1. Experimental Procedures

A. Synthetic Procedures

Reagents and standards

All reagents and standards were acquired from Sigma-Aldrich in the highest grade available. Aqueous solutions were prepared in Milli-Q water. Both native and mass-labelled analytical reference standards used for characterization were acquired from Wellington Laboratories (Guelph, Ontario, Canada). Commercial zeolite samples (CP814-E22, referred to as Beta-22, CP811C-300, referred to as Beta-300 and USY) were acquired via Zeolyst International. The Activated Carbon was a powder type Norit SX 1G (Cabot).

Synthesis of all-silica and high-silica zeolites

All-silica zeolite Beta was prepared in fluoride media, according to a method described earlier in literature.[1] Tetraethylorthosilicate (TEOS) was used as silica source and an aqueous solution of tetraethylammonium hydroxide (TEAOH) was used as organic structure directing agent (OSDA). The final gel composition was: SiO_2 : 0.55 TEAOH : 0.55 HF : 9 H_2O. Crystallization of the zeolite was carried out in a Teflon liner under static conditions at 408 K for 168 hours. After crystallization, the solid product was separated from the liquid phase by filtration and washed repeatedly with deionized water. The zeolite product was obtained after thermal treatment at 823 K for 6 hours.

All-silica silicalite-1 was prepared in basic media according to a procedure described in literature.[2] Silica sol was used as silica source, ethylamine (C_2H_7N) and tetrapropylammonium bromide (TPABr) were used as OSDA. The final gel composition was: SiO_2 : 0.1 C_2H_7N : 0.1 TPABr : 0.15 NaOH : 50 H_2O. Crystallization of the zeolite was carried out in a Teflon liner under static conditions at 453 K for 20 hours. After crystallization, the solid product was washed and thermally activated in a similar way as all-silica zeolite Beta.

Synthesis of high-silica chabazite was performed in basic media, like described earlier in literature.[3] USY zeolite was used as silica source and TEAOH as OSDA. The final gel composition was: SiO_2 : 0.2 TEAOH : 0.2 NaOH : 5 H_2O. Crystallization of the zeolite was carried out in a Teflon liner under static conditions at 433 K for 72 hours. After crystallization, the solid product was washed and thermally activated in a similar way as all-silica zeolite Beta.

Synthesis of mesoporous silica materials

Two highly ordered hexagonal mesoporous silica materials (SBA-15 and MCM-41) were synthesized according to the respective literature methods.[4,5] For the synthesis of SBA-15, TEOS was used as silica source and Pluronic P123 (a nonionic alkyl poly(ethylene oxide) oligomeric surfactant) as OSDA. Typically, 4 g of Pluronic P123 and 8.5 g of TEOS were dissolved in 30 g of water and 120 g of a 2 M HCl solution and stirred at 308 K for 20h. The solid product was then washed with water, air-dried at 298 K and thermally activated at 773 K for 6 h.

For the synthesis of MCM-41, TEOS was again used as silica source and cetyltrimethylammonium bromide (CTABr) as OSDA. The procedure started by dissolving 2.50 g of CTABr in 50 mL of water. Afterwards, 60 g of ethanol and 13.2 g of ammonium hydroxide were added and stirred for 15 min to obtain a homogeneous solution. Then 4.67 g of TEOS was added and the resulting solution was stirred for 2 h. The precipitate was washed with water and methanol. The solid product was dried overnight at 343 K and thermally treated at 823 K for 8 h.

B. Characterization

FTIR spectroscopy

Fourier transform infrared (FTIR) spectroscopy was used to investigate the hydroxyl stretching region of the zeolites. IR spectra of self-supporting wafers (~10 cm^2/g) were measured on a Nicolet 6700 FTIR spectrometer with DTGS detector (128 scans, 2 cm^{-1} resolution). Prior to the measurement, the samples were dried under vacuum to 723 K for 1 h. Spectra were recorded under vacuum at 423 K.

Physisorption measurements

N_2 physisorption experiments were performed using a Micromeritics 3Flex apparatus at 77 K. Samples (ca. 50 mg) were activated at 413 K under dynamic vacuum (10^{-3} mbar) prior to the measurements. Micropore volumes were calculates using the t-plot model. Surface areas were calculated using the multipoint BET (Brunauer-Emmett-Teller) method, all in accordance with the Rouquerol consistency criteria. Water vapor physisorption was performed on the same apparatus with degassed water at 298 K. Degassing consisted of connecting a pressure resistant stainless steel canister with water (ca. 15 mL) to the 3Flex apparatus and cooling it to freezing temperature (273 K). After 15 min of cooling the head space of the container was removed under dynamic vacuum (10^{-3} mbar), the canister's connection valve was closed and water was left to defrost. The process was repeated 3 times to ensure complete degassing.

TGA measurements

TGA measurements were performed on a Netzsch STA 449C. The measurements were performed under oxygen and start at room temperature. The temperature is increased with a constant ramp of 10 K/min up to 1273 K. Data were analyzed with the Netzsch Proteus Thermal Analysis Software.

XRD measurements

Powder X-ray diffraction (XRD) patterns of all-silica zeolite Beta were recorded on a Malvern PANalytical Empyrean diffractometer in transmission mode over a 1.3–45° 2θ range, using a PIXcel3D solid-state detector and Cu anode (Cu Kα1: 1.5406 Å; Cu Kα2: 1.5444 Å). Data were analyzed with the PANalytical Data Viewer Software.

HPLC-MS analysis

Samples containing perfluorinated carboxylates or sulfonates were analyzed by LC-ESI-(-)-MS/MS using a Waters UPLC and a XEVO Triple Quad tandem mass spectrometer. Analytes were separated on a Waters Acquity BEH Shield RP_{18} column (2.1 × 100 mm; 1.7 µm) at 313 K. An elution gradient was used, with 2 mM ammonium acetate either in 95:5 (*v/v*) water:MeOH (solvent A), or in MeOH (solvent B). Two multiple reaction monitoring (MRM) transitions were used for each analyte. The method was validated and the method precision (which is the most important performance parameter for this study) ranged from < 1 % (repeatability) tot 2-4 % (intermediate precision). During analysis, a quality control scheme was in place to monitor good performance of the method. Further details can be found in literature.[6]

Calorimetry measurements

The adsorption enthalpies (ΔH_{ads}) were determined by a titration method in a cell placed into a Tian−Calvet-type microcalorimeter, TAM III, provided by TA Instruments. In each experiment, 1.5 mg of sample was placed in a stainless steel ampule. Then 800 mL of water was introduced into the cell. The cell was then fixed on the calorimetric titration setup and introduced into the thermopiles. An ampule with only the solvent was used as a reference. After thermal equilibration at 298 K and while keeping the suspension stirred, a stock solution of PFOA (initial bulk concentration: 2.1g/L) was introduced step by step into the calorimetric cell via a fine cannula with a motor-driven syringe pump. A total volume of 200 mL of stock solution was added in steps of 10 mL with 1.5 h of equilibrium time between each injection. This process yielded a calorimetric peak that contained two contributions: one from adsorption and one corresponding to a dilution effect. The contribution of the dilution effect was measured via a blank sample, in order to subtract it from the total calorimetric peak. Homemade software was used to compute the amount of

PFOA adsorbed in the calorimetric experiment, the heat of dilution and the adsorption enthalpy. This was done using the following experimental data: heat measured at each injection, the adsorption isotherm and the dilution enthalpy curve. Integrated enthalpies of adsorption were plotted as a function of equilibrium concentration determined from adsorption isotherms for each injection.

Solid-state NMR experiments

Solid-state NMR measurements were carried out on a 600 MHz Varian NMR spectrometer using 1.6 mm HXY MAS probe. Samples were spun at 32 kHz unless otherwise stated. In the ^{1}H-^{1}H homonuclear correlation experiment, four consecutive cycles of POST-C7 recoupling scheme were used for the excitation and reconversion of ^{1}H double-quantum (DQ) coherences. Repetition delay was 0.2 s for the 'AllSiBeta 500' sample (= all-silica zeolite Beta, maximally loaded after equilibration with a 500 mg PFOA/L stock solution) and 0.5 s for the 'PFOA' sample (= pure, crystalline PFOA). During the experiments, samples were cooled down to 278 K to enhance the signal. The ^{19}F-^{29}Si heteronuclear correlation spectrum was measured by exciting fluorine nuclei with the $\pi/2$ pulse of 1.7 μs and transferring polarization to silicon nuclei using a ramped-amplitude cross-polarization (CP) block of 5 ms. For each of the 22 slices along the indirect dimension (t_1), 7360 scans were accumulated with 1 s repetition delay. The ^{13}C and ^{19}F MAS NMR spectra were measured using the Hahn-echo sequence with the echo delay of one rotation period. In the ^{13}C MAS experiments, the recycling delay was 3 s, and 260 000, 50 000, and 12 000 scans were acquired for the 'AllSiBeta 500', 'AllSiBeta 250' (= all-silica zeolite Beta loaded with a 250 mg PFOA/L stock solution), and 'PFOA' samples, respectively. During signal acquisition, high-power fluorine XiX decoupling was applied. In the ^{19}F MAS experiments, the recycling delay was 5 s and up to 64 scans were acquired. The ^{1}H-^{13}C heteronuclear correlation experiment consisted of the ^{1}H excitation pulse of 1.5 μs and a CP block of 5 ms. 12 slices along t_1 were recorded with 32 000 scans each; repetition delay was 0.5 s. The ^{19}F-^{19}F homonuclear correlation experiment comprised a single BABA cycle for the DQ excitation and another one for the reconversion. The sample was spun at 40 kHz. The $\pi/2$ pulse of 1.7 μs was used, and the 2D spectrum was obtained after acquiring 300 slices along t_1 with 32 scans each and 1 s delay between consecutive scans. The ^{1}H, ^{13}C and ^{29}Si spectral axes were calibrated relative to the signals of TMS, and ^{19}F relative to the signal of $CFCl_3$.

C. Experiments

Adsorption experiments

All batch adsorption experiments were performed in polypropylene vials, in order to avoid PFAS adsorption onto the surface of glass vials. For all the experiments, a commercial powder activated carbon (Norit SX 1 G) was used as benchmark material. For the determination of the single compound adsorption isotherms, an amount of 5 mg of adsorbent was contacted with 5 mL of an aqueous sample with a known PFOA or PFOS concentration (C_0). PFOA stock concentrations ranged from 0.1 mg/L to 500 mg/L, while PFOS stock concentrations ranged from 0.1 mg/L to 250 mg/L (Table S1). A lower maximum concentration was used for PFOS in order to avoid micelle formation; PFOS has a lower critical micelle concentration (CMC) than PFOA. Stock concentrations for other PFAS alternatives were similar to those of PFOS. The samples were shaken for 24 hours where after PFAS concentrations of the aqueous solutions were measured via HPLC-MS (see above). PFAS uptake on the zeolite adsorbents was calculated using equation 1, where V is the sample volume (L), q (mg/g) is the amount of PFAS adsorbed per g of dry matter (m) and C_e (mg/L) is the equilibrium PFAS concentration in the aqueous solutions, upon contact with the adsorbent.

$$q = (C_0 - C_e)\, V_{sample} / m_{adsorbent} \quad (1)$$

After the experiments, all results were fitted to the Langmuir and Freundlich adsorption model and isotherms were plotted according to the model with the best fit. For kinetic experiments, 5 mg of adsorbent was contacted with 5 mL of a 100 mg/L solution of either PFOA or PFOS. Contact times were varied, ranging from 5 min up to 24 h. For pH screening experiments, 5 mg of adsorbent was contact with 5 mL of a 100 mg/L solution of PFOA. After initial equilibration, pH was adjusted by adding adequate amounts of either HCl or NaOH in small steps. For competitive experiments, 5 mg of adsorbent was mixed with 5 mL of a 100 µM aqueous solution of PFOA or PFOS. This time, five organic compounds (caprylic acid, phenol, sodium dodecyl sulfate (SDS), benzoic acid and adipic acid) were simultaneously present in the sample, either in a 1:1 or 1:3 (PFAS : organic compound) molar ratio for every individual organic compound. In the case of 1:1 ratio, there was a total fivefold molar excess of organic compounds over PFOA or PFOS. In the case of 1:3 ratio, there was a total fifteenfold molar excess of organic compounds over PFOA or PFOS. For the experiments with competition of inorganic ions, stock solutions were prepared with 100 µM of PFOA together with either $CaCl_2$ or $KHCO_3$. Concentrations of these salts where adjusted to have either 100 µM or 300 µM of the inorganic anion.

Measurements of the PFAS concentrations and calculations of PFAS uptakes were performed as described previously.

Regeneration of the zeolite adsorbents

The loaded zeolite samples were heated in a muffle furnace at a ramp of 10 K/min until the temperature reached 633 K. The temperature was then kept constant for 10 min. Afterwards, sufficient time was given for the zeolite samples to cool down to room temperature.

D. Molecular simulations

Calculations of the adsorption energies

The DFT simulations of the adsorption of PFOA and caprylic acid in all-silica zeolite Beta were performed using the Quantum Espresso package [7], which is implemented under periodic boundary conditions with plane wave functions as a basis set. These calculations were performed with the consideration of a supercell (1 × 2 × 1) constructed from the unit cell of the all-silica zeolite Beta containing a dimer of either PFOA or caprylic acid. The geometry optimizations of all tested dimer conformations (head-head, head-tail and tail-tail) were performed with the generalized gradient approximation (GGA/PBE) [8] coupled with the DFT-D2 scheme [9] in order to compute the contributions of the dispersion forces. The relative ion positions were relaxed until all of the force components were lower than 0.001 Ry/Bohr, while the unit cell parameters were kept constant. The ion cores were described by Vanderbilt ultrasoft pseudopotentials [10], and the Kohn Sham one-electron states were expanded in a planewave basis set with a kinetic cutoff energy of 35 Ry (350 Ry for the charge density). The calculations were performed at the Γ-point. This allows to define an energy ranking of all the confined conformations for both PFOA and caprylic acid with the head-head configuration taken as a reference. The PFOA/zeolite and caprylic acid/zeolite interaction energies of the most stable conformations (head-head) were computed according to equation 2.

$$\text{Interaction Energy} = E_{\text{dimer in all-silica zeolite}} - E_{\text{dimer}} - E_{\text{all-silica zeolite}} \quad (2)$$

The terms $E_{\text{dimer in all-silica zeolite}}$, E_{dimer} and $E_{\text{all-silica}}$ zeolite correspond to the total energy of the optimized 'dimer in all-silica zeolite' structures, the single-point total energy of the dimer in gas phase and the single point total energy of the all-silica zeolite Beta.

Calculation of chemical shifts

Structural models of crystalline PFOA and of all-silica zeolite Beta were geometry optimized with the DFT-based relaxation using CASTEP software package (Materials Studio v. 5.5.3, Accelrys Software Inc.). Plane-wave basis, generalized gradient approximation of Perdew-Burke-Ernzerhof, and ultrasoft pseudopotentials (generated on-the-fly with CASTEP) were employed. Upon relaxation, the force on each atom was smaller than 0.01 eV/Å and stress was below 0.03 GPa. In the DFT-based relaxation, kinetic-energy cutoff for the plane-wave basis was set to 650 eV, and the reciprocal-space sampling was performed with the k-point grid spacing of 0.042 $Å^{-1}$ or less. First-principles calculations of isotropic chemical shifts of ^{13}C and ^{29}Si nuclei were carried out with the GIPAW/DFT approach using the NMR CASTEP package. The kinetic-energy cutoff for the plane-wave basis for these calculations was increased to 700 eV and a finer grid of k-points was used, having the spacing of 0.028 $Å^{-1}$ or less. GIPAW calculations yielded isotropic chemical shieldings σ^{iso}, from which isotropic chemical shifts were obtained via equation 3, with σ^{ref} being set to 169 ppm for ^{13}C and 325.8 ppm for ^{29}Si nuclei, respectively. These shielding values have led to the best agreement between the calculated and the experimental isotropic ^{13}C and ^{29}Si chemical shifts for many different crystalline solids.

$$\delta_{CS}^{iso} = \sigma^{ref} - \sigma^{iso} \quad (3)$$

5.5.2. Supporting Figures

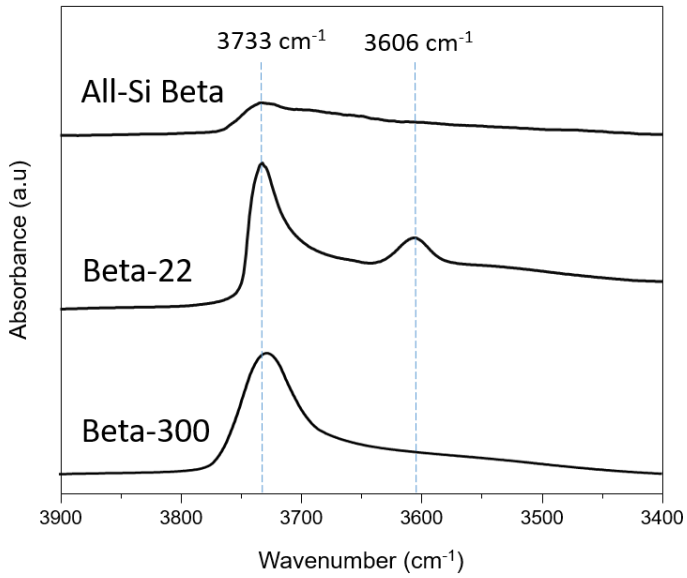


Figure S5.1: FTIR spectrum of the hydroxyl stretching region for as-synthesized all-silica Beta (All-Si Beta) and for the commercial zeolite Beta types Beta-22 and Beta-300. The band at 3606 cm^{-1} corresponds with bridging OH groups due to the Al-content. The band at 3733 cm^{-1} corresponds to non-acidic hydroxyl groups at defect sites inside the crystals or at the outer surface. In the spectrum of All-Si Beta, the ν_{OH} vibration of the bridging OH-groups, which is characteristic for Al-containing, commercial zeolite Beta, is fully absent. The only band in the ν_{OH} range of All-Si-Beta is that of the non-acidic hydroxyl groups at defect sites inside the crystal's framework (3733 cm^{-1}). However, this band is much less intense than for deeply dealuminated commercial Beta-300, indicating a much smaller amount of point defects and hence a much higher degree of hydrophobicity in All-Si Beta.

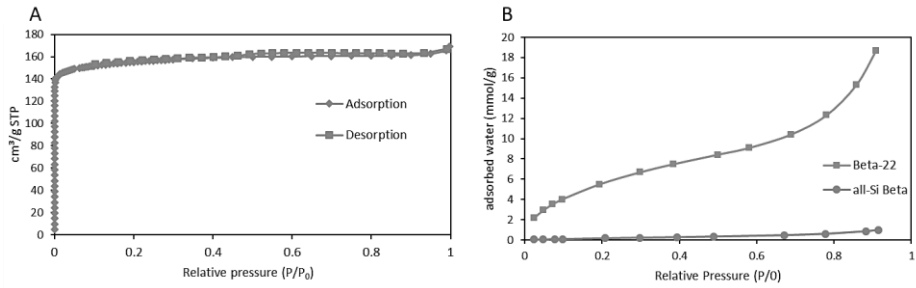


Figure S5.2: Characterization of all-silica zeolite Beta via N_2 and water vapor physisorption isotherms. (A): N_2 physisorption isotherm of all-silica zeolite Beta, resulting in a calculated t-plot micropore volume of 0.21 cm^3/g and a BET surface of 624 m^2/g. (B): Water vapor physisorption isotherms for all-silica zeolite Beta (all-Si Beta) and for a more hydrophilic zeolite Beta type (Beta-22, with SiO_2/Al_2O_3 = 22).

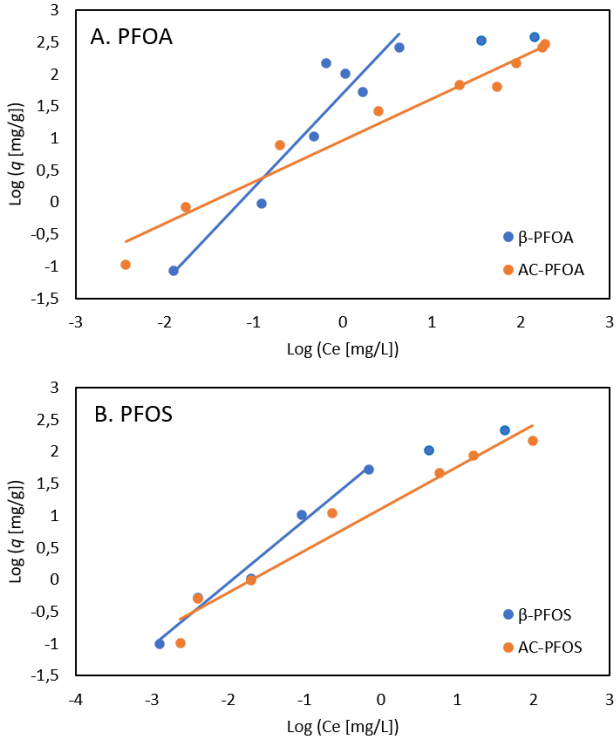


Figure S5.3: Adsorption isotherms for the adsorption of PFOA (A) and PFOS (B) on all-silica zeolite Beta (β) and activated carbon (AC) plotted on a log-log graph. Isotherms are plotted over the linear region only. *q* = mg PFAS adsorbed per g of dry matter adsorbent; Ce = equilibrium concentration in water.

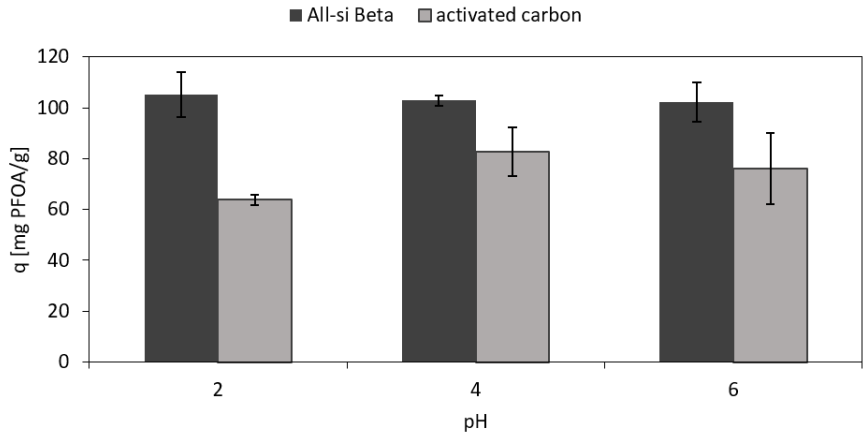


Figure S5.4: The effect of pH upon the adsorption of PFOA on all-silica zeolite Beta and activated carbon. *q* = mg PFAS adsorbed per g of dry matter adsorbent. Starting concentration = 100 mg PFOA/L. pH was adjusted by adding adequate amounts of HCl or NaOH. Error bars indicate standard deviation for triplicate experiments.

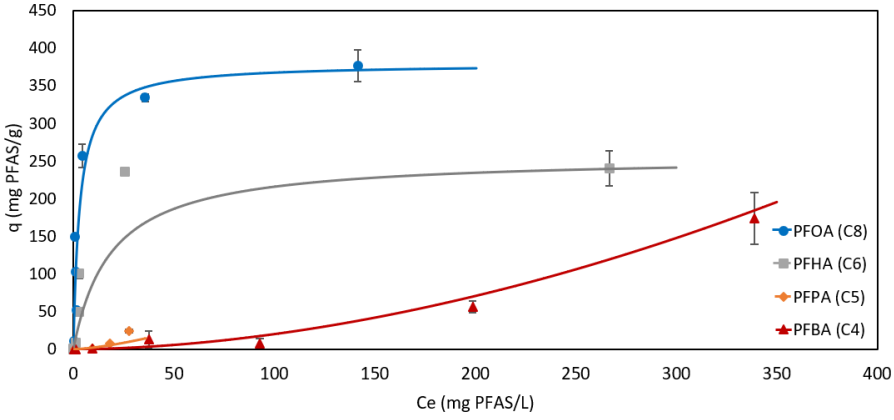


Figure S5.5: Adsorption isotherms for linear perfluorinated carboxylic acids of varying chain length on all-silica zeolite Beta. *q* = mg PFAS adsorbed per g of dry matter adsorbent; C_e = equilibrium concentration in water. PFOA = perfluorooctanoic acid (C_8), PFHA = perfluorohexanoic acid (C_6), PFPA = perfluoropentanoic acid (C_5), PFBA = perfluorobutanoic acid (C_4). For PFOA and PFHA, Langmuir isotherms are plotted. For PFPA and PFBA, Freundlich isotherms are plotted. Errors bars indicate standard deviation for triplicate experiments.

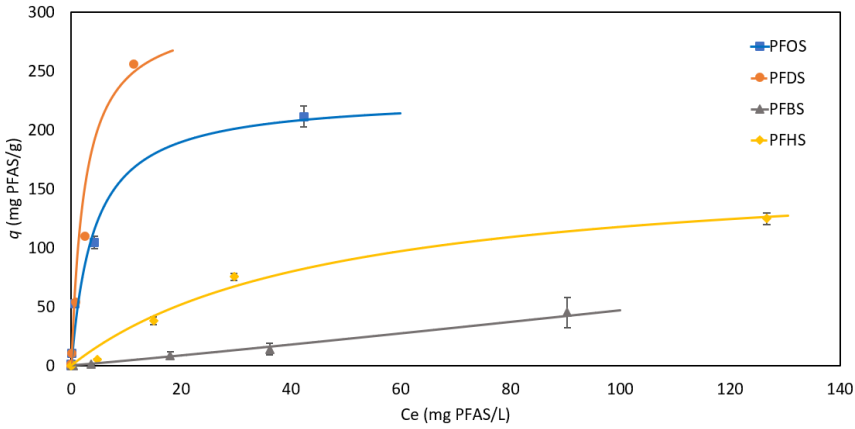


Figure S5.6: Adsorption isotherms for linear perfluorinated sulfonic acids of varying chain length on all-silica zeolite Beta. q = mg PFAS adsorbed per g of dry matter adsorbent; C_e = equilibrium concentration in water. Also longer perfluorinated chains fit very well in the channels of all-silica zeolite Beta; a very high affinity and capacity is seen for perfluorodecanesulfonic acid (PFDS, C_{10}). PFOS = perfluorooctanesulfonic acid (C_8), PFHS = perfluorohexanesulfonic acid (C_6), PFBS = perfluorobutanesulfonic acid (C_4). For PFDS, PFOS and PFHS, Langmuir isotherms are plotted. For PFBS, a Freundlich isotherm is plotted. Errors bars indicate standard deviation for triplicate experiments.

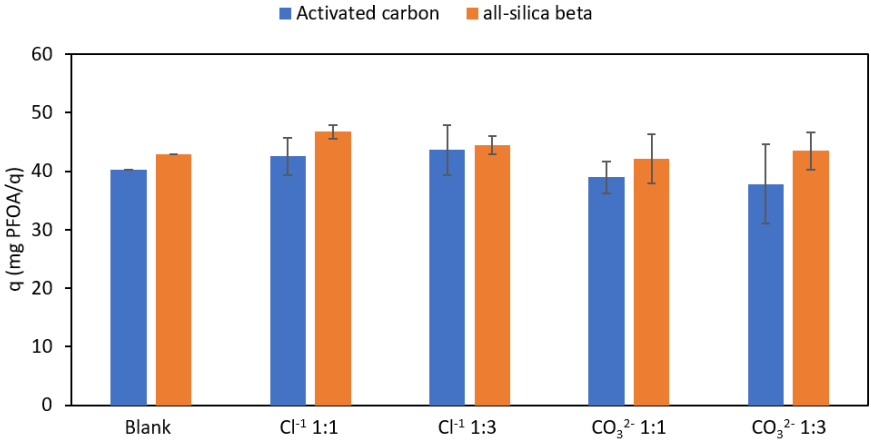


Figure S5.7: PFOA adsorption on all-silica Beta and activated carbon under competition of inorganic anions (100 µM of PFOA and 100 µM (1:1) or 300 µM (1:3) of a single inorganic anion). q = mg PFAS adsorbed per g of dry matter adsorbent. $CaCl_2$ was added to adjust chlorine concentrations, whereas $KHCO_3$ was added to adjust carbonate concentrations. Error bars indicate standard deviation for triplicate experiments.

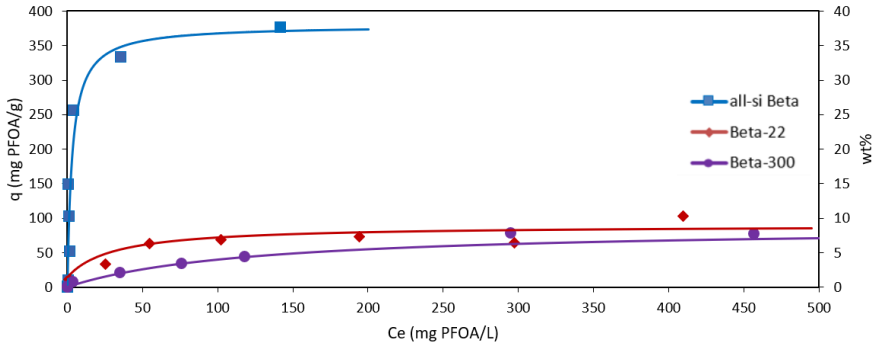


Figure S5.8: Adsorption isotherms for PFOA on all-silica Beta (β) and the aluminum-containing zeolites Beta-22 and Beta-300. The latter number refers to the SiO_2/Al_2O_3 ratio. q = mg PFAS adsorbed per g of dry matter adsorbent; C_e = equilibrium concentration in water.

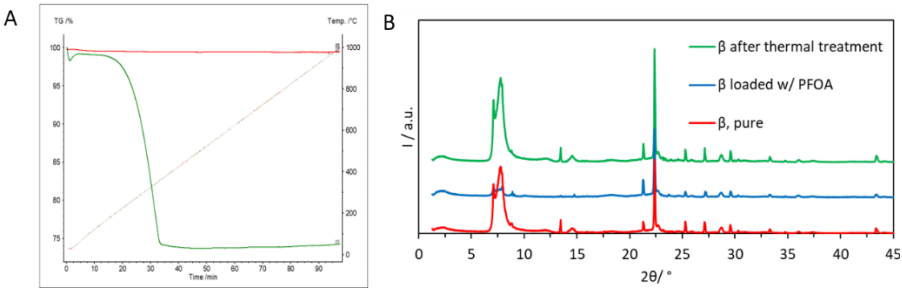


Figure S5.9: Studying the impact of thermal treatment on a PFOA-saturated all-silica zeolite Beta. **(A)**: Thermogravimetric analysis of pure, crystalline and as-synthesized all-silica zeolite Beta (red) and of all-silica zeolite Beta, fully loaded with PFOA (green). The temperature profile is indicated by the dotted line. The relative weight loss of the PFOA loaded zeolite Beta clearly shows that all PFOA is removed at a temperature of 623 K. **(B)**: XRD patterns of pure, crystalline and as-synthesized all-silica zeolite Beta (red), all-silica zeolite Beta fully loaded with PFOA (blue) and of all-silica zeolite Beta after loading with PFOA and thermal treatment at 623 K (green). No loss of crystallinity of zeolite Beta is seen after adsorption and desorption of PFOA.

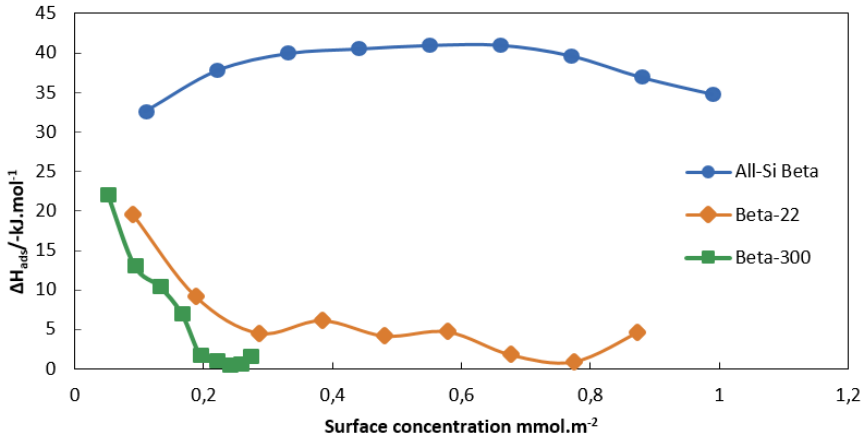


Figure S5.10: Integral adsorption enthalpies for all-silica zeolite Beta and the aluminum-containing zeolites Beta-22 and Beta-300 as a function of the surface concentration of PFOA, measured via calorimetry.

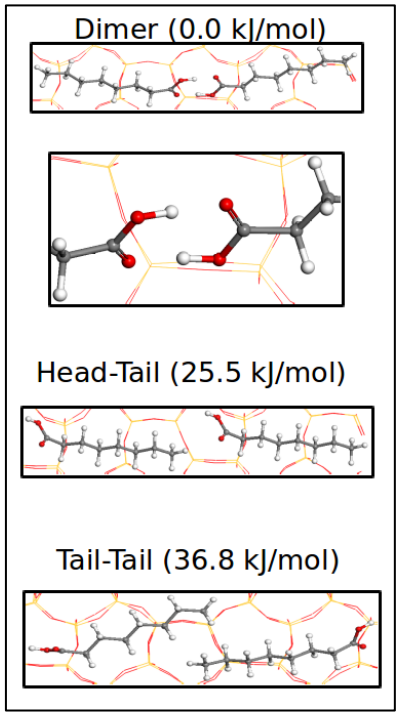


Figure S5.11: Snapshots of DFT-optimized caprylic acid conformations adsorbed in all-silica zeolite Beta, as well as their associated total energy differences with respect to the head-head dimer taken as reference.

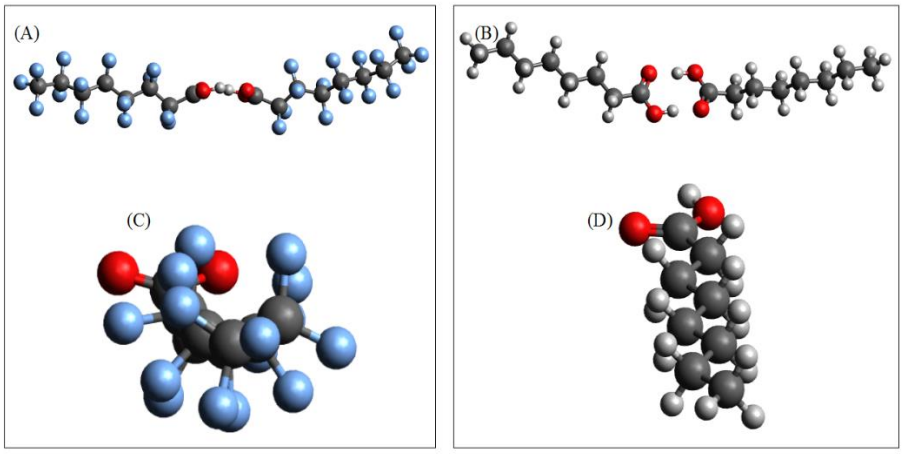


Figure S5.12: Snapshots of the geometry optimized PFOA **(A)** and caprylic acid **(B)** dimers. The helical and zig-zag conformations of the PFOA **(C)** and the caprylic acid **(D)** chains, respectively, are also depicted.

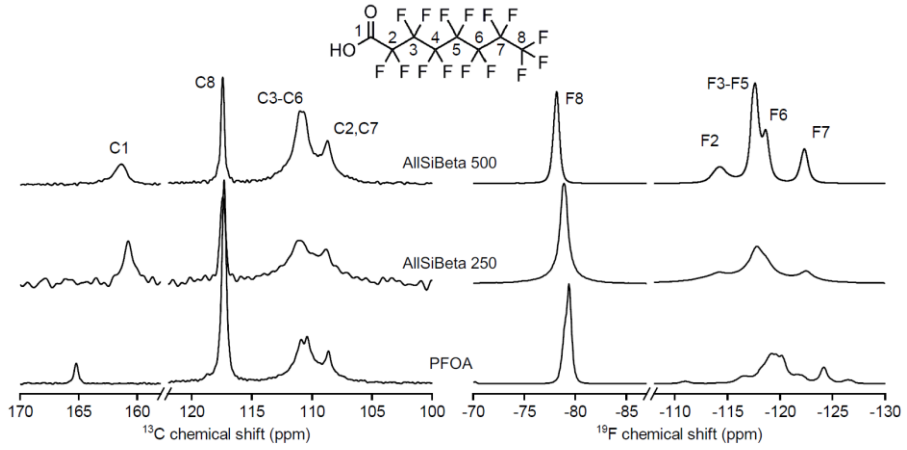


Figure S5.13: ^{13}C and ^{19}F MAS NMR spectra of pure, crystalline PFOA and of PFOA loaded into the all-silica zeolite Beta in two different concentrations (AllSiBeta 250 = moderate concentration, AllSiBeta 500 = maximal concentration). ^{13}C and ^{19}F NMR signals were assigned to individual carbon and fluorine sites of PFOA based on the DFT/GIPAW calculations of the chemical shifts of the crystalline PFOA, and by ^{1}H-^{13}C heteronuclear and ^{19}F-^{19}F homonuclear correlation measurements on the sample with PFOA incorporated into the zeolite (see Figure S5.11).

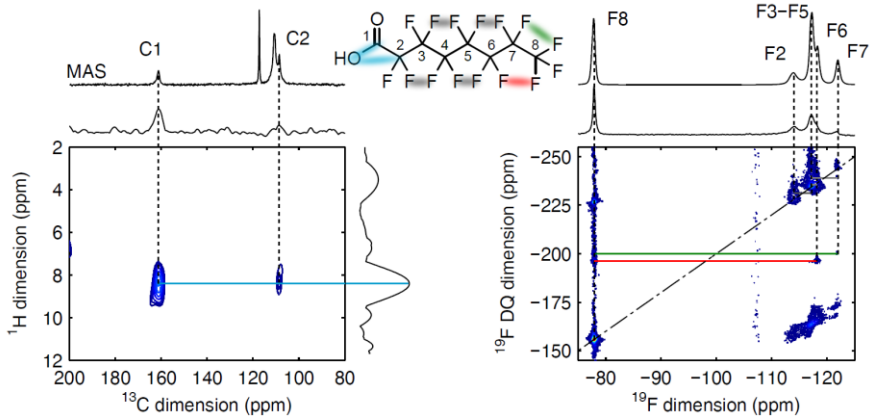


Figure S5.14: Two-dimensional ^{1}H-^{13}C heteronuclear correlation (left) and ^{19}F-^{19}F homonuclear correlation (right) NMR spectra of PFOA loaded into the all-silica zeolite Beta (highest concentration, AllSiBeta 500). Above the two-dimensional spectra, skyline projections of the spectra onto the ^{13}C and ^{19}F dimension are compared to the ^{13}C and ^{19}F MAS NMR spectra, respectively. Solid horizontal lines in the two-dimensional spectra mark selected correlations (proximities) among atoms. Their color code is explained in the inserted scheme of the PFOA molecule.

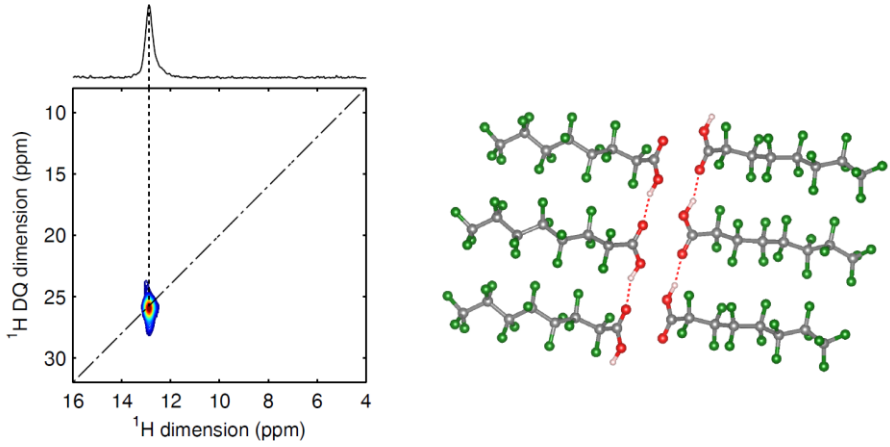


Figure S5.15: Two-dimensional ^{1}H-^{1}H DQ-SQ homonuclear correlation NMR spectrum of pure, crystalline PFOA (left) and schematic presentation of the arrangement of PFOA molecules and of the hydrogen-bonding among these molecules in the crystals (right). Hydrogen bonds are presented with red dotted lines.

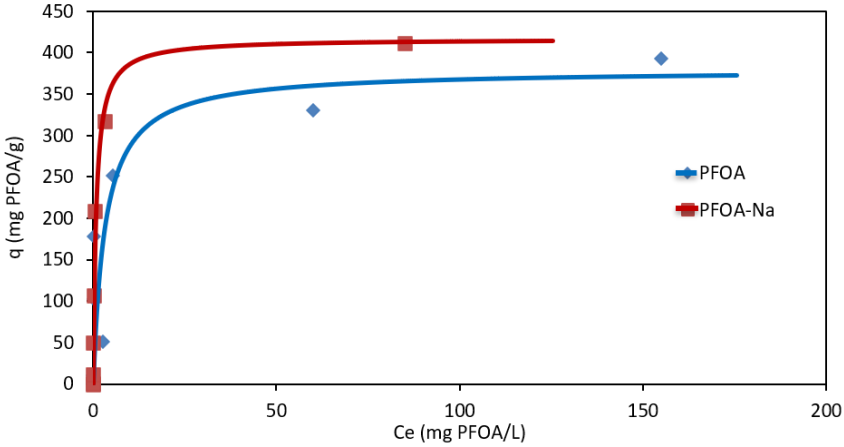


Figure S5.16: Langmuir adsorption isotherms for PFOA and its sodium salt on all-silica zeolite Beta. q = mg PFAS adsorbed per g of dry matter adsorbent; C_e = equilibrium concentration in water.

5.5.3. Supporting Tables

Table S5.1: Model parameters obtained by fitting the adsorption data of different zeolite Beta types and activated carbon to the Langmuir and Freundlich adsorption models. q_m [mg/g] and K_L [l/mg] are Langmuir parameters. q_m is the maximum adsorption capacity, while K_L is an indicator of the affinity of the adsorbent. K_F [(l/g)^n] is the Freundlich parameter and n^{-1} is the Freundlich exponent. K_F is an indicator for the adsorption capacity, while n represents the heterogeneity of the adsorption sites. n/a = not available, in case of a very bad fit to the model.

		Langmuir			Freundlich		
Adsorbent	**Adsorbate**	**q_m (mg/g)**	**K_L (l/mg)**	**R^2**	**n^{-1}**	**K_F (l/g)^n**	**R^2**
All-si Beta	PFOA	379,2	0,31	0,90	0,28	103,55	0,82
All-si Beta	PFOS	228,7	0,24	0,98	0,76	29,73	0,94
All-si Beta	PFBA	n/a	n/a	n/a	1,82	0,00	0,96
All-si Beta	PFPA	n/a	n/a	n/a	1,46	0,08	0,80
All-si Beta	PFHA	256,4	0,05	0,98	0,82	9,51	0,88
All-si Beta	PFBS	n/a	n/a	n/a	1,06	0,35	0,99
All-si Beta	PFHS	173,1	0,02	0,99	0,86	2,58	0,98
All-si Beta	PFDS	303,0	0,41	0,94	0,80	55,70	0,98
Beta-22	PFOA	90,1	0,04	0,92	0,59	3,96	0,95
Beta-22	PFOS	147,1	0,05	0,95	0,78	3,84	0,99
Beta-300	PFOA	87,7	0,01	0,94	0,65	1,98	0,98
Beta-300	PFOS	49,0	0,08	0,89	0,66	2,91	0,97
AC	PFOA	392,7	0,01	0,91	0,93	2,21	0,98
AC	PFOS	171,7	0,06	0,99	0,39	25,58	0,99

Table S5.2: Stock concentrations of PFOA and PFOS solutions used for the determination of the single compound adsorption isotherms.

PFAS	Stock concentrations (mg PFAS/L)								
PFOA	0.1	1	10	50	100	150	250	350	500
PFOS	0.1	0.5	1	10	50	100	250		

5.5.4. References Supporting Information

[1] D. P. Serrano, R. Van Grieken, P. Sánchez, R. Sanz, L. Rodríguez, *Microporous and Mesoporous Materials* **2001**, *46*, 35–46.

[2] C. Wang, J. Liu, J. Yang, J. Li, *Microporous and Mesoporous Materials* **2017**, *242*, 231–237.

[3] N. Martín, M. Moliner, A. Corma, *Chem. Commun.* **2015**, *51*, 9965–9968.

[4] D. Zhao, Q. Huo, J. Feng, B. F. Chmelka, G. D. Stucky, *J. Am. Chem. Soc.* **1998**, *120*, 6024–6036.

[5] M. Grün, I. Lauer, K. K. Unger, *Adv. Mater.* **1997**, *9*, 254–257.

[6] A. Alves, G. Jacobs, G. Vanermen, A. Covaci, S. Voorspoels, *Talanta* **2015**, *144*, 574–583.

[7] P. Giannozzi, S. Baroni, N. Bonini, M. Calandra, R. Car, C. Cavazzoni, D. Ceresoli, G. L. Chiarotti, M. Cococcioni, I. Dabo, et al., *J. Phys.: Condens. Matter* **2009**, *21*, 395502.

[8] J. P. Perdew, K. Burke, M. Ernzerhof, *Phys. Rev. Lett.* **1996**, *77*, 3865–3868.

[9] S. Grimme, Journal of Computational Chemistry **2006**, 27, 1787–1799.

[10] D. Vanderbilt, *Phys. Rev. B* **1990**, *41*, 7892–7895.

CHAPTER 6

STRUCTURED ZEOLITIC ADSORBENTS FOR THE ADSORPTIVE SEPARATION OF PFASS BY DROPLET COAGULATION TECHNIQUES

Matthias Van den Bergh,[a,b] Steven Mullens,[b] and Dirk De Vos[a]

Unpublished results

[a] M. Van den Bergh, Prof. D. E. De Vos
Centre for Membrane Separations, Adsorption, Catalysis and Spectroscopy for Sustainable Solutions (cMACS)
KU Leuven
Celestijnenlaan 200F, 3001 Leuven, Belgium
[b] M. Van den Bergh, S. Mullens
Flemish Institute for Technological Research, VITO
Boeretang 200, 2400 Mol, Belgium

Abstract

This chapter focuses on the shaping and structuration of zeolite Beta as adsorbent for PFAS contaminants. First, different types of binder materials were screened for their compatibility with zeolite Beta; no negative impact on PFAS adsorption could be seen. Second, microspheres for application in a packed bed adsorption column were synthesized with a commercial zeolite Beta by gravitational droplet extrusion. Highly spherical microspheres of around 2 mm wide could be synthesized with this shaping procedure, even when only low amounts of active material are available. However, shaping of the zeolite adsorbent reduced both adsorption kinetics and capacity, as compared to the original zeolite material. Application of the gravitational droplet extrusion process for all-silica zeolite Beta instead of Beta-22 proved cumbersome.

Contributions

M.V.d.B. wrote the manuscript. S.M. and D.D.V. supervised the work.

6. Structured zeolitic adsorbents for the adsorptive separation of PFASs by droplet coagulation

6.1. Introduction

6.1.1. Structured active materials

In the previous chapters, most adsorption experiments have been performed as batch experiments with powder-like adsorbents. After adsorption equilibrium is reached, the adsorbent is removed from the treated solution by sedimentation or filtration. This lab practice is advantageous for screening different adsorbents and/or many parameters, but it has several drawbacks when applied *in situ* for the treatment of waste water. Adsorption uptake is slow compared to water treatment in fixed bed columns, while adsorbent removal (after equilibration) via sedimentation is time-consuming. Adsorbent removal by filtration can be costly or lead to very high pressure drops over the filter, depending on the powder particle size and filter type. Therefore, most treatment systems that deal with large volumes of water (and thus moderate to high flow rates) use adsorption columns in which the adsorbent is applied as granular structures of controlled shape and size. This can go from very dense packed bed columns to very loose fluidized beds (see Chapter 2). Also size and shape of the particulate matter can vary widely, depending on the adsorbent type and treatment conditions, among others. In columns with particulate adsorbents, there is generally a trade-off between contact surface and time on the one hand, and pressure drop and flow rate on the other hand. A densely packed bed with e.g. metal oxide nanoparticles will have a very high contact area, resulting in a high adsorption capacity per unit bed length. Resistance to flow will be high though, resulting in a high pressure drop and increased cost of operation.

Even though the use of larger adsorbent particles can be advantageous compared to the powder form, the void space of adsorption beds packed with particulate materials can still be of random and tortuous nature. This leads to increased pressure drops and column inhomogeneities, which lead to unwanted process characteristics. Shaping of the active material into a hierarchically porous structure can overcome these drawbacks and is often a critical step in process optimization. Applying the active material in a structured, homogeneous shape can result in enhanced kinetics, more uniform processes (in time and space), higher surface area and hence optimized driving forces and in better adsorbent properties like stability or separability.[1,2] Several shaping techniques exist for transforming a microporous, inorganic powder into an hierarchical structure with meso- or macroporosity. Most literature on the shaping and structuration of inorganic materials deals with

catalysts, but the principles and methodologies are also valid for (inorganic) adsorbents. In general, two broad strategies can be defined: the active material can either be coated on a porous support, or meso- and/or macroporosity can be introduced in the active material itself; one then speaks of a self-supporting structure.[3,4] Within both strategies, one can choose between different types and shapes of (support) structure, degree and type of porosity, number and type of binders and other additives, shaping methodologies, etc. This all leads to a wide variety in shaping procedures and possibilities. Conventional (support) structures are, among others, (i) spheres, (ii) monoliths with straight channels (also called honeycombs), (iii) foams, (iv) knitted wire packings and (v) corrugated sheets packing. These structures can be ceramic or metallic. [5,6]

6.1.2. 3D-printing

A relatively new and innovative manner of support manufacturing is 3D-printing or 3DFD (Three Dimensional Fiber Deposition). This is a very flexible technique with a large freedom of design: the preferred channel structure and ideal flow pattern can be chosen in advance and manufactured very precisely. This allows optimization of mass and heat transfer while keeping flow resistance and pressure drop low. With 3DFD, it is possible to create shapes and structures that are almost impossible to construct with more convenient shaping procedures.[7] Of course, not every material can be printed as such. Solvents, binders and other additives have to be carefully selected and added to a printable paste, adding an extra degree of complexity. 3D-printed catalysts or adsorbents are self-supporting structures, hence no volume in the reactor or column is lost to an inert support material.[8,9] At the *Coating and Shaping Technologies* (CAST) research team of VITO, not only zeolites like ZSM-5, but also ZIFs (Zeolite Imidazolate Frameworks, e.g. ZIF-8) and SAPOs (a silicoaluminophosphate molecular sieve, e.g. SAPO-34) have been successfully applied for 3D-printed structures. [10–14] 3D-printing of both catalysts and adsorbents is definitely a rapid growing field, with an ever increasing number of publications and inventions. [15–18]

6.1.3. Coating

Coating of monoliths (or other support structures) and shaping of microspheres are other possibilities for the structuration and application of inorganic, active materials as catalyst or adsorbent. Coating of a zeolite material can generally be achieved by two different techniques: wash coating or hydrothermal coating. Wash coating involves the deposition of crystalline zeolite particles on a support from a slurry or suspension. This procedure is also known as dip coating or slurry coating.[19] Highly porous coatings can be obtained via wash coating, but addition of binders is often necessary in order to obtain sufficient mechanical stability. These binders are

generally suspensions of nano-sized silica or alumina particles. Addition of binders can reduce the activity and/or selectivity of the active zeolite material due to blocking of channels and/or active sites or due to active phase dilution, even though in some cases there is no impact or even a beneficial effect, due to synergistic interactions. [20,21] Higher zeolite loadings (i.e. thicker coatings) can be achieved by increasing the zeolite concentration in the casting suspension or by multiple treatments.

Hydrothermal coating involves the *in situ* growth of zeolite crystals on the surface of the support. Since the support acts as a base for the nucleation of zeolite crystals, a chemical bond between the support and the zeolite coating is formed. This results in a higher chemical, thermal and mechanical stability of the binderless coating, compared to wash coating. As a downside, high crystalline (inter)growth can result in a compact coating which then leads to diffusion limitation. A non-dense porous film is always preferred for low diffusive resistance and high specific surface area, but the mechanical stability of the coating always needs to remain sufficiently high. This unavoidable trade-off between porosity and mechanical stability is one of the big challenges in zeolite coating.[22] Another downside of the hydrothermal coating is the tendency of the zeolite crystals to grow in the hydrothermal solution instead of on the surface support, hereby lowering the selectivity of the coating synthesis. [23] The zeolite loading during hydrothermal coating is limited in a single coating step. Coating thickness can be increased by extending the synthesis time but this effect diminishes in time. For increasing the coating thickness, it is better to apply multiple coating steps. By increasing the number of coating steps, not only thickness but also density and crystal size will increase, since underlying zeolite coatings will act as nucleation seeds. Additionally, also Si/Al ratio can change with multiple coatings, thus changing the surface chemistry and hence catalyst activity or adsorbent capacity of the zeolite material.[13,23]

6.1.4. Microspheres

Last but not least, shaping as microspheres is still very relevant for the packing of adsorbent and catalyst beds. Even though new and innovative techniques like 3DFD open up new possibilities, spheres are still the most convenient shape for inorganic or ceramic materials, for a wide variety of applications. Their uniform shape and smooth surface minimizes pressure drop and mechanical attrition of the material in case of liquid flows. The smaller the radius of the microspheres, the higher the specific surface area, which increases the activity of a catalyst or the capacity of an adsorbent. Smaller particles also have lower internal diffusion limitation, but flow resistance in a packed bed column can be higher when using smaller particles. Depending on the application and column design, an optimal microsphere size has

to be found.[24,25] Microspheres can be either dense or porous and differ in morphology. In general, there are three morphology options: (i) matrix microspheres, (ii) hollow microspheres or (iii) core-shell microspheres (see **Figure 6.1**). Matrix microspheres are the most simple form of spheres and they consist of a complete matrix of the same material. Hollow microspheres consist of a shell that contains an empty void space. Evidently, they have a lower density than matrix microspheres. Hollow spheres are often used as fillers because they reduce the density of the material while mechanical strength and insulating properties remain high.[26–28] Core-shell microspheres have a core and a shell with different material properties. This can be a difference in porosity, chemical composition or both. The boundary between the core and the shell can be discrete or gradual. In general, the latter is preferred to overcome diffusion limitation.[29,30]

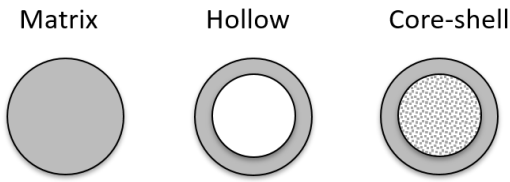


Figure 6.1: Different microsphere morphologies.

6.1.5. Microsphere formation

There are many different methods to produce spherical particles. Bohner *et al.* (2013) classified the different procedures according to (i) the type of reagents used, (ii) the media in which the spheres are formed, (iii) the dispersion tool, (iv) the consolidation reaction, (v) the size of the resulting spheres and (vi) the ceramic/inorganic phase that is included in the spheres.[31] Critical steps in the formation of microspheres are granulation and coagulation. Granulation is the formation of a spherical shape (droplet) while coagulation is the consolidation of this sphere into a solid structure. Pype classified microspheres according to the type of granulation and coagulation.[32] Both processes can be either chemical or physical in nature. During chemical granulation, spherical shapes are formed due to chemical interactions in a solution. A typical example of this is the precipitation of metal hydroxide particles after the addition of an alkaline solution to a solution of trivalent or tetravalent metal cations (e.g. Al^{3+} or Ti^{4+}). Since this precipitation is often a rapid process, it is difficult to control the formation and size of the spheres.[33] Another type of chemical granulation is the sol-emulsion-gel synthesis. A water-in-oil emulsion is formed by intensive stirring, with metal precursors dissolved in the water droplets. The emulsion is stabilized by the addition of surfactants, hence creating inverted micelles that act as microreactors for the metal precursors. Gelation inside the micelles is triggered by changing the temperature or pH of the solution. This

method lends itself to the formation of core-shell particles. The size of the spheres is directed by the size of the micelles, which is not always easy to control. Therefore, sizes of different spheres can vary largely within the same system.[34,35]

During physical granulation, fine powder particles are already present prior to shaping, and sphere formation occurs through agglomeration of these powder particles. Agglomerates can be formed by e.g. mixing a powder with a binder solution using high shear mixers. Once again, size and shape are difficult to control with this type of process, yet it is a popular method for microsphere formation due to its high productivity and low cost.[36,37] Spray drying is another well-known method for physical granulation. A suspension, containing a powder (the active material), binder and solvent is dispersed into fine droplets under high pressure in a drying chamber. In this process, granulation is effected by a nozzle sprayer while consolidation occurs through drying. Even though this process might look difficult to control, rather uniform particles (mostly matrix spheres) can be obtained.[38,39]

6.1.6. Droplet extrusion

As stated earlier, the droplet size will have a large influence on important material properties like capacity, activity and diffusive limitations. Hence it is important to (i) control the size of the spheres and (ii) to have a uniform size distribution among the shaped particles. It is in this regard that droplet extrusion procedures have been developed. These techniques are able to create monodisperse particles with droplet sizes that can be rather strictly controlled. Droplet extrusion processes are either based on droplet formation due to gravity and capillary forces or on the breaking of laminar fluid flows into smaller droplets. Break-up of a fluid flow is normally achieved by vibrating a nozzle head.

The first type of droplet extrusion is called gravitational droplet extrusion (**Figure 6.2**, left). Droplets are formed at the tip of a nozzle due to an interplay between gravity (downward force) and capillary forces (i.e. surface tension, an upward force). It is one of the most simple techniques for shaping microspheres. Microspheres of homogeneous size can be obtained; their radius is mostly determined by the viscosity and surface tension of the suspension, rather than by tip diameter. So size control is limited, but the very simple set-up allows easy lab experiments and screening experiments with little active material. This can be advantageous when working with very specific, on purpose synthesized active materials, rather than with commercial bulk inorganics.

A more advanced shaping technique is the vibrating nozzle technology. In this technique, a vibration (with a strictly controlled frequency and amplitude) is applied

to a nozzle in order to break the laminar flow of a suspension into droplets. In contrast to gravitational droplet extrusion, this method allows both high flexibility and strict control of droplet size and shape (**Figure 6.2**, right).

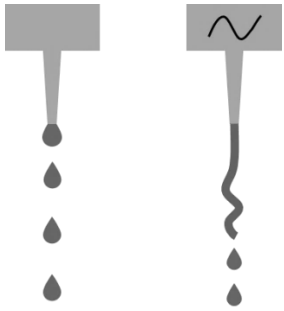


Figure 6.2: Graphical representation of droplet formation by gravitional droplet extrusion (left) and vibrational droplet extrusion (right).

6.1.7. Droplet coagulation

So far, only the granulation of spherical droplets has been discussed. No matter the shaping procedure, all spheres have to be consolidated in the coagulation step. As for the granulation, many different methods exist, some more common than others. When the chemical composition of the solidified sphere is different from the starting material, we speak of chemical coagulation. Physical coagulation involves the solidification of the droplets due to changing physical conditions. Examples are spray drying or freeze drying with liquid nitrogen. With freeze drying, a highly porous structure can be obtained after removal of the frozen water crystals via sublimation. Shrinkage of the spheres is limited (as compared to air drying) and the spherical shapes are well preserved due to the rapid freezing process. [40] Pore volume and pore sizes can to a certain extent be controlled by adjusting the freezing rate (allowing the growth of smaller or larger water crystals) or by implementation of additives.[41,42] Another type of physical coagulation is solidification of a binder melt by lowering the temperature. This simple process, called prilling, will transform the suspension droplets into solid matrices, but control of porosity is very limited.[43] A last example of physical coagulation is phase inversion, well known in the synthesis and tuning of porous membranes but also applicable to microspheres. Solidification of the spheres is achieved by immersing the droplets in a nonsolvent. Exchange of the suspension solvent with the nonsolvent will cause precipitation of the microspheres, while phase separation and mass transfer create a porous structure.[44]

Chemical coagulation, where the chemical composition of the microsphere is altered to obtain solidification, might be the most common method. An example is sol-gel

synthesis, which bears some resemblances to zeolite synthesis. Hydrolysis of a metal alkoxide (e.g. tetraethylorthosilicate, TEOS) will initiate condensation reactions, creating a sol of colloidal silica particles. Changing the pH of this sol will lead to coagulation of the colloids and the formation of a gel.[45] This gel is subsequently dried, resulting in a solid matrix.

Ionotropic gelation is another method and the most common procedure at VITO. This method is based on the solidification of a (sodium) alginate polymer network, an organic and linear polysaccharide. It consists of two monomeric units, being α-L-guluronic acid (G) and 1,4-linked β-D-mannuronic acid (M). These monomeric units can be combined to form three different types of block co-polymers: homopolymeric blocks of either M or G (called M- and G-blocks) or a heteropolymeric block with an alternating G and M pattern (GM-block) (**Figure 6.3**).[46] Homopolymeric blocks can vary in length, while GM-blocks can also vary in G-M pattern. Of course, also the three different block co-polymers can be randomly combined, leading to a large variety in different alginate polymers. The chemical composition of the polymer and its molecular weight will largely influence the viscosity of the polymer solution, which will hence also affect the shaping procedure.[47] Alginate is derived from alginic acid, and its many anionic carboxylate groups are neutralized by counter cations, commonly sodium. The usefulness of sodium alginate lies in its ability to form a rigid 3D-network upon ion exchange with multivalent cations (most often Ca^{2+}). Multivalent cations can act as bridging (or chelating) agents between the hydroxyl and carboxyl groups of the guluronate blocks, which causes crosslinking and hence gelation/solidification of the alginate network.[48,49] Since this effect is most powerful for G-blocks, the degree of gelation and resulting gel strength can be tuned by altering the G-block content of an alginate polymer.[50] Crosslinking due to ionotropic gelation can be intramolecular or intermolecular. Intramolecular interactions bond groups from the same alginate chain; this results in a planar geometry. Intermolecular crosslinking between different alginate chains, on the other hand, occurs perpendicular to the planar orientation of the chains. The type and geometry of alginate crosslinking are largely determined by the nature and valence of the metal counter cation, which is a tunable parameter. Even though the possibilities and flexibility of microsphere formation might seem limited compared to e.g. 3DFD, the use of different crosslinking ions and salts allows the formation of innovative materials with added functionalities.[51–53] In practice, ionotropic coagulation is often combined with gravitational and vibrational droplet extrusion by simply collecting the suspension droplets in a container with a Ca^{2+} solution.

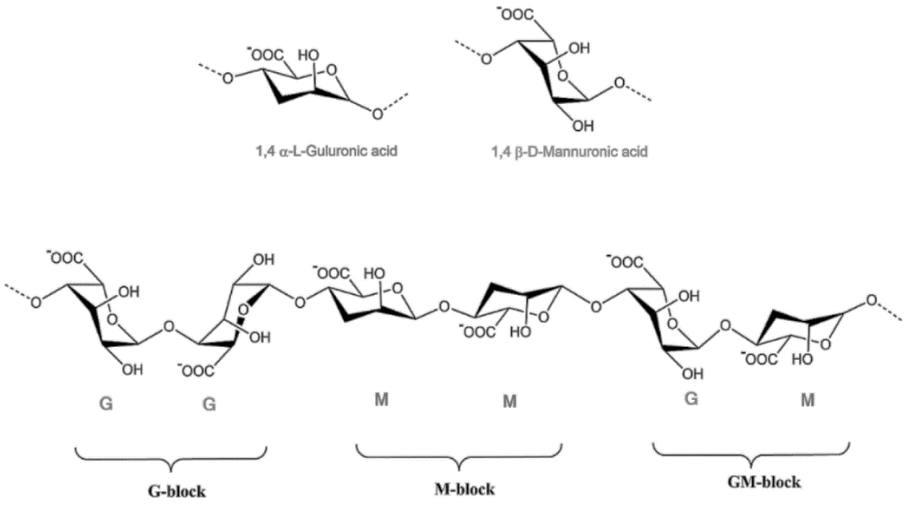


Figure 6.3*:* Overview of the monomeric units and different block co-polymers of alginate polysaccharides. Figure taken from Abasalizadeh et al. [54]

6.1.8. Other components of the suspension recipe

So far, this extensive introduction towards the structural shaping of catalysts and adsorbents has focused on the different shaping techniques and aspects thereof. In the previous paragraph, the function and role of the alginate polymer on the suspension chemistry has been discussed. However, this is not the only ingredient of a suspension for microsphere production, besides the active material itself and the solvent. Appropriate chemistry and rheology of a suspension are crucial for any kind of shaping technology. Hence development of a good suspension *recipe* constitutes a large part of the research work on this topic. Therefore, in the last part of this introduction, the role and impact of the binder will be shortly discussed. The advantages of structural shaping of active materials have already been discussed, but to obtain the required mechanical strength and stability, the use of a binder is often needed. The ultimate goal is to have both high strength and porosity; however there is often a trade-off between these two criteria. Careful selection of the best possible binder can result in the optimal balance between strength and porosity. Addition of a binder does not only influence the final strength of the structure, but also the suspension viscosity and drying behavior. A good binder can reduce shrinking during drying and calcination; this lessens the probability of crack formation which negatively influences the mechanical properties.[55] Different binders can be used simultaneously, in order to fine-tune several parameters, e.g. via binary binder systems, superior synergistic mechanical properties can be obtained.[56] Addition of binders can alter the acidity of the suspension solution, hereby affecting inter- and intramolecular interactions that act during gelation, solidification and calcination. Since so many physical and chemical factors play a role

during the different stages of material shaping, the effect of a binder is still difficult to predict and research on this topic is still often a matter of *trial and error*. More research in the future will lead to a higher level of understanding and smarter binder selection.[57]

6.2. Results and discussion

6.2.1. Binder screening and selection

As preparatory work for the actual shaping of the adsorbent, the best possible binder had to be selected. A good binder increases the mechanical stability of the end product, contributes to good suspension chemistry and viscosity and has little or minimal impact on the adsorption behavior of the active adsorbent. Since all-silica zeolite Beta has a higher capacity and affinity for PFASs than most inorganic adsorbents, a reduction in affinity and capacity after mixing the pure Beta material with an inorganic binder was expected. This reduction can be further amplified upon shaping by a reduced specific surface area of the microspheres, compared to the initial powder. All these factors have to be considered during the screening of hybrid zeolite-binder mixtures. A series of different inorganic binders (**Table 6.1**) were selected for mixing with all-silica zeolite Beta. All binders were known for their use in the shaping of active materials, whether for 3D-printing, coating or microsphere formation. Every binder was mixed with all-silica zeolite Beta or with the commercial zeolite Beta CP814E-22 (also dubbed Beta-22). The latter is an Al-containing zeolite Beta (SiO_2/Al_2O_3 = 22) and not as hydrophobic as all-silica zeolite Beta. The differences in material properties and adsorption behavior between all-silica zeolite Beta and Beta-22 were discussed before in Chapters 4 and 5. Beta-22 is commercially available in large quantities, while only ca. 50 g of all-silica zeolite Beta can be produced per synthesis (3 weeks). Since experiments with gravitational and/or vibrational droplet coagulation require a considerable amount of active material, Beta-22 instead of the better adsorbent all-silica zeolite Beta was used in the primary shaping experiments. It is therefore important to screen the compatibility of the different binders not only with the all-silica zeolite Beta, but also with Beta-22.

In a first stage, all binders were mixed in a 80:20 (zeolite:binder) mass ratio. SEM pictures (see **Figure 6.4**) clearly show the original zeolite Beta crystals (easily recognized by their characteristic truncated bipyramidal structure) with smaller binder particles attached to them. The zeolite-binder powders were then screened for the adsorption of PFOA at three different starting concentrations (1, 100 and 500 mg PFOA/L) in order to gauge both affinity (at low concentrations) and capacity (at higher concentrations).

Table 6.1: Overview of the selected binders for the structuration of all-silica zeolite Beta and Beta-22.

Binder	Composition	Type
Bentonite	Clay mineral (aluminosilicate)	Powder
$AlPO_4$	Synthetic aluminium phosphate ($AlPO_4$)	Powder
Ludox AS-40 (cryo)	Freeze-dried colloidal silica	Powder
Ludox AS-40 sol.	40 wt% suspension of colloidal silica	Solution
Dispersal P2	Highly dispersed boehmite (AlO(OH))	Powder
Lithopix P1	50 wt% suspension of $AlPO_4$	Solution
Ceramabind (644-A-115X)	Acidic suspension of colloidal alumina	Solution

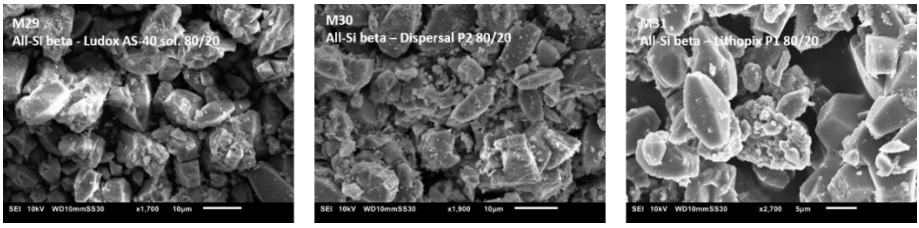


Figure 6.4: SEM pictures of the calcined powder mixtures M29 (all-silica zeolite Beta – Ludox AS-40 80:20), M30 (all-silica zeolite Beta – Dispersal P2 80:20) and M31 (all-silica zeolite Beta – Lithopix P1 80:20).

Figure 6.5 shows the results for PFOA adsorption on different all-silica zeolite Beta/binder mixtures. It is clear that no single binder had a significant negative effect on the uptake of PFOA, when compared to PFOA adsorption on the pure all-silica zeolite Beta sample. This is rather remarkable, even though inorganic materials like clay and alumina are known to adsorb PFASs in soil.[58,59] Given the fact that all-silica zeolite Beta outperforms many other adsorbents with respect to affinity and capacity, a somewhat negative influence of the binder was expected. On top of that, there is a dilution effect: the hybrid powders only contain 80 wt% of the zeolite adsorbent, compared to 100 wt% for the reference sample. An identical screening was performed for the Beta-22/binder mixtures; the results of which are shown in **Figure S6.1.** The trend of the data is almost identical to that for all-silica zeolite Beta: no significant negative (or positive) impact of the binder can be seen. Considering the results at low, middle and high PFOA concentrations for both all-silica zeolite Beta and the commercial Beta-22, Ludox AS-40, Dispersal P2 and Lithopix P1 seemed to show the best overall results and were selected for further investigation. At this stage, it is not clear whether the impact of the binder is minimal or non-existent. In the latter case, the small differences in adsorption capacity for PFOA of the hybrid materials are due to experimental error and variation and the three selected binders

are not necessarily better than other binders. Nevertheless, they are all common binders for the shaping of zeolites (at VITO) and therefore an appropriate choice.

For all selected binders, the zeolite:binder ratio was varied to 70:30 and 90:10, to gauge the effect of binder content. These powder mixtures were again screened for their adsorption capacity and affinity for PFOA at three different concentrations, similar to the screening experiment above (see **Figure 6.6**). According to these results, there is again no simple conclusion to which binder type and ratio is the most preferable for PFOA uptake. In order to make a final selection also factors like cost, ease of handling, availability and applicability in the shaping process have to be considered. Ludox AS-40 and Dispersal P2 were picked for further experiments, with Lithopix P1 as back-up if one of the two other binders would fail. Lithopix P1 is an acidic solution (pH ~2) and was therefore considered as not optimal for compatibility with neutral to basic zeolite Beta suspensions (see further). In contrast, Ludox AS-40 is a colloidal silica solution with a pH of 9.1.

6.2.2. Droplet extrusion of Beta-22 based suspensions

Next, an experimental set-up for the shaping of zeolitic microspheres was created. The advantages (and disadvantages) of microspheres over other shaping techniques have been discussed in Paragraph 6.1.4. An additional argument for experimenting with gravitational droplet extrusion is the fact that it is well fit for small lab scale experiments. Since especially all-silica zeolite Beta is only available in limited quantities, gravitational droplet extrusions still allows us to screen many different suspension recipes and extrusion parameters, without consuming large amounts of active material. Vibrational droplet extrusion experiments, for instance, can consume up to kilograms of active material per experiment. A schematic overview and photograph of the experimental set-up for gravitational droplet extrusion are shown in **Figure 6.7**. The suspension, containing the zeolite adsorbent, binder material and alginate polymer, is forced toward the nozzle by air pressure. This air pressure can be controlled and determines the flow rate of the suspension through the nozzle. A flow rate that is too high will not allow droplet formation at the tip of the nozzle. A very low flow rate, on the other hand, results in very slow and possibly irregular droplet formation, hence an optimum flow rate has to be found. This optimum depends on the viscosity of the suspension and the nozzle diameter, among other factors, and has to be determined by trial and error for every experiment. After shaping and consolidation, the dried microspheres are thermally treated by calcination. During this process, the alginate polymer network is destroyed, leaving behind a completely inorganic microsphere. Additionally, sintering processes between the zeolite and binder particles can occur (see for instance **Figure 6.8**).

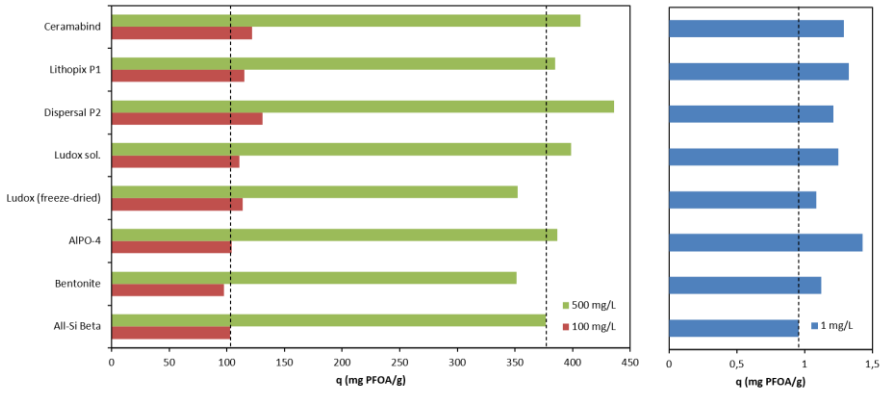


Figure 6.5: PFOA adsorption on mixtures of all-silica zeolite Beta and different inorganic binders at three different starting concentrations for PFOA. Left: 100 and 500 mg PFOA/L (to probe capacity of the adsorbents). Right: 1 mg PFOA/L (to probe affinity). Dashed lines are used to indicate the adsorption capacity of pure all-silica zeolite Beta. *q* = mg PFAS adsorbed per g of dry matter zeolite-binder mixture.

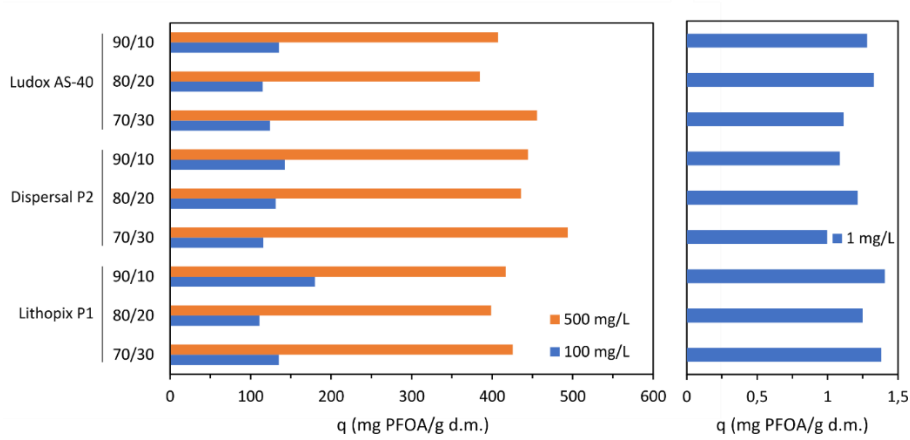


Figure 6.6: PFOA adsorption on different mixtures of all-silica zeolite Beta and three different inorganic binders. The concentrations refer to the starting concentrations of the stock solution. *q* = mg PFAS adsorbed per g of dry matter zeolite-binder mixture.

Prior to actual shaping experiments, the suspension recipe had to be finetuned. The *recipe* includes the amount, type and ratio of the different *ingredients*. This affects, among others, the viscosity and particle size distribution of the suspension, two very important factors in droplet extrusion experiments. In a first stage, only suspensions with Beta-22 were prepared, in order to save on the less available self-synthesized all-silica zeolite Beta. A suspension recipe for Beta-22 and Ludox AS-40 as binder was used as a starting point. This recipe (named V1; see **Table 6.2** for an overview of all recipes) was used earlier at VITO for the catalyst shaping of (aluminated) zeolite Beta. For gravitational droplet extrusion, a viscosity of 0.12-0.3 Pa.s (measured at a

shear stress of 60 s^{-1}) is considered optimal, based on previous in-house experiences. A viscosity that is too low results in a suspension solution that will just flow through the nozzle without breaking into droplets. A viscosity that is too high leads to a suspension that is difficult to pump through the hose and the nozzle of the set-up. A suspension with higher viscosity is also more prone to blocking the nozzle opening by particle obstruction. Since suspension V1 was not viscous enough, the water content was reduced, resulting in recipe V2. With this suspension, the first shaping experiments were started. In general, the relative content of active material, binder, alginate and water in all the different recipes were relatively constant and similar to the reference recipe V2 (**Table 6.2**).

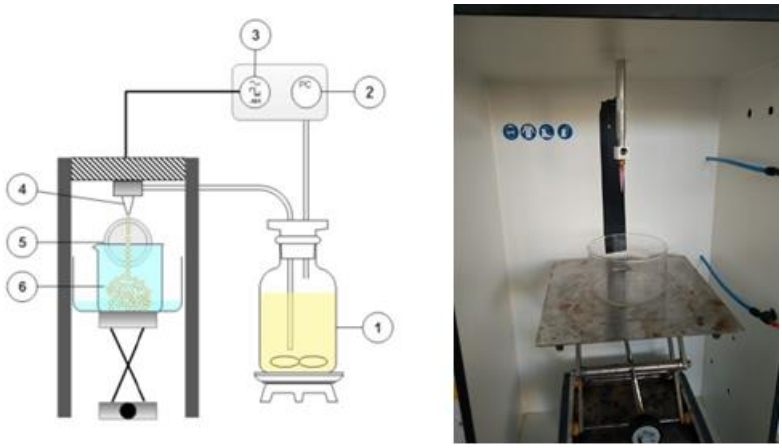


Figure 6.7: Left: Schematic overview of the gravitational coagulation set-up. (1) Feed vessel with suspension; (2) Air pressure controller; (4) Nozzle; (6) Coagulation bath. The numbered parts that are not mentioned apply to a set-up for vibrational coagulation and not for gravitational coagulation. Figure by J. Pype. Right: picture of the experimental set-up.

Considering particle size distribution, a rather uniform distribution with an average particle size around 10 µm is aimed for. This particle size is small enough to prevent frequent obstruction of the nozzle tip, while it still allows small aggregates of zeolite Beta and binder particles to be formed. Remind that the original zeolite Beta crystals are 0.5 to 4 µm wide, with the commercial Beta-22 crystals being smaller (<1 µm) than the self-synthesized all-silica zeolite Beta crystals (2-4 µm). Unfortunately, obstructed nozzle heads did occur frequently due to broad particle size distributions of the suspensions, with the 90th percentile often above 100 µm. Regarding this, aggregate size distribution is more critical than the median particle size of the starting materials, because a small fraction of large agglomerates is enough to cause frequent obstructions. One way to resolve obstruction issues is by ball milling the suspension before dripping. During ball milling, large particles in the suspension are

being grinded by ceramic balls into smaller particles. Ball milling for 24 hours could significantly reduce particle sizes, see e.g. **Table 6.3** for recipe V4.

Table 6.2: Overview of the different recipes used for the shaping of Beta-22 microspheres via gravitational droplet extrusion. Only the recipes in bold were successful. n/a = not available.

Recipe	Binder Type	Zeolite	Binder	Alginate 4 wt%	Water	Viscosity (Pa.s)
V1	Ludox AS-40 80/20	8 g	5 g	12.2 g	41.6 g	0.092
V2	Ludox AS-40 80/20	12 g	5 g	12.2 g	27.7 g	0.23
V5	Ludox AS-40 80/20	8 g	5 g	12.2 g	35 g	0.13
V7	Ludox AS-40 70/30	7 g	7.5 g	12.2 g	33.5 g	0.12
V8	Ludox AS-40 90/10	9 g	2.5 g	12.2 g	36.5 g	0.16
V3	Dispersal P2 80/20	8 g	2 g	12.2 g	44.6 g	0.69
V4	Dispersal P2 80/20	8 g	2 g	18.3 g	67.0 g	0.24
V6	Dispersal P2 80/20	8 g	2 g	12.2 g	67 g	n/a
V9	Dispersal P2 70/30	7 g	3 g	12.2 g	38 g	0.31
V10	Dispersal P2 90/10	9 g	1 g	12.2 g	38 g	0.031
V11	Dispersal HP 14/7 80/20	8 g	2 g	12.2 g	38 g	0.29
V12	Dispersal HP 14/7 70/30	7 g	3 g	12.2 g	38 g	0.37
V13	Dispersal HP 14/7 90/10	9 g	1 g	12.2 g	38 g	0.20

Colloidal (in)stability is another important factor to consider. Colloidal stability means that a suspension remains homogeneous for an extended period of time, while in an unstable suspension, the solid colloidal particles tend to aggregate and/or precipitate as sediments. Of course, phase separation in suspensions for adsorbent shaping should be avoided at all costs. Colloidal stability depends on particle size, viscosity and interparticle interactions, among others, but it is very difficult to control this by just one single parameter. Not all recipes could be successfully used for the shaping of microspheres, for instance all recipes with the binder type Dispersal P2 resulted in unstable suspensions with large flocs and rapid phase separation. Some microspheres could be shaped with recipe V4 (**Table 6.2**) right after the suspension preparation but the nozzle heads had to be replaced very frequently due to rapid obstruction of the nozzle. Even after thorough ball milling, these problems still persisted. Eventually, Dispersal P2 was replaced by Dispersal HP14/7; this is an alternative type of boehmite with citric acid grafted on the alumina surface. This surface modification results in a lower zeta (ζ) potential and lowers the pH of the suspension solution to ca. 4, generating a more stable colloidal suspension. The ζ potential is the electrical potential at the slipping plane of a surface and a practical (i.e. more easy to measure) indicator of surface potential. The negatively charged citrate groups at the surface of the binder increase electrostatic repulsion between the colloidal particles and hence successfully prevent aggregation. The ζ potential of

zeolite Beta itself is further discussed in paragraph 6.2.5. With Dispersal HP14/7, zeolite Beta-boehmite microspheres could finally be produced. An overview of all recipes that led to the successful shaping of zeolitic (Beta-22) microspheres shaped by gravitational droplet extrusion is given in **Table 6.2**. These different suspensions were combined with different nozzle diameters, leading to a collection of as-synthesized microspheres, an overview of which is given in **Table 6.4**. It is important to note that nozzle diameter has only a limited impact on microsphere size, since it is mostly the interplay between surface tension and gravity that determines the radius of the extruded droplets in gravitational droplet extrusion.

Table 6.3: Effect of ball milling on the average diameter of agglomerates in recipe V4 for different percentiles.

Recipe V4	**Percentile diameter (µm)**			
	d_{10}	d_{50}	d_{90}	d_{99}
No ball milling	39	120	252	419
10h ball milling	8	44	175	295
24h ball milling	5	23	74	173

As shown by previous experiments, the mixing of zeolite Beta with a binder does not negatively impact the affinity and the capacity for PFOA uptake. The structuration of the zeolite into microspheres may however significantly impact adsorption kinetics. At the same time, adsorption kinetics are very important when using the beads in an adsorption column later on. On the one hand, by packing the loose zeolite powder into a dense microsphere, an additional mass diffusion barrier is created. On the other hand, meso- and macropores are created during the shaping process, resulting in a total pore volume (and hence porosity) of the microspheres that is much higher than that of a pure zeolite Beta powder (see **Table 6.5**). The complete process of microsphere formation and calcination creates an open, porous structure. These newly created macropores (or channels) can be clearly seen on SEM pictures of fractured microspheres and are 2 to 5 µm wide (**Figure 6.8**). This is also apparent from the N_2 physisorption isotherms: the isotherms for Beta-22 based microspheres (**Figure S6.2**) are very similar to the isotherm for pure, as-synthesized all-silica zeolite Beta (**Figure S6.3**). It is only at P/P_0 close to 1 that the microsphere isotherms diverge from the all-silica zeolite Beta isotherm and show a significant surge, due to macroporosity. Measured BET surfaces for the structured microspheres are slightly lower (but not drastically) compared to the pure zeolite Beta powder (**Table 6.5**). Micropore volumes (calculated with the t-plot method and compared to the pure zeolite powder) are halved though, while total pore volumes are more than doubled.

Table 6.4: Overview of self-shaped microspheres obtained by gravitational droplet extrusion. All microspheres are based on Beta-22.

Name	Recipe	Binder type	Nozzle diam.	Remarks
M48	V2	Ludox 80/20	0.84 mm	
M49	V2	Ludox 80/20	0.58 mm	
M50	V5	Ludox 80/20	1.19 mm	
M51	V5	Ludox 80/20	0.41 mm	
M52	V4	Dispersal P2 80/20	1.19 mm	24h of ball milling
M53	V4	Dispersal P2 80/20	0.58 mm	24h of ball milling
M54	V7	Ludox 70/30	1.19 mm	
M55	V7	Ludox 70/30	0.58 mm	
M56	V8	Ludox 90/10	1.19 mm	
M57	V8	Ludox 90/10	0.58 mm	
M59	V11	Dispersal HP14/7 80/20	1.19 mm	
M60	V11	Dispersal HP14/7 80/20	0.58 mm	
M61	V12	Dispersal HP14/7 70/30	1.19 mm	
M62	V12	Dispersal HP14/7 70/30	0.58 mm	
M63	V13	Dispersal HP14/7 90/10	1.19 mm	
M64	V13	Dispersal HP14/7 90/10	0.58 mm	

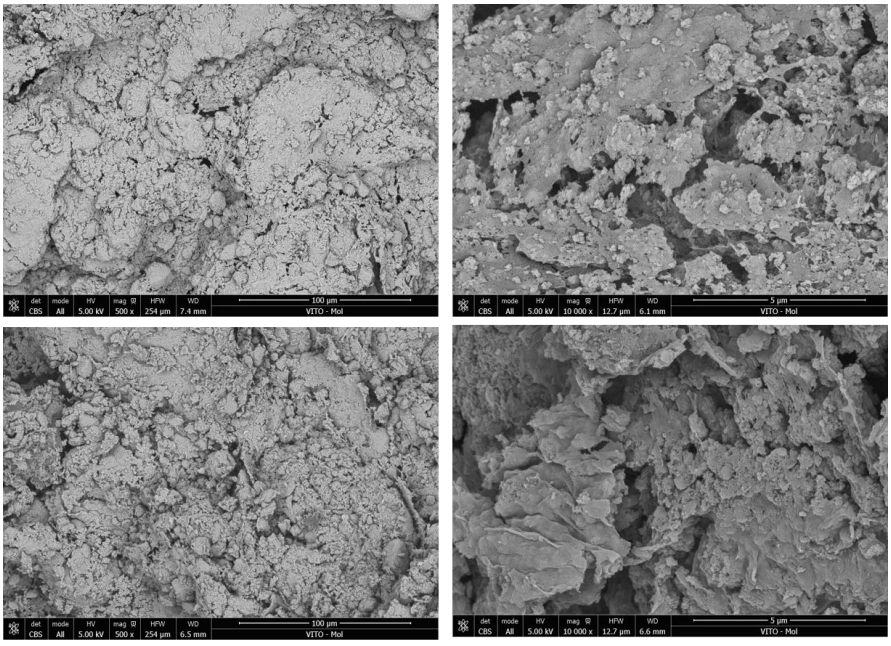


Figure 6.8: SEM pictures of a single type of microspheres (Beta-22/Ludox AS-40 80/20). Top: outer microsphere surface. Bottom: inner surface of fractured microspheres. The microspheres are fractured in order to have a clear view on the interior. More SEM pictures are shown further in this chapter.

Table 6.5: Surface and pore properties of all-silica zeolite Beta and Beta-22 (powder) vs. extruded microspheres based on Beta-22. Micropore volumes are based on t-plot, total pore volumes are based on DFT (see 6.5.1. for experimental details).

Material	BET surface (m^2/g)	Micropore vol. (cc/g)	Total pore vol. (cc/g)
Powder: as-synthesized all-silica zeolite Beta	623	0.21	0.77
Powder: commercial Beta-22	650	0.19	0.85
Microsphere: Beta-22/Ludox AS-40 80/20 (0.84 mm tip size)	522	0.097	0.80
Microsphere: Beta-22/Ludox AS-40 80/20 (0.58 mm tip size)	490	0.068	0.79

6.2.3. Screening of as-synthesized microspheres for PFAS adsorption

Several types of extruded microspheres were screened for their kinetics in the adsorption of PFOA. This was done for both whole microspheres as well as for crushed microspheres. Comparing whole vs. crushed microspheres allows to investigate the impact of the microsphere structure on diffusion limitation, while comparing crushed microspheres vs. the original zeolite Beta powder allows to study the impact of binder mixing, suspension preparation and the shaping process as a whole. **Figure 6.9** shows the time profiles for PFOA adsorption on M48 and M49, two microspheres made from Beta-22/Ludox AS-40 80/20. Despite the experimental variation that is clearly visible from the data, it is fair to suggest that there is both a slower and a lower PFOA uptake for the whole microspheres as compared to the crushed spheres. This indicates that shaping the zeolite into a solid structure indeed creates an additional diffusion limitation, but also lowers the number of available adsorption sites per g of material. The latter could be due to obstruction or destruction of micropores, initially present in the zeolite crystals, or due to the somewhat lower specific surface area.

When comparing PFOA adsorption on the crushed (M48) microspheres vs. the original zeolite Beta powder, we see that both the speed (kinetics) and extent (capacity) of adsorption are very similar. This again shows that mixing of the zeolite material with a binder has little to no impact on PFOA adsorption. Additionally, it shows that the impact of sintering during calcination is limited. If sintering reactions between the zeolite and the binder would significantly reduce surface area and/or microporosity, then this effect would still be apparent after crushing the microspheres into a course powder. This also means that the lower capacity for the microspheres as a whole is completely due to the packing of the materials into a solid structure. Even though there is definitely a delay in PFOA uptake for the

microspheres, this delay is considered acceptable and allow the spheres to be used in a packed bed column in the future. Nevertheless, a reduction in the average sphere diameter might further benefit the application of these microspheres in packed bed columns, by increasing the specific surface area of the spheres and by reducing the diffusion limitation barriers.

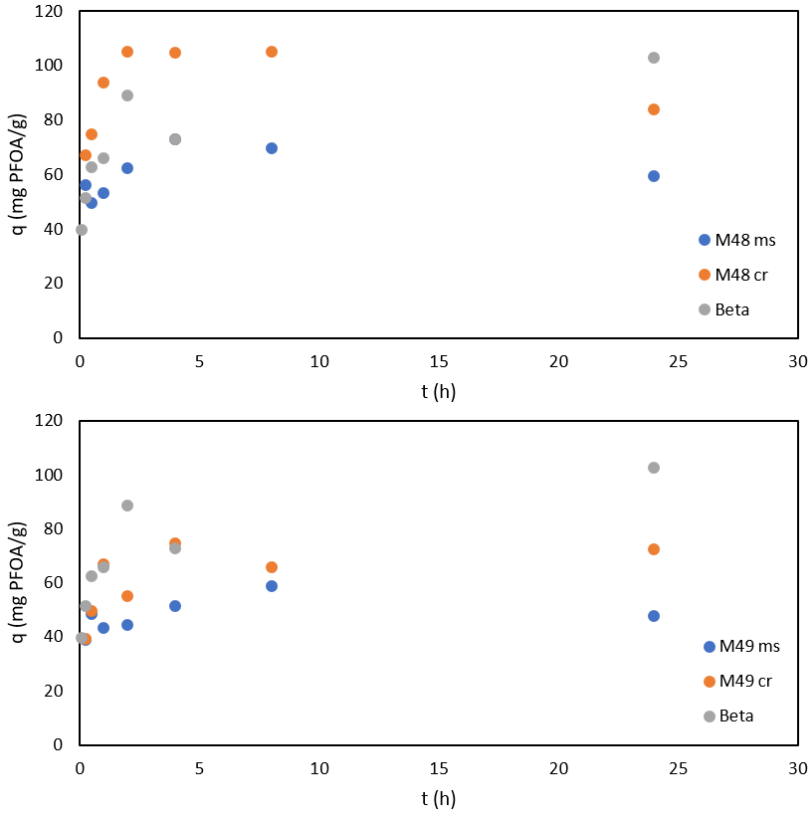


Figure 6.9: PFOA adsorption kinetics for M48 and M49, compared to the all-silica zeolite Beta powder (= Beta). Whole microspheres are denoted 'ms'; crushed microspheres are denoted 'cr'**.** M48 and M49 are microspheres based on 80/20 Beta-22/Ludox AS-40 suspension. Starting solution: 100 mg PFOA/L. Data points indicate single measurements, no triplicates were measured for this experiment.

The kinetic experiment was repeated for two types of microspheres (M63 and M64, only differing in extrusion tip size) based on Dispersal HP14/7 as binder in a 90/10 ratio (**Figure 6.10**). There is more experimental variation on the data, compared to the Ludox based microspheres, but it seems fair to conclude that the difference between the whole and crushed microspheres is much smaller for Dispersal based microspheres. Unfortunately, extensive characterization (see next section) of the

Dispersal microspheres is lacking; so no link with pore volume and specific surface area can be made for now. It still shows however that binder selection is important and that the impact of a certain binder sometimes manifests itself only in a later research stage: remind that no significant difference in PFOA uptake between Ludox AS-40 and Dispersal P2 was seen during the initial screening of different binder types. It is difficult to tell to which extent the adsorption behavior of the Dispersal microspheres is changed when shifting from Dispersal P2 towards the citric acid-modified Dispersal HP14/7. The results from **Figure 6.10** suggest that also Dispersal HP14/7 does not significantly impede PFOA adsorption on zeolite Beta.

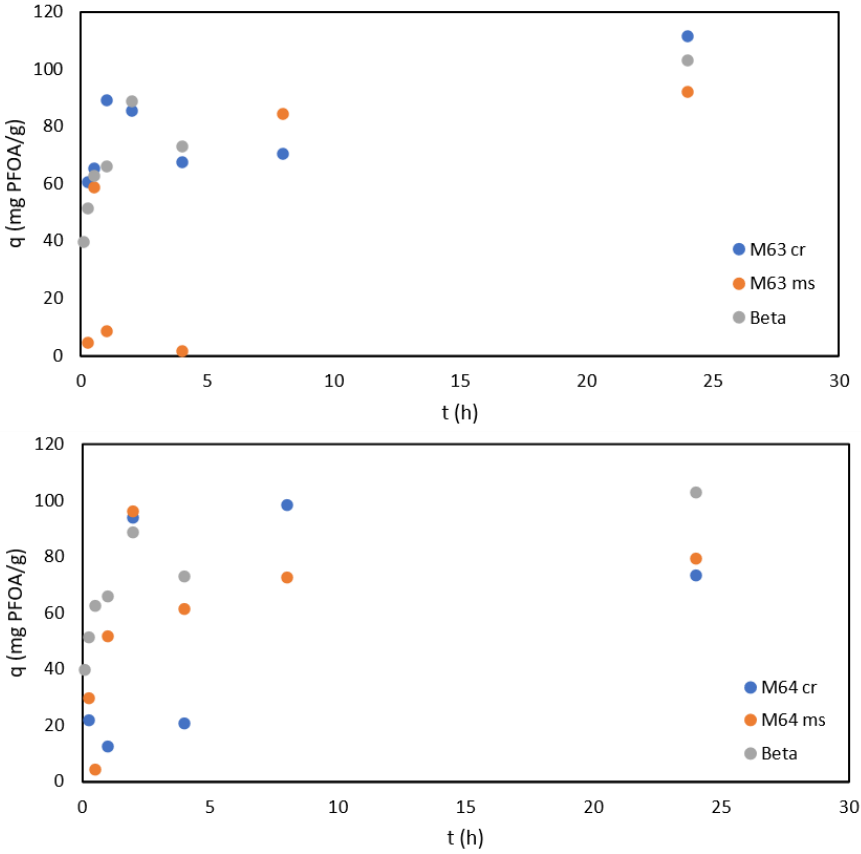


Figure 6.10: PFOA adsorption kinetics for M63 and M64, compared to the all-silica zeolite Beta powder (= Beta). Whole microspheres are denoted 'ms'; crushed microspheres are denoted 'cr'**.** M63 and M64 are microspheres based on 90/10 Beta-22/Dispersal HP14/7 suspension. Starting solution: 100 mg PFOA/L. Data points indicate single measurements, no triplicates were measured for this experiment.

6.2.4. Microsphere characterization

As noted before, adsorption kinetics are very important when an adsorbent is meant to be applied in a (packed bed) adsorption column. This is not the only important aspect however; mechanical stability and resistance to attrition are crucial. High flow rates and pressure drops over an adsorption column can cause excessive wear on the packed bed material, leading to premature adsorbent replacement, high costs and fine grit residues in the equipment. Mechanical strength of a series of microspheres was gauged via crushing experiments. In this type of experiment, single microspheres are loaded under an ever increasing mechanical pressure until they crack. The maximum pressure that can be applied before the microspheres crack is called the side crushing strength (SCS) and an indication of mechanical strength. The higher the SCS value for a certain type of microsphere, the higher its ability to withstand mechanical attrition in column operations. A selection of the SCS results is shown in **Figure 6.11**. The results are listed according to binder type, binder content and nozzle diameter (used during the gravitational extrusion process). Note that SCS values are expressed in terms of MPa, hence *strength* is in fact not a correct (but still a common) term and *maximum tensile stress* would be more correct. SCS values were calculated by dividing the maximum applied load (N) before cracking/failure by the area ($4\pi r^2$,with r being the radius) of the spheres. Hence smaller microspheres will have a higher SCS than larger microspheres if they crack under the same external load.[60]

No clear trend could be seen in the mechanical strength results. Considering the spheres with 20 wt% of Ludox AS-40 as binder, there is an increase in mechanical strength with decreasing nozzle diameter, but this trend is absent for the spheres with 30 wt% of Ludox binder. There is no rise in SCS with increasing binder content, something that could have been expected since the binder particles act as 'glue' between the zeolite crystals. There is in fact no other reason to increase binder content than to increase mechanical strength and stability; so it is very remarkable that this is not apparent in the SCS experiments. The SCS values on **Figure 6.11** are averages of 10 individual samples for every type of microsphere. Sometimes, the deviation of the mechanical strength between samples of the same microsphere type was rather large, resulting in higher average values (see **Figure S6.4**). But as often as not, SCS values for samples of the same type were very consistent and significantly different from other microsphere types. This variation in results can be partly explained by the experimental variation which is typically relatively high for this kind of measurements. Small deviations in the sphericity of the microspheres can also contribute, because they directly impact the surface (area) on which the crushing pressure is exerted. Finally, inhomogeneities in the shaping suspension will

result in inhomogeneities in the resulting microspheres, another factor contributing to a larger deviation in SCS values.

In order to gain more insight in the results of both the adsorption and mechanical strength experiments, several characterization techniques were applied on the as-shaped microspheres. An overview of the most common characterization techniques to elucidate the composition and structure of shaped adsorbents and catalysts at VITO is given in **Table 6.6**. Not all of these techniques were applied on all of the different microsphere type, but several types were nevertheless characterized in detail.

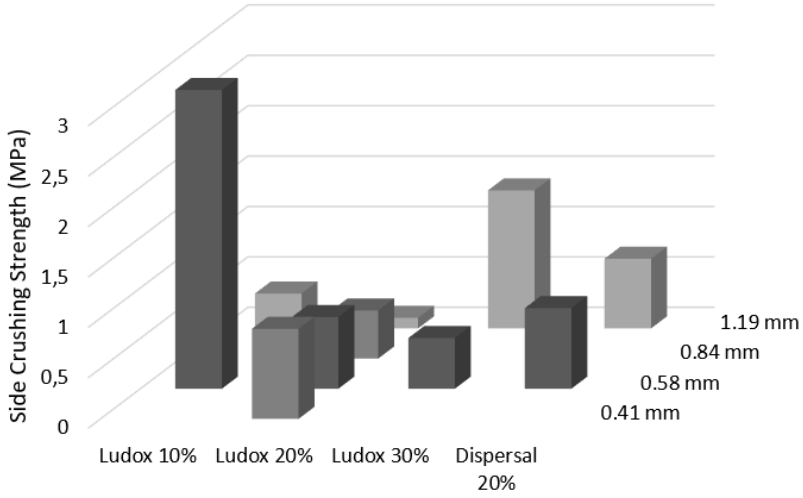


Figure 6.11: Side crushing strength results for different types of microspheres, varying in binder content and nozzle diameter. Each result is an average of 10 individual samples.

First, shrinkage during drying and calcination of the as-shaped microspheres was studied via optical microscopy and image analysis. Extensive shrinkage is undesired since it can cause cracks in the exterior and/or interior of the sphere. Shrinkage upon drying the spheres is driven by water evaporation, while shrinkage during calcination is driven by the removal of the alginate network, sintering reactions and other local composition changes.[61] Extensive (and swift) shrinking increases the risk of microspheres with low sphericity (often expressed via the Feret ratio).[62] A low sphericity is undesired since it leads to inhomogeneous spheres for which the mechanical strength of the spheres depends on their orientation. Moreover, it can lead to inhomogeneous flow paths and higher pressure drops in an adsorption column. Here, the example of two Ludox-based microsphere types is given. **Figure 6.12** shows the shrinkage of the microspheres upon drying and after calcination. A shrinkage of 22% and 26% (measured for a set of spheres) was witnessed for the

M48 and M49 microspheres upon drying, while no further shrinkage after calcination was seen. The results for other types of microspheres were very similar. The degree of shrinkage seems well within range of what is reported in literature (varying from 10 to 50% shrinkage). Also visually no cracks could be seen, indicating that the drying and calcination processes do not seem to initiate structural weaknesses in the microspheres. Also the sphericity of the microspheres is very high, as can be seen on the microscopic pictures used for image analysis (**Figure S6.5** and **Figure S6.6**).

Table 6.6: Overview of the most common characterization techniques for as-shaped microspheres and the information retrieved thereof.

Characterization technique	Retrieved information
Optical Microscopy	Size distribution and sphericity, shrinkage upon drying and calcination
Side Crushing Strength (SCS)	Mechanical strength
Scanning electron microscope (SEM)	Open and closed porosity, element distribution
Thermogravimetric analysis (TGA)	Inorganic and organic content, before/after drying/calcination
Dilatometry	Sintering behavior of microspheres
X-ray diffraction (XRD)	Study of crystalline matter in the microspheres
Hg-porosimetry	Porosity, pore size distribution, specific surface

Scanning Electron Microscopy (SEM) images of different microsphere types were used to study the changes of the zeolite and binder particles upon shaping and calcination, and to investigate the porosity and structure of the microsphere's surface and interior. Microspheres were sliced in two in order to have a clear view on the interior (see Supporting Information for experimental details). A selection of SEM images is shown in **Figure 6.13**, zooming in on both the exterior and interior of Beta-22/Ludox (80/20) microspheres. It can be seen that both the surface and the interior have an open, porous structure, with channels up to 2-5 µm wide. In general, the microspheres are homogeneous and no irregularities can be seen. The impact of increasing the binder content (from 20 to 30 wt%) can be clearly seen on the SEM pictures of **Figure S6.7**. Especially at the outer surface, the channels that were numerously present for the spheres with 20 wt% Ludox are now fully absent. Increasing the binder content in this case leads to a more homogeneous and more densely packed microsphere interior. Lowering the binder content did not result in a more loose and coarse structure of the microspheres though (**Figure S6.8**). Changing the binder type from Ludox AS-40 to Dispersal P2 (both 20 wt%) leads to small differences in sphere morphology: the outer surface is a bit more dense and the interior channels are somewhat smaller, but in general the differences are small (**Figure S6.9**).

SEM pictures can give useful information on the sphere morphology, structure and porosity, all parameters which influence adsorption performance and mechanical stability. In this case, nevertheless, no clear indications for explaining the differences seen in side crushing strength could be deduced. All spheres discussed in this paragraph were extruded from a 1.19 mm nozzle, but also SEM pictures of similar spheres extruded from a smaller tip (0.58 mm) were taken. The nozzle size had no impact on the structure and morphology of the spheres. Unfortunately, no SEM pictures of microspheres with Dispersal HP14/7 were taken at the time; such pictures could potentially explain the faster PFOA adsorption on these spheres as compared to Ludox based microspheres.

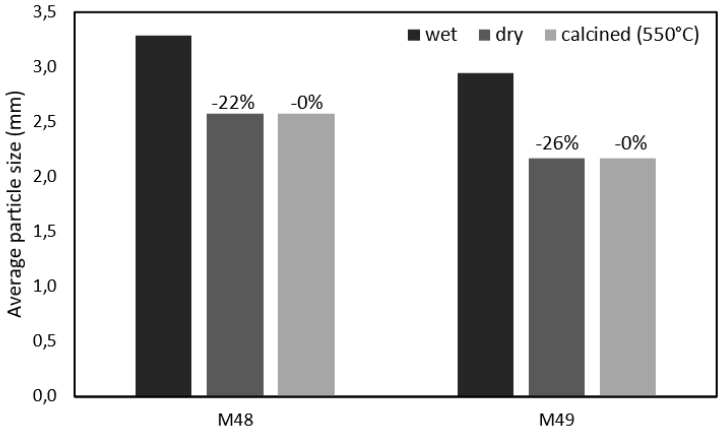


Figure 6.12: Shrinkage overview upon drying and calcination of Ludox-based microspheres. Shrinkage is measured for a set of 5 microsphere per sample type. M48 = Microspheres extruded from a 0.84 mm nozzle, suspension = Beta-22/Ludox AS-40 80/20. M49 = Microspheres extruded from a 0.58 mm nozzle, suspension = Beta-22/Ludox AS-40 80/20.

Also SEM-EDX measurements were made for the different microsphere types discussed above. EDX stands for Energy-dispersive X-ray spectroscopy, an analytical technique used for elemental analysis. When EDX is combined with SEM, elemental mapping is possible and (in)homogeneities in zeolite and binder distributions are made visible. It is difficult though to differentiate between the zeolite and binder particles on the SEM-EDX pictures (see **Figure 6.14** and **Figure 6.15**). The microspheres studied here are based on Beta-22, a commercial zeolite Beta with both Si and Al (and of course O) in the framework (SiO_2/Al_2O_3 = 22). Since Ludox is a colloidal silica suspension, no hetero-atoms can be seen. Similarly, Dispersal is a fine boehmite (AlO(OH)) powder without any element that is not present in Beta-22. Also Ca is present in the microspheres, because of ion-exchange during the coagulation procedure with alginate.

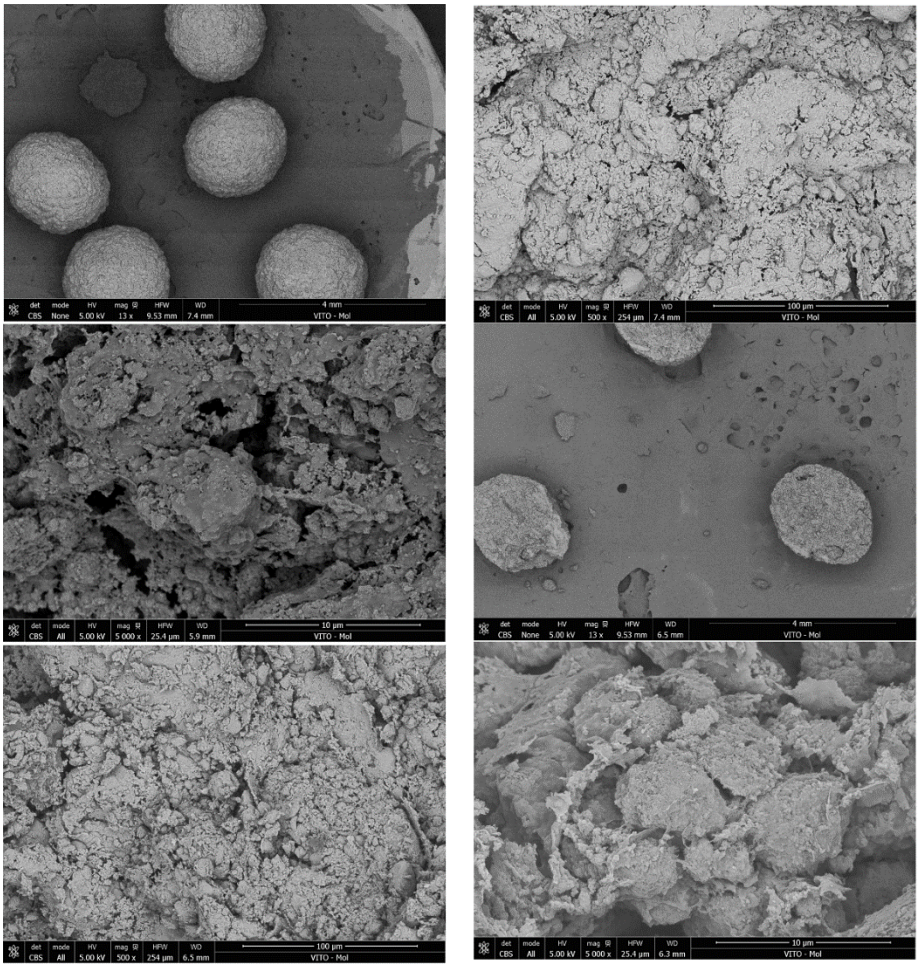


Figure 6.13: SEM images of M50 microspheres: Beta-22/Ludox AS-40 80/20 extruded from a 1.19 mm nozzle. From left to right, bottom to top: SEM images of the external surface (4 mm, 100 µm, 10 µm); SEM images of the interior/fracture plane (4 mm, 100 µm, 10 µm).

Figure 6.14 shows elemental mapping pictures for Ludox AS-40 based microspheres. It is impossible to clearly discern zeolite and binder, but hotspots that are only visible for either Si or Al can indicate inhomogeneous distribution of zeolite and binder. This only occurs for the microspheres with 20 wt% binder and corresponds with the rather coarse morphology of these spheres that could be seen on the SEM pictures (**Figure 6.13**), showing relatively large channels and clusters. SEM-EDX maps for spheres with 10 and 30 wt% of Ludox binder show a very homogeneous distribution of all elements, conform their SEM images that showed a less rough morphology and finer particles (**Figure S6.8** and **Figure S6.7**). Note that for all microspheres, Ca distribution is very homogeneous, an indication that the alginate polymer network

was well entangled with the inorganic zeolite and binder particles. When comparing the impact of the binder type, the increase in Al intensity and spreading when using a boehmite binder (Dispersal P2) instead of a silica binder (Ludox) can be clearly seen (**Figure 6.15**). Also here, and in line with the respective SEM pictures, a finer elemental distribution is seen for the Dispersal based microspheres, as compared with the 20 wt% Ludox microspheres. To summarize, no big conclusions considering adsorption performance and/or mechanical stability can be drawn, based on the SEM and SEM-EDX analysis. It can be confirmed, however, that the internal structure of the as-shaped microspheres meets the expectations and that no structural aberrations are generated during the shaping and calcination process.

Finally, mercury intrusion porosimetry was used to evaluate the porosity, pore size distribution and pore volume of the microspheres. Compared to BET surface measurements, Hg porosimetry will give more information about the connected pore volume and macroporosity and might be more valuable in order to assess and explain diffusion and kinetic differences between different types of microspheres. Both inter- and intra-particle pores can be characterized using this technique. Cumulative pore volume and pore size distribution plots for all Ludox based microspheres are shown on **Figure S6.10**. Mostly pores up to 0.3 µm wide can be seen for spheres extruded from a 1.19 mm tip, while pores up to 0.08 – 0.1 µm are seen for spheres extruded from a 0.58 mm tip. When comparing Dispersal P2 and Dispersal HP14/7, in different weight ratios and for different tip sizes, only small differences in pore size (distribution) and porosity are seen. These spheres have mostly pores up until 0.2-0.5 µm wide, with cumulative pore volumes of ca. 1200 cc/g (**Figure S6.11** and **Figure S6.12**). On average, these values are not significantly higher than for the Ludox-based microspheres, which could possibly have explained the faster PFOA uptake on the Dispersal HP14/7-based microspheres as witnessed during the kinetic experiment.

Based on all these characterizations of the as-shaped microspheres, some significant differences between the various types can be seen. As for the adsorption and SCS results, it is difficult to see a direct correlation with variables like binder type or content. The variation of the results, for different types of experiments and characterizations, seems to be random at times, which makes it difficult to draw strict conclusions on the correct synthesis parameters and to steer the shaping of zeolite Beta microspheres in the best possible direction. Unstable and/or inhomogeneous suspensions will lead to inhomogeneities in the shaping process and in the resulting structures. The understanding and optimization of the shaping procedures is hence not finished.

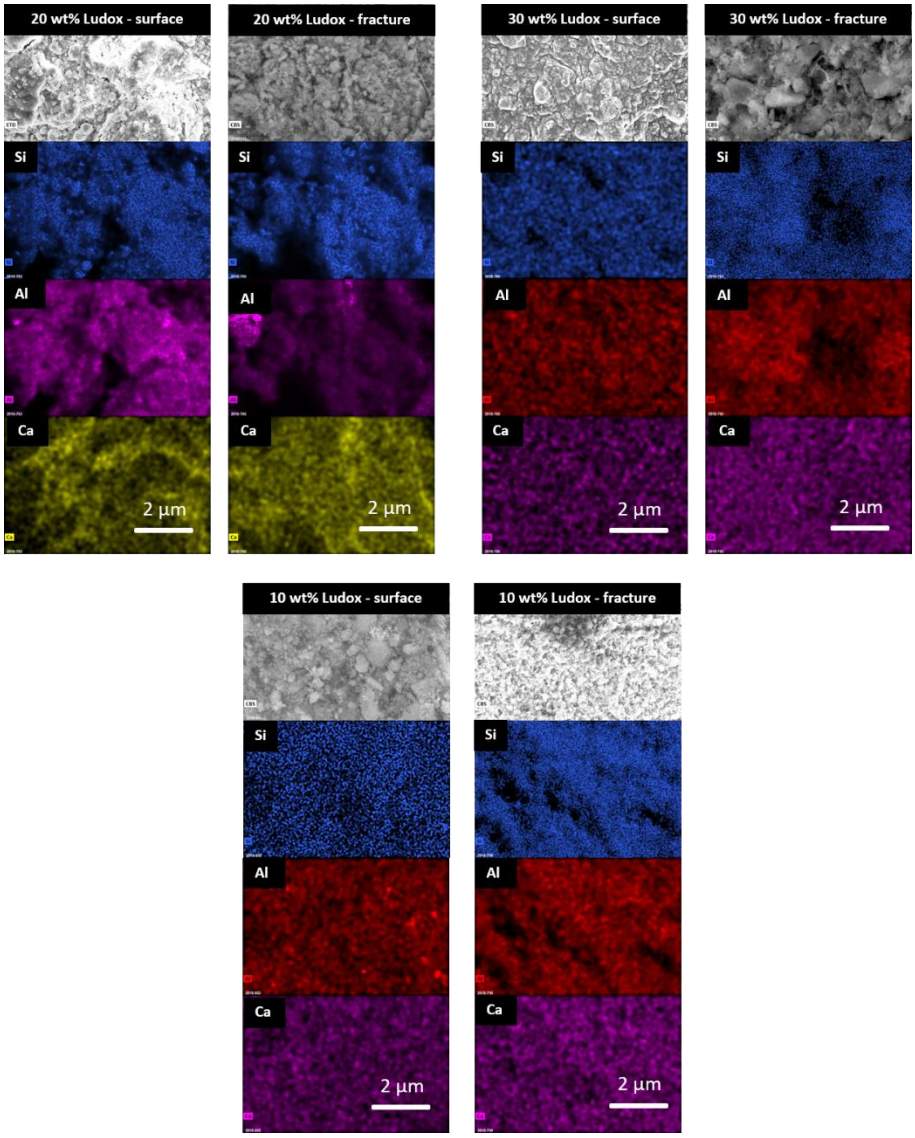


Figure 6.14: SEM-EDX analysis of microspheres with different weight ratio of Ludox AS-40 binder. For every microsphere type, both the outer surface and the interior were analyzed.

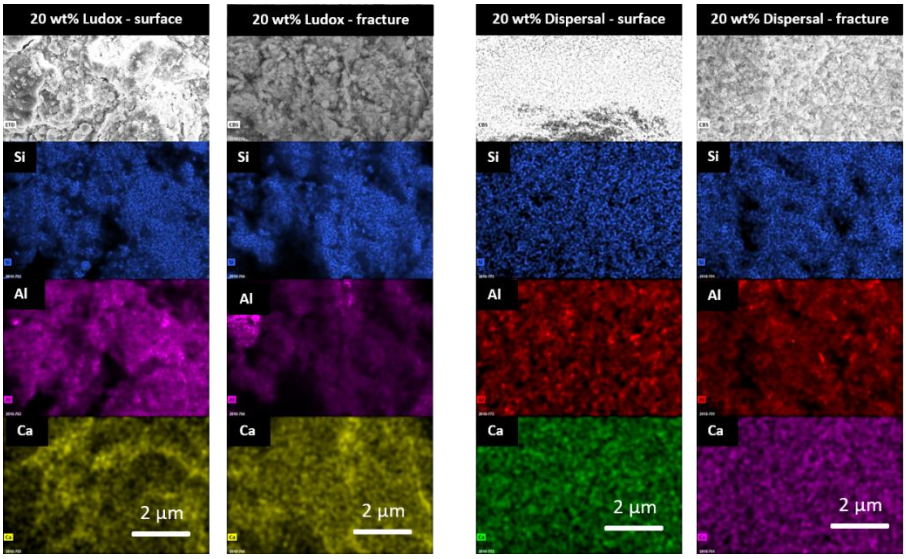


Figure 6.15: SEM-EDX analysis of microspheres with different binder types: Ludox AS-40 (colloidal silica) vs. Dispersal P2 (boehmite). For both microsphere types, the outer surface and the interior were analyzed.

6.2.5. Shaping of all-silica zeolite Beta microspheres

After an initial experimentation with the shaping of Beta-22 based microspheres and their subsequent screening and characterization, experiments were started for the shaping of microspheres based on all-silica zeolite Beta. Since the all-silica variant of zeolite Beta performs much better for PFAS adsorption than the commercial, Al-containing Beta-22, also their respective microspheres are expected to perform much better on PFAS uptake. It can be anticipated that the behavior of all-silica zeolite Beta in a suspension will differ from that of Beta-22 due to differences in surface chemistry. The latter is a hydrophilic cation-exchanger, while the former is a non-ionic and very hydrophobic material. Also the crystal size is different: 2-5 µm for the as-synthesized all-silica zeolite Beta compared to ca. 0.5 µm for Beta-22. This all has an influence on the electrical double layer of the particles and inter-particle interactions. This on its turn influences the rheology, colloidal stability and particle size distribution of the suspension. Nevertheless, all-silica zeolite Beta crystals still have polar silanol functionalities at the crystals' edges, and wetting of small quantities of zeolite powder

during adsorption experiments with aqueous PFAS solutions has never been a problem. However, during suspension preparation, large agglomerates of all-silica zeolite Beta and binder were formed. These could be clearly seen, both visually as well as with particle size distribution measurements. Tuning the relative proportions

of water and alginate in the suspension recipe did not resolve this issue, where it did previously for suspensions with Beta-22. The formation of large agglomerates was definitely caused by the surface chemistry of all-silica zeolite Beta, and not (or not dominantly) by interactions of the zeolite with the binder and/or alginate polymer. This was seen when measuring particle size distribution for a 2 wt% suspension of all-silica zeolite Beta in pure water, compared to a similar suspension for Beta-22 (**Figure S6.13**). Aggregates up to 1 mm were present in the all-silica Beta suspension, whereas most Beta-22 particles are between 1-50 µm. Note that both zeolite Beta types have crystal sizes in the order of 0.2-5 µm, so both types form agglomerates when suspended in water, albeit to a largely different extent.

In order to study the surface chemistry of all-silica and commercial zeolite Beta – and their differences – more deeply, zeta (ζ) potentials over a relevant range of pH values were measured for both zeolites (**Figure 6.16**). The isoelectric point (IEP) titrations revealed a higher (i.e. more positive/less negative) ζ potential for all-silica zeolite Beta. All-silica zeolite Beta has an IEP of ca. 4.2, whereas Beta-22 has a negative ζ potential over a wide range of pH values. This can be attributed to the higher surface acidity of Beta-22 because of the isomorphic substitution of aluminum in the framework and because of the higher amount of framework defects.[63] A larger absolute value of the ζ potential will increase repulsive forces between particles of the same type and enhance colloidal stability. Nevertheless, the pH levels of most suspensions that were made are around 8, so also all-silica zeolite Beta crystals should have a negative ζ potential at this pH level (albeit probably less negative than Beta-22).

Enhancing the colloidal stability of all-silica zeolite beta suspensions can be attempted by either changing the physical or chemical conditions of the zeolite particles or of the suspension as a whole. Mechanical disruption of the large agglomerates can be tried by planetary ball milling or high shear mixing. The latter did not prove to be an efficient method for suspension homogenization, but planetary ball milling showed to be rather effective; 5 minutes of milling was sufficient to significantly reduce the particle size (and homogenize the distribution) of a Beta-300 suspension. Alginate can only be added to the suspension afterwards because the energy-intensive milling process would mechanically disrupt the alginate chains.[64] A disadvantage of the planetary ball milling however is that relatively large quantities of suspension (and thus zeolite) are required, making it more difficult to experiment with all-silica zeolite Beta suspensions.

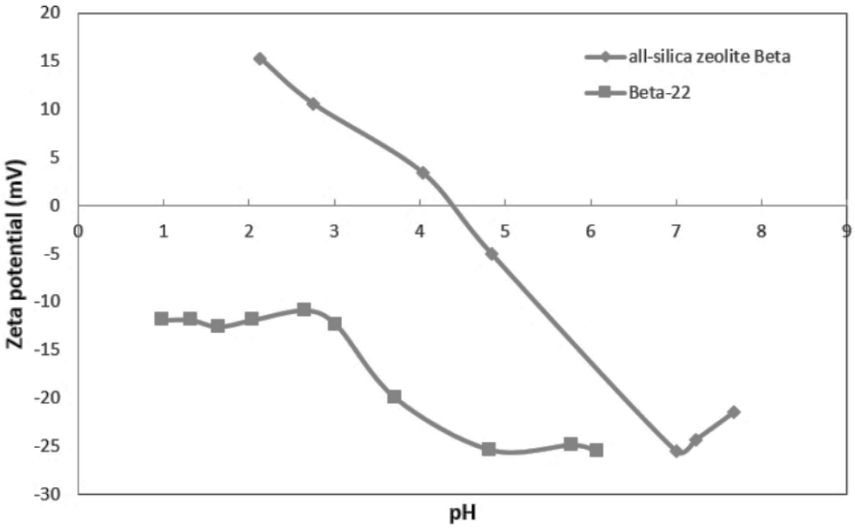


Figure 6.16: Isoelectric point titration of all-silica zeolite Beta and the aluminum containing Beta-22. For every measurement, 40 mg of sample was suspended in 20 mL of demineralized water. pH correction in the vials was done by addition of HCl or NaOH.

Unfortunately, further experiments for the preparation and extrusion of all-silica zeolite Beta suspensions, as well as other experiments to alter the surface chemistry of the all-silica zeolite Beta crystals and/or viscosity of the suspension had to be postponed. The following experiments were still planned:

- Use of a different alginate type; one with a higher viscosity than the BR-W type that was commonly used, e.g. BR-GM;
- Use of a different binder, e.g. methylcellulose (MC) for higher viscosity;
- Changing the surface chemistry of all-silica zeolite beta by silylation.

Therefore, all experimental efforts for the shaping of microspheres with as-synthesized all-silica zeolite Beta were unsuccessful so far. As an alternative, pelletizing of the pure zeolite powder was tried by means of an hydraulic press. Unfortunately, the resulting pellets were brittle and mechanically not strong enough for adsorption column experiments.

6.3. Conclusion

This chapter focused on the shaping and structuration of zeolite Beta as adsorbent for PFAS contaminants. Microspheres for application in a packed bed adsorption column were synthesized by gravitational droplet extrusion. This is a relatively simple shaping procedure, well suited for shaping and screening experiments with

an active material that is limited in availability (all-silica zeolite Beta). In a first stage, different types of binder material were mixed with both all-silica zeolite Beta and the commercial, Al-containing Beta-22. Remarkably, the addition of binder to the adsorbent material had no significant negative impact on PFAS adsorption. Considering PFAS uptake, there was little difference among the various binder types. Ludox AS-40 (colloidal silica suspension) and Dispersal (boehmite fine powder) were selected to start the actual shaping experiments.

The type and relative proportions of the suspension ingredients had a significant impact on the viscosity and particle size distribution of the resulting suspension. These parameters had to be tuned before the suspensions could be used for gravitational droplet extrusion. Highly spherical microspheres could be synthesized with this shaping procedure, even with low amounts of active material. The spheres were screened for PFAS uptake with a focus on adsorption kinetics. Compared to the crushed spheres, a slower uptake for PFOA on the shaped microspheres was observed: PFOA adsorption after 1h was ca. 40% lower. The results were appropriate to allow for the microspheres to be used in a packed bed column in the future, but further optimization will be beneficial.

In order to explain the variation that was seen in mechanical strength and PFAS uptake for different types of microspheres (varying in binder type, binder ratio and extrusion nozzle radius), extensive characterization of the as-shaped microspheres was performed. As for the adsorption and crushing strength results, some significant differences in morphology and porosity could be seen, but it is difficult to find a direct correlation with other variables like binder type or content. At this point, more insight in how to optimally influence the shaping process and resulting sphere characteristics is needed.

Transferring the gravitational droplet extrusion process to all-silica zeolite Beta proved cumbersome. Different surface chemistry (due to the non-ionic and nearly defect-free, hydrophobic nature of the all-silica zeolite Beta framework) of the adsorbent significantly altered the suspension behavior. Large agglomerates were formed, resulting in low colloidal stability and rapid phase separation. Tuning the recipe did not resolve this issue, but large agglomerates could be broken by planetary ball milling. Also surface modification of the zeolite powder can potentially increase colloidal stability. These experiments, together with the actual shaping of all-silica zeolite Beta microspheres, were unfortunately postponed.

6.4. References

[1] T. Sen, Y. Kawajiri, M. J. Realff, *Ind. Eng. Chem. Res.* **2019**, *58*, 5750–5767.

[2] F. Akhtar, L. Andersson, S. Ogunwumi, N. Hedin, L. Bergström, *Journal of the European Ceramic Society* **2014**, *34*, 1643–1666.

[3] S. Mitchell, N.-L. Michels, K. Kunze, J. Pérez-Ramírez, *Nature Chem* **2012**, *4*, 825–831.

[4] S. Mitchell, N.-L. Michels, J. Pérez-Ramírez, *Chem. Soc. Rev.* **2013**, *42*, 6094–6112.

[5] J. Lefevere, S. Mullens, V. Meynen, J. Noyen, *Chemical Papers* **2014**, *68*, 1143–1153.

[6] K. Pangarkar, T. J. Schildhauer, J. R. van Ommen, J. Nijenhuis, F. Kapteijn, J. A. Moulijn, *Ind. Eng. Chem. Res.* **2008**, *47*, 3720–3751.

[7] H. Thakkar, S. Eastman, A. Hajari, A. A. Rownaghi, J. C. Knox, F. Rezaei, *ACS Appl. Mater. Interfaces* **2016**, *8*, 27753–27761.

[8] J. Lefevere, S. Mullens, V. Meynen, *Chemical Engineering Journal* **2018**, *349*, 260–268.

[9] J. Lefevere, B. Claessens, S. Mullens, G. Baron, J. Cousin-Saint-Remi, J. F. M. Denayer, *ACS Appl. Nano Mater.* **2019**, *2*, 4991–4999.

[10] J. N. Stuecker, J. E. Miller, R. E. Ferrizz, J. E. Mudd, J. Cesarano, *Ind. Eng. Chem. Res.* **2004**, *43*, 51–55.

[11] R. M. Ferrizz, J. N. Stuecker, J. Cesarano, J. E. Miller, *Ind. Eng. Chem. Res.* **2005**, *44*, 302–308.

[12] J. A. Lewis, *Advanced Functional Materials* **2006**, *16*, 2193–2204.

[13] J. V. Noyen, A. D. Wilde, M. Schroeven, S. Mullens, J. Luyten, *International Journal of Applied Ceramic Technology* **2012**, *9*, 902–910.

[14] J. Lefevere, M. Gysen, S. Mullens, V. Meynen, J. Van Noyen, *Catalysis Today* **2013**, *216*, 18–23.

[15] C. R. Tubío, J. Azuaje, L. Escalante, A. Coelho, F. Guitián, E. Sotelo, A. Gil, *Journal of Catalysis* **2016**, *334*, 110–115.

[16] X. Zhou, C. Liu, *Advanced Functional Materials* **2017**, *27*, 1701134.

[17] S. Couck, J. Lefevere, S. Mullens, L. Protasova, V. Meynen, G. Desmet, G. V. Baron, J. F. M. Denayer, *Chemical Engineering Journal* **2017**, *308*, 719–726.

[18] S. Couck, J. Cousin-Saint-Remi, S. Van der Perre, G. V. Baron, C. Minas, P. Ruch, J. F. M. Denayer, *Microporous and Mesoporous Materials* **2018**, *255*, 185–191.

[19] J. Zhu, Y. Fan, N. Xu, *Journal of Membrane Science* **2011**, *367*, 14–20.

[20] J. M. Zamaro, E. E. Miró, *Chemical Engineering Journal* **2010**, *165*, 701–708.

[21] F.-C. Buciuman, B. Kraushaar-Czarnetzki, *Catalysis Today* **2001**, *69*, 337–342.

[22] G. B. F. Seijger, O. L. Oudshoorn, W. E. J. van Kooten, J. C. Jansen, H. van Bekkum, C. M. van den Bleek, H. P. A. Calis, *Microporous and Mesoporous Materials* **2000**, *39*, 195–204.

[23] Z. Shan, W. E. J. van Kooten, O. L. Oudshoorn, J. C. Jansen, H. van Bekkum, C. M. van den Bleek, H. P. A. Calis, *Microporous and Mesoporous Materials* **2000**, *34*, 81–91.

[24] J. Roosen, J. Pype, K. Binnemans, S. Mullens, *Ind. Eng. Chem. Res.* **2015**, *54*, 12836–12846.

[25] J. Pype, B. Michielsen, S. Mullens, V. Meynen, *Sustainable Materials and Technologies* **2017**, *14*, 19–28.

[26] J. Bertling, J. Blömer, R. Kümmel, *Chemical Engineering & Technology* **2004**, *27*, 829–837.

[27] J. Z. Liang, F. H. Li, *Polymer Testing* **2006**, *25*, 527–531.

[28] K. C. Yung, B. L. Zhu, T. M. Yue, C. S. Xie, *Composites Science and Technology* **2009**, *69*, 260–264.

[29] S. Freiberg, X. Zhu, *Int. J. Pharm.* **2004**, *282*, 1–18.
[30] M. S. Fleming, T. K. Mandal, D. R. Walt, *Chem. Mat.* **2001**, *13*, 2210–2216.
[31] M. Bohner, S. Tadier, N. van Garderen, A. de Gasparo, N. Döbelin, G. Baroud, *Biomatter* **2013**, *3*, e25103.
[32] J. Pype, Exploring Droplet Coagulation for Shaping Ceramics: A Physico-Chemical Study, PhD Thesis, Universiteit Antwerpen, **2018**.
[33] P. Chen, I. Chen, *J. Am. Ceram. Soc.* **1992**, *75*, 2610–2612.
[34] S. D. Ramamurthi, Z. Xu, D. A. Payne, *Journal of the American Ceramic Society* **1990**, *73*, 2760–2763.
[35] A. Jamekhorshid, S. M. Sadrameli, M. Farid, *Renewable and Sustainable Energy Reviews* **2014**, *31*, 531–542.
[36] M. Bardin, P. C. Knight, J. P. K. Seville, *Powder Technology* **2004**, *140*, 169–175.
[37] M. B. Mackaplow, L. A. Rosen, J. N. Michaels, *Powder Technology* **2000**, *108*, 32–45.
[38] S. J. Lukasiewicz, *Journal of the American Ceramic Society* **1989**, *72*, 617–624.
[39] M. Vicent, E. Sánchez, T. Molina, M. I. Nieto, R. Moreno, *Journal of the European Ceramic Society* **2012**, *32*, 1019–1028.
[40] A. Kaushal, S. M. Olhero, B. Singh, D. P. Fagg, I. Bdikin, J. M. F. Ferreira, *Ceramics International* **2014**, *40*, 10593–10600.
[41] W. L. Li, K. Lu, J. Y. Walz, *International Materials Reviews* **2012**, *57*, 37–60.
[42] S. Deville, *Journal of Materials Research* **2013**, *28*, 2202–2219.
[43] P. Pivette, V. Faivre, G. Daste, M. Ollivon, S. Lesieur, *Journal of Thermal Analysis and Calorimetry* **2009**, *98*, 47–55.
[44] A. Kausar, Polymer-Plastics Technology and Engineering **2017**, 56, 1401–1420.
[45] C. J. Brinker, G. W. Scherer, Sol-Gel Science: The Physics and Chemistry of Sol-Gel Processing, Academic Press, **2013**.
[46] K. Kashima, M. Imai, *Advancing Desalination* **2012**.
[47] S. Fu, A. Thacker, D. M. Sperger, R. L. Boni, I. S. Buckner, S. Velankar, E. J. Munson, L. H. Block, *AAPS PharmSciTech* **2011**, *12*, 453–460.
[48] R. G. Schweiger, *J. Org. Chem.* **1962**, *27*, 1789–1791.
[49] R. G. Schweiger, *J. Org. Chem.* **1964**, *29*, 2973–2975.
[50] R. Hassan, I. Zaafarany, A. Gobouri, H. Takagi, "A Revisit to the Corrosion Inhibition of Aluminum in Aqueous Alkaline Solutions by Water-Soluble Alginates and Pectates as Anionic Polyelectrolyte Inhibitors," **2013**.
[51] J. E. Gregor, E. Fenton, G. Brokenshire, P. Van Den Brink, B. O'Sullivan, *Water Research* **1996**, *30*, 1319–1324.
[52] C. Brandes, M. Hoog Antink, S. Kroll, L. Treccani, K. Rezwan, *Journal of the European Ceramic Society* **2016**, *36*, 1241–1251.
[53] S. Periyasamy, V. Gopalakannan, N. Viswanathan, *Carbohydrate Polymers* **2017**, *174*, 352–359.
[54] F. Abasalizadeh, S. V. Moghaddam, E. Alizadeh, E. akbari, E. Kashani, S. M. B. Fazljou, M. Torbati, A. Akbarzadeh, *J Biol Eng* **2020**, *14*, 8.
[55] Y. Y. Tay, D. I. Stewart, T. W. Cousens, *Engineering Geology* **2001**, *60*, 263–274.
[56] K.-Y. Lee, H.-K. Lee, S.-K. Ihm, *Top Catal* **2010**, *53*, 247–253.
[57] J. Lefevere, L. Protasova, S. Mullens, V. Meynen, *Materials & Design* **2017**, *134*, 331–341.
[58] R. M. Wallace, P. J. Chen, S. A. Henck, D. A. Webb, *Journal of Vacuum Science & Technology A* **1995**, *13*, 1345–1350.
[59] F. Wang, K. Shih, *Water Research* **2011**, *45*, 2925–2930.
[60] D. Staub, S. Meille, V. L. Corre, J. Chevalier, L. Rouleau, *Oil Gas Sci. Technol. – Rev. IFP Energies nouvelles* **2015**, *70*, 475–486.
[61] P. Smrdel, M. Bogataj, A. Mrhar, *Scientia Pharmaceutica* **2008**, *76*, 77–90.

[62] W. Yu, B. C. Hancock, *International Journal of Pharmaceutics* **2008**, *361*, 150–157.
[63] S. G. Hegde, R. Kumar, R. N. Bhat, P. Ratnasamy, *Zeolites* **1989**, *9*, 231–237.
[64] A. Barbetta, E. Barigelli, M. Dentini, *Biomacromolecules* **2009**, *10*, 2328–2337.
[65] C. Couroyer, M. Ghadiri, P. Laval, N. Brunard, F. Kolenda, *Oil & Gas Science and Technology - Rev. IFP* **2000**, *55*, 67–85.

6.5. Supporting Information

6.5.1. Experimental Section

Reagents and standards

All reagents and standards (except when noted otherwise) were acquired from Sigma-Aldrich in the highest grade available. Aqueous solutions were prepared in Milli-Q water. Both native and mass-labelled analytical reference standards used for characterization were acquired from Wellington Laboratories (Guelph, Ontario, Canada). Commercial zeolite samples (CP814-E22, referred to as Beta-22 and CP811C-300, referred to as Beta-300) were acquired via Zeolyst International. Dispersal P2 and Dispersal HP14/7 were acquired via Sasol. Sodium alginate Br-W was supplied by Brace GmBH (Alzenau, Germany).

Preparation of hybrid zeolite-binder mixtures

All binders were mixed with the zeolite powder in a 90:10, 80:20 or 70:30 (zeolite:binder) mass ratio. When the binder was a powder, water was added to obtain a slurry. Slurries and powders were adequately mixed in a planetary mixer. The resulting zeolite binder mixtures were dried overnight at 60°C and subsequently calcined (5h at 550°C, heating ramp 1.5 °C/min at ambient air and pressure).

Microsphere shaping by gravitational droplet extrusion

Suspensions were prepared by planetary mixing the zeolite powder with the respective binder, alginate BR-W solution and deionized (DI) water. When necessary, agglomerates were eliminated by adding grinding balls (3 mm yttrium stabilized zirconia in ratio 2:1 powder/grinding balls) to the suspension and keeping the container in motion on the rolling bench for several hours. Droplets were generated by air pressure and extruded through a nozzle tip of variable size (min. 0.58 mm, max. 1.19 mm). The droplets were collected in the coagulation bath (4 wt% $CaCl_2$ solution) and left overnight for solidification. During extrusion, isopropyl alcohol (IPA) was sprayed on the liquid interface to reduce surface tension, hence lowering the impact when the falling droplets hit the interface. The microspheres were thoroughly washed with DI water and IPA, before drying overnight at 60 °C. Lastly, the spheres were calcined at 550 °C for 6h, with a heating rate of 1.5 °C/min at ambient air and pressure.

Adsorption experiments

Adsorption experiments for the screening of zeolite-binder powder mixtures were similar to the batch adsorption experiments as described earlier in the experimental sections of Chapter 4 and 5. For these experiments, 5 mg of powder mixture was

dissolved in 5 mL of stock solution (1, 100 or 500 mg PFOA/L). For kinetic experiments, 5 mg of adsorbent was contacted with 5 mL of a 100 mg/L solution of either PFOA or PFOS. Contact times were varied, ranging from 5 min up to 24 h. In these kinetic experiments, the adsorbent was a pure zeolite Beta sample or a sample of self-shaped microspheres, either crushed or as whole structures. Therefore, adsorbent loading was not always exactly 5 mg/5mL, but varied between 4-6 mg per 5 mL. The same number of spheres was used throughout the kinetic experiments, whether for the crushed form or the whole spheres. Measurements of the PFAS concentrations and calculations of PFAS uptakes were performed as described previously.

Viscosity measurements

The viscosity of the prepared suspensions was analyzed at room temperature with a Haake Mars Rheometer using a concentric cup measuring geometry (cup Z43 DIN 53018 and rotor Z41 DIN 53018). The dynamic viscosity was recorded over a range of shear rates (0.01–1000 s^{-1}) and data points were gathered when reducing the shear rate.

Porosimetry

Macroporosity (pores between 0.01-10 µm) of the shaped microspheres was analyzed with Hg-porosimetry (Pascal Mercury Porosimeters, Thermo Scientific). The specific surface areas of the microspheres were measured by N_2 physisorption (Autosorb-1, Quantachrome), using the BET method. Samples were measured at -196 °C. Prior to the sorption measurements, all samples were degassed for 16h at 200 °C to remove all adsorbed water. The t-plot method using the De Boer thickness equation was used to derive micropore volume and the external surface area. The micropore surface area was obtained by subtracting the external surface area from the calculated BET surface. The volume of pores < 50 nm was measured at a P/P_0 value of 0.95.

Particle size distribution

Particle size distribution of suspensions was measured via light diffraction combined with a dynamic image analysis system (Microtrac S3500). Each sample was subjected to ultrasound for 30 s and measured for 30 s at 40% of the maximum flow.

Optical microscopy and image analysis

The microspheres were examined by optical microscopy with a Zeiss Discovery V12 stereomicroscope, equipped with a Plan Apo S 1.0 w FWD 60 mm objective. Images of the spheres were taken with an Axiocam 506 camera connected to the

microscope. Image processing was performed by Zen software. Image conversion and analysis was performed using the ImageJ software with the Bio-Format plugin.

Scanning Electron Microscope (SEM) and elemental mapping

The as-shaped microspheres were examined with a cold field emission gun scanning electron microscope (FEGSEM) of the type Nova Nano SEM 450 (FEI, USA) at 20 kV. The spheres were encapsulated in an epoxy resin before measurement. For analysis of microsphere cross-sections, the samples were cut and polished. Element mappings of the surface and cross-sections of the spheres were performed with a Bruker XFlash Detector 5030 and a Bruker QUANTAX-200 EDS system.

Crushing strength experiments

The mechanical strength of the microspheres was assessed by side crushing strength (SCS) testing on a Instron 5582 universal hydraulic testing machine. Side crushing strength (σ_f) was calculated with the following equation:[65]

$$\sigma_f = 2.8 \frac{P_f}{\pi D^2}$$

With P_f being the load (N) at breaking point and D the diameter (m) of the spheres. 10 samples were crushed for every type of microsphere to obtain an average strength and calculate the standard deviation.

Isoelectric point titration (ζ potential measurement)

Zeta potential measurements were performed with a Zetaprobe analyzer (Colloidal Dynamics, FL, USA). For every measurement, 40 mg of sample was suspended in 20 mL of demineralized water, mixed in an ultrasonication bath for 30 min. pH correction in the vials was done by addition of HCl or NaOH.

6.5.2. Supporting Figures

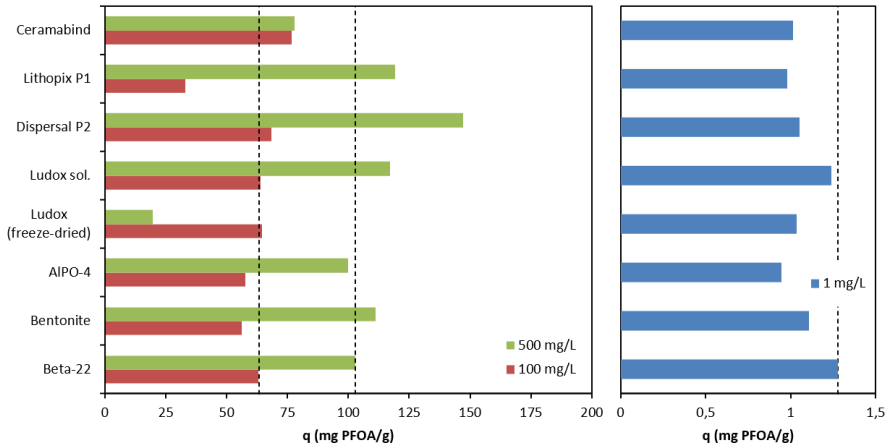


Figure S6.1: PFOA adsorption on mixtures of Beta-22 (commercial name: CP814E-22) and different inorganic binders at three different initial PFOA concentrations. Left: 100 and 500 mg PFOA/L (to probe capacity of the adsorbents). Right: 1 mg PFOA/L (to probe affinity). Dashed lines are used to indicate the adsorption capacity of pure Beta-22. *q* = mg PFAS adsorbed per g of dry matter zeolite-binder mixture.

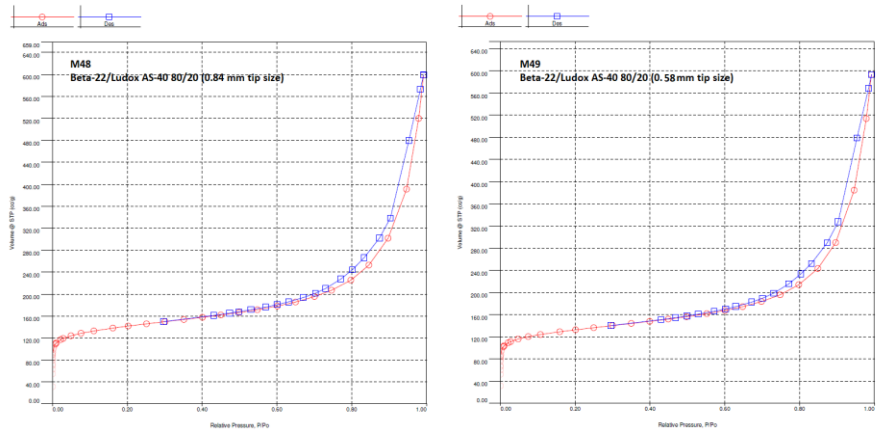


Figure S6.2: N_2 physisorption isotherms for M48 (left) and M49 (right). M48 = Microspheres extruded from a 0.84 mm nozzle, suspension = Beta-22/Ludox AS-40 80/20. M49 = Microspheres extruded from a 0.58 mm nozzle, suspension = Beta-22/Ludox AS-40 80/20.

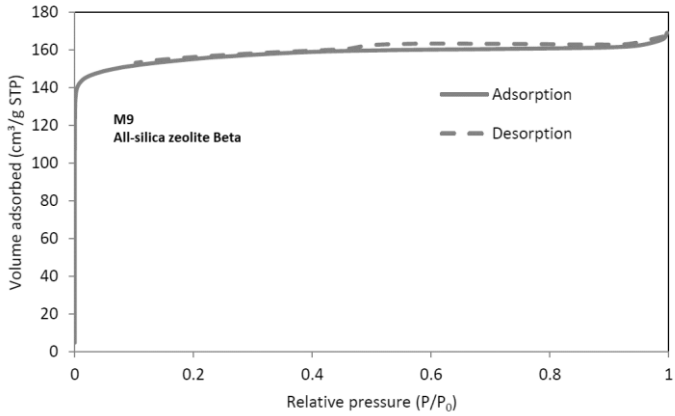
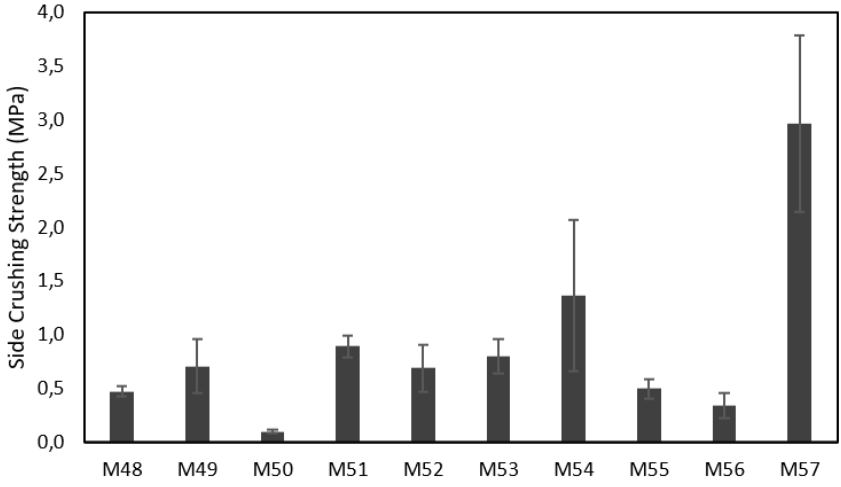


Figure S6.3: N_2 physisorption isotherm for pure, as-synthesized all-silica zeolite Beta.



Name	Binder type	Nozzle size
M48	Ludox 80/20	0.84 mm
M49	Ludox 80/20	0.58 mm
M50	Ludox 80/20	1.19 mm
M51	Ludox 80/20	0.41 mm
M52	Dispersal P2 80/20	1.19 mm
M53	Dispersal P2 80/20	0.58 mm
M54	Ludox 70/30	1.19 mm
M55	Ludox 70/30	0.58 mm
M56	Ludox 90/10	1.19 mm
M57	Ludox 90/10	0.58 mm

Figure S6.4: Results of the side crushing strength (SCS) experiments (**Figure 6.11**) for different types of microspheres. The error bars show the standard deviation, based on 10 samples for every microsphere type.

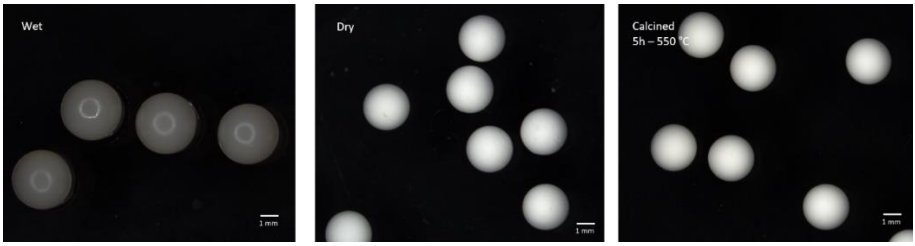


Figure S6.5: Image analysis for M48 microspheres. M48 = microspheres extruded from a 0.84 mm nozzle, suspension = Beta-22/Ludox AS-40 80/20. Images were taken with a Zeiss Discovery V12 microscope and Axiocam 506 camera.

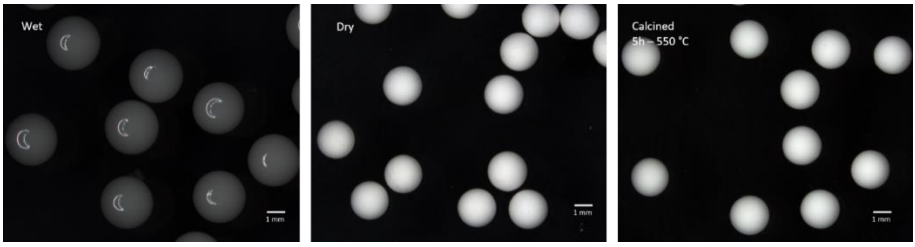


Figure S6.6: Image analysis for M49 microspheres. M49 = microspheres extruded from a 0.58 mm nozzle, suspension = Beta-22/Ludox AS-40 80/20. Images were taken with a Zeiss Discovery V12 microscope and Axiocam 506 camera.

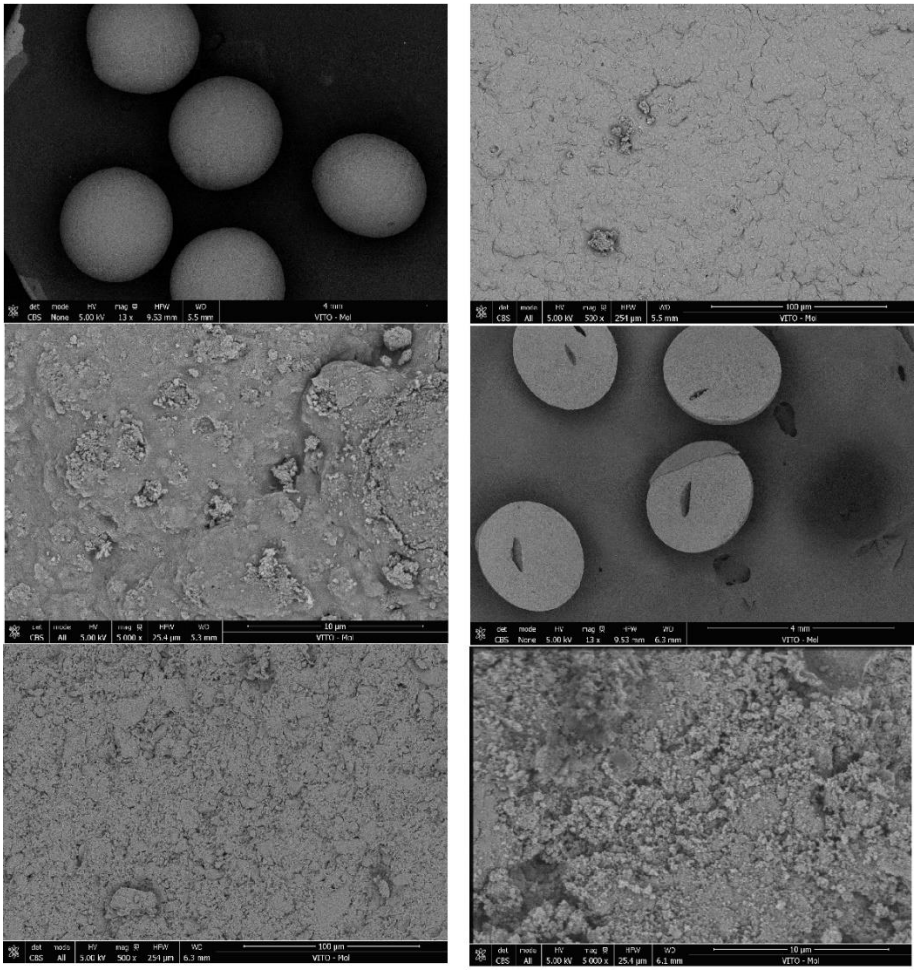


Figure S6.7: SEM images of M54 microspheres: Beta-22/Ludox AS-40 70/30 extruded from a 1.19 mm nozzle. From left to right, bottom to top: SEM images of the external surface (4 mm, 100 µm, 10 µm); SEM images of the interior/fracture plane (4 mm, 100 µm, 10 µm).

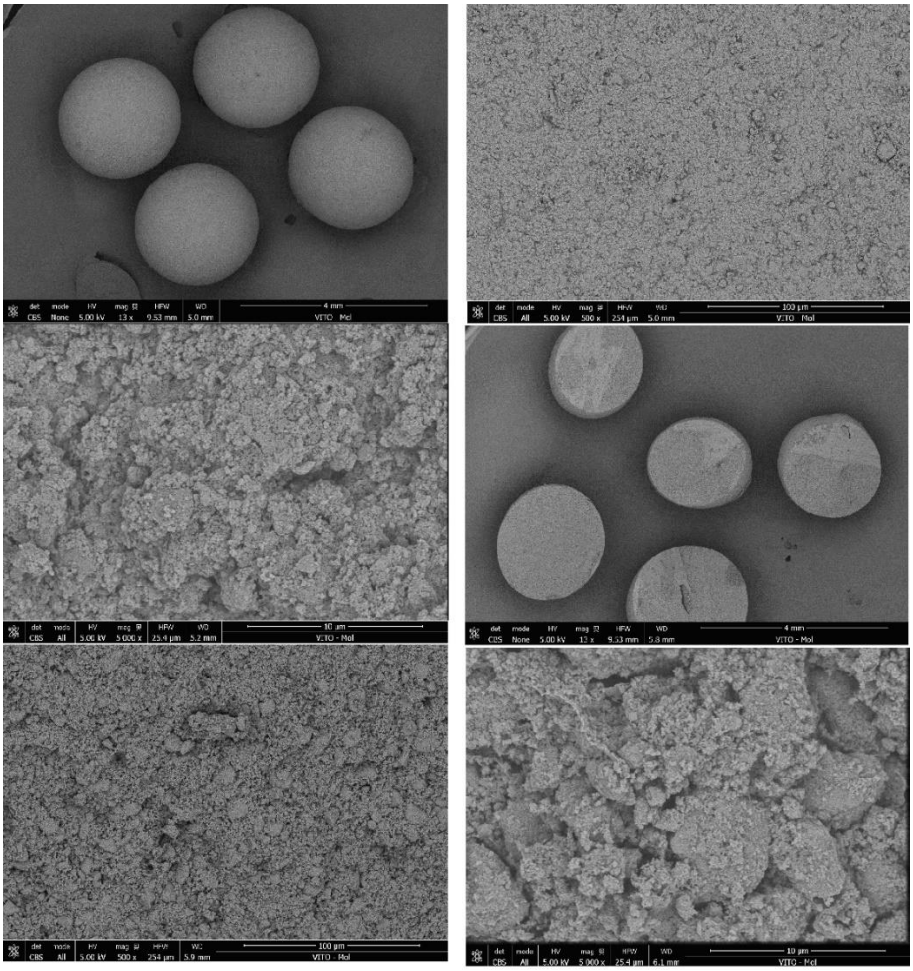


Figure S6.8: SEM images of M56 microspheres: Beta-22/Ludox AS-40 90/10 extruded from a 1.19 mm nozzle. From left to right, bottom to top: SEM images of the external surface (4 mm, 100 µm, 10 µm); SEM images of the interior/fracture plane (4 mm, 100 µm, 10 µm).

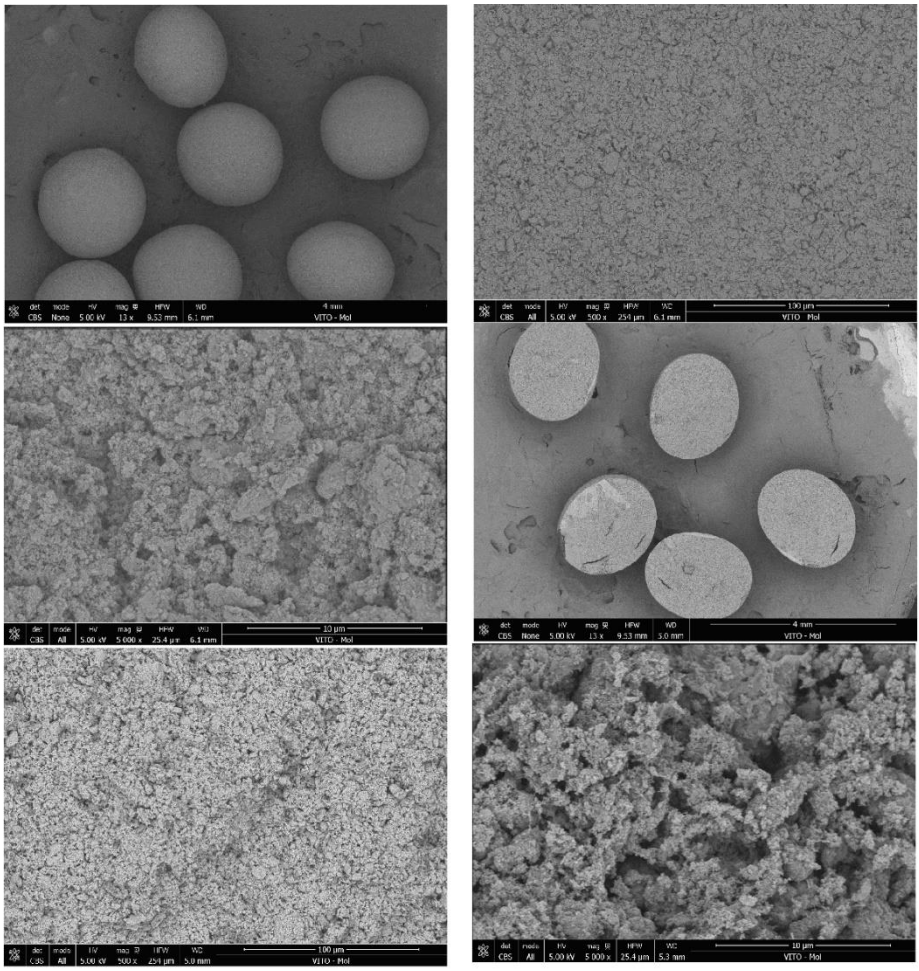


Figure S6.9: SEM images of M52 microspheres: Beta-22/Dispersal P2 80/20 extruded from a 1.19 mm nozzle. From left to right, bottom to top: SEM images of the external surface (4 mm, 100 µm, 10 µm); SEM images of the interior/fracture plane (4 mm, 100 µm, 10 µm).

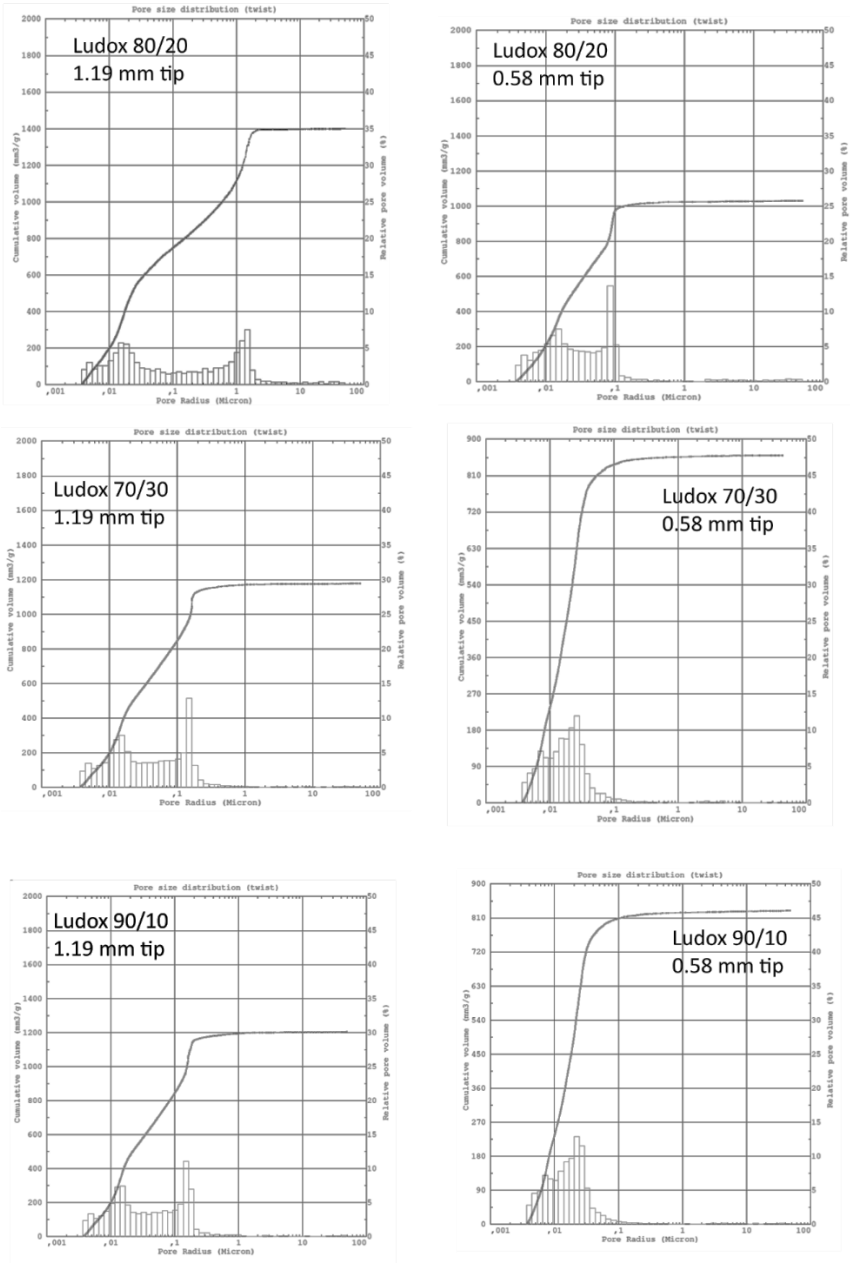


Figure S6.10: Pore volume and pore size distribution plots of Ludox based microspheres, derived from mercury intrusion porosimetry measurements.

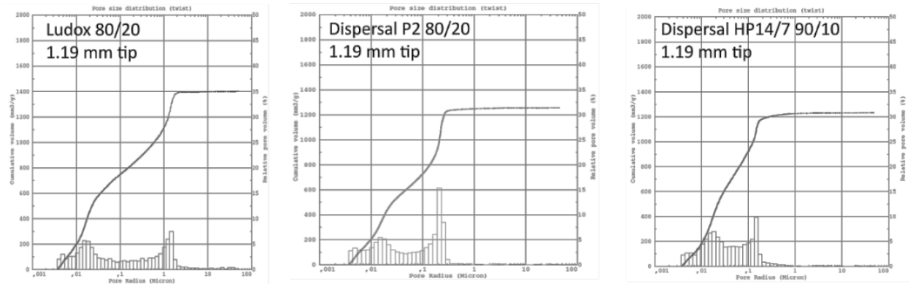


Figure S6.11: Pore volume and pore size distribution plots of microspheres made with different types of binders. Values are derived from mercury intrusion porosimetry measurements.

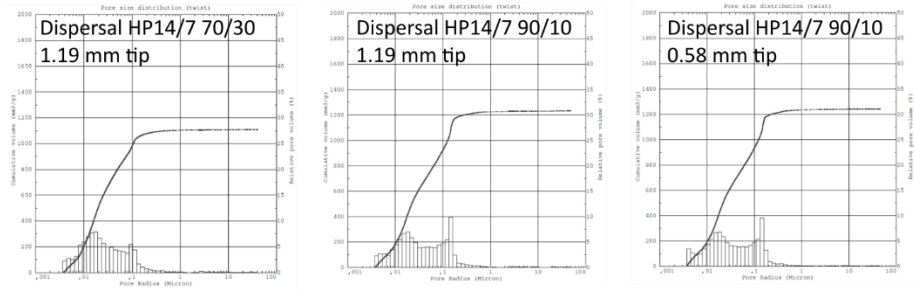


Figure S6.12: Pore volume and pore size distribution plots of microspheres made with different weight ratio of Dispersal HP14/7 and/or extruded from different tip sizes. Values are derived from mercury intrusion porosimetry measurements.

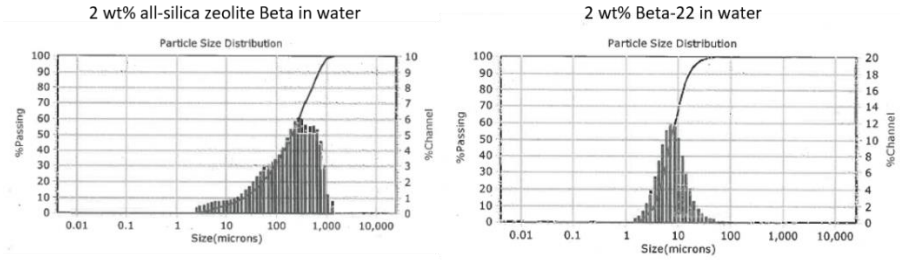


Figure S6.13: Particle size distributions of 2 wt% suspensions of all-silica zeolite Beta (left) and Beta-22 (right) in pure water.

CHAPTER 7

SCOPE EXTENSION, FUTURE PERSPECTIVES AND GENERAL CONCLUSION

Matthias Van den Bergh[a] and Dirk De Vos[a]

[a] M. Van den Bergh, Prof. D. De Vos
Centre for Membrane Separations, Adsorption, Catalysis and Spectroscopy for Sustainable Solutions (cMACS)
KU Leuven
Celestijnenlaan 200F, 3001 Leuven, Belgium

Abstract

In this final chapter, the conclusions drawn on the experimental work in this manuscript are given. Additionally, the future perspectives of this research are discussed.

Contributions

M.V.d.B. wrote the manuscript. D.D.V. supervised the work.

7. General conclusions and future perspectives

7.1. Conclusions

Perfluorinated alkylated substances (PFASs) are persistent organic pollutants that have been used and emitted extensively in the past 60 years. Their physicochemical properties make them a unique class of chemicals; the perfluorinated carbon chain is extremely hydrophobic and oleophobic, while the acidic head group gives them surfactant properties and makes them water soluble. They are inert towards many types of reactive agents and cannot be degraded by heat, UV-light or microbiota. They are used as emulsifier (easily forming micelles), coating (repelling water, oil and stains), lubricant (having extremely low surface tension) and have many other functions, in industry and in household applications. Their unique physicochemical properties are predominantly caused by the peculiar nature of fluorine, with C-F as one of the strongest bonds in organic chemistry.

Historical and current emissions of these persistent chemicals have led to a build-up of PFAS contaminations in the environment. Because of their solubility in water streams, highly concentrated point emissions have been diluted into very diffuse pollutions of water streams. Due to the chronic toxic effects and the widespread presence of these PFASs in waste water and drinking water, governments worldwide have imposed restrictions on the usage but also on the emissions and concentrations of the most relevant PFASs in water. This does not necessarily reduce the production, consumption and emission of PFASs, since the fluorochemical industry is switching towards the best available alternatives that are very similar to the historically most used PFOA and PFOS. The recent introduction of environmental quality standards and this shift towards perfluorinated alternatives impose the urgent need for a clean-up strategy and removal technologies for (lowly concentrated) PFAS pollutions.

Several treatment techniques (e.g. sonolysis and electro- or photochemical catalysis) are being investigated for the remediation of PFAS pollutions in water, but they suffer from high energy requirements. They also need several pre-treatment steps, making them inefficient for the treatment of large volumes of water. In this regard, adsorption is arguably the best technique to treat large volumes while keeping energy costs modest. Even when using one of the aforementioned techniques, adsorption is often essential for concentrating the influent stream. This makes the selection of an adsorbent with adequate capacity and high selectivity for PFASs of utmost importance. Most studies on PFAS adsorbents have a strong focus on maximum adsorption capacity and less on affinity (at low concentrations) and

selectivity for PFASs (over other organic compounds commonly present in waste and surface water). However, affinity and selectivity are crucial prerequisites for the removal of low-level PFAS pollutions. High adsorption capacity is desirable but if the adsorbent can be regenerated, it is not the most pivotal adsorbent feature.

The importance of adsorption parameters other than capacity was first demonstrated for citric acid, a common organic acid. Compared to more common, commercial strong anion exchangers, a higher selectivity (over sulfate) and regeneratability was achieved using the weak anion exchanger poly(4-vinylpyridine) (PVP). This made PVP very suitable for the recovery of citric acid under industrially relevant conditions (e.g. at low pH or at moderate pH with high sulfate levels). Especially the robustness of PVP towards sulfate competition was in striking contrast with other resins, which showed dramatic reductions in citric acid adsorption in the presence of sulfate. The good adsorptive features of PVP for citric acid recovery could be attributed to the weak basicity of the pyridine group: it facilitates an easier desorption and circumvents selectivity problems when adsorption is dominated by electrostatic interactions, as is the case for most commercial strong and weak anion exchangers. This showed the potential of carefully selecting and tuning an adsorbent, with respect to the organic acid to be recovered. This approach was therefore also adopted for PFAS adsorption.

Microporous, siliceous materials were investigated for their potential as PFAS adsorbents, with a focus on hydrophobic, all-silica or high-silica zeolites. It was suggested in previous studies that hydrophobicity is favorable factor for PFAS adsorption, but hydrophobic, all-silica zeolites were never studied before for this type of application.[1,2] The as-synthesized materials were compared to the current benchmark adsorbent for PFAS removal, being activated carbon. Activated carbon has a relatively high adsorption capacity and it is a widely applicable adsorbent for many types of (organic) compounds, but it therefore lacks a selectivity mechanism for PFASs over other organic compounds. Based on various adsorption experiments (screening for capacity, affinity, selectivity and kinetics), all-silica zeolite Beta proved to be an outstanding adsorbent for PFAS adsorption. Zeolite Beta is a zeolite type with wide (12-membered) ring openings and straight pore channels in the *a*- and *b*-direction of the zeolite, providing an open and accessible framework. PFAS uptake was higher (PFOA) or similar (PFOS) for all-silica zeolite Beta, compared to activated carbon. A similar trend was seen for the kinetics of the adsorption process. It was especially for PFAS selectivity that all-silica zeolite Beta showed truly outstanding results. PFOA uptake was undisturbed by competition of other organic compounds, even when these compounds were present in a 15-fold molar excess. In contrast, PFOA uptake on activated carbon was drastically reduced. Also PFOS adsorption on

all-silica zeolite Beta was barely affected by severe competition, whereas PFOS uptake on activated carbon was again reduced significantly. This was remarkable, since both adsorbents were on par for PFOS adsorption in single-component experiments.

The comparison of all-silica zeolite Beta with other microporous and mesoporous (silica-based) materials showed that i) hydrophobicity of the material and ii) adequate (micro)porosity and specific surface area are important parameters for PFAS adsorption. Both criteria have to be fulfilled simultaneously in order to achieve both high affinity and capacity. Adsorption of PFAS on zeolites is limited by the radius of the pore windows, with 12-membered ring openings appearing to be the minimal window size to allow adequate PFAS adsorption. All-silica zeolites have no framework charge due to the absence of aluminium, but this is not sufficient to achieve high hydrophobicity; also the framework should be free of connectivity defects that create silanol nests. This was clearly shown by comparing the high PFOA uptake on all-silica zeolite Beta with the low uptake on the commercial zeolite Beta-300 (with a very high SiO_2/Al_2O_3 ratio of 300).

The question why all-silica zeolite Beta has such a high affinity and selectivity for PFASs was resolved by combining the results of advanced characterization techniques and computational modelling. Calorimetry measurements showed that PFOA adsorption on the different zeolite Beta types is associated with a negative adsorption enthalpy, both at low and at higher occupation of the zeolite surface. Adsorption enthalpies for all-silica zeolite Beta were much more negative (-30 to -40 kJ mol^{-1}) than for the aluminated zeolite Beta types (-20 to 0 kJ mol^{-1}). This was partly a surprise, since the hydrophobic clustering of PFAS molecules was believed to be predominantly driven by entropic (and thus not enthalpic) effects. The combination of both an enthalpic and entropic effect is clearly an advantage for a strong adsorption interaction. Through Density Functional Theory (DFT) simulations, the total energy of different optimized conformations of PFOA molecules in zeolite Beta was calculated, demonstrating a strong preference of PFOA for head-head interactions. The stability of these head-head interactions results from the formation of carboxylic acid dimers, driven by H-bonding. The same scenario was observed for caprylic acid (the non-fluorinated C_8 analogue of PFOA), associated, however, with a guest/zeolite Beta interaction energy (-181.1 kJ mol^{-1}) that is much lower than that obtained for the head-head conformation of PFOA (-264.6 kJ mol^{-1}). This showed that the observed selectivity of all-silica zeolite Beta for PFOA is enthalpy-driven, confirming the calorimetry results. According to the simulations, the PFOA molecules are aligned according to the straight channels in the *a*- and *b*-directions, but not along the tortuous channels in the *c*-direction. DFT simulations also showed that a

helical conformation of PFOA is slightly more favorable than a zig-zag one, in contrast to caprylic acid for which a zig-zag structure is more stable. Since the helical conformation is slightly shorter than the zig-zag one, PFOA might also have a steric advantage over caprylic acid when the zeolite is fully packed.

Experimental evidence supporting the computational predictions was offered by solid-state NMR spectroscopy. ^{19}F MAS and ^{1}H-^{13}C CPMAS NMR spectra of pure, crystalline PFOA and of PFOA loaded into all-silica zeolite Beta showed large similarity and confirmed the presence of PFOA inside the zeolite. The 2D ^{1}H-^{1}H homonuclear correlation spectrum of the zeolite Beta loaded with the highest concentration of PFOA indicated that PFOA within the zeolite most likely forms head-to-head hydrogen-bonded dimers, while close inspection of the ^{19}F-^{29}Si heteronuclear correlation spectrum suggested that the hydrophobic part of PFOA is located within the straight channels. It therefore also suggested that the end of the tail and the (polar) head of the molecule are situated in or closer to the channel intersections. All NMR findings were in line with the computational predictions. Summarizing, it was made clear that the adsorption of PFOA on all-silica zeolite Beta is very favorable in terms of enthalpy, due to the PFOA molecules forming hydrogen bonded pairs in the intersections, while the perfluorinated chains are situated in the hydrophobic, straight (*a*- and *b*-) channels of the zeolite. Even though not measured, also favorable entropy changes upon adsorption are believed to play an import role in these hydrophobic interactions. The helical conformation of the perfluorinated chains makes a very tight packing at maximal capacity sterically possible, explaining the exceptionally high affinity and selectivity of all-silica zeolite Beta for PFOA and similar perfluorinated compounds.

Its outstanding adsorptive properties position all-silica zeolite Beta as the lead candidate for combating PFAS pollution via adsorption. Most treatment systems that deal with large volumes of water use packed bed adsorption columns in which the adsorbent is applied as particles of controlled shape and size. Shaping of the active material into a hierarchically porous structure can reduce high pressure drops and avoid random and tortuous flow paths. Applying the active material in a structured, homogeneous shape can furthermore result in enhanced kinetics, more uniform processes (in time and space), higher surface area and hence optimized driving forces and in better adsorbent properties like stability or separability. To prepare all-silica zeolite Beta for future application in a packed bed adsorption column, the possibility of shaping zeolite Beta based microspheres was explored. Among several existing shaping processes and adsorbent structures, microspheres are still one of the most convenient shapes for inorganic or ceramic materials. Their smooth shape

and surface minimize pressure drop and mechanical attrition of the material in liquid flows.

Zeolite Beta microspheres were synthesized by gravitational droplet extrusion; this shaping procedure is well suited for shaping and screening experiments at lab scale. Different types of binder material were screened with both all-silica zeolite Beta and the commercial, Al-containing Beta-22 for their compatibility with PFAS adsorption. Very remarkably (but desirably), the addition of binder to the adsorbent material had no significant negative impact on PFAS adsorption. Ludox AS-40 (colloidal silica suspension) and Dispersal (highly dispersed boehmite powder) were selected to start the actual shaping experiments. They were dispersed in a suspension together with zeolite Beta and a BR-W alginate polymer. The type and relative proportions of the suspension ingredients had a significant impact on the viscosity and particle size distribution of the resulting suspension. After optimizing the suspension recipe, highly spherical microspheres of Beta-22 could be synthesized with both Ludox and Dispersal as binder type. Compared to the pure zeolite adsorbent, the shaped microspheres showed a lower capacity and slower PFOA uptake due to the additional mass diffusion limitation that is inherent to structured materials.

The shaping of microspheres based on the better PFAS adsorbing all-silica zeolite Beta was unsuccessful so far. Different surface chemistry (reflected in a very disparate zeta potential) led to low-viscosity suspensions, large agglomerates and low colloidal stability (i.e. rapid settling of particulate matter). Mechanically disrupting the agglomerates by ball-milling or chemical modification of the zeolite surface (by e.g. silylation) can potentially resolve this issue. To accomplish this, further insight in how the suspension composition and extrusion process affect the resulting microsphere characteristics is needed.

7.2. Future perspectives

We strongly believe that all-silica zeolite Beta is one of the best PFAS adsorbents known and investigated up until this day. Adsorbents with higher capacity exist (e.g. some anion-exchangers) but they suffer from low selectivity and are hence ineffective in treating large volumes of surface or waste water with relatively low PFAS concentrations. In contrast, all-silica zeolite Beta is highly selective towards C_8 PFASs against a complex background of dissolved organic matter. It has a strong potential to be effectively used for *in situ* treatment of waste and surface waters and we are convinced it can be the crux in a novel treatment for aqueous PFAS remediation. Such a novel technique is essential in order to comply with the environmental quality standards, recently introduced by the EU and implemented

on a regional level. These will be strictly monitored from 2027 onwards, hence time is limited for resolving this stringent issue. Calling this all-silica zeolite Beta the crux or foundation of a novel treatment stresses the importance of the adsorbent material, but it also implies that still other factors are essential in order for this solution to be fully applied. Four main aspects that need further exploration and development can be distinguished; i) extending the scope of PFASs than can be removed, ii) regeneration of the adsorbent by PFAS degradation, iii) shaping of the adsorbent and optimization of the adsorption process and iv) upscaling of the all-silica zeolite Beta synthesis process.

7.2.1. Scope extension to PFAS alternatives

PFOA and PFOS have been the most relevant and most widely used PFASs for decades. Hence, in terms of emissions and pollution of water bodies (and other compartments), PFOA and PFOS removal is still a critical topic. A growing number of countries has imposed restrictions though on these chemicals; therefore current emissions of PFOA and PFOS are lower than they used to be (but still not zero).[3,4] This does not mean that (global) PFAS emissions are lower too; firstly, a part of PFOA and PFOS productions has been moved from the Western industrial countries to emerging Asian countries. Secondly, the restrictions on PFOA and PFOS have pushed industrial players to use perfluorinated alternatives. Since PFOA and PFOS have such unique (and desirable) features, these alternatives are often intended to be as similar (in chemical properties) to PFOA and PFOS as possible. These alternatives can be broadly divided into five subclasses; i) shorter perfluorinated alkylated acids, ii) non-functionalized, perfluorinated alkyl chains, iii) (per)fluorotelomers, iv) perfluoro(poly)ethers and v) perfluorinated liquids such as perfluorotrialkylamines.[5–7] This industrial shift from C_8 perfluorinated acids towards other alternatives has already been witnessed in several environmental monitoring studies, both in Europe as well as in other continents. Many of these alternatives are not strictly regulated (yet), because they are believed to be less toxic (e.g. due to a shorter half-life in the human body) and their spreading is not as apparent yet. Nevertheless, the risks of long term exposure and usage of these compounds is often not fully known yet.[8] Because they are intended to be so similar to PFOA and PFOS, it is reasonable to assume that (some of) these alternatives are also persistent and not harmless for humans and/or ecosystems.

A good adsorbent for PFOA and PFOS is of high value, even when it is only efficient in removing these two PFASs. The historical emissions of PFOA and PFOS are of such degree that the removal of these PFASs has the highest priority, especially regarding the new legislation on these compounds in several countries. Nevertheless,

restrictions on some of the most widely used alternatives can be expected in the future. Already now, industrial players are searching for the best possible solution(s) to reduce the emissions of the perfluorinated alternatives they use. The field of applicability and durability of all-silica zeolite Beta as PFAS adsorbent would increase tremendously if it would also efficiently remove some or most of these alternatives. Based on the research in this PhD thesis, it is known that both hydrophobicity and steric constraints play an important role in the removal of PFOA and PFOS. This gives a clue on which PFAS alternatives could be adsorbed by all-silica zeolite Beta with similar capacity and selectivity as for PFOA and PFOS. Linear perfluorinated alkyl chains might adsorb very well on all-silica zeolite Beta, with or without functional group(s) in or at the end of the chain. For perfluorinated acids though, chain length is important; the shorter the perfluorinated carbon chain, the less hydrophobic the molecule will be. The relative contribution of the polar acid group to the hydrophobic/hydrophilic character of the PFCA increases with decreasing chain length. Non-functionalized and linear perfluorinated aliphatic molecules, like perfluorooctane and perfluorodecane, might adsorb extremely well on all-silica zeolite Beta because they are ultra-hydrophobic and have similar dimensions as PFOA and PFOS. This was also confirmed in a set of preliminary of experiments (see Chapter 5); both perfluorinated carboxylic and sulfonic acids of varying chain length adsorb very well on all-silica zeolite Beta, with C_6 as minimal chain length. Adsorption of shorter-chain PFASs (e.g. perfluorobutanesulfonic acid (PFBS), C_4) was significantly lower, due to the reduced hydrophobicity. Also aliphatic compounds like perfluorooctane and perfluorodecane are adsorbed in very high quantities on all-silica zeolite Beta.

On the other hand, branched molecules like perfluorotrialkyl amines will be very difficult to adsorb because of steric obstruction; they will not have a proper fit in the channels of zeolite Beta. It cannot be wished or expected that all-silica zeolite Beta performs well in adsorbing every type of PFAS, since this group of chemicals is very diverse and the broader the adsorbate scope, the lower the selectivity for specific PFASs may be. Nevertheless, it is an interesting and necessary step to fully explore the complete scope of PFASs that all-silica zeolite Beta is able to remove in high quantities and/or with high affinity and selectivity. This will maximally exploit the applicability and potency of this adsorbent for future *in situ* PFAS removal. It must also be further investigated if these PFAS adsorbates can be adsorbed simultaneously and in what order. Preliminary experiments show that PFCAs are preferred over similar PFSAs (e.g. PFOA > PFOS) and that different types of PFASs (e.g. PFOA, PFOS, FPHS and PFBS) can be simultaneously removed from real waste waters, as long as the adsorbent is not fully saturated. Confidential experiments on strongly polluted groundwater samples show high and simultaneous uptake of C_6-

C_{10} PFCAs and PFSAs against a natural background, underlining the potential of all-silica zeolite Beta for the remediation of *real life* polluted waters.

A final thought on this matter: if emissions for a series of PFAS alternatives will be more strictly regulated in the future, industrial players might also adapt to the remediation techniques available. This means that out of two similarly performing PFASs, the one that can be the best removed by e.g. all-silica zeolite Beta might preferentially be used in industry.

7.2.2. Regeneration and PFAS degradation

In order for an adsorbent to be used over and over again, it has to be regenerated once saturated. Several methods for adsorbent regeneration exist (see Chapter 2), each method having its (dis)advantages. Common PFAS adsorbents like activated carbon and anion-exchangers can only be regenerated by mild thermal treatment or by using organic solvents and/or strong acids or bases, creating stoichiometric amounts of waste products and leading to high consumption of these chemicals. For relatively cheap adsorbents like activated carbon, the cost of regeneration can be higher than the cost of the material itself; therefore the saturated adsorbent is often discharged and landfilled. This is not a durable solution; both the adsorbent and the PFAS pollutants have a linear life cycle and end as waste product. Saturated all-silica zeolite Beta can be regenerated by thermal treatment at high temperature (360 °C), without damaging the zeolite's framework or its crystallinity. The possibility of a thermal regeneration is a big asset for all-silica zeolite Beta, especially so when compared to organic adsorbents like activated carbon or macrocyclic polymers (e.g. β-cyclodextrins), or organic ion-exchange resins. These materials cannot be treated at these high temperatures. Nevertheless, at this point it is not yet clear i) what happens to the PFAS compounds upon thermal treatment at high temperatures (> 300 °C) and ii) how adsorption on all-silica zeolite Beta evolves after multiple adsorption-regeneration cycles.

Looking further than just the regeneration of the adsorbent, inorganic microporous materials like zeolites might be suited for both the adsorption and degradation of PFASs. This would not only prepare the zeolitic adsorbent for another adsorption cycle, but actually end the problem of PFAS pollution. Without PFAS degradation, adsorption is a good technique for the remediation of water streams but it only transfers the PFAS contamination to another phase. Very little is known about PFAS recycling , but in general it is deemed not economically viable if not in a highly concentrated, industrial context; hence destroying the PFAS compounds would be the best solution to avoid discharging the PFASs as waste product. Acidic zeolites

have already proven to assist in the hydrolysis of short (chloro)fluorocarbons at elevated temperatures, but catalyzed thermal degradation (i.e. hydrolysis under steaming conditions) of longer perfluorinated surfactants remains a largely unexplored research topic.[9,10] Considering what is known about the thermal degradation of fluorinated compounds, the hydrolysis of short fluorocarbons like CF_4 requires very high temperatures (> 500 °C) in combination with steam, even with the use of a catalyst.[10] PFOA and PFOS, however, are known to undergo spontaneous loss of the carboxylic acid group at lower temperatures (150-300 °C, depending on the counter ion).[11] Such a dissociation results in the formation of a perfluoro-olefin, but little is known about the further reactions of these olefins. It is still unclear if they can be degraded via hydrolysis, and if so, under which conditions. Furthermore, the hydrolysis of PFASs yields HF. The combination with steam at elevated temperatures results in very corrosive conditions to which the catalysts are exposed, making catalyst stability a core issue.

Knowing that the hydrophobicity of all-silica zeolite Beta is essential for high PFAS adsorption, it cannot be expected from this zeolite to act both as adsorbent and catalyst; catalytic activity by zeolites is often driven by their surface acidity (Brønsted and/or Lewis acid sites) and the presence of these acid sites would jeopardize the hydrophobicity of all-silica zeolite Beta. But an adsorbent and catalyst material can potentially be combined: either in series (an adsorbent bed followed by a catalyst bed) or by combining both materials into a hybrid adsorbent-catalyst structure. The scope of catalysts can then be extended to other material types like metal oxides (alumina, zirconia, titania) and non-porous metal phosphates (Al-, Zr- and Ti-phosphate). All these materials have been reported for their catalytic activity and stability in the thermal degradation of chlorofluorocarbons.[9,12–16] Deposition of nano-sized oxide and phosphate clusters on the outer surface of all-silica zeolite Beta is a potential strategy to combine the adsorptive characteristics of the latter material with the catalytic features of the oxides and phosphates. Such an approach for preparing highly dispersed clusters of metal oxides or phosphates within a zeolite matrix is known: the polymerizable complex method. The idea behind this method is to create a poly-ester resin with strongly chelating side groups, by polymerizing citric acid and ethylene glycol. The resin will chelate with the metal precursors and prevent the precipitation of large metal clusters. In this way, highly dispersed nanosized metal clusters can be prepared and deposited on the outer surface of zeolites.[17]

Ideally, this type of research would result in the incorporation of an adsorbent and catalyst in a single (hybrid) material or in a mixture of materials. Such a (mixed) adsorbent can then be regenerated by the catalytic hydrolysis of PFASs. The effect

of HF and steam on all-silica zeolite Beta during this hydrolysis might be particular: part of the zeolite lattice could be destroyed, generating a secondary pore system. But this could simultaneously provide a source of Si that can be used (elsewhere) for healing framework connectivity defects. This would protect or even enhance the structural integrity of all-silica zeolite Beta and assure its hydrophobic character. The appropriate characteristics for a subsequent PFAS adsorption would be conserved, making the adsorbent reusable for many adsorption cycles and preventing the disposal of PFAS-saturated adsorbents (**Figure 7.1**).

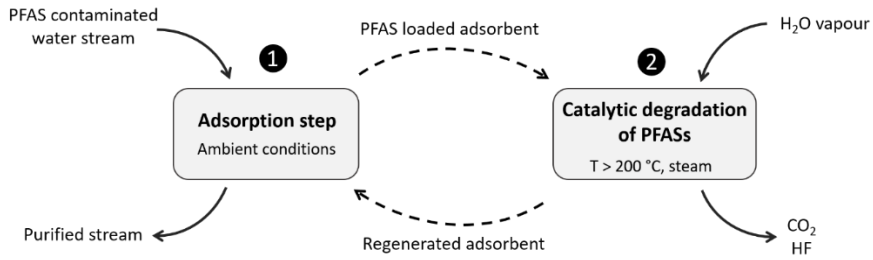


Figure 7.1: Schematic visualization of an adsorption-regeneration cycle.

7.2.3. Adsorbent structuration and optimization of the adsorption process

As explained in detail in Chapter 6, the structuration of adsorbent materials offers several advantages over the use of loose powders. Any type of structuration, whether it be shaping of microspheres, pelletizing the zeolite powder or e.g. coating of a honeycomb extrudate is considered essential for *in situ* application of all-silica zeolite Beta as PFAS adsorbent. Further research is required to structure all-silica zeolite Beta in the best possible way for real water treatment applications. Together with this structuration, the adsorption process as a whole requires further optimization of process and flow conditions: which pressure and temperature are optimal for PFAS removal? Which flow rates will be used and how will adsorption columns be dimensioned? What will be the pressure drop over the column and how severe will mechanical attrition of the adsorbent be? How often will the adsorbent need to be regenerated and how much will this cost? All these questions and respective parameters are related to each other and therefore they need to be resolved simultaneously. This an intensive and in-depth research study of its own and a big step up from screening adsorbent powders in the lab. Nevertheless, it is a final and crucial step before real life application of all-silica zeolite Beta for PFAS removal in water streams is possible.

7.2.4. Upscaling the synthesis process of all-silica zeolite Beta

In this PhD, all-silica zeolite Beta has been synthesized on lab scale, which is a time-consuming synthesis process with a yield on gram scale. In order for this material to be applied on full scale in adsorption columns, the synthesis process requires significant upscaling. Every upscaling process has its pitfalls: the correct synthesis conditions (gel composition, crystallization time and temperate, etc.) can change upon upscaling due to differences in mass and energy transfer, among others. For all-silica zeolite Beta to be synthesized on large scale, it might be interesting to start from a commercially available Beta-22 or Beta-300 and to dealuminate the zeolite, followed by framework healing (i.e. eliminating connectivity defects). We believe this is a feasible, but not yet known synthesis procedure for all-silica zeolite Beta at large scale.

A significant amount of research work still needs to be done, possibly comprising even a few PhD projects. Nevertheless, with the discovery of all-silica zeolite Beta as PFAS adsorbent, we have made a critical step forwards toward a feasible and efficient novel treatment for the remediation of PFAS contaminated water streams and bodies.

7.3. References

[1] V. Ochoa-Herrera, R. Sierra-Alvarez, *Chemosphere* **2008**, *72*, 1588–1593.

[2] P. Meng, S. Deng, X. Lu, Z. Du, B. Wang, J. Huang, Y. Wang, G. Yu, B. Xing, *Environmental Science & Technology* **2014**, *48*, 13785–13792.

[3] C. Lindim, J. van Gils, I. T. Cousins, *Water Research* **2016**, *103*, 124–132.

[4] A. Pistocchi, R. Loos, *Environ. Sci. Technol.* **2009**, *43*, 9237–9244.

[5] R. Holt, **2011**.

[6] Z. Wang, I. T. Cousins, M. Scheringer, K. Hungerbühler, *Environment International* **2013**, *60*, 242–248.

[7] P. B. Poulsen, A. A. Jensen, E. Wallström, E. Aps, *Environmental Project* **2005**, *1013*, 2005.

[8] N. Sheng, R. Cui, J. Wang, Y. Guo, J. Wang, J. Dai, *Arch Toxicol* **2018**, *92*, 359–369.

[9] M. Tajima, M. Niwa, Y. Fujii, Y. Koinuma, R. Aizawa, S. Kushiyama, S. Kobayashi, K. Mizuno, H. Ohuchi, *Applied Catalysis B: Environmental* **1996**, *9*, 167–177.

[10] Y. Takita, T. Ishihara, *Catalysis Surveys from Asia* **1998**, *2*, 165–173.

[11] S. Rayne, K. Forest, Journal of Environmental Science and Health, Part A **2009**, 44, 1145–1199.

[12] Y. Takita, T. Tanabe, M. Ito, M. Ogura, T. Muraya, S. Yasuda, H. Nishiguchi, T. Ishihara, *Industrial & Engineering Chemistry Research* **2002**, *41*, 2585–2590.

[13] X. Deng, Z. Ma, Y. Yue, Z. Gao, *Journal of Catalysis* **2001**, *204*, 200–208.

[14] P. Ning, X. Wang, H.-J. Bart, T. Liu, J. Huang, Y. Wang, H. Gao, *Journal of Environmental Engineering* **2011**, *137*, 897–902.

[15] Y. Takita, J.-I. Moriyama, Y. Yoshinaga, H. Nishiguchi, T. Ishihara, S. Yasuda, Y. Ueda, M. Kubo, A. Miyamoto, *Applied Catalysis A: General* **2004**, *271*, 55–60.

[16] X.-F. Xu, J. Y. Jeon, M. H. Choi, H. Y. Kim, W. C. Choi, Y.-K. Park, *Journal of Molecular Catalysis A: Chemical* **2007**, *266*, 131–138.

[17] M. Kakihana, K. Domen, *MRS Bulletin* **2000**, *25*, 27–31.

LIST OF PUBLICATIONS

Peer-reviewed publications

1) Van den Bergh, M., Van de Voorde, B., De Vos, D. Adsorption and Selective Recovery of Citric Acid with Poly(4-vinylpyridine). *ChemSusChem*, (2017) *10* (24), 4864-4871.

2) Van den Bergh, M., Krajnc, A., Voorspoels, S., Tavares, S.R., Mullens, S., Beurroies, I., Maurin, G., Mali, G., De Vos, D.E. Highly Selective Removal of Perfluorinated Contaminants by Adsorption on All-Silica Zeolite Beta. *Angewandte Chemie-International Edition*, (2020) *59* (34) 14086-14090

3) In print: Van den Bergh, M., Smolders, S., De Vos, D. *Adsorption, Liquid Separation* in Kirk-Othmer Encyclopedia of Chemical Technology (2020)

Patent (pending)

Van den Bergh, M., De Vos, D. Adsorptive Removal Of Perfluorinated Or Partially Fluorinated Surfactants - PCT/EP2020/068275

Appearance of the research in the general media

1) "Nieuwe filtertechnologie kan oplossing bieden voor fluorvervuiling." Nieuwsbericht KU Leuven, 16 oktober 2020
2) "Spons van zand gaat eeuwige chemicaliën te lijf." De Standaard, 16 oktober 2020.
3) "Minerale spons om giftige PFAS uit het water te filteren." Innovationorigins.com, 19 oktober 2020.
4) "Nieuwe filtertechnologie als oplossing voor forever chemicals." Engineeringnet.be, 19 oktober 2020.
5) "Eindelijk een filter voor gevaarlijke chemicaliën." VETO, 24 november 2020.